Platinum Complexes as Potential Photochemotherapeutic Agents

A Thesis Submitted for the Degree of

Doctor of Philosophy

by

Sarah J. Farley, *MChem.*

School of Chemistry

Faculty of Science and Engineering

University of Edinburgh

August 2009

Abstract

A major challenge of platinum anticancer therapy lies in overcoming the severe side-effects associated with treatment. Photoactivatable Pt^{IV} azido complexes, which are stable in the dark and reduced to cytotoxic Pt^{II} species upon irradiation, have recently emerged as a potential site-specific treatment. This thesis is concerned with the investigation of Pt^{II} and Pt^{IV} azido complexes as potential cytotoxic and photochemotherapeutic agents.

Pt^{II} azido complexes such as $[Pt(en)(N_3)_2]$ were shown to bind to both 5'-guanosine monophosphate (5'-GMP) and glutathione, at a much reduced rate compared with their Pt^{II} chlorido analogues. Interestingly, and unexpectedly, these Pt^{II} azido complexes showed moderate cytotoxicity towards the A2780 cancer cell line (IC_{50} 21–47 μM). Binding to 5'-GMP was observed to occur more rapidly upon irradiation with UVA light, although the extent of binding was low and the complexes did not demonstrate phototoxicity towards HaCaT keratinocytes.

The pendant hydroxyl group of a Pt^{II} azido complex was functionalised with a fluorescent probe; conjugation to one axial hydroxyl ligand of a Pt^{IV} azido complex was also achieved. The latter conjugate showed a rapid increase in fluorescence intensity upon irradiation, resulting from loss of the axial ligands upon photoreduction. The functionalisation of quantum dots with Pt^{II} complexes was also investigated. Water soluble CdSe-ZnS quantum dots were synthesised and derivatised with an amine ligand to which platinum was bound. Conjugation of apo-transferrin to quantum dots was also achieved, with subsequent platinum binding yielding a conjugate with improved aqueous solubility and fluorescence properties. However, the conjugate was inactive towards the A2780 cancer cell line, likely due to surface modifications preventing cellular internalisation. Pt^{II} chlorido and azido conjugates with a porphyrin were synthesised and found to show differing behaviour upon irradiation with visible light; evidence of hydrogen peroxide generation from the chlorido complex was much reduced in the case of

the azido complex; it is suggested this may result from quenching of reactive oxygen species by the azide anion released upon irradiation.

Pt^{II} chlorido and azido complexes of highly coloured azo ligands were synthesised in an attempt to shift the wavelength of activation into the visible region. TD-DFT calculations allowed frontier orbital analysis and assignment of the transitions in the absorption spectra. Irradiation of the Pt^{II} azido complexes with UVA or broadband visible light led to their decomposition; one water-soluble complex was found to show moderate cytotoxicity and phototoxicity; in addition, its intense blue colour allowed for visual monitoring of this complex inside cells.

Declaration

I hereby declare that except where specific reference is made to other sources, the work contained in this thesis is the original work of the author. It has been composed by myself and has not been submitted, in whole or in part, for any other degree, diploma, or other qualification.

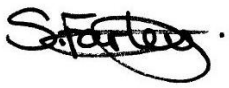

Sarah Farley

August 2009

Acknowledgements

I would firstly like to thank Professor Peter Sadler, for all his help, support and kindness in the last few years.

Many thanks are due to Dr Arindam Mukherjee, who has helped me so much especially in the last year, both with the quantum dot work and with suggestions for many other areas of my project, and from whom I have learnt so much. Thanks also to Dr Vivienne Munk, who helped me to get started on the project, to Dr Juan Mareque, who initially introduced me to quantum dots, to Dr Luca Salassa, for his help with TD-DFT calculations, and to Professor Zijian Guo and Dr Jun Du for their kind hospitality during my visit to China in 2006.

Thanks to Dr Ana Pizarro and Soledad Betanzos Lara for performing the cytotoxicity tests on my complexes, and to Dr Julie Woods and Kim Robinson, from the University of Dundee, for phototoxicity testing. I am grateful to Professor Simon Parsons (University of Edinburgh) and Dr Guy Clarkson (University of Warwick) for crystal structure determination, to Dr Juraj Bella (Edinburgh) and Drs Adam Clarke and Ivan Prokes (Warwick) for assistance with NMR experiments, and Dr Lijiang Song (Warwick) for the acquisition of mass spectra.

Many thanks to Annette Burgess and Jayne Patience, for all their help regarding our move from Edinburgh to Warwick in June 2007.

A huge thank you to the members of the Sadler group, for all their help, support, encouragement and friendship, especially since our move to Warwick. Particular thanks to Dr Arindam Mukherjee, Dr Abraha Habtemariam, Dr Ana Pizarro and Dr Nicky Farrer for all their advice and encouragement, and to Hazel Phillips, Julie Ann Lough, Dr Stefan Weidt and Soledad Betanzos Lara for their friendship over the last few years.

I would like to say the biggest thank you to all of my friends, from Horsham, Durham, Edinburgh and Warwick, and finally to my parents for all their love and support.

Contents

Chapter 1

Introduction

1.1 Introduction

This thesis is concerned with the design of photoactivatable platinum complexes and their potential application as anticancer agents. In this Chapter, an introduction to platinum drugs in clinical use and the current research in this area is given, followed by a discussion of photochemistry with emphasis on metal complexes and its use in medicine. An introduction to the previous work in the area of photoactivatable platinum anticancer complexes is then given.

1.2 Metal-based Drugs

It is now apparent that around 24 elements are essential to human life,[1] with inorganic elements playing crucial roles in many biological processes. The rich redox and coordination chemistry of a number of transition metals is utilised in many catalytic and electron transfer processes; it has been estimated that the activity of around 12% of all enzymes can be attributed to metal centres.[2]

Metal ions are electron deficient and thus show affinity for electron rich biomolecules such as proteins and DNA. However, their reactivity is very much dependent upon speciation, and with scope to vary the coordination number, geometry, oxidation state, thermodynamic and kinetic stability of metal complexes, interest is increasing in their potential medicinal applications.

The use of metals in medicine dates back to antiquity; it is believed the use of gold as a therapeutic agent began in Ancient China around 2500 BC,[3] whilst the antimicrobial properties of silver compounds were recognised by the Romans.[4] The last century has seen the use of bismuth compounds in the treatment of gastrointestinal disorders,[5] as well as the development of gold complexes in the treatment of rheumatoid arthritis;[6] both of which are still in use today. However, the field of medicinal inorganic chemistry was sparked by the discovery, in 1969, of the anticancer activity of *cis*-$[Pt(NH_3)_2Cl_2]$ (cisplatin).[7] Since platinum anticancer agents are a focus of this work they shall be discussed in detail below,

however it is important to note the development of this field in the last forty years. A wide range of inorganic and organometallic complexes are in clinical use or are under investigation as therapeutic agents, including those of gadolinium as imaging contrast agents,[8] vanadium as insulin mimetics,[9] and titanium,[10] ruthenium,[11] gallium[12] and gold[13] as anticancer agents, among others.

1.3 Platinum Anticancer Agents

Cancer is a term for a group of over 100 diseases characterised by abnormal cell growth. Cancers typically acquire six hallmark capabilities: a self-sufficiency in growth signals with insensitivity to anti-growth signals, sustained angiogenesis (growth of blood vessels), a limitless replicative potential, the evasion of apoptosis and the ability to invade other tissues.[14] The treatment of cancer includes surgery, external or internal radiotherapy (using X-rays or a radioactive source, respectively) and/or chemotherapy with cytotoxic drugs, of which there are several types:[15] DNA alkylating agents, antimetabolites, mitotic and topoisomerase inhibitors, hormone treatments and cytotoxic antibiotics. Although not strictly alkylating agents, platinum drugs are related to the first class, and since their routine use began thirty years ago have become the world's best selling anticancer agents; it is estimated that over 70% of cancer patients receive a platinum drug as part of their treatment.[16]

1.3.1 Cisplatin

The biological activity of cisplatin was serendipitously discovered by Barnett Rosenberg in 1969 who, studying the effect of electric fields on *E. coli*, noted abnormal filamentous growth attributed to platinum complexes formed from the electrode.[17] Several such complexes were then tested and found to have potent anticancer activity,[7] resulting in cisplatin entering clinical trials in 1971. Following FDA approval in 1978, it is now used in the treatment of ovarian,

cervical, bladder, small-cell lung and head and neck cancers,[18] and has revolutionised the treatment of testicular cancer; rendering a disease which once killed around 80% of all patients curable in over 90% of cases.[19]

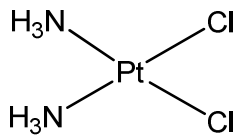

Cisplatin

Figure 1.1 The structure of cisplatin, the first platinum anticancer agent.

Cisplatin is administered by infusion or intravenous injection, following which the high extracellular chloride concentration (~100 mM) prevents hydrolysis of the two chlorido ligands during distribution throughout the body. For many years, uptake into cells was believed to occur *via* passive diffusion,[20] however in recent years evidence has mounted for the involvement of a number of active transport processes,[21] the most important of which involves the copper transporter protein CTR1. This was shown to be a major determinant of the initial influx of platinum drugs, with one experiment showing its loss reduces cisplatin influx by 81% in the first five minutes of exposure, and renders cells resistant to even high concentrations of the drug.[22] It has been suggested that CTR1 employs a different mechanism for the transport of copper and cisplatin,[23] and although the mechanism has yet to be elucidated, the interaction of platinum complexes with a methionine motif found in this protein has been reported.[24]

Upon entry into the cytoplasm, where the chloride concentration falls to ~25 mM, cisplatin becomes hydrolysed to the mono- and diaqua species *cis*-$[Pt(NH_3)_2(H_2O)Cl]^+$ and *cis*-$[Pt(NH_3)_2(H_2O)_2]^{2+}$, and it is the binding of these to DNA which results in a cytotoxic effect.[25] Hydrolysis is the rate-limiting step in this interaction, with half-lives for loss of the first and second chloride

determined as 1.9 h and 2.1 h respectively (310 K).[26] The preferred binding site on DNA is the N7 of guanine residues, since this is the most electron rich site and, additionally, allows for hydrogen bonding interactions between the amine N–H of cisplatin and the O6 of guanine.[27] The major DNA adducts formed are 1,2-d(GpG) intrastrand cross-links between two adjacent guanines (Figure 1.2), accounting for 65% of the total, with other adducts including 1,2-d(ApG) (25%) and 1,3-d(GpNpG) (5–10%) intrastrand links, with a small percentage of interstrand cross-links and monofunctional adducts.[28]

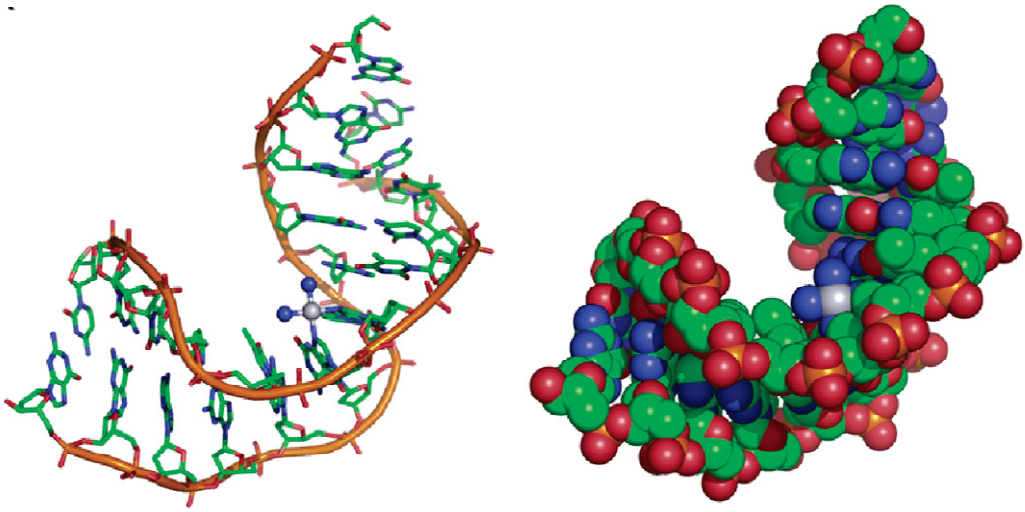

Figure 1.2 Two representations of the 1,2-d(GpG) adduct formed by the interaction of cisplatin with duplex DNA. Adapted from reference 25.

The formation of platinum adducts significantly alters the structure of DNA, with studies revealing destabilisation of the duplex, unwinding and bending. 1,2-Intrastrand cross-links were shown to unwind the DNA duplex in the locality of the platination site, inducing a bend towards the major groove and a widened, shallow minor groove.[29]

Several classes of protein can bind to the exposed minor groove surface, the most studied of which are the high-mobility group (HMG) box proteins. Following binding, the protein inserts a phenylalanine side chain between the two guanine bases in the platinated cross-link,[30] and may serve to shield the cross-link from repair, ultimately leading to apoptosis. However, the exact mechanism by which platinum–DNA adducts trigger apoptosis is unclear; they are known to modulate several signal transduction pathways, which may lead to replication arrest, transcription inhibition and cell cycle arrest,[31] although much work is needed in order to gain further understanding of these processes.

1.3.2 Platinum Anticancer Agents in Clinical Use

Despite the success of cisplatin there are a number of problems associated with its use, namely poor saline solubility and resistance as well as toxic side effects including nausea and vomiting, nephro- and neurotoxicity. Whilst the former can be partially managed with antiemetics, and nephrotoxicity with hydration therapy, neurotoxicity is dose-limiting and may be severe enough to necessitate withdrawal of treatment.[31] Consequently, the search for new platinum drugs to circumvent such effects is extensive and ongoing; although despite the synthesis of thousands of complexes, around 35 have undergone clinical testing with only five approved for clinical use.[32] These are discussed in the following sections.

1.3.2.1 Carboplatin

The toxicity of cisplatin has been attributed in part to its high reactivity, resulting from the lability of the Pt–Cl bonds. It was hypothesised that the incorporation of a more stable leaving group would render the complex less reactive towards biomolecules, thereby minimising side-reactions and lowering toxicity yet retaining antitumour efficacy. This led to the development of the second

generation drug carboplatin, containing the chelating 1,1-cyclobutanedicarboxylato ligand (Figure 1.3).

Despite its introduction as early as the 1980s, the nature of the interaction of carboplatin with DNA is yet to be fully elucidated and two main mechanisms have been proposed:[33] the aquation hypothesis, involving hydrolysis of the chelating ligand and subsequent reaction with DNA in a similar fashion to cisplatin, or the activation hypothesis, involving biological activation (for example, enzymatically or by reaction with thiols) to a species which can then react with DNA.[34] Additionally, direct reactions with DNA have also been suggested due to unexpectedly rapid reactions with 5'-GMP.[35] Although there is a lack of evidence for these latter theories, they are consistent with the observed activity of carboplatin despite its chemical inertness.

Therapeutically, an increased dose relative to cisplatin is required, however whilst a 100-fold greater concentration is necessary to achieve the same rate of DNA platination as cisplatin *in vitro*, only a 4–20 fold increase is needed to achieve the same in patients.[36] Furthermore, such doses of carboplatin are comparatively well-tolerated. Nausea, vomiting and neurotoxicity are markedly reduced and nephrotoxicity is absent at standard doses; instead, the dose-limiting toxicity of carboplatin is myelosuppression (a reduction in bone marrow function). As a result of this higher tolerance, carboplatin has largely replaced cisplatin in clinical use where possible.

However, compared with cisplatin, carboplatin shows somewhat reduced efficacy in head and neck, bladder and oesophageal cancers, although is comparable in ovarian and both small-cell and non-small-cell lung cancers;[32] thus showing no real increase in the range of sensitive tumours. This is attributed to the fact that both complexes form similar DNA adducts, since these are largely dictated by the non-leaving am(m)ino ligands, which are ammonia groups in both cases.

1.3.2.2 Oxaliplatin

The third generation drug oxaliplatin was approved for use in major European countries in 1999, followed by the United States in 2002.[37] This complex contains a 1,2-diaminocyclohexane (DACH) ligand as the non-leaving group (Figure 1.3), hence the Pt–DNA adducts formed differ from those of cisplatin and carboplatin; although 1,2-d(GpG) cross-links are still the major platinated species, the bulky DACH ligand confers differing chemical and steric characteristics to the adducts. This is likely to result in differential recognition and protein binding to these adducts compared with those of cisplatin and carboplatin, implicated in the fact that oxaliplatin shows potency in tumours that are resistant to these drugs. It is now the first line treatment for metastatic colorectal cancer, and has recently undergone Phase III trials for the treatment of pancreatic cancer,[37] a notoriously difficult cancer to treat. However, the difference in tumour specificity could also be related to a difference in uptake. Studies have determined that organic cation transporters (OCTs) markedly increase cellular accumulation of oxaliplatin, but not cisplatin or carboplatin, and that the cytotoxicity of oxaliplatin is reduced upon administration with an OCT inhibitor. It is suggested that an organic group on the non-leaving ligand is required for selective uptake by OCTs.[38]

Tolerance to oxaliplatin is similar to that of carboplatin, with sensory neuropathy the dose-limiting toxicity, as is common with all DACH-containing complexes.[19] Oxaliplatin is now the best selling of all platinum anticancer agents and has become a blockbuster drug, with sales of over $1.6 billion in 2005/2006.[21]

1.3.2.3 Nedaplatin, Lobaplatin and Heptaplatin

Three other platinum complexes have also gained regionally limited approval. Nedaplatin is approved for use in Japan in the treatment of lung, ovarian and colorectal cancers; however shows major cross-resistance with cisplatin.[39] Lobaplatin is used in China to treat metastatic breast and small-cell lung

tumours,[40] with heptaplatin used in South Korea for gastric cancers.[41] However, their toxicities remain similar to that of carboplatin and, although effective in a slightly wider range of tumours, they again do little to circumvent the problem of resistance, which shall be discussed in the following section.

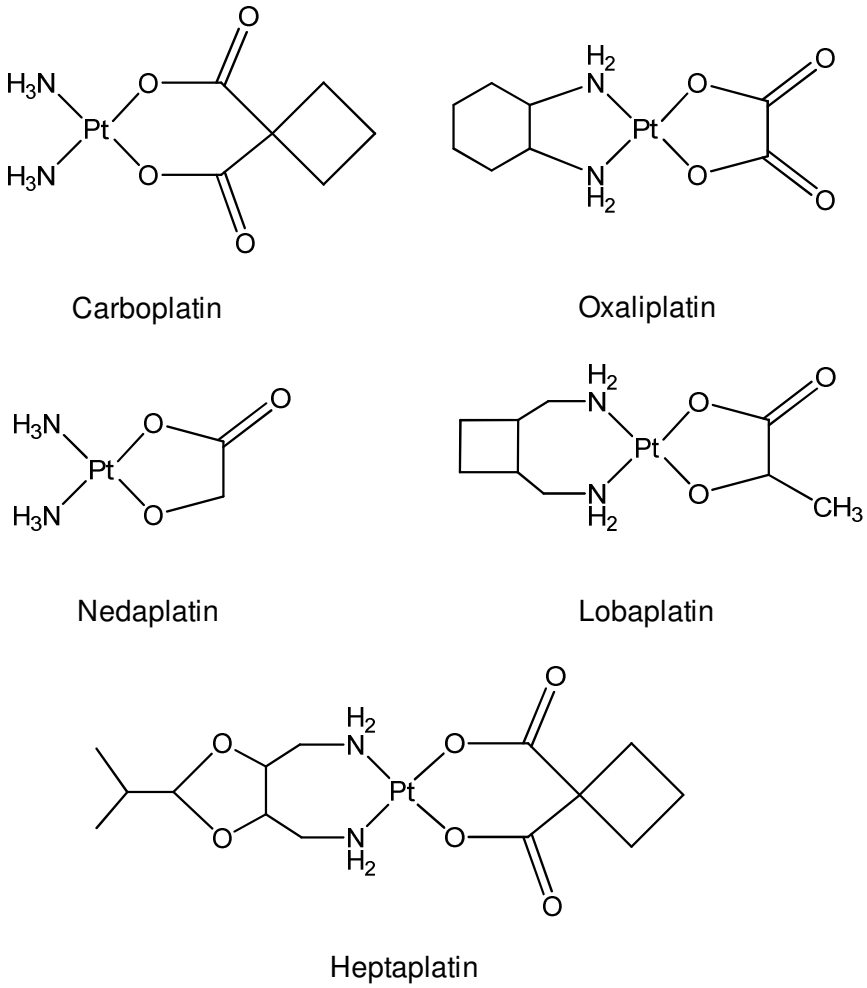

Figure 1.3 Five platinum compounds approved for use in cancer treatment.

1.3.3 Resistance to Platinum Anticancer Agents

The second- and third generation platinum drugs discussed here show some improvements over cisplatin; these include greater water solubility, a slightly broader spectrum of activity and, in particular, a reduction in toxic side effects.

However, they do little to circumvent another major problem of platinum chemotherapy: that of resistance. This can be either inherent, or acquired following initial treatment, and can occur by several different mechanisms.

Reduced drug accumulation is commonly reported in platinum-resistant cell lines, and is believed to result from a decrease in uptake rather than an increase in efflux.[42] Reasons behind this are unclear; in addition to the copper transporter CTR1, a number of other transporters are likely to be capable of accommodating cisplatin uptake, and studies of sensitive and resistant cell lines have not been able to identify a single one whose decreased presence on the plasma membrane significantly contributes to a reduction in accumulation.[43] However, there are also arguments for the role of increased efflux, with evidence of extrusion after chelation by glutathione and in an unknown form *via* the copper efflux system.[43]

A major resistance mechanism involves the deactivation of complexes prior to reaching their active site of DNA; in fact, it has been estimated that only 1% of intracellular platinum reaches the nucleus.[44] The high affinity of platinum for sulfur donor ligands results in binding to intracellular thiols, with the cysteine-containing tripeptide glutathione, present in millimolar concentrations within cells, believed to play an important role in deactivation. There have been many reports showing that the toxicity of platinum drugs decreases with increasing cellular glutathione levels,[45] however reducing these levels with drugs such as buthionine sulfoximine has led to only low to moderate increases in cisplatin sensitivity.[46] Furthermore, recent work has suggested that higher molecular weight thiols may be of greater importance than glutathione in deactivation reactions. Experiments involving the incubation of cisplatin with whole cell extracts revealed that two-thirds of the resulting platinum adducts had a molecular mass >3 kDa, and Pt(glutathione)$_2$ species could not account for more than 20% of the total platinum adducts.[47] The high molecular weight adducts could not be identified due to the sheer abundance of proteins in the cell with which platinum could react, however the likely role of metallothioneins in deactivation is well-documented.[48] These metal-binding proteins are sulfur rich, containing twenty

cysteine residues, and incorporation of platinum into the metallothionein structure is an efficient means of sequestering these drugs.

Resistance can also arise from the increased tolerance to, or repair of, Pt–DNA adducts. The recognition of such adducts can either lead to induction of apoptosis by activation of the appropriate signalling pathways, as discussed in section 1.3.1, or to damage repair, which will increase the probability of cell survival. Adducts are primarily removed by nucleotide excision repair (NER), in which the damaged DNA segment is excised by hydrolysis of the backbone phosphodiester bonds, followed by replacement of the missing nucleotides by DNA polymerase.[49] It is known that cells deficient in NER are more sensitive to platinum drugs, and that repair is enhanced in platinum-resistant cell lines.[50] In addition, mismatch repair and recombinatorial repair mechanisms have also been implicated;[25] it has been suggested that the latter may also be active against the small proportion of interstrand cross-links. However, studies have indicated that an enhancement of DNA repair is not sufficient to render cells resistant to platinum drugs in the absence of other resistance mechanisms.[50]

1.3.4 The Design of New Platinum Anticancer Agents

In the years following the development of cisplatin, Cleare and Hoeschele published a set of structure-activity relationships[51] which focused the research efforts in this field onto complexes similar in nature to cisplatin; namely *cis*-$[PtA_2X_2]$, where A = amine possessing at least one N–H bond, and X = anionic leaving group with intermediate binding strength (e.g. chloride). However, whilst thousands of complexes have been screened, only five have entered clinical use, and no drug has yet emerged in which the range of sensitive tumours is much greater, and the toxicity significantly lower, than that of cisplatin. It is becoming increasingly apparent that in order to overcome these problems, new design concepts are needed. Hence in recent years the emphasis has shifted and many recent complexes violate these rules; they are designed to

have a different mechanism of action, mode of activation, or platination profile to cisplatin in attempts to produce a more effective platinum anticancer agent. Some examples are discussed below.

1.3.4.1 Sterically Hindered Complexes

cis–[$Pt(NH_3)$(2-picoline)Cl_2] (picoplatin) was designed in an attempt to reduce drug deactivation by intracellular thiols.[52] The methyl group of the 2-picoline ring lies over the top of the platinum square plane, providing steric hindrance to the formation of a trigonal bipyramidal intermediate necessary in substitution reactions. The hydrolysis rates of picoplatin are two to three times slower than those of cisplatin,[52] with the rate of reaction towards glutathione also reduced, and the influence of the 2-picoline ring highlighted by comparison with the 3-picoline analogue.[53] Although reaction rates with DNA were also decreased, the extent of platination by this complex was shown to be similar to that of cisplatin.[54] It was suggested that DNA adducts may be recognised differently to those of cisplatin by the excision repair systems, which could explain the observed lack of cross-resistance. Picoplatin shows *in vitro* toxicity intermediate between that of cisplatin and carboplatin,[55] and is currently undergoing Phase III clinical trials for the treatment of small-cell lung cancer.[21]

1.3.4.2 *Trans* Complexes

It had been observed in early studies of platinum complexes that *trans*-[$Pt(NH_3)_2Cl_2$] (transplatin) was inactive.[56] This was partially attributed to its lack of ability to form 1,2-d(GpG) intrastrand cross-links, responsible for the activity of its isomer cisplatin, although stable monoadducts are formed. Furthermore, transplatin is kinetically much more reactive to nucleophiles in both the dichloro and monoaqua forms than is cisplatin, reacting up to 1000 times faster with glutathione. Such high activity is likely to result in rapid deactivation

prior to reaching DNA. However, by varying the nature of the amine ligands, several classes of active *trans* complexes have been identified; three shall be discussed here.

The complex *trans*-[Pt(*E*-iminoether)$_2$Cl$_2$] (Figure 1.4) forms monofunctional adducts at the N7 of guanine residues; experiments with single-stranded oligonucleotides, which were subsequently hybridised, suggested the local distortion of DNA and bending towards the minor groove, with a lack of adduct recognition by HMG proteins.[57] The monofunctional adducts can readily cross-link proteins, enhancing the ability to terminate DNA polymerisation and inhibiting removal of the adduct by nucleotide excision repair. However, more recent studies suggested that *trans*-[Pt(*E*-iminoether)$_2$Cl$_2$] does not interact with short duplexes lacking terminal guanine residues, as a result of the steric demand of the iminoether groups. The replacement of one iminoether group with NH_3 allowed for binding at central guanines, whilst retaining the toxicity of the bis-iminoether complex.[58] It has also been suggested that the steric bulk of the iminoether ligand may retard any deactivation reactions with thiol-containing biomolecules. These imino complexes have shown good activity in a range of cell lines.[59]

Trans-Pt^{II} complexes with branched chain aliphatic amines also show very promising cytotoxicity. *Trans*-[Pt(dimethylamine)(isopropylamine)Cl$_2$] (Figure 1.4) has been shown to form mainly interstrand cross-links with DNA, between a guanine residue and its complementary cytosine, and induce apoptosis.[60] Recent work suggests that hydrolysis rates of this and two related branched-amine complexes are rapid (half-lives 1.3–3.5 h at 298 K), however the extent of hydrolysis is low: <1% at equilibrium.[61] It was noted that more sterically hindered complexes hydrolyse more slowly, and a lower extent of hydrolysis at equilibrium appears to correlate with higher cytotoxicity, suggesting more efficient DNA targeting. The effect of replacing one aliphatic amine with various pyridyl moieties has also been investigated, with the cytotoxicity very much dependent upon the substituents on the pyridyl ring.[62]

In the last few years, *trans* complexes with N_2O_2 donor sets have been investigated,[63] where the chlorido groups are replaced by carboxylates to improve aqueous solubility (Figure 1.4). Like carboplatin, these complexes are surprisingly stable to hydrolysis, although their toxicity is similar to that of the chlorido analogues.[64] The use of carboxylate ligands appears to result in increased cellular accumulation, furthermore there is much scope to fine-tune the properties of these complexes by varying the nature of the oxygen donor ligands.

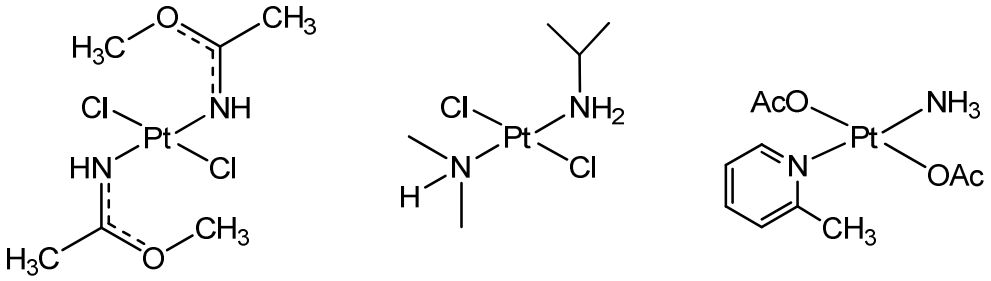

Figure 1.4 Three *trans*-platinum complexes currently under investigation.
Left: an iminoether complex, middle: a complex with branched chain aliphatic amines, right: a complex containing the N_2O_2 donor set.

1.3.4.3 Multinuclear Complexes

Multiplatinum complexes have been under investigation since the late 1980s. The rationale behind their development was the belief that complexes structurally dissimilar to cisplatin could form markedly different DNA adducts, potentially leading to differences in recognition and repair, and activity in a wider range of tumour types.

The most successful and widely studied is the trinuclear complex BBR3464 (Figure 1.5), in which the platinum centres are separated by diaminohexane linkers, and the two terminal platinums bind one chlorido ligand each. This complex has a high affinity for DNA due to its positive charge, and binds rapidly

forming 1,4-interstrand cross-links involving two guanine residues. These adducts do not significantly distort DNA, suggesting recognition by HMG proteins is poor; in addition, their flexibility renders them less likely to be recognised and removed by the nucleotide excision repair system.[65] However, these complexes are able to induce conformational changes in DNA, particularly from B-type to Z-type and A-type.[66] Cell tests reveal BBR3464 to be highly cytotoxic, showing mean IC_{50} values more than one order of magnitude lower than cisplatin in an assay of seven cell lines,[67] with evidence that the drug can overcome both acquired and inherent cisplatin resistance.[68] However, BBR3464 is also highly toxic to healthy cells, with the maximum tolerated dose at least 60 times lower than that of cisplatin.[66] Nephro- and neurotoxicity are not observed, and the dose-limiting toxicity is neutropenia (a reduction in the number of white blood cells). BBR3464 has undergone a number of clinical trials over the past ten years, including recent Phase II trials for gastric adenocarcinoma, ovarian and small-cell lung cancer; however, the results were not substantially different from those of cisplatin, possibly resulting from extensive binding and degradation by human plasma proteins.[66]

Triplatin NC (Figure 1.5) is a more recent trinuclear complex in which the chlorido ligands are replaced by diaminohexane groups. This increases the overall charge on the complex to +8 and introduces further hydrogen bonding capability, but removes the ability to form coordination bonds with DNA. Instead, this complex shows an unprecedented non-covalent interaction known as the "phosphate clamp", binding to the phosphate oxygens of the backbone.[69] This complex shows micromolar activity against a human ovarian cancer cell line,[70] the first platinum complex with only non-covalent DNA interactions to do so.

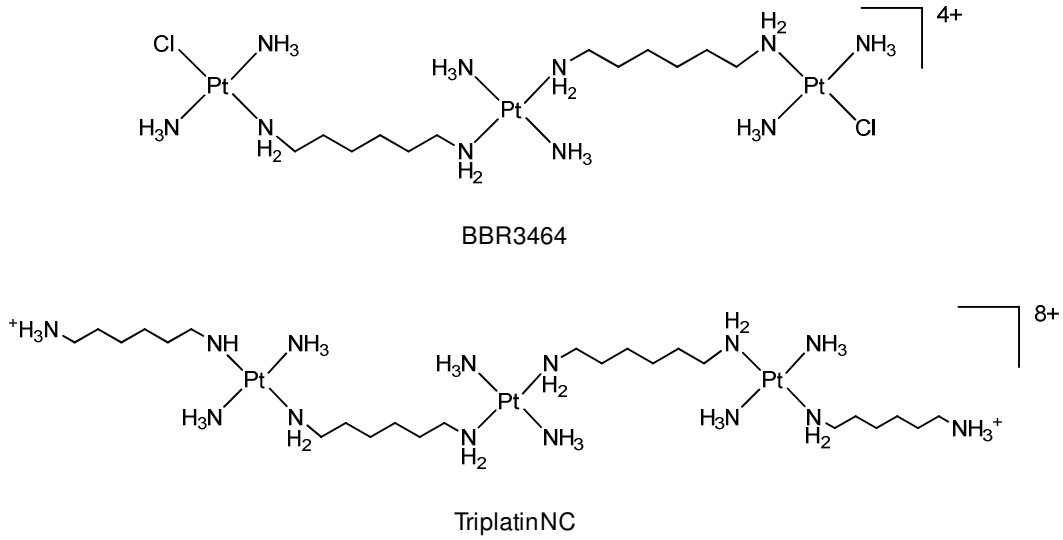

Figure 1.5 The multinuclear platinum complexes BBR3464 and TriplatinNC.

1.3.4.4 Pt^{IV} Complexes

The cytotoxicity of Pt^{IV} complexes has been recognised since the early work on cisplatin,[17] and over the years research interest in this area has increased with the recognition that Pt^{IV} complexes can offer several advantages over those of Pt^{II}. Firstly, Pt^{IV} complexes are much more kinetically inert, and as such the probability of deactivating side-reactions, a major problem with Pt^{II} complexes, is greatly reduced. They are also generally more lipophilic than those of Pt^{II}, allowing for greater diffusion through cell membranes with less reliance upon facilitated transport mechanisms for cellular uptake. Furthermore, the addition of two "axial"[71] ligands gives great scope for structural variation and modifying the properties of the complex.

It is widely accepted that Pt^{IV} complexes act as prodrugs and must be reduced to Pt^{II} in order to exert a cytotoxic effect; their reduction potentials are therefore of great importance. The axial ligands have the greatest influence on this property, determined by their size and electron withdrawing ability.[72] Complexes with axial chlorido ligands are the most readily reduced, followed by

acetato/carboxylato, and those with axial hydroxyl groups have the lowest relative reduction potential and therefore are the least readily reduced.[73]

There have been some attempts to correlate these reduction potentials with DNA binding ability, cellular reduction rates and cytotoxicity. The most readily reduced complexes showed increased DNA binding ability,[74] and the proportions of three Pt^{IV} complexes reduced intracellularly, two hours after administration, was found to correlate with their reduction potentials.[75] Correlations with cytotoxicity cannot be so readily drawn, since dramatic changes in lipophilicity, uptake and reactivity will occur upon reduction, which can occur either intra- or extracellularly.

The location of reduction, nature of the reducing species, and the overall fate of the complex depends upon the Pt^{IV} complex in question. There are a number of biomolecules available in the bloodstream and in cells capable of effecting such a reduction, such as glutathione, ascorbate, metallothioneins and even nucleotides.[72] It is suggested that complexes with axial chlorido groups, such as [Pt(1,2-diaminocyclohexane)Cl_4] (tetraplatin, Figure 1.6), are rapidly reduced extracellularly to form Pt^{II} biotransformation products.[76] Those with axial acetato groups, such as *cis,cis,trans*-[Pt(NH_3)(cyclohexylamine)$Cl_2(OAc)_2$] (satraplatin, Figure 1.6) are likely to be reduced at a lesser rate in the bloodstream, allowing for a small degree of hydrolysis of the chlorido ligands.[72] *In vivo* metabolism of satraplatin is not well understood; although the major metabolite is the Pt^{II} analogue formed by loss of the axial acetato groups, at least six biotransformation products, both Pt^{IV} and Pt^{II}, have been identified.[77] Recent research has shown that the reduction of satraplatin can be mediated by haem proteins, consistent with the shorter half-life observed in whole blood extracts compared with plasma alone.[78] Complexes with lower reduction potentials, such as *cis,cis,trans*-[Pt(isopropylamine)$_2Cl_2(OH)_2$] (iproplatin, Figure 1.6) are likely to remain in the Pt^{IV} state until reduced intracellularly, likely by glutathione. One study shows a positive correlation between iproplatin and tetraplatin cytotoxicity and cellular glutathione levels, and suggests the more significant correlation for iproplatin

arises since its high reduction potential would necessitate a strong reducing agent such as glutathione, whereas tetraplatin could also be reduced by weaker reductants such as ascorbate.[79]

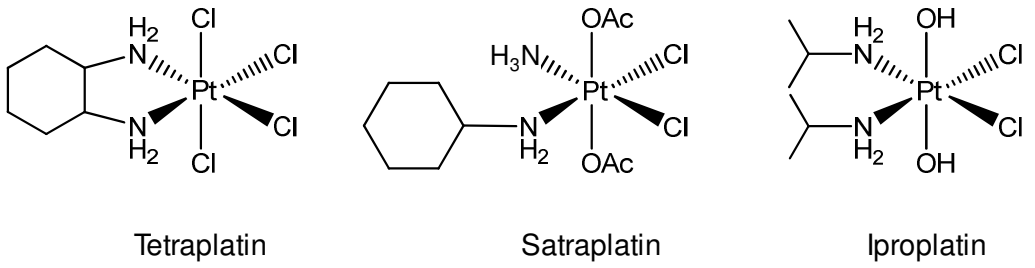

Tetraplatin Satraplatin Iproplatin

Figure 1.6 Three Pt^{IV} complexes which have been investigated in clinical trials.

The three aforementioned Pt^{IV} complexes have all entered clinical trials. Tetraplatin had showed high activity both *in vivo* and *in vitro* to a number of cell lines,[32] likely due to increased cellular accumulation (four-fold compared with cisplatin).[80] However, four different Phase I trials revealed severe and irreversible neurotoxicity, and trials were discontinued. Iproplatin reached Phase III clinical trials for ovarian cancer, but was ultimately abandoned due to lower activity compared with cisplatin. Satraplatin, an orally-administered drug, first entered clinical trials over 15 years ago and has recently completed Phase III trials in combination with prednisolone for the treatment of hormone-refractory prostate cancer. However, results failed to show a significant increase in overall survival compared with cisplatin,[81] and an FDA application for drug approval was withdrawn. However, given its convenience of administration, mild toxicity profile and lack of cross-resistance with cisplatin, further clinical trials involving satraplatin may be likely.

Pt^{IV} complexes remain an active area of research. Recent developments include new insights into the reaction of iproplatin with glutathione; this was previously

believed to involve reduction to the Pt^{II} chlorido species, however formation of a Pt^{II} bis-glutathione complex has been demonstrated.[82] A new class of Pt^{IV} complexes with long-chain carboxylate ligands has shown very high toxicity, with IC_{50} values in the low micromolar and even nanomolar range.[83] Furthermore, an increasingly attractive strategy is the incorporation of bioactive moieties into the axial ligands, which would be released upon reduction; this could aid in targeting or give complexes with a dual mode of action, and is explored further in Section 1.3.4.5.

1.3.4.5 Functionalisation and Targeting of Platinum Anticancer Complexes

The drawbacks of current platinum anticancer complexes include the lack of selectivity for cancerous over healthy cells (a problem common to the majority of anticancer agents), and deactivation of the drugs before reaching their intended site of DNA. The idea of incorporating a moiety that can increase selectivity, either for cancer cells or for a particular cellular target, is becoming an increasingly attractive strategy in drug design. There are many examples of such approaches applied to platinum complexes in the literature, hence only a few shall be considered here.

Attention has recently focused upon novel methods of delivery of cytotoxic platinum complexes, aiming to increase selective uptake into cancer cells. A liposomal formulation of cisplatin, known as lipoplatin (Figure 1.7), is among the most widely studied. The liposomes in which cisplatin is encapsulated (average size 110 nm) are coated with hydrophilic polyethylene glycol (PEG) chains, hence are able to evade removal by macrophages, and show a long *in vivo* retention time (>100 h). Since tumours are often hyperpermeable to macromolecules due to their compromised vasculature (the EPR effect), lipoplatin shows accumulation in both primary and metastatic tumour tissue up to 200 times greater than in surrounding healthy tissue. As of 2008, lipoplatin was involved in three Phase III clinical trials, two against non-small-cell lung cancer and a third for head and neck

cancers. The results of previous trials have suggested a vast reduction in side effects compared with other platinum drugs and an improved spectrum of activity, and further Phase III trials are planned. Additional delivery methods have included the use of dendrimers, polymers and micellar systems.[84] More recently, the encapsulation of cisplatin into the cavity of the iron binding protein apoferritin was reported (Figure 1.7).[85] The resulting conjugate showed a 4.5-fold increase in cellular uptake relative to cisplatin alone, and appeared to release the toxic moiety slowly over time. Au-Fe_3O_4 nanoparticles have also been used as target-specific nanocarriers of a toxic platinum moiety, targeted to Her-2 breast cancer cells by the monoclonal antibody herceptin.[86]

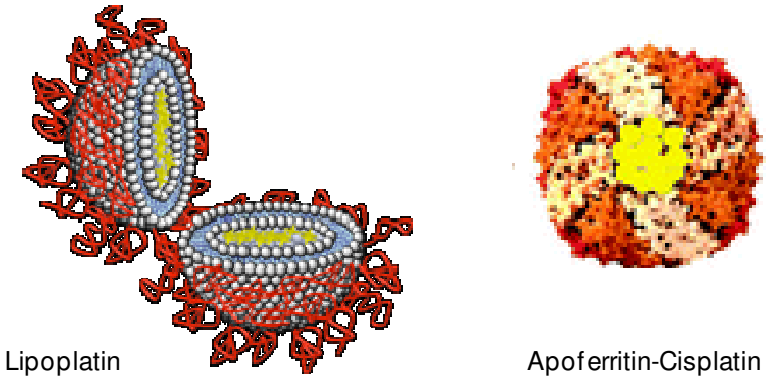

Figure 1.7 Schematic diagrams of two novel methods for the delivery of platinum anticancer complexes. In both cases, the platinum complexes are represented by the yellow colour. Adapted from references 32 and 85.

Many studies have investigated the attachment of DNA-targeting species, such as intercalators, to cytotoxic Pt^{II} complexes. Construction of the intercalating moiety to enable platinum binding allows the synthesis of complexes with a potentially bifunctional mode of DNA interaction; furthermore, changes in the nature of DNA adducts may result in complexes with a different activity profile to cisplatin. The complex [Pt(en)Cl(ACRAMTU-S)]$(NO_3)_2$, (ACRAMTU = [2-(acridin-9-

ylamino)ethyl]-1,3-dimethylthiourea), denoted Pt–ACRAMTU and depicted in Figure 1.8, was found to interact with DNA *via* a dual mechanism involving intercalation of the ACRAMTU moiety and monofunctional platination. Contrary to cisplatin, platination occurs at the guanine N7 and adenine N3 sites, and is directed towards the minor groove by the sequence and groove specificity of the intercalator.[87] In another recent example, a targeted interaction with G-quadruplex DNA was achieved with a platinum–quinacridine hybrid complex, which showed a dual noncovalent and covalent binding mode to further stabilise the G-quadruplex structure.[88]

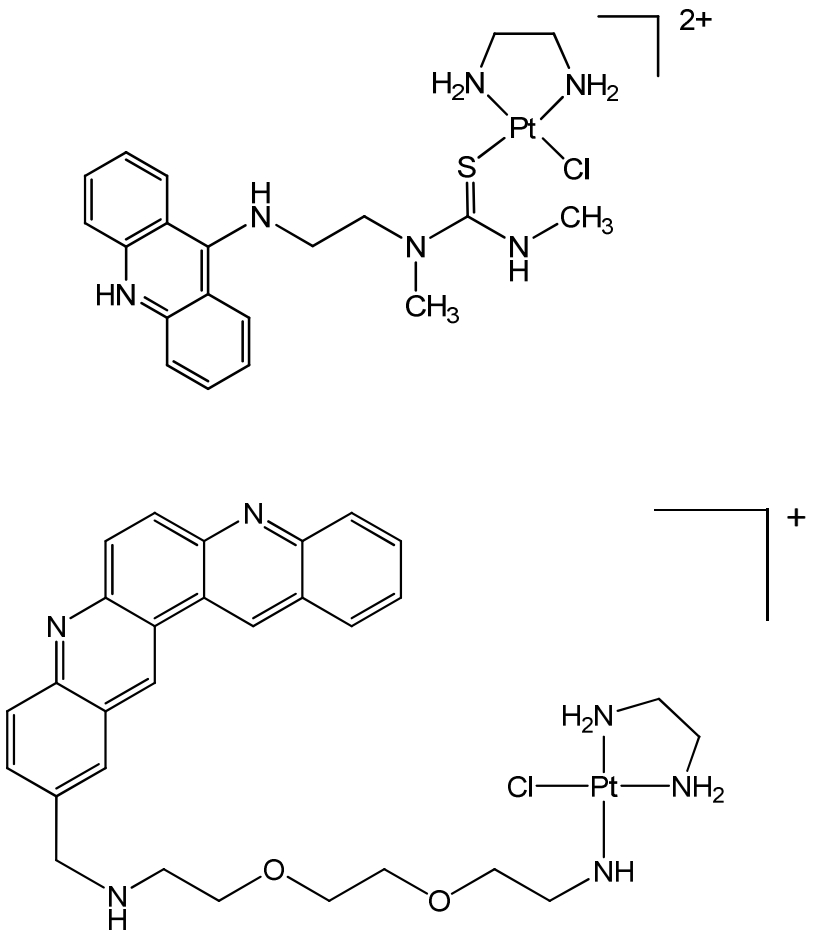

Figure 1.8 The structures of two platinum-intercalator complexes.
Top: Pt–ACRAMTU, and bottom: a Pt-quinacridine complex to target G-quadruplex DNA.

Other studies have shown the effects of varying the linker length between an intercalator (9-aminoacridine-4-carboxamide) and a platinum moiety ([Pt(en)Cl_2]); compounds with shorter linker chain lengths were found to show greater alteration of sequence specificity than those in which the linker was longer, where the platination profile was more similar to cisplatin.[89]

An additional strategy gaining increasing interest is the functionalisation of the axial ligands of Pt^{IV} complexes. Since the reduction of these complexes involves loss of the axial ligands, intracellular reduction should release these along with a toxic platinum complex; a wide range of ligands could potentially be employed to give targeted complexes or those with a dual mode of action.

In one such example, Lippard *et al* synthesised a series of estrogen-tethered Pt^{IV} complexes (Figure 1.9),[90] since it is known that exposure to the hormone sensitises estrogen-receptor positive (ER(+)) cells towards cisplatin treatment, *via* overexpression of a protein shielding the platinated adduct from repair. The complexes were found to selectively induce overexpression in ER(+) and not ER(–) cells, and were consequently more toxic to the former cell line.

Lippard *et al* have also synthesised a Pt^{IV} conjugate functionalising both axial ligands independently: one with a targeting species, a folate derivative exploiting the overexpression of the folate receptor on a variety of tumour cells, and the second with a delivery aid, a single-walled carbon nanotube to aid internalisation into cells (Figure 1.9). Cell entry *via* endocytosis was confirmed, as well as reduction to a cytotoxic Pt^{II} species able to cross-link DNA.

Dyson *et al* employed the ligand ethacrynic acid (Figure 1.9), a known inhibitor of the enzyme glutathione-S-transferase, which catalyses the conjugation of cisplatin to glutathione.[91] The greater cytotoxicity of these conjugates compared with cisplatin was suggested to arise from the release of the inhibitor upon reduction and its subsequent effects on glutathione levels.

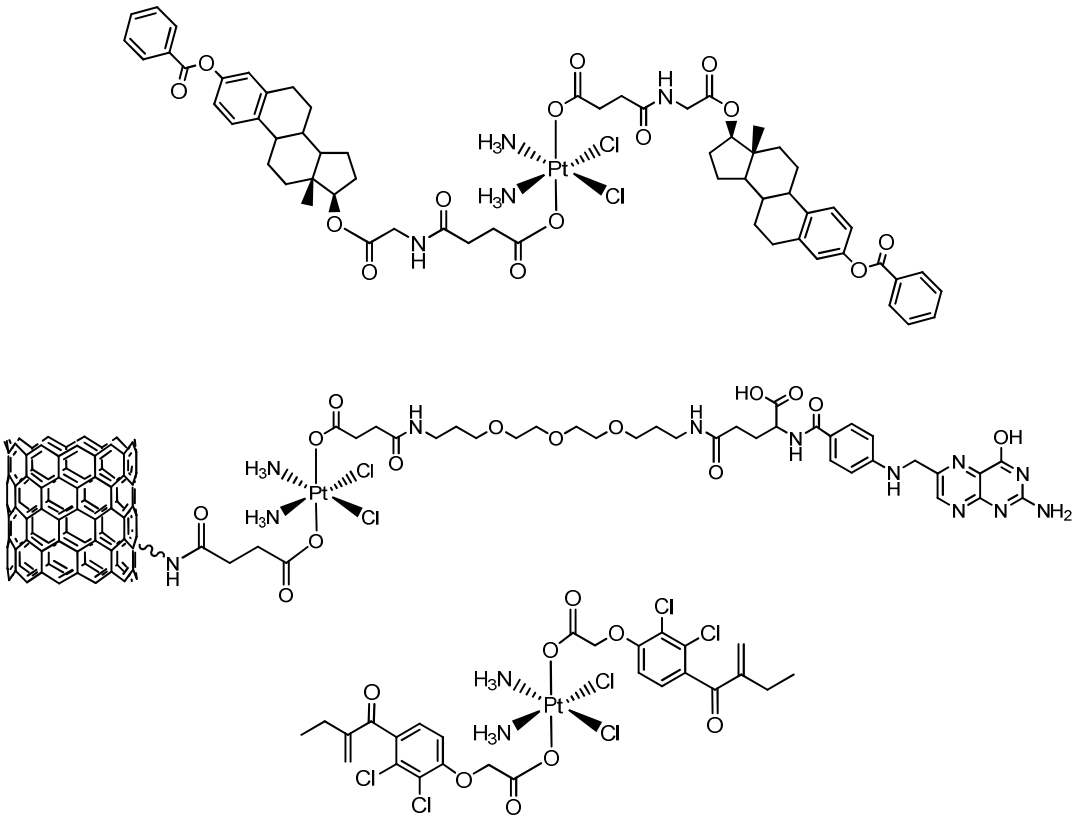

Figure 1.9 Pt^{IV} complexes with functionalised axial ligands.
Top: An estrogen conjugate, middle: a complex containing a carbon nanotube and a folate derivative, and bottom: a complex containing ethacrynic acid.

Many of the strategies described above are designed with the aim of minimising activity in healthy cells, and thus reducing toxic side effects associated with treatment. This was also the rationale behind the development of photoactivatable platinum anticancer complexes, with which this thesis is concerned. Prior to discussion of previous work on these complexes, some background to photochemistry and its use in medicine will be given.

1.4 Photochemistry[92,93,94]

Photochemistry is concerned with the effects of light on chemical systems, and is discussed here with reference to coordination compounds. This section considers the formation of excited states and different types of electronic transition, followed by deactivation pathways to the ground state. The photochemistry of platinum complexes is then discussed.

During the interaction of light with a complex, photoexcitation can occur if the difference in energy between the ground state and an excited state matches that of the incident photon. The transition dipole moment is a transient dipolar polarisation created by this interaction, and the intensity of the transition is proportional to the square of this term.

Transitions with a nonzero transition dipole moment therefore have nonzero intensity, and are designated allowed transitions, whilst in forbidden transitions the dipole moment is zero, with the magnitude governed by selection rules.

– The spin selection rule declares that transitions between states of different multiplicity are forbidden; i.e. the relative orientations of spins in the complex must not change.
– The Laporte, or symmetry selection rule declares that transitions between states of equal parity are forbidden; for example d–d transitions in metal complexes.

The intensity of the transition can be quantified by the amount of light absorbed, according to the Beer-Lambert Law:
$A = \varepsilon c l$
where A is absorbance, c is the concentration (M), ε is the molar extinction coefficient (M^{-1} cm^{-1}) and l is the pathlength of the light beam (cm).
Absorbance is defined as $A = \log_{10}(I/I_0)$, where I_0 is the incident light intensity and I the transmitted intensity.

1.4.1 Types of Electronic Transition

Electronic transitions are classified according to the localisation of the electron density and its change during the transition. There are four main types of transition, as described below.

– Transitions between molecular orbitals (MOs) based on the central (metal) atom in a complex, subdivided into ligand field (LF) transitions (e.g. d–d), Rydberg transitions (populating an orbital of higher quantum number), and inter-valence charge transfer transitions (between metal atoms in polymetallic complexes).
– Ligand based transitions; either intraligand (ILCT), where the two MOs are based on the same ligand, or ligand-to-ligand charge transfer transitions (LLCT), involving two different ligands of the same complex.
– Transitions involving charge transfer between orbitals that are primarily ligand in character and those primarily metal in character, classified according to direction: Ligand-to-metal charge transfer (LMCT) or Metal-to-ligand charge transfer (MLCT).
– Transitions between complex and solvent; charge-transfer-to-solvent (CTTS).

Ligand field transitions correspond to a redistribution of electrons in partially filled d orbitals; since this does not involve a change in parity, these transitions are formally forbidden in octahedral complexes. However, they often occur, albeit weakly, since the Laporte selection rule can be relaxed in one of two ways: firstly the complex may deviate from perfect symmetry, due to the differing nature of its ligands or environmental distortions, and secondly the complex can undergo asymmetric vibration, also destroying the centre of symmetry.

The direction of charge transfer transitions (metal-to-ligand or ligand-to-metal) depends on the relative energy of the orbitals and their population; for example, if the ligand orbitals are filled and those of the metal are not, an LMCT may arise,

conversely if the metal is electron rich (in a low oxidation state) and the ligand has low-lying, accessible empty orbitals, an MLCT may result.
Since charge-transfer transitions are formally allowed they give rise to much more intense bands in absorption spectra, and this is one means of identifying such a transition. Another is that charge-transfer transitions typically display solvatochromism, a shift in transition frequency with solvent polarity; this is characteristic of transitions in which a large shift of electron density occurs.

Intraligand charge-transfer transitions can occur in complexes containing organic ligands with multiple bonds. These transitions are both spin- and orbital-allowed, and hence give rise to intense bands in the spectra, the position of which do not depend significantly on the metal or other ligands in the complex.

1.4.2 Deactivation from Excited States

Generation of an excited singlet state typically populates the higher vibrational levels of that state, from which the complex rapidly relaxes back to the lowest level by a process known as vibrational relaxation. From here, several processes are possible: either photophysical, which regenerate the ground state of the complex, or photochemical, in which reactions occur in the excited state to generate new products.

1.4.2.1 Photophysical Deactivation and Luminescence

Photophysical deactivation pathways can either be non-radiative, in which the excitation energy is dissipated to the solvent as heat, or radiative, where relaxation to the ground state is accompanied by emission of a photon (luminescence). The loss of energy to molecular rotation, vibrations and heat means the photon emitted is of lower energy than that absorbed, hence complexes are often excited in the

UV region but emit in the visible. This difference in energy is known as the Stokes Shift.

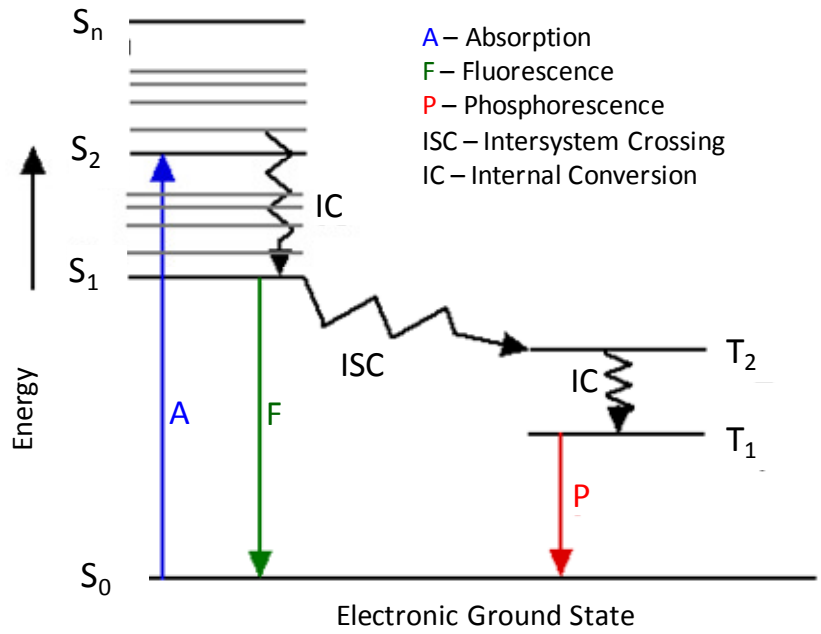

Figure 1.10 A Jablonski diagram summarising the potential deactivation pathways of a complex in an excited state.

There are two main luminescent processes: fluorescence and phosphorescence, which differ in the nature of the excited state from which the emission occurs. Where this is a singlet state (usually S_1), the process is known as fluorescence. Being a formally allowed process, the emission rate is rapid and fluorescence lifetimes are short, typically around 10 ns. Molecules in the S_1 excited state can also undergo spin conversion to the first triplet state, T_1, *via* intersystem crossing; emission from this state is termed phosphorescence. As the transition from T_1 to S_0 is spin forbidden, the rate of relaxation from the triplet state is much reduced

compared with the singlet, and as a result phosphorescence lifetimes are of the order of milliseconds or seconds.

A decrease in intensity of fluorescence is known as quenching, and can be induced by many processes. A common process is collisional quenching, in which the fluorophore is deactivated upon contact with another molecule in solution. Molecular oxygen is a good example of a quencher, hence many samples show fluorescence only in degassed solutions. The mechanism of quenching depends upon the molecules involved, and can include electron transfer and increased intersystem crossing. The latter is typically seen in the presence of heavy metals, which are known to be excellent quenchers. Heavy atoms, either within the fluorophore or in close contact, increase the rate of intersystem crossing to the triplet state by strengthening spin-orbit coupling. This radiationless transition to the triplet state completes with the emissive transition from S_1 to S_0, hence quenching the fluorescence.

1.4.2.2 Photochemical Reactions of Coordination Compounds

A photochemical reaction is a process in which part of the excited state energy is used to produce a chemical change in the complex. In certain cases, photochemical reactions compete efficiently with photophysical decay pathways to dissipate the energy gained upon excitation. The reactivity of the excited state is different from that of the ground state, and otherwise inaccessible products can often be formed upon irradiation. The main photoreactions can be classified as photoredox, photoisomerisation and photosubstitution, and are discussed below.

a) Photoredox reactions

Although several reactions can be classified as photoredox, this section shall consider only addition and elimination reactions. These involve a change in oxidation state of the central atom and in coordination number of the complex,

and often involve the formation of intermediates, so do not always result in a stable product.

Oxidative addition reactions occur in metal complexes with vacant coordination sites and a low oxidation state, and involve the insertion of a metal into a covalent bond. They can occur photochemically when the Lewis acidity of the central atom is increased upon excitation. Reductive elimination reactions involve the elimination of two ligands adjacent in the coordination sphere of the metal, and are favoured where the new bond formed between them is strong, such as in the case of N_2 produced from reductive elimination of azido ligands. LMCT transitions are often implicated in photochemical reductive eliminations.

b) Photoisomerisation reactions

Reactions leading to isomerisation of a substrate can occur by several mechanisms including bond rotation, skeletal rearrangement or atom or group transfer, and the *cis-trans* photoisomerisation of square planar complexes is thought to involve both tetrahedral and trigonal intermediates. Studies of Pt^{II} complexes indicate that the photoactive states are mostly spin-forbidden ligand-field states, and that photoisomerisations occur from the lowest triplet state. Photochemical isomerisation reactions can give mixtures rich in thermodynamically unstable isomers.

c) Photosubstitution reactions

These reactions involve an exchange of ligands on the central metal atom with retention of coordination number. Photochemical substitutions can form different products to those accessible thermally, and occur up to 14 orders of magnitude faster. Substitution generally occurs from ligand-field triplet excited states, and can be achieved by irradiation in the region of ligand-field transitions; for d^6 configurations, this often results in the labilisation of all ligands, with substitution

of one. Photosubstitution is also often induced concurrently with photoredox reactions upon irradiating in the region of charge-transfer transitions.

1.4.3 Photochemistry of Platinum Complexes

The photochemistry of platinum complexes is extensive and varied, with much of the work concerned with the luminescent properties of square planar Pt^{II} complexes, which shall not be discussed here. This section will concentrate on the chemistry of platinum azide complexes, and the photoreduction of Pt^{IV} complexes, due to their relevance to this work.

As discussed in section 1.4.2.2, the fate of a complex upon irradiation is dependent upon the transitions accessible given the energy of the incident light. Lower energy ligand-field transitions can induce photoisomerisation or substitution reactions, whilst ligand-to-metal charge transfer transitions typically result in photoreduction.

c) Platinum Azide Complexes

The photoactivity of the azide (N_3) moiety is well demonstrated in both organic and inorganic compounds,[95] and it has been stated that almost any transition metal azide complex is light sensitive, regardless of oxidation state.[96] Metal azido complexes can undergo a variety of photoreactions,[95] including photosubstitution, photoisomerisation, formation of a nitrido (≡N) complex with a two-electron oxidation of the central metal, or oxidation of the azide anion to a radical with a one-electron reduction of the metal.

An example of the latter reaction, the photoinduced, reductive transelimination of nitrogen from a Pt^{IV} azido complex, was first reported in 1978.[97]

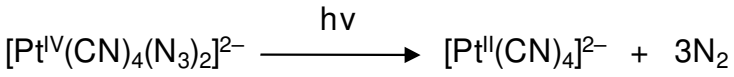

Irradiation into the LMCT ($N_3 \rightarrow Pt$) band was accomplished with UVA light (314 nm), and the elimination reaction was shown to involve the formation of two azide radicals and no Pt^{III} intermediate.

This was followed by reports of successive reductive eliminations from $[Pt(N_3)_6]^{2-}$ In this case, irradiation into the LMCT band induces cleavage of two ligands from the metal in a one-photon, two-electron elimination to yield a Pt^{II} species. Subsequent irradiation of this species induces further elimination and a reduction to Pt^0.[98]

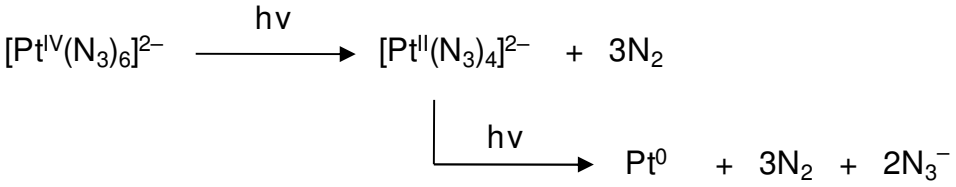

The photoreduction of the Pt^{II} complex *cis*-$[Pt(N_3)_2(PPh_3)_2]$ yields a Pt^0 complex as shown below, and conversion to the *trans* isomer is also seen. It is of interest that this photoreduction occurs at wavelengths above 350 nm, since only ligand-field transitions are present in this region, and these would be expected to give rise to photoisomerisation or substitution products only.[95]

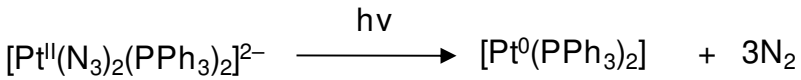

Pt^{II} diazido complexes of α-diimine ligands have also been found to act as efficient photosensitisers in the production of singlet oxygen ($^1O_2$), with the excited states arising from MLCT transitions implicated in the mechanism.[99] The

efficiency was found to be dependent upon the nature of the α-diimine ligand,[100] and quantum yields comparable with haematoporphyrin, a known sensitiser for singlet oxygen.[99]

d) Photoreduction of Pt^{IV} Complexes

The photochemical reduction of Pt^{IV} to Pt^{II} is reasonably well documented, and can show some interesting features. For example, as in the case of $[Pt(PPh_3)_2(N_3)_2]^{2-}$, the photoreduction of $[PtCl_6]^{2-}$ occurs at all wavelengths at which the complex absorbs light, even in regions where only ligand-field transitions are present.[101] The ability to effect reductions at significantly lower energy than would be expected could be of benefit in many applications.

A recent investigation into several Pt^{IV} complexes with bipyridine ligands, such as *trans*-$[Pt(bipy)(MeNH_2)_2Cl_2]Cl_2$, found that such complexes undergo initial hydrolysis of chloride, followed by photoisomerisation and reduction in daylight. This was accompanied by formation of HOCl, presumably arising from the reductive elimination of the axial ligands, and this study served to highlight the importance of considering photochemical reactions of Pt^{IV} complexes when considering any potential applications.[102]

The photochemistry of Pt^{IV} complexes has been exploited in the sensitisation of TiO_2 surfaces. TiO_2 is a known photocatalyst, and modification with $[PtCl_6]^{2-}$ allows for activation with visible wavelengths. The photosensitisation mechanism is believed to involve an electron injection from the photogenerated Pt^{III} intermediate to titanium dioxide, leading to the formation of reactive oxygen species. Cell tests have indicated the platinum-modified TiO_2 is phototoxic to a murine macrophage cell line.[103]

1.5 Photochemistry in Medicine

The use of light in the treatment of disease dates back over 4000 years to the Ancient Egyptians, who combined the ingestion of psoralen-containing plants with exposure to sunlight in the treatment of the skin disorder vitiligo; the same active ingredient is used worldwide today in phototherapy for the treatment of psoriasis.[104] However, the field of modern phototherapy did not begin until the 1960s, with the observation that a porphyrin could be used as a photosensitiser in the destruction of tumour tissue.[105]

The use of light in medicine is an attractive prospect, since site-selective irradiation allows for targeting of the therapeutic effect. However, there are several factors that can limit its application, and must be considered in the design of photoactive drugs.

The wavelengths at which the drug can be activated is perhaps the most important consideration. The use of UV light below 300 nm is not possible, since these wavelengths induce extensive damage to tissues, DNA and proteins. Higher wavelengths are less damaging, but penetration through tissues is poor below around 600 nm, as a result of absorption by biomolecules such as haemoglobin, cytochromes and melanin, and scattering by organelles. Light in the region of 600–1000 nm shows the deepest penetration through tissue[106] (Figure 1.11) and is known as the "therapeutic window"; it is these wavelengths which are most suitable for phototherapy. In addition, the dosage of light required to produce a therapeutic effect must also be taken into account.

There are also practical considerations: whilst irradiation of the skin is easily achievable, other parts of the body are less accessible and this has limited the use of phototherapy to date. However, advances in laser technology have begun to circumvent this problem, and it is now possible to irradiate various parts of the body including the lung, bladder, cervix, colon and oesophagus. Furthermore, the rapid developments in fibre optic technologies in recent years will soon allow

other areas of the body to be reached, and the application of phototherapy to be increased.

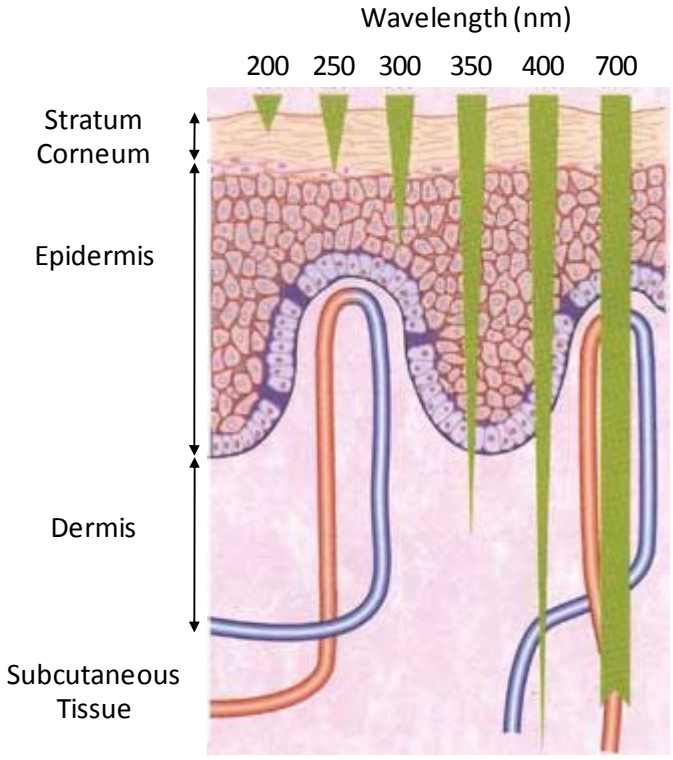

Figure 1.11 The skin penetration depths of different wavelengths of light.[106,107]

1.5.1 Photodynamic Therapy

Photodynamic therapy (PDT) is a treatment involving the selective damage of tissue using a photosensitising drug, light and oxygen. It is currently used in the treatment of accessible cancers including those of the skin, mouth, oesophagus and bladder, as well as several inflammatory skin conditions, and the eye disease age-related macular degeneration.

Following administration of the photosensitiser (intravenously for most cancers and topically for skin conditions), irradiation in the target region with an appropriate wavelength of light excites the photosensitiser to a singlet excited

state. From here, it can undergo intersystem crossing to a triplet state. Relaxation to the ground state is spin-forbidden, favouring the transfer of energy to molecular oxygen. This regenerates the ground state of the photosensitiser and forms singlet oxygen, $^1O_2$, responsible for the cytotoxicity. Although this mechanism is predominant, interactions of the photosensitiser with biomolecules, and subsequent reactions of both can lead to the generation of other reactive oxygen species, such as superoxide anions (O_2^-), superoxide radicals ($O_2^{\bullet}$) and hydroxyl radicals ($OH^{\bullet}$).[105]

Singlet oxygen is a very reactive species that induces cell death *via* rapid and indiscriminate reactions with biomolecules. Its lifetime in aqueous solutions is very low, around 2 μs; it therefore has a very limited spatial range of activity, likely confined to the cell in which it was created, and hence damage to healthy tissue is minimised. Although direct cell effects are the main cause of cell death, research has indicated that a significant proportion also die following irradiation, since an induced shutdown of vasculature deprives them of oxygen and nutrients, and mitochondrially-controlled apoptosis has also been implicated.[105]

The photosensitisers employed are typically porphyrins or porphyrin-like molecules such as chlorins, with a strong absorbance in the visible region and the ability to accumulate preferentially inside tumour cells, and all are very efficient singlet oxygen generators. The first approved photosensitiser, Photofrin®, is a mixture of haematoporphyrin derivatives of varying linkages, lengths and stereochemistries (Figure 1.12), with an absorption maximum around 630 nm, and can be activated to a depth of about 5 mm in tissue. Foscan®, a chlorin derivative, requires a much lower drug and light dose to achieve similar responses to photofrin, and has a shorter retention time in the body.[104,105]

More recently, the lanthanide complex lutetium texaphyrin (Lutrin) has also been approved for use in cervical, prostate and brain tumours, with several other potential new photosensitisers in clinical trials.[108] Other metal complexes, which are phototoxic by a different mechanism to that of photodynamic therapy, are discussed in Section 1.5.2.

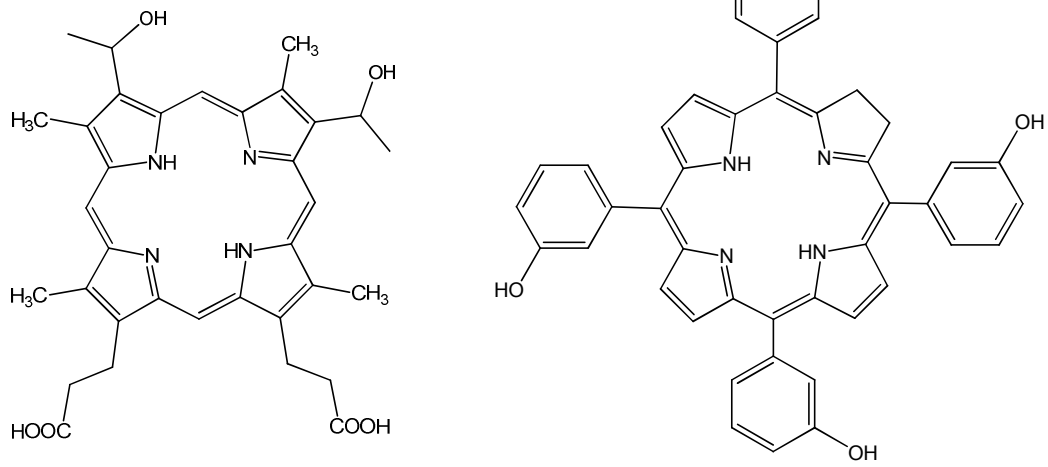

Haematoporphyrin Foscan

Figure 1.12 Two drugs in clinical use for photodynamic therapy.

PDT is non-invasive, and is typically well-tolerated by patients. The targeted treatment also means that the incidence of side effects common to chemotherapy can be minimised.

Figure 1.13 Patients receiving photodynamic therapy. Images courtesy of Dr Sam Eljamel, Ninewells Hospital, Dundee.

However, the disadvantages of PDT include sensitivity to sunlight, which can persist for weeks after treatment, and its reliance on oxygen, since many tumour cells are known to be hypoxic.

1.5.2 Phototoxic Metal Complexes

In the development of metal complexes as potential anticancer agents, one design concept receiving increasing interest in recent years is that of photoactivation.

The complex *cis*-$[Ru(bipy)_2(NH_3)_2]^{2+}$ (bipy = 2,2-bipyridine), upon irradiation with $\lambda < 400$ nm, was found to undergo sequential loss of the ammonia ligands in aqueous solution to form the bis-aqua complex; in the presence of 9-ethylguanine, bisadducts of this species were formed. This complex was also found to be phototoxic to human skin fibroblasts (Hs-27).[109] A dinuclear Ru^{II} arene complex, $[\{(\eta^6\text{-indan})RuCl\}_2(\mu\text{-2,3-dpp})](PF_6)_2$ (2,3-dpp = 2,3-bis(2-pyridyl)pyrazine) was found to undergo indan loss upon irradiation with UVA light in aqueous solution, with an increase in the fluorescence of this arene. DNA binding was also markedly increased upon irradiation, with the formation of both mono- and bifunctional adducts; additionally, the photoreaction appeared independent of oxygen.[110]

The dinuclear rhodium complex *cis*-$[Rh_2(\mu\text{-}O_2CCH_3)_2(dppz)(bipy)]^{2+}$ (dppz = dipyrido[3,2-*a*:2',3'-*c*]phenazine) is one of several rhodium complexes investigated for phototoxicity. This complex shows low toxicity in the dark, but a 79% increase in toxicity upon irradiation with visible light, similar to that of haematoporphyrin, with efficient photocleavage demonstrated upon irradiation.[111]

The group of Chakravarty has investigated the DNA-photocleavage properties of several different metal complexes. A series of copper complexes of the formula [Cu(L-arg)(B)Cl]Cl, where B is a heterocyclic base such as pyridine, were shown to effectively cleave DNA upon irradiation with UVA (365 nm) or red (647.1 nm)

light in a metal-assisted photoexcitation process forming singlet oxygen.[112] Similarly, the vanadium complex $[VOCl(dppz)_2]Cl$[113] also cleaved DNA by a similar mechanism involving singlet oxygen upon irradiation with UVA light, but with near-IR wavelengths ($\geq$ 750 nm), the involvement of only $OH^{\bullet}$ radicals was found. This complex was found to be non-toxic in the dark, but phototoxic upon irradiation with both UVA and visible light, although IC_{50} values were lower for the former. Photoinduced binding to the protein bovine serum albumin was also seen, and implicated in a potential role as an antimetastatic agent. The analogous iron complex,[114] [FeL(B)], (B = dppz, L = a tetradentate *N,O,O,O* phenolate-based ligand) showed photocleavage upon irradiation with red light, also involving $OH^{\bullet}$ radicals, and phototoxicity in the human cervical cancer cell line (HeLa) and human keratinocyte cell line (HaCaT); upon UVA irradiation, IC_{50} values were in the nanomolar range.

1.5.3 Photoactivated Pt^{IV} Complexes

The idea of administering a prodrug which becomes activated upon irradiation has recently been applied to platinum chemotherapy, and could potentially lead to a novel class of photoactivated anticancer agents which do not rely upon the presence of oxygen. Many Pt^{IV} complexes are known to be inert *in vivo* and activated by reduction to Pt^{II}; and it is known that such a reduction can occur photochemically. Therefore, it was hypothesised that a non-toxic, Pt^{IV} prodrug could be designed which, upon site-selective irradiation, could be reduced in the region of the tumour to yield a cytotoxic Pt^{II} species. Since such complexes are a focus of this project, these are discussed in detail below.

Initial studies in this area employed Pt^{IV} complexes containing equatorial iodido ligands[115] (Figure 1.14), since the Pt–I ligand-to-metal charge transfer (LMCT) band is of sufficiently low energy to allow photolysis by visible light. The nature of the axial ligand was found to greatly influence both the photochemistry and the dark stability of the complexes; that with axial chlorido groups being too unstable

in serum for further study. In nucleobase and DNA binding experiments, the complex with axial acetato groups showed no reaction to 5'-GMP in the dark, but formed the bisadduct Pt(en)(5'-GMP)$_2$ upon irradiation;[116] similarly, little DNA platination occurred after 24 the dark, but rose to 60% after 6 h irradiation. The hydroxyl analogue was also photolabile, however the predominant photoproducts were believed to be Pt^{IV} species, and were unreactive to 5'-GMP upon irradiation; the extent of DNA platination was also low (~10%).

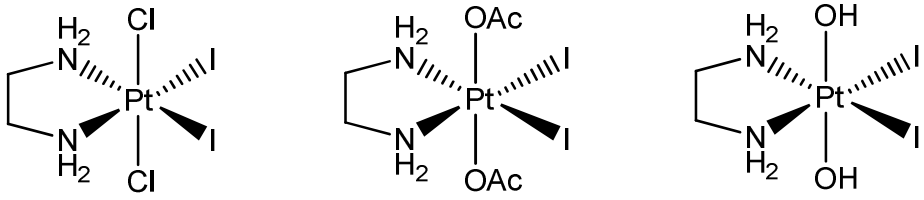

Figure 1.14 Photoactivatable Pt^{IV} prodrugs containing equatorial iodido ligands.

In additional experiments, the hydroxyl analogue was found to react rapidly with glutathione, forming a ring-opened Pt^{II} species *via* initial attack of the thiol on an iodido ligand.[117] Since poor stability towards thiols such as glutathione leads to rapid deactivation of such complexes *in vivo*, these complexes were deemed unsuitable for further study.

It was believed that replacement of the equatorial iodido ligands with a more strongly-binding ligand could produce a more stable Pt^{IV} species, however it was also necessary to retain photoactivity. The pseudo-halogen group azide (N_3) was chosen which, being a nitrogen donor, can form strong bonds to platinum; additionally, the photoactivity of metal-azide complexes is well documented.[118]

Initial studies on the Pt^{IV} azido complexes *cis,cis,trans*-[Pt(NH_3)$_2$(N_3)$_2$(OH)$_2$] and *cis,trans*-[Pt(en)(N_3)$_2$(OH)$_2$] showed them to be remarkably stable in the dark in the presence of glutathione and 5'-GMP, with no observable reactions over a

period of many weeks. Upon irradiation with visible light (457.9 nm), however, rapid binding to the N7 atoms of 5'-GMP and d(GpG) was observed.[119] Subsequent transcription mapping studies of plasmid DNA treated with *cis,trans*-[Pt(en)$(N_3)_2(OH)_2$] and visible light revealed platination sites similar to those of cisplatin, occurring mainly at GG sequences; HPLC analysis of a 40-bp DNA duplex treated with the complex also found preferential formation of GG cross-links.[120]

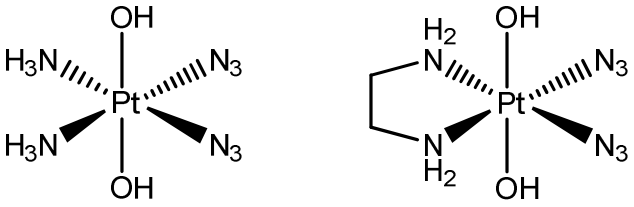

Figure 1.15 The structures of two photoactivatable Pt^{IV} azido complexes

However, cell morphology studies suggested these complexes may have a different mode of action to drugs such as cisplatin.[121] *Cis,cis,trans*-[Pt$(NH_3)(N_3)_2(OH)_2$] and *cis,trans*-[Pt(en)$(N_3)_2(OH)_2$] were both found to show negligible toxicity in the dark, but were phototoxic to both the 5637 and 5637 cisplatin-resistant human bladder cancer cell lines upon irradiation with UVA light (365 nm). Morphology studies showed that, in contrast to cisplatin, treated cells showed "ballooning" after 6 h irradiation, and 17 h after the irradiation period cellular shrinkage and loss of contact with neighbours was observed, as well as significant nuclear packing. After 90 h, cells were shrunken and most lacked a nucleus. These results were markedly different from those of cisplatin treated cells, and not fully consistent with an apoptotic pathway of cell death.

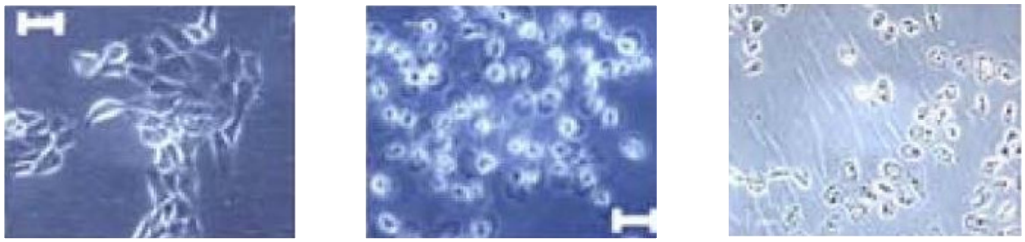

Figure 1.16 Phase contrast microscopy images of 5367 bladder cancer cells following exposure to *cis,cis,trans*-$[Pt(NH_3)(N_3)_2(OH)_2]$. From reference 121.

An interesting discovery was that complexes with the azide ligands in a *trans* geometry appear to show higher activity than their *cis* analogues, which is surprising since the *cis* complexes could be regarded as a prodrug for cisplatin, and the *trans* complexes would presumably be unable to form 1,2-d(GpG) cross-links with DNA. Nevertheless, irradiation studies of *trans,trans,trans*-$[Pt(NH_3)_2(N_3)_2(OH)_2]$ in the presence of 5'-GMP showed rapid formation of the bisadduct *trans*-$[Pt(NH_3)_2(5'\text{-GMP-N7})_2]^{2+}$, and phototoxicity tests revealed this complex to be as cytotoxic as cisplatin upon irradiation with UVA light, whilst non-toxic in the dark.[122] A range of trans-azido complexes has since been synthesised and shown good phototoxicity,[123,124] with one in particular, *trans,trans,trans*-$[Pt(NH_3)(py)(N_3)_2(OH)_2]$ (py = pyridine), showing cytotoxicity between 13 and 80 times greater than cisplatin upon irradiation, dependent upon cell line.[123] This complex appears to have a novel mechanism of action, forming *trans* azido/guanine and *trans* diguanine Pt^{II} adducts; both intrastrand and interstrand, and DNA–protein, cross-links were detected. DNA damage was found to be different from that induced by cisplatin or transplatin, and repair synthesis also markedly lower.

Work is continuing to elucidate the mechanism of action of these Pt^{IV} azido complexes and their degradation pathways upon irradiation. A reductive elimination was initially proposed, in which the two azido ligands leave as radicals and rapidly combine to form molecular nitrogen, resulting in cytotoxic Pt^{II} species. However, recent experiments have suggested this is an oversimplification, with photoproducts highly dependent upon solvent and pH. Various photoproducts have been detected upon UVA irradiation of *cis,cis,trans*-$[Pt(^{15}NH_3)_2(N_3)_2(OH)_2]$, including N_2, N_3^-, $^{15}NH_3$, unlabelled NH_3 (presumably arising from N_3), and O_2, as well as Pt^{IV} photoisomerisation products, several Pt^{II} species, and an insoluble precipitate thought to be a polymeric hydroxo-/oxo bridged platinum species; nitrene intermediates have also been implicated.[125] Rapid photoreductions have been found in the presence of biomolecules; for example, during the irradiation of *trans,trans,trans*-$[Pt(NH_3)_2(N_3)_2(OH)_2]$ in the presence of 5'-GMP, the bisadduct *trans*-$[Pt(NH_3)_2(5'\text{-GMP-N7})_2]^{2+}$ was detected after only one minute.[122.126] However, irradiation studies of *cis,cis,trans*-$[Pt(NH_3)_2(N_3)_2(OH)_2]$ with 1-methylimidazole, in a 1:1 ratio, gave rise to a number of photoproducts, including, surprisingly, the tetrasubstituted product $[Pt(1\text{-methylimidazole})_4]^{2+}$.[127]

1.6 The Aims of this Work

The general aims of this work were to further investigate the chemistry of platinum azido complexes as potential photoactivatable anticancer agents, in particular to explore routes to their functionalisation and for shifting the wavelength of activation further into the visible region.

The functionalisation of cytotoxic complexes with bioactive ligands, such as a fluorescent probe or a cancer-cell targeting species, could aid elucidation of their mechanism of action or improve specificity for cancer cells. Therefore one aim of this work was to develop platinum azido complexes with functional groups to

which bioactive ligands could be attached, and to investigate the attachment of such species to these complexes.

The ideal wavelengths of activation for a photoactivatable drug are between 700–1000 nm, the region in which light can penetrate deepest into tissue, however the Pt^{IV} azido complexes currently studied absorb in the UV region. A further aim was to investigate the incorporation of ligands absorbing strongly in the visible region, which may allow the possibility of activation upon irradiation in this region, and lead to novel photochemical pathways.

1.7 References

[1] Z. Guo and P. J. Sadler, *Angew. Chem. Int. Ed.*, 1999, **38**, 1512.

[2] R. Huang, A. Wallqvist and D. G. Covell, *Biochem. Pharmacol.*, 2005, **69**, 1009.

[3] B. Merchant, *Biologicals*, 1998, **26**, 49.

[4] A. Gupta and S. Silver, *Nat. Biotechnol.*, 1998, **16**, 888.

[5] G. F. Baxter, *Chem. Br.*, 1992, **28**, 445.

[6] R. Y. Keers, *Thorax*, 1980, **35**, 884.

[7] B. Rosenberg, L. van Camp, J. E. Trosko and V. H. Mansour, *Nature*, 1969, **222**, 385.

[8] M. Schaefer, *Met. Based Drugs.*, 1997, **4**, 159.

[9] K. H. Thompson, J. H. McNeill and C. Orvig, *Chem. Rev.*, 1999, **99**, 2561.

[10] F. Caruso and M. Rossi, *Met. Ions. Biol. Syst.*, 2004, **42**, 353.

[11] S. J. Dougan and P. J. Sadler, *Chimia*, 2007, **61**, 704.

[12] A. V. Rudnev, L. S. Foteeva, C. Kowol, R. Berger, M. A. Jakupec, V. B. Arion, A. R. Timerbaev and B. K. Keppler, *J. Inorg. Biochem*., 2006, **100**, 1819.

[13] S. J. Berners-Price and A. Filipovska, *Aust. J. Chem*., 2008, **61**, 66.

[14] D. Hanahan and R. A. Weinberg, *Cell*, 2000, **100**, 57.

[15] A. L. Thomas, R. A. Sharma and W. P. Steward, in *The Molecular Biology of Cancer*, ed. M. Khan and S. Pelengaris, Blackwell, Oxford, UK, 2007, ch. 16, pp 444–463.

[16] C. X. Zhang, S. J. Lippard, *Curr. Opin. Chem. Biol*., 2003, **7**, 481.

[17] B. Rosenberg, L. van Camp and T. Krigas, *Nature*, 1965, **205**, 698.

[18] C. F. J. Barnard, *Plat. Met. Rev.,* 1989, **33**, 162.

[19] P. J. O'Dwyer, J. P. Stevenson and S. W. Johnson, in *Cisplatin: Chemistry and Biochemistry of a Leading Anticancer Drug*, ed. B. Lippert, Wiley, Weinheim, Germany, 1999, ch.2, pp 31–73.

[20] S. P. Binks, M. Dobrota, *Biochem. Pharmacol.*, 1990, **40**, 1329.

[21] F. Arnesano and G. Natile, *Coord. Chem. Rev.*, 2009, **253**, 2070.

[22] C. A. Larson, B. G. Blair, R. Safaei and S. B. Howell, *Mol. Pharmacol.*, 2009, **75**, 324.

[23] D. Sinani, D. J. Adle, H. Kim and J. Lee, *J. Biol. Chem.*, 2007, **282**, 26775.

[24] F.Arnesano, S. Scintilla and G. Natile, *Angew. Chem. Int. Ed.*, 2007, **46**, 9062.

[25] Y. Jung and S. J. Lippard, *Chem. Rev.*, 2007, **107**, 1387.

[26] D. P. Bancroft, C. A. Lepre and S. J. Lippard, *J. Am. Chem. Soc.*, 1990, **112**, 6860.

[27] J. Reedijk, *Plat. Met. Rev.*, 2008, **52**, 2.

[28] M. Kartalou and J. M. Essigmann, *Mutat. Res.*, 2001, **478**, 1.

[29] A. Galasko and S. J. Lippard, *Biochemistry.*, 1998, **37**, 9230.

[30] U.-M. Ohndorf, M. A. Rould, W. He, C. O. Pabo and S. J. Lippard, *Nature*, 1999, **399**, 708.

[31] D. Wang and S. J. Lippard, *Nat. Rev. Drug. Discov.*, 2005, **4**, 307.

[32] T. Boulikas, A. Pantos, E. Bellis and P. Christofis, *Cancer Ther.*, 2007, **5**, 537.

[33] G. Natarajan, R. Malathi and E. Holler, *Biochem. Pharmacol.*, 1998, **58**, 1625.

[34] M. Pavelka, M. F. A. Lucas and N. Russo, *Chem. Eur. J.*, 2007, **13**, 10108.

[35] U. Frey, J. D. Ranford and P. J. Sadler, *Inorg. Chem.*, 1993, **32**, 1333.

[36] M. A. Jakupec, M. Galanski, B. K. Keppler, H. G. Koch, M. Muller, B. C. Burckhardt and G. Burckhardt, *Rev. Physiol. Biochem. Pharmacol.*, 2003, **146**, 1.

[37] J. Graham, M. Muhsin and P. Kirkpatrick, *Nat. Rev. Drug Discov.*, 2004, **3**, 11.

[38] S. Zhang, K. S. Lovejoy, J. E. Shima, L L. Lagpacan, Y. Shu, A. Lapuk, Y. Chen, T. Komori, J. W. Gray, X. Chen and S. J. Lippard and K. M. Giacomini, *Cancer Res.*, 2006, **66**, 8847.

[39] M. Ita, M. Okafuji, K. Fukada, K. Mitsuoka, T. Hanakita and Y. Hayatsu, *Oral Oncol*., 2003, **39**, 144.

[40] B. K. Keppler, *Rev. Physiol. Biochem. Pharmacol*., 2003, **146**, 1.

[41] J.-H. Ahn, Y.-K. Kang, T.-W. Kim, H. Bahng, H.-M.Chang, W.-C. Kang,W. K. Kim, J.-S. Lee, and J.-S. Park, *Cancer Chemother. Pharmacol*., 2002, **50**, 104.

[42] S. W. Johnson, K. V. Ferry and T. C. Hamilton, *Drug Res. Updates*, 1998, **1**, 243.

[43] M. D. Hall, M. Okabe, D.-W. Shen, X.-J. Liang and M. M. Gottesman *Annu. Rev. Pharmacol. Toxicol*. 2008, **48**, 495.

[44] F. Yu, J. Megyesi and P. M. Price, *Am. J. Physiol. Renal Physiol*., 2008, **295**, F44.

[45] A. K. Godwin, A. Meister, P. J. O'Dwyer, C. S. Huang, T. C. Hamilton and M. E. Anderson, *Proc. Natl. Acad. Sci. U. S. A.,* 1992, **89**, 3070.

[46] P. Mistry, S. Y. Loh, L. R. Kelland and K. R. Harrap, *Int. J. Cancer,* 1993, **55**, 848.

[47] Y. Kasherman, S. Sturup and D. Gibson, *J. Med. Chem*., 2009, **52**, 4319.

[48] M. Knipp, *Curr. Med. Chem*., 2009, **16**, 522.

[49] A. M. Pizarro and P. J. Sadler, in *Nucleic Acid-Metal Ion Interactions*, ed. N. V. Hud, Royal Society of Chemistry, Cambridge, England, 2008, ch. 10, pp 350–398.

[50] E. R. Jamieson and S. J. Lippard, *Chem. Rev.*, 1999, **99**, 2467.

[51] M. J. Cleare and J. D. Hoeschele, *Bioinorg. Chem*., 1973, **2**, 187.

[52] Y. Chen, Z. Guo, S. Parsons and P. J. Sadler, *Chem. Eur. J.*, 1998, **4**, 672.

[53] Y. Chen, Z, Guo, J. A. Parkinson and P. J. Sadler, *J. Chem. Soc. Dalton Trans*., 1998, 3577.

[54] Y. Chen, J. A. Parkinson, Z. Guo, T. Brown and P. J. Sadler, *Angew. Chem. Int. Ed.*, 1999, **38**, 13.

[55] J. Holford, S. Y. Sharp, B. A. Murrer, M. Abrams and L. R. Kelland, *Br. J. Cancer*, 1998, **77**, 366.

[56] B. Rosenberg, *Plat. Met. Rev*., 1971, **15**, 42.

[57] O. Novakova, J. Kasparkova, J. Malina, G. Natile, and V. Brabec, *Nucleic Acids Res.*, 2003, **31**, 6450.

[58] C. Alvheim, N. Frøystein, J. Vinje, F. P. Intini, G. Natile, Y. Liu, R. Huang and E. Sletten, *Inorg. Chim. Acta*, 2009, **362**, 907.

[59] F. P. Intini, A. Boccarelli, V. C. Francia, C. Pacifico, M. F. Sivo, G. Natile, G. Giordano, P. De Rinaldis, M. Coluccia, *J. Biol. Inorg. Chem.*, 2004, **9**, 768.

[60] E. I. Montero, J. M. Perez, A. Schwartz, M. A. Fuertes, J. M. Malinge, C. Alonso, M. Leng, and C. Navarro-Ranninger, *ChemBioChem*, 2002, **3**, 61.

[61] L. Cubo, A. G. Quiroga, J. Zhang, D. S. Thomas, A. Carnero, C. Navarro-Ranninger and S. J. Berners-Price, *Dalton Trans.*, 2009, 3457.

[62] R. M. Medina, J. Rodriguez, A. G. Quiroga, F. J. Ramos-Lima, V. Moneo, A. Carnero, C. Navarro-Ranninger and M. J. Macazaga, *Chemistry & Biodiversity*, 2008, **5**, 2090.

[63] S. M. Aris and N. P. Farrell, *Eur. J. Inorg. Chem.*, 2009, **10**, 1293.

[64] A. G. Quiroga, J. M. Perez, C. Alonso, C. Navarro-Ranninger and N. P. Farrell, *J. Med. Chem*., 2006, **49**, 224.

[65] J. Kašpárková, J. Zehnulova, N. P. Farrell and V. Brabec, *J. Biol. Chem.*, 2002, **277**, 48076.

[66] N. J. Wheate and J. G. Collins, *Coord. Chem. Rev*., 2003, **243**, 133.

[67] J. D. Roberts, J. Peroutka and N. Farrell, *J. Inorg. Biochem*., 1999, **77**, 51.

[68] G. Pratesi, P. Perego, D. Polizzi, S. C. Righetti, R. Supino, C. Caserini, C. Manzotti, F. C. Giuliani, G. Pezzoni, S. Tognella, S. Spinelli, N. Farrell and F. Zunino, *Br. J. Cancer*, 1999, **80**, 1912.

[69] S. Komeda, T. Moulaei, K. Kruger Woods, M. Chikuma, N. P. Farrell and L. Dean Williams., *J. Am. Chem. Soc.*, 2006, **128**, 16092.

[70] A. L. Harris, X. Yang, A. Hegmans, L. Povrik, J. J. Ryan, L. R. Kelland and N. P. Farrell, *Inorg. Chem.*, 2005, **44**, 9598.

[71] Although the terms “axial” and “equatorial” ligands are not strictly relevant for octahedral complexes, the convention in literature is to refer to the two ligands lying above and below the plane of the amine ligands as “axial”, and this terminology shall be used in this work.

[72] M. D. Hall and T. W. Hambley, *Coord. Chem. Rev.*, 2002, **232**, 49.

[73] L. T. Ellis, H. Er and T. W. Hambley, *Aust. J. Chem*., 1995, **48**, 793.

[74] S. Choi, C. Filotto, M. Bisanzo, S. Delaney, D. Lagasee and J. L. Whitworth, *Inorg. Chem*., 1998, **37**, 2500.

[75] M. D. Hall, G. J. Foran, M. Zhang, P. J. Beale and T W Hambley, *J. Am. Chem. Soc.*, 2003, **125**, 7274.

[76] S. G. Chaney, S. Wyrick and G. K. Till, *Cancer Res.*, 1990, **50**, 4539.

[77] L. R. Kelland, *Exp. Opin. Invest. Drugs*, 2000, **9**, 1373.

[78] J. L. Carr, M. D. Tingle and M. J. McKeage, *Cancer Chemother*.

Pharmacol., 2002, **50**, 9.

[79] P. Wardman, *J. Phys. Chem. Ref. Data*, 1989, **18**, 1637.

[80] A. Rahman, J. K. Roh, M. K. Wolpert-DeFilippes, A. Goldin, J. M. Venditti and P. V. Woolley, *Cancer Res.*, 1988, **48**, 1745.

[81] H. Choy, C. Park and M. Yao, *Cancer Ther*., 2008, **5**, 563.

[82] E. Volckova1, E. Weaver and R. N. Bose, *Eur. J. Med. Chem.*, 2008, **43**, 1081.

[83] M. R. Reithofer, A. Schwarzinger, S. M. Valiahdi, M. Galanski, M. A. Jakupec and B. K. Keppler, *J. Inorg. Biochem.*, 2008, **102**, 2072.

[84] K. J. Haxton and H. M. Burt, *J. Pharm. Sci*, 2009, **98**, 2299.

[85] Y. Zhen, X. Wang, H. Diao, J. Zhang, H. Li, H. Sun and Z. Guo, *Chem. Commun.*, 2007, 3453.

[86] C. Xu, B. Wang and S. Sun, *J. Am. Chem. Soc.*, 2009, **131**, 4216.

[87] R. Guddneppanavar, G. Saluta, G. L. Kucera and U. Bierbach, *J. Med. Chem.,* 2006, **49**, 3204.

[88] H. Bertrand, S. Bombard, D. Monchaud and M.-P. Teulade-Fichou, *J. Biol. Inorg. Chem*., 2007, **12**, 1003.

[89] M. J. McKeage and V. Murray, *J. Inorg. Biochem*., 2001, **85**, 209.

[90] K. R. Barnes, A. Kutikov and S. J.Lippard, *Chem. Biol.*, 2004, **11**, 557.

[91] W. H. Ang, I. Khalaila, C. S. Allardyce, L. Juillerat-Jeanneret and P. J. Dyson, *J. Am. Chem. Soc.*, 2005, **127**, 1382.

[92] J. Sykora and J. Šima, *Coord. Chem. Rev*., 1990, **107**, 1.

[93] D. F. Shriver and P. W. Atkins, *Inorganic Chemistry*, Oxford University Press, Oxford, 3rd edn, 2002.

[94] C. E. Wayne and R. P. Wayne, *Photochemistry*, Oxford University Press,

Oxford, 1996.

[95] J. Šima, *Coord. Chem. Rev*., 2006, **250**, 2325.

[96] A. Vogler, C. Quett and H. Kunkely, *Ber. Bunsen-Ges. Phys. Chem.,* 1988, **92**, 1486.

[97] A. Vogler, A. Kern and J. Huttermann, *Angew. Chem. Int. Ed. Engl.*, 1978, **7**, 524.

[98] A. Vogler and J. Hlavatsch, *Angew. Chem. Ind. Ed. Engl*., 1983, **22**, 154.

[99] V. Anbalagan, *J. Coord. Chem.*, 2003, **56**, 161.

[100] S. S. Kamath and T. S. Srivastava, *J. Photochem. Photobiol. A*., 1990, **52**, 83.

[101] R. E. Cameron and A. B. Bocarsly, *Inorg. Chem.*, 1986, **25**, 2910.

[102] Y. Nakabayashi, A. Erxleben, U. Letinois, G. Pratviel, B. Meunier, L. Holland and B. Lippert, *Chem. Eur. J.*, 2007, **13**, 3980.

[103] A. Janczyk, A. Wolnicka-Głubisz, K. Urbanska, G. Stochel and W. Macyk, *J. Photochem. Photobiol. B.*, 2008, **92**, 54.

[104] L. B. Josefsen and R. W. Boyle, *Metal-Based Drugs*, 2008, 1.

[105] I. J. Macdonald and T. J. Dougherty, *J. Porphyrins Phthalocyanines*, 2001, **5**, 105.

[106] S. Wan, J. A. Parrish, R. R. Anderson and M. Madden, *Photochem. Photobiol.*, 1981, **34**, 679.

[107] The Amjo Corporation, www.lightsforhealth.com, accessed August 2009.

[108] N. J. Farrer and P. J. Sadler, *Aust. J. Chem*., 2008, **61**, 669.

[109] T. N. Singh and C. Turro, *Inorg. Chem*., 2004, **43**, 7260.

[110] S. W. Magennis, A. Habtemariam, O. Novakova, J. B. Henry, S. Meier, S. Parsons, I. D. H. Oswald, V. Brabec and P. J. Sadler, *Inorg. Chem.*, 2007,

46, 5059.

[111] A. M. Angeles-Boza, P. M. Bradley, P. K.-L. Fu, M. Shatruk, M. G. Hilfiger, K. R. Dunbar, and C. Turro, *Inorg. Chem.*, 2005, **44**, 7262.

[112] A. K. Patra, T. Bhowmick, S. Roy, S. Ramakumar and A. R. Chakravarty, *Inorg. Chem.,* 2009, **48**, 2932.

[113] P. K. Sasmal, S. Saha, R. Majumdar, R. R. Digheb and A. R. Chakravarty *Chem. Commun.*, 2009, 1703–1705.

[114] S. Saha, R. Majumdar, M. Roy, R. R. Dighe and A. R. Chakravarty*, Inorg. Chem.,* 2009, **48**, 2652.

[115] N. A. Kratochwil, M. Zabel, K.-J. Range and P. J. Bednarski, *J. Med. Chem*., 1996, **39**, 2499.

[116] N. A. Kratochwil, J. A. Parkinson, P. J. Bednarksi and P. J. Sadler, *Angew. Chem. Int. Ed*., 1999, **38**, 1460.

[117] N. A. Kratochwil, Z. Guo, P. del Socorro Murdoch, J. A. Parkinson, P. J. Bednarski and P. J. Sadler, *J. Am. Chem. Soc*., 1998, **120**, 8253.

[118] J. Sima, *Coord. Chem. Rev.*, 2006, **250**, 2325.

[119] P. Müller, B. Schröder, J. A. Parkinson, N. A. Kratochwil, R. A. Coxall, A. Parkin, S. Parsons and P. J. Sadler, *Angew. Chem. Int. Ed*., 2003, **42**, 335.

[120] J. Kašpárková, F. S. Mackay, V. Brabec and P. J. Sadler, *J. Biol. Inorg. Chem*, 2003, **8**, 741.

[121] P. J. Bednarski, R. Grunert, M. Zielzki, A. Wellner, F. S. Mackay and P. J. Sadler, *Chem. Biol.*, 2006, **13**, 61.

[122] F. S. Mackay, J. A. Woods, H. Moseley, J. Ferguson, A. Dawson, S. Parsons and P. J. Sadler, *Chem. Eur. J*., 2006, **12**, 3155.

[123] F. S. Mackay, J. A. Woods, P. Heringova, J. Kašpárková, A. M. Pizarro, S.

A. Moggach, S. Parsons, V. Brabec and P. J. Sadler, *Proc. Natl. Acad. Sci. U.S.A.*, 2007, **104**, 20743.

[124] F. S. Mackay, S. A. Moggach, A. Collins, S. Parsons and P. J. Sadler, *Inorg. Chim. Acta.*, 2009, **362**, 811.

[125] L. Ronconi and P. J. Sadler, *Chem. Commun*., 2008, 235.

[126] F. S. Mackay, Ph.D. Thesis, The University of Edinburgh, 2006.

[127] H. I. A. Phillips, L. Ronconi and P. J. Sadler, *Chem. Eur. J*., 2009, **15**, 1588.

Chapter 2

Experimental Methods

This chapter describes the main experimental methods used in this work. Details relating to individual experiments can be found in subsequent chapters where relevant.

2.1 Nuclear Magnetic Resonance (NMR) Spectroscopy[1,2,3]

NMR spectroscopy is among the most powerful tools available for the structural determination of compounds. ^{1}H NMR was routinely used in this work to characterise the compounds synthesised, to investigate their stability over time, and to follow reactions in solution. The following paragraphs give a background to the technique and the NMR methods used in this work.

2.1.1 Overview of Technique

Certain nuclei possess spin, a property related to the number of unpaired protons and neutrons within the nucleus. This is characterised by the nuclear spin quantum number I, which can take integer and half-integer values. Spin-½ nuclei are the most favourable for NMR observation; those for which $I = 0$ have no overall spin and are NMR silent, and nuclei for which $I > ½$, termed quadrupolar nuclei, can give unfavourable spectra and are less commonly studied.

Nuclei possessing spin have associated with them a weak magnetic field. When placed in an external field (B_0), they begin to precess about the axis of this field, known as Larmor precession. This occurs at the Larmor frequency (ν), which is proportional to the strength of the applied field with proportionality constant γ, the magnetogyric ratio. This is characteristic to each nucleus, and an indication of how "strongly magnetic" the particular nucleus is.

A nucleus of spin I can adopt $2I+1$ orientations, which are degenerate in the absence of an external magnetic field. When such a field is applied the degeneracy is removed, hence a spin-½ nucleus can align in two ways, parallel (α) or

antiparallel (β) to the external field, with the former of slightly lower energy. Application of electromagnetic radiation at the appropriate energy (the Larmor frequency) can induce excitation of the lower energy state to the higher; this is nuclear magnetic resonance.

Considering nuclei in bulk, a slight excess of spins will be present in the low energy orientation, resulting in a bulk magnetisation vector, **M**, along the +*z* axis, parallel to the applied field. The application of a second field, B_1, at the Larmor frequency rotates the magnetisation away from the +*z* axis; in the case of a 90° pulse, which equalises the population of the α and β states, it is rotated into the *x*-*y* plane, generating an oscillating voltage in the transmitter coil. As the magnetisation gradually returns to the +*z* axis (the equilibrium state) by the process of relaxation, the oscillating voltage decays producing the free induction decay (FID), which is then subject to a Fourier analysis to obtain an NMR spectrum.

2.1.2 Chemical Shift

The electron cloud surrounding the nucleus will also circulate in the applied field, generating a small field of its own which acts in opposition. This shields the nucleus to some extent from the applied field, changing the rate of precession and the frequency required to induce resonance. Differences in chemical environment and thus electron cloud density will provide different levels of shielding, hence resonance will be induced at different frequencies. This variation in frequency is known as the chemical shift, with symbol δ and units of ppm.

2.1.3 Resonance Intensities

The intensity of a peak (the total area beneath it, obtained by integration) is proportional to the number of protons giving rise to it. Although the accuracy is generally low, and can vary between resonances in the spectrum, it is usually

sufficient to compare ratios and determine the number of protons giving rise to each particular signal, and for this reason is also of use in structure determination.

2.1.4 Spin-spin Coupling

The small magnetic field influencing a nucleus will also affect the electrons in the bond; thus the orientation of one nucleus can be relayed to another through chemical bonds. The two possible orientations of a ^{1}H nucleus will result in two slightly different local fields at another, so resonance occurs at two different frequencies. The signal is split into a doublet, with the frequency difference between the two lines known as the coupling constant, *J*. Multiplicities resulting from coupling reflect the 2n*I*+1 rule; for spin-½ nuclei, the relative intensities of the lines are given by the coefficients of Pascal's triangle. Coupling is generally seen over two or three bonds (geminal and vicinal coupling respectively), although certain factors can increase the magnitude of coupling over a longer range. Protons that are equivalent will show no coupling to each other. Coupling thus aids assignment of peaks in the NMR spectrum by indicating which nuclei are joined by chemical bonds.

As well as to each other, protons can also show coupling to other NMR-active nuclei close in the bonding network. Since ^{13}C is only 1.1% abundant, ^{13}C–^{1}H couplings are rarely apparent in ^{1}H NMR spectra, although ^{13}C satellites can be seen on either side of strong peaks, each comprising 0.5% of the total peak intensity. In this work, $^{3}J(^{195}Pt–^{1}H)$ couplings were often observed in ^{1}H NMR spectra, since this NMR active isotope of platinum, ^{195}Pt, is 33.8% abundant. In Pt^{II} complexes, these satellites are often significantly broadened by chemical shift anisotropy relaxation, although are sharper in the more symmetrical, octahedral Pt^{IV} complexes.[4] The geometry change also accounts for the reduced magnitude of coupling constants seen in Pt^{IV} complexes compared with Pt^{II} (ratio around 1 : 1.5), attributed to a decrease in *s* character of the resulting hybridised orbitals.[5]

2.1.5 Water Suppression

The spectra of many samples in this work were recorded in aqueous solutions in order to be of biological relevance. In certain cases 90% H_2O/10% D_2O was chosen over 100% D_2O; this allows for peaks of exchangeable protons (such as those of amines and hydroxyl groups) to be seen. In such cases, a large HOD peak dominates the spectrum and requires suppression. Two main techniques can be used to achieve this. Presaturation uses a weak, continuous wave at the water frequency during the relaxation delay, so as to saturate the water resonance; however, exchangeable protons may also be saturated by this method.[6] Other techniques involve the use of magnetic field gradients, such as Excitation Sculpting (also known as Double Pulsed Field Gradient Spin Echo (DPFGSE) or Shaka water suppression).[7] However, in this case, signals close to the water peak can also be suppressed and therefore reduced in intensity.

2.1.6 ^{13}C NMR

^{13}C NMR is routinely used for the characterisation of organic compounds, despite the low natural abundance (1.1%) and poor sensitivity of the nucleus. Spectra are typically recorded with broadband decoupling of protons to remove ^{13}C–^{1}H splittings; this results in a simplification of the spectrum so that a single line is observed for each chemically distinct carbon. Unlike in ^{1}H NMR, the integral of a peak is not generally proportional to the number of carbons contributing to it, so signals cannot be reliably integrated. Signal strength can be enhanced by the use of experiments such as Polarisation ENhancement During Attached Nucleus Testing (PENDANT),[6] in which polarisation transfer from ^{1}H to ^{13}C is employed. In these experiments, the pulse sequences are designed such that signals display positive or negative intensities depending upon the number of protons directly attached to the carbon, to aid in the assignment of the spectrum.

2.1.7 Two-dimensional Techniques

Two-dimensional NMR techniques involve the addition of a second frequency axis and give information on how spins are related in a molecule. Homonuclear (^{1}H–^{1}H) or heteronuclear (for example ^{13}C–^{1}H) correlation experiments can be performed.

COrrelation SpectroscopY (COSY) is a homonuclear experiment, allowing two or three bond couplings to be identified. Following application of a 90° pulse and a delay, a second 90° pulse is applied to transfer magnetisation partially from one spin to its *J*-coupled partner. During the following time delay (known as mixing time), magnetisation evolves partially with the frequency of the second nucleus. A plot of the two frequency axes reveals cross peaks, indicating which nuclei have exchanged magnetisation during the experiment and hence which are *J*-coupled to each other.

Nuclear Overhauser Effect SpectroscopY (NOESY) exploits the transfer of magnetisation from one spin to another close in space through dipolar interactions, upon irradiation at the resonant frequency of one of them. This homonuclear ^{1}H–^{1}H experiment consists of three 90° pulses; during the delay between the second and third, magnetisation is transferred between neighbouring spins *via* the NOE. This allows for the identification of protons that are spatially close, which is of great importance in structural elucidation of proteins or other molecules with stereochemical differences.

Heteronuclear Multiple Quantum Coherence (HMQC) is a two-dimensional, heteronuclear inverse detection experiment correlating, in this case, ^{13}C and ^{1}H resonances by the *J*-coupling interactions between them. As with the experiments described previously, these are observed as cross peaks on a two-dimensional spectrum. HMQC is selective for direct, $^{1}J(^{13}\text{C}–^{1}\text{H})$ couplings, so correlates protons only with the carbons to which they are directly bound. Since this experiment relies on inverse detection, quaternary carbons, to which no protons

are bound, are invisible to this technique. These experiments aid in the complete assignment of ^{1}H and ^{13}C signals.

2.1.8 Experimental

NMR spectra were recorded on the following Bruker Spectrometers: DMX 500 MHz, DPX 360 MHz or AV 800 MHz (University of Edinburgh), and DPX 400 MHz, AV 400 MHz or DRX 500 MHz (University of Warwick). 1D and 2D spectra were recorded using standard Bruker pulse sequences modified by Dr Juraj Bella or Dr Dusan Uhrin (University of Edinburgh), and Dr Adam Clarke or Dr Ivan Prokes (University of Warwick). Unless otherwise stated, spectra were acquired in 5 mm quartz NMR tubes at 298 K. ^{1}H chemical shifts were referenced to residual protio-solvent resonances:[8] δ = 7.26 (chloroform), 2.50 (DMSO), 3.31 (methanol) and 2.92 (DMF). For D_2O and H_2O/D_2O solutions, 0.7–4 μL of a 1% dioxane solution was added as an internal calibrant (δ = 3.75). Spectral data were processed using either XWIN-NMR (Version 2.0 or 3.6, Bruker UK Ltd) or MestReC (Version 4.9.9.9, Mestrelab Research, Spain).

2.2 Ultraviolet-Visible (UV-Vis) Spectroscopy

As a more detailed discussion of the theory behind UV-Vis spectroscopy can be found in Chapter 1, this section describes only the methods and instrumentation used. Further details of individual experiments can be found in the appropriate Chapters.

Spectra were acquired on a Varian Cary 300 spectrophotometer with a Cary temperature controller; the temperature was set to 298 K or 313 K depending on the experiment. Spectra were recorded from 800–210 nm, at 1 nm intervals at a rate of 420 nm/min. Hellma® self-masking, black walled quartz cuvettes (1 cm pathlength, 0.7 mL volume) were used for standard absorption measurements;

transparent cuvettes were used for irradiation studies as described in section 2.3. HPLC grade methanol, UV grade dioxane or deionised water were used as solvents. Spectra were processed using Varian Cary WinUV software (Version 3.00, Varian Inc., USA).

Molar extinction coefficients (ε) were calculated according to the Beer-Lambert law, $A = \varepsilon cl$. For a given compound, spectra at five different concentrations were obtained, and for each absorption band the resulting plot of absorbance at λ_{max} against concentration is linear; the value of ε is obtained by calculating the gradient of the line.

2.3 Irradiation Studies

The majority of the irradiation studies, using both UVA and visible light, were carried out using a photoreactor designed for drug photostability testing (Figure 2.1, A). Additionally, Light Emitting Diodes (LEDs) were also used for the irradiation of certain complexes. All irradiations were carried out in either 5 mm precision grade NMR tubes or Hellma® transparent UV quartz cuvettes (1 cm pathlength, 3.5 mL volume).

2.3.1 Photoreactor

UV irradiations were performed using a Luzchem LZC-ICH2 photoreactor equipped with 16 LZC-UVA lamps (Hitachi), delivering almost pure (>95%) UVA light centred at 365 nm (Figure 2.1, B). Typically only four lamps were used during each experiment to give power levels in the range of 1.7–2.2 mW cm^{-2}.

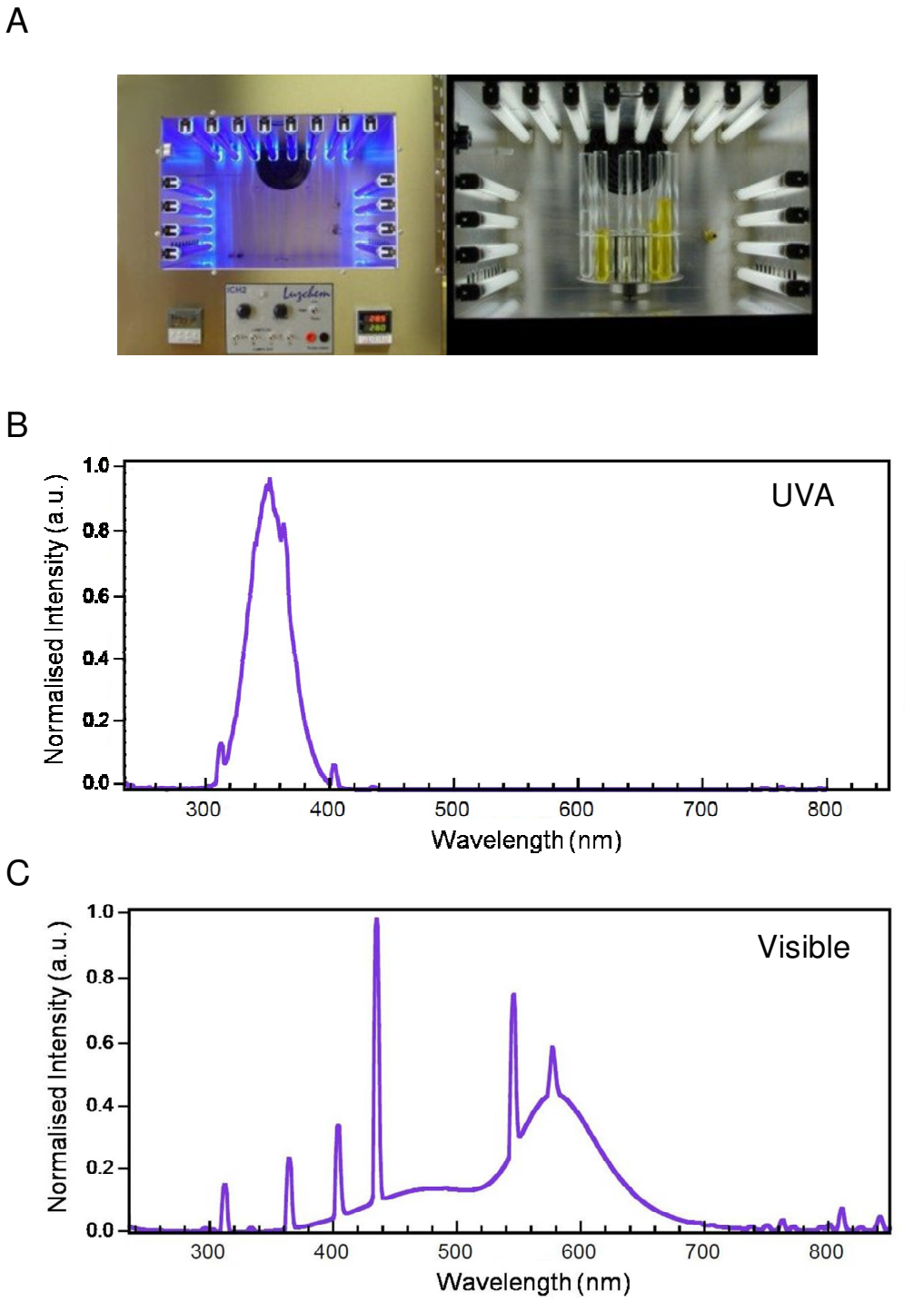

Figure 2.1 A: The photoreactor in operation, showing both UVA and visible lamps, B: the spectral output of LZC-UVA lamps, C: that of LZC-VIS lamps. Obtained from http://www.luzchem.com.

For visible irradiation studies, the photoreactor was equipped with 16 LZC-VIS lamps (Sylvania cool white). These lamps are regarded as a broadband visible light source; although small amounts (<6%) of UV light are present according to the spectral output (Figure 2.1, C), power levels in the UV region were measured prior to use and determined to be negligible. These lamps were subsequently used without any source of light filtration. All 16 lamps were used to give power levels in the range of 0.27–0.29 mW cm^{-2}.

Power levels were measured using the appropriate probe window (UV or visible), calibrated against an OAI-306 power meter from Optical Associates Inc. Irradiations were carried out at either 300 K or 310 K depending upon the complex studied; further details can be found in subsequent chapters.

2.3.2 Light Emitting Diodes (LEDs)

For certain complexes, irradiations in the visible region were also carried out using LED light sources, as these have a much narrower emission profile than the visible lamps and can be chosen according to the absorption bands of the complex.

Green LEDs (λ_{max} = 525 nm) were obtained from Farnell UK Ltd, the spectral output of these is shown in Figure 2.2. A typical setup involved four LEDs soldered in series, irradiating a UV cuvette in a blackened box. Power levels were measured as 0.19 mW cm^{-2} using a ILT1400-A radiometer photometer from International Light Technologies, equipped with F/W windows as appropriate for visible light. Irradiations were carried out at room temperature, with no significant heating effect noted during the experiment.

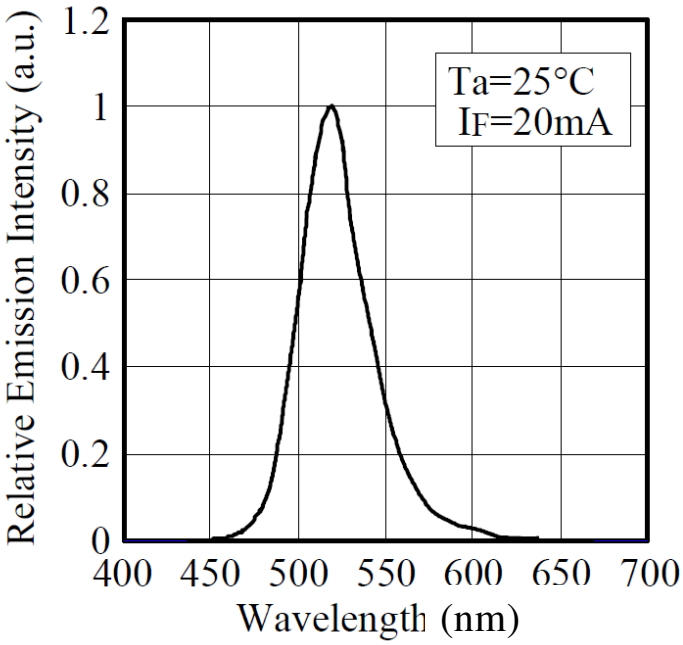

Figure 2.2 The spectral output of the green LEDs. Obtained from http://uk.farnell.com.

2.4 Fluorescence Spectroscopy

As a discussion of fluorescence can be found in Chapter 1, this section describes only the methods and instrumentation used.

Fluorescence spectra were acquired at room temperature on a JASCO FP-6500 spectrofluorimeter, running Spectra Manager for Windows 95/NT software, version 1.53.06 build 1. Samples were placed in a Hellma® fluorescence cuvette (pathlength 1 cm, volume 3.5 mL). The excitation wavelength (λ_{ex}) and scan range were varied depending upon the complex under investigation; further details are given in subsequent chapters where relevant. Unless otherwise stated, the band widths for excitation and emission were set to 5 nm, with spectra averaged over five acquisitions.

2.5 X-ray Crystallography[9]

Single crystal X-ray diffraction is used for the determination of atomic positions, bond lengths and angles in molecules in the crystalline state.

The technique exploits the fact that X-rays are diffracted by electrons when passed through a crystal, since their wavelengths are comparable to the spacing between the lattice planes of the crystal. This scattering can be recorded as a pattern of spots of varying intensity: a diffraction pattern. The geometry of the pattern is related to that of the unit cell, and can give information on the repeat distance between molecules. The symmetry is related to the crystal system and space group, and the intensities of the spots give information as to the positions of the atoms within the unit cell. The structure is then solved using, for example, Patterson or direct methods, to give approximate atom positions. This is then further refined to give more accurate atom positions and displacement parameters.

Certain diffraction data were collected and refined by Professor Simon Parsons and colleagues at the University of Edinburgh, on a Bruker (Siemens) Smart Apex CCD Diffractometer using Mo Kα radiation equipped with an Oxford Cryosystems low-temperature device operating at 150 K. Other data were collected and refined by Dr Guy Clarkson at the University of Warwick, using Mo Kα radiation on an Oxford Diffraction Gemini four-circle system, with Ruby CCD area detector, at 296 K.

All structures were solved by Professor Simon Parsons and colleagues, or by Dr Guy Clarkson, using direct SHELXS-97[10] methods, with additional light atoms found by Fourier methods, and refined against F^2 using SHELXL-97.[11] Hydrogen atoms were added at calculated positions, and anisotropic displacement parameters were used for all non-H atoms.

2.6 Elemental Analysis[12]

Elemental analysis is one of the most definitive ways of analysing the purity of a compound, by determining the percentages of elements in a sample and comparing the result to a theoretical value. Several elements can be analysed, although carbon, hydrogen and nitrogen (CHN) analyses are the most common, and are the only type used in this work.

A known mass of sample is subject to high temperature oxidation in a pure oxygen environment, producing a gaseous mixture of CO_2, CO, H_2O, N_2 and various oxides of nitrogen. These are passed into a furnace in which nitrogen oxides are reduced to nitrogen, oxygen is removed, and CO is converted to CO_2. The mixture is then analysed by a series of detectors; nitrogen content is quantified from the gaseous element, hydrogen from the water content, and carbon from the carbon dioxide present.

Analyses were performed by the CHN service staff at the University of Edinburgh or at Warwick Analytical Services, both using an Exeter Analytical Elemental Analyser (CE440). Analyses were also carried out at the University of St Andrews, using a Carlo-Erba CHNS Analyser.

2.7 Mass Spectrometry[1,12]

Mass spectrometry allows the mass of the molecule of interest to be determined, and also gives information on its construction and isotopic distribution.

This technique separates gaseous ions on the basis of their mass-to-charge ratio (*m/z*), hence requires that the molecule of interest is charged and in the gas phase. Various ionisation methods are available in order to achieve this; in this work electrospray was used, which is among the softest of ionisation techniques. A solution is passed through the exit of a fine needle held at an electric potential, then dispersed into a mist of droplets, from which solvent is lost to leave an aerosol of protonated sample which is desorbed into the gas phase.

Ion analysis was performed using either an Ion Trap or Time of Flight (TOF) mass analyser. The ion trap consists of a ring electrode, to which a voltage is applied inducing the ions to circulate in the cavity. Scanning the voltage causes the ions to be destabilised and leave the cavity at varying rates depending upon their *m/z*, where they then pass to a detector. In a TOF analyser, ions are accelerated into a field-free drift tube, where lighter particles will accelerate faster than heavy ones and have a shorter time of flight along the tube; they are thus analysed by their arrival time at the detector.

Electrospray ionisation mass spectra were obtained either on a Micromass Platform II Mass Spectrometer (University of Edinburgh), a Bruker Esquire2000 Spectrometer or a Bruker MicroTOF Spectrometer with the help of Dr Lijiang Song (University of Warwick). Samples were prepared either in water or a methanol/water mixture, and the cone voltage and source temperature varied depending upon the sample. Data were processed using DataAnalysis 3.3 (Bruker Daltonics).

2.8 pH Measurements

All pH values were measured at room temperature, using a Hydrus 500 pH meter equipped with glass semi-micro combination electrodes from Thermo Scientific. The electrodes were filled with either KCl or KNO_3 solutions, and were calibrated with standard buffer solutions from Sigma-Aldrich at pH 4, 7 and 10. The pH values of NMR samples in D_2O were recorded without correction for the effect of deuterium on the glass electrode, and are termed pH^*.

2.9 Fast Protein Liquid Chromatography (FPLC)[13]

FPLC is a chromatographic technique used for the separation and purification of proteins. The sample to be separated is loaded onto a column packed with a stationary phase; the means by which separation is achieved is dependent upon the

type of stationary phase. In this case Sephacryl was used, a gel filtration medium that separates molecules based on their size. This consists of small porous polymer beads with pores of different sizes. Larger particles cannot readily enter pores, so have less volume to traverse and elute from the column more quickly. Smaller particles can enter into the pores (to various extents depending upon their size), hindering their progress down the column and resulting in a longer retention time. The grade of Sephacryl employed here was S-200, which is suitable for proteins and macromolecules with molecular weights in the range of 5–250 kDa.

FPLC was performed on a BioCAD 700E Perfusion Chromatography workstation (PerSpective Biosystems), running BioCAD Perfusion Chromatography Workstation software, version 3.01. An XK16 Pharmacia Biotech column was used, packed with Sephacryl S-200. Samples were concentrated to < 2 mL in 1X PBS prior to injection, and products were eluted with 1X PBS (pH 7.4).

2.10 Inductively Coupled Plasma Mass Spectrometry (ICP-MS)[14]

ICP-MS combines the ionisation power of an inductively coupled plasma (ICP) with the high sensitivity of mass spectrometry, to give a technique capable of quantifying metals and non-metals in concentrations as low as parts per trillion.

Plasma is generated from the ionisation of argon gas by free electrons, and maintained at a high temperature (7500 K). Samples to be analysed are passed through a nebuliser into the plasma chamber, where they are atomised and ionised by loss of an electron. The resulting ions are extracted into another chamber containing a quadrupole mass analyser which separates the ions based on their mass-to-charge ratio; since all ions are singly charged, this ratio is equal to the mass of the ion. The magnitude of each peak is directly proportional to the concentration of an element in a sample; quantitative results are therefore generated by comparing signal intensities to those from calibration standards.

ICP-MS was carried out using an Agilent 7500 series machine with the help of Dr Ana Pizarro. Standard solutions were prepared in 3% nitric acid from commercially available stock solutions (typically 1000 ppm, Sigma Aldrich) of Cd, Se, Zn, S and Pt. These were analysed to give a calibration curve from which unknown concentrations of the element could be determined.

2.11 Cytotoxicity Studies

Cytotoxicity testing was carried out by Dr Ana Pizarro and Miss Soledad Betanzos Lara at the University of Warwick. Complexes were tested against the A2780 human ovarian cancer cell line, according to a previously published protocol.[15]

The A2780 human ovarian cancer cell line was obtained from the ECACC (European Collection of Cell Culture, Salisbury, UK). Cells were grown as monolayers in RPMI 1640 medium with L-glutamine (Gibco BRL, Paisley, UK) supplemented with 5% foetal calf serum and penicillin (110 U mL^{-1}) and streptomycin (100 μg mL^{-1}) and were maintained under standard tissue culture conditions of 310 K and 5% CO_2. Experiments were performed on cells within 10 passages of each other.

After plating, human ovarian A2780 cancer cells were treated with the complexes on day 2, at concentrations ranging from 0.1 to 200 μM. Solutions of the complexes were made up in 0.5% DMSO (v/v) to assist dissolution. Each concentration was added in triplicate and cisplatin control was added to the plate as a reference. Cells were exposed to the complexes for 24 h, washed with PBS, supplied with fresh medium, allowed to grow for three doubling times (72 h), and then the protein content measured (proportional to cell survival) using the sulforhodamine B (SRB) assay.[16]

2.12 Phototoxicity Studies

Phototoxicity testing was carried out by Dr Julie Woods and Kim Robinson from the Photobiology unit of the Department of Dermatology, University of Dundee, at Ninewells Hospital, Dundee, Scotland. Complexes were tested against HaCaT keratinocytes, a human skin cell line.

Phototoxicity was assessed using the neutral red phototoxicity assay; a test designed to compare the toxicity of a drug plus light, compared with the drug alone. Complexes were dissolved in Earle's balanced salt solution and sterile filtered (0.22 μm) before being applied to cells. All experiments were carried out in a specially adapted photobiology laboratory, with ambient light levels <1 lux (Solatell). Cells were seeded at a density of ~7 x 10^4 cells per cm^2 and left to adhere overnight. After washing cells with PBS, test compounds were added in Earle's solution and incubated for 1 h (310 K/5% CO_2). After this time, cells were irradiated by a bank of 2 ft x 6 ft Cosmolux RA Plus (Cosmedico) 15500/100 W UVA light sources (5 J cm^{-2}, λ_{max} = 365 nm), each filtered to attenuate UVB/UVC wavelengths. The total irradiation time was 50 min, to give a dose equivalent to ~15–60 min sunlight received on a typical UK midday, and reflects the clinical conditions used for light-activated drugs. Following irradiation, the salt solution was removed, the cells thoroughly washed, and then returned to the incubator in complete growth medium. Phototoxicity was determined 24 h later using neutral red uptake.[17,18] The amount of test compound required to inhibit dye uptake by 50% (IC_{50} value) was determined by nonlinear regression (GraphPad Prism). Experiments were performed in triplicate and each repeated two to three times, with chlorpromazine as positive control.

2.13 References

[1] L. M. Harwood and T. D. W. Claridge, *Introduction to Organic Spectroscopy*, Oxford University Press, New York, 1999.

[2] P. J. Hore, *Nuclear Magnetic Resonance*, Oxford University Press, New York, 2004.

[3] J. B. Lambert, H. F. Shurvell, D. A. Lightner and R. G. Cooks, *Organic Structural Spectroscopy*, Prentice Hall, New York, 1998.

[4] S. J. Berners-Price, L. Ronconi and P. J. Sadler, *Prog. Nucl. Magn. Reson. Spectrosc*., 2006, **49**, 65.

[5] F. P. Pruchnik, *Organometallic Chemistry of the Transition Elements*, Springer, New York, 1990.

[6] S. Braun, H. -O. Kalinowski and S. Berger, *150 and More Basic NMR Experiments*, Wiley-VCH, Weinheim, 2nd edn., 1998.

[7] T. -L. Hwang and A. J. Shaka, *J. Magn. Reson. Ser. A*., 1995, **112**, 275.

[8] H. E. Gottlieb, V. Kotlyar and A. Nudelman, *J. Org. Chem.*, 1997, **62**, 7512.

[9] W. Clegg, *Crystal Structure Determination*, Oxford University Press, New York, 1998.

[10] G. M. Sheldrick, *SHELXS-97: Program for the Solution of Crystal Structures*, University of Göttingen, Göttingen, 1997.

[11] G. M. Sheldrick, *SHELXL-97: Program for the Refinement of Crystal Structures*, University of Göttingen, Göttingen, 1997.

[12] D. A. Skoog, F. J. Holler and T. A. Nieman, *Principles of Instrumentation Analysis*, Harcourt Brace and Company, Orlando, 1998.

[13] P. L. R. Bonner, *Protein Purification*, Taylor and Francis Group, Abingdon, 2007.

[14] *Inductively Coupled Plasma Mass Spectrometry: A Primer*, Agilent Technologies Inc., 2008.

[15] R .E. Aird, J. Cummings, A. A. Ritchie, M. Muir, R. E. Morris, H. Chen, P. J. Sadler and D. I. Jodrell, *Br. J. Cancer*, 2002, **86**, 1652.

[16] P. Skehan, R. Storeng, D. Scudiero, A. Monks, J. McMahon, D. Vistica, J. T. Warren, H. Bokesch, S. Kenney and M. R. Boyd, *J. Natl. Cancer Inst*., 1990, **82**, 1107.

[17] E. Borenfreund and J. A. Puerner, *Toxicol Lett*., 1985, **24**, 119.

[18] N. J. Traynor, P. E. Beattie, S. H. Ibbotson, H. Moseley, J. Ferguson and J. A. Woods, *Toxicol Lett.*, 2005, **158**, 220.

Chapter 3

Platinum Azido Complexes and Routes to Functionalisation

3.1 Introduction

Pt^{IV} azido complexes, of the general formula $[Pt(amine)_2(N_3)_2(OH)_2]$, have recently emerged as potential photoactivated anticancer agents.[1] Such complexes are stable and non-toxic in the dark, yet upon irradiation can show cytotoxicity up to 80 times greater than cisplatin.[2] Work is continuing in our laboratory to further elucidate their mechanism of action, and to design new complexes with enhanced phototoxicity.

These appear to be the only examples of platinum azido complexes investigated for cytotoxic activity. In the years following the discovery of cisplatin, numerous Pt^{II} analogues were synthesised and tested, varying the nature of the amines and leaving group, and in 1973 Cleare and Hoeschele published a set of structure-activity relationships aimed at focusing future design onto complexes with the most promising features.[3] Regarding the nature of the leaving group, Cl^- was considered optimal, since experimental evidence had shown that very labile groups (H_2O, NO_3^-) gave complexes with high but indiscriminate toxicity, whilst complexes with strongly bound ligands (I^-, SCN^-, NO_2^-) showed little to no activity.[3] These findings were correlated with the order of leaving ability for X in the reaction $[Pt(dien)X]^+$ + pyridine, which had been experimentally determined as $NO_3^- > H_2O > Cl^- > Br^- > I^- > N_3^- > SCN^- > NO_2^- > CN^-$.[4] Therefore, although Pt^{II} azido complexes had seemingly never been tested, they were likely predicted to be inactive in line with experimental evidence from iodido and isothiocyanato complexes.

Nevertheless, the severe side effects associated with cisplatin therapy later led to the study of complexes with a more stable leaving group, in the belief that side reactions may be hindered and toxicity lowered, but antitumour efficacy retained. This concept was validated by carboplatin, a second-generation drug containing cyclobutanedicarboxylate, a bidentate oxygen donor ligand. The rate of hydrolysis of carboplatin is approximately 100 times lower than that of cisplatin, and DNA adduct formation at least 10-fold slower,[5] resulting in the need for higher doses

to achieve a therapeutic effect. However, due to the substantial decrease in toxicity, such doses can be tolerated and carboplatin has largely replaced cisplatin in many cases of platinum chemotherapy. This theme of enhanced stability continued with the development of oxaliplatin, containing the bidentate oxalato group; indeed many new platinum complexes in recent clinical trials contain bidentate oxygen donor ligands.[6]

Moreover, although general trends are often observed, the hydrolysis and nucleobase binding rates of metal complexes are not always strongly correlated with their cytotoxicity. One example concerning the cytotoxicity of metal azide complexes can be found in literature, involving two monofunctional Ru^{II} arene complexes $[(\eta^6\text{-hmb})Ru(en)(N_3)][PF_6]$ and $[(\eta^6\text{-bip})Ru(en)(N_3)][PF_6]$ (where en = ethylenediamine, hmb = hexamethylbenzene and bip = biphenyl).[7] The hydrolysis of these complexes (hmb, 21.3 min, bip, 367 min) was found to be slower than those containing chloride, bromide or iodide, with a 40-fold rate difference in comparison to the chlorido analogues, and the extent of hydrolysis was <5% in both cases. A degree of binding to 5'-GMP was also detected, although at a slower rate than hydrolysis. Surprisingly, however, both complexes showed good cytotoxicity, with IC_{50} values of 18 μM (hmb) and 4 μM (bip).

It was therefore decided to investigate a range of Pt^{II} azido complexes, with regard to their potential cytotoxicity. Additionally, since many transition metal azido complexes, including those of Pt^{II}, are known to be photoactive,[8] such complexes could potentially show phototoxic behaviour. Oxidation of these Pt^{II} complexes could also generate novel Pt^{IV} azido analogues, to add to the library of such complexes previously studied.

In addition to ethylenediamine, which is known to form cytotoxic Pt^{II} chlorido[9] and phototoxic Pt^{IV} azido complexes,[10] it was decided to investigate ligands incorporating hydroxyl or amine groups, which would remain uncoordinated, or "pendant", upon complex formation; it has been suggested that the hydrogen bonding capability of these groups could facilitate interactions with DNA.[11] Furthermore, these pendant functional groups could provide a handle with which

to functionalise these complexes. This could enable the incorporation of, for example, targeting agents or fluorescent probes, to increase affinity for target sites or investigate the mechanism of action. This concept is explored in Chapter 4.

This Chapter describes the synthesis, stability and cytotoxicity of a series of Pt^{II} chlorido and the corresponding Pt^{II} azido complexes, with photoreactions and phototoxicity also explored. The complexes studied are shown in Figure 3.1.

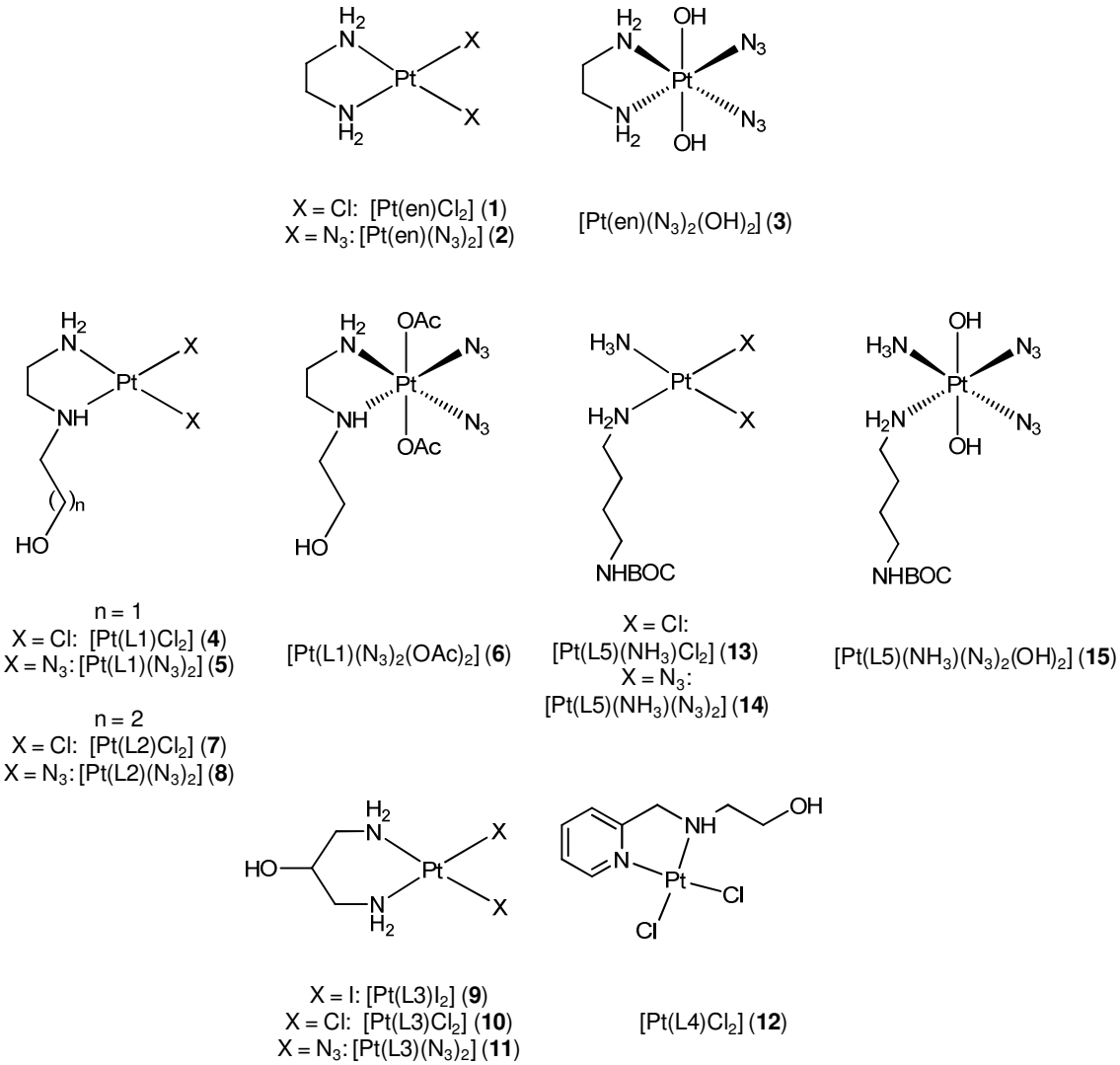

Figure 3.1 The platinum complexes studied in this Chapter.

3.2 Experimental

3.2.1 Materials

$K_2[PtCl_4]$ was purchased from Precious Metals Online. 1,4-Diaminobutane, 2-(2-aminoethylamino)ethanol (**L1**), ethanolamine, 2-pyridinecarboxaldehyde, di-*tert*-butyl dicarbonate and guanosine 5'-monophosphate (5'-GMP) were obtained from Aldrich. 1,3-diamino-2-propanol (**L3**) and silver nitrate were obtained from Fluka. 3-(2-aminoethylamino)-1-propanol (**L2**) was purchased from TCI Europe, hydrogen peroxide (30%) from VWR, ethylenediamine and sodium azide from Fisher, and reduced glutathione (GSH) from Acros Organics. Other reagents were obtained from commercial sources. All reagents were used as received, with the exception of ethylenediamine, which was distilled over sodium and stored under argon prior to use.

3.2.2 Synthesis

Caution! Heavy metal azide complexes are known to be unstable and/or explosive, especially when subject to friction or high temperatures.[12] Therefore it is imperative that care is taken when handling platinum azide complexes in the solid form; plastic spatulas are used instead of metal, glass frits are avoided, and these complexes are never heated to temperatures exceeding 313 K.

$[Pt(en)Cl_2]$ (1)

$K_2[PtCl_4]$ (500 mg, 1.20 mmol) was dissolved in water (5 mL), ethylenediamine (80 µL, 1.20 mmol) was added, and the solution stirred at room temperature for 3 h. The yellow solid was removed by filtration, washed with water, ethanol and diethyl ether, and dried under vacuum.

Yield: 277 mg (71%).

Elemental analysis: Found: C, 7.50; H, 2.31; N, 8.22. $PtC_2H_8N_2Cl_2$ requires: C, 7.37; H, 2.47; N, 8.57%.

^{1}H NMR (400 MHz, DMSO-d_6): δ 5.32 (s, 4H, NH_2), 2.23 (s, 4H, CH_2).

[Pt(en)(N_3)$_2$] (2)

[Pt(en)Cl_2] (250 mg, 0.77 mmol) was suspended in water (15 mL), to this was added $AgNO_3$ (254 mg, 1.50 mmol), and the mixture stirred at 328 K in the dark for 16 h. The AgCl precipitate was filtered off using an inorganic membrane filter (Sartorius Minisart®, 0.2 μm). NaN_3 (497 mg, 7.7 mmol) was added, the solution immediately filtered again to remove any AgN_3, and stirred at room temperature in the dark for 3 h. The volume was reduced and the solution stored at 277 K overnight, after which a yellow solid was filtered off, washed with water, ethanol and diethyl ether, and dried under vacuum.

Yield: 187 mg (72%).

Elemental analysis: Found: C, 7.23; H, 2.32; N, 32.75. $PtC_2H_8N_8$ requires: C, 7.08; H, 2.38; N, 33.08%.

^{1}H NMR (400 MHz, DMSO-d_6): δ 5.27 (s, 4H, NH_2), 2.26 (s, 4H, CH_2).

[Pt(en)(N_3)$_2$(OH)$_2$] (3)

[Pt(en)(N_3)$_2$] (72 mg, 0.21 mmol) was suspended in water (25 mL), to this was added H_2O_2 (903 μL, 8.84 mmol, 30 % solution), and the mixture stirred at room temperature in the dark for 16 h. Following this, the solution was passed through an inorganic membrane filter to remove any residual AgN_3. The volume was reduced and the solution stored at 277 K overnight, after which a yellow solid was filtered off, washed sparingly with water, ethanol and diethyl ether, and dried under vacuum.

Yield: 32 mg (41%).

Elemental analysis: Found: C, 6.43; H, 2.60; N, 29.65. $PtC_2H_{10}N_8O_2$ requires: C, 6.44; H, 2.70; N, 30.02%.

^{1}H NMR (400 MHz, 90% H_2O/10% D_2O): δ 2.93 (s, $^3J(^{195}Pt\text{-}^1H)$ 27 Hz, 4H, CH_2).

[Pt(L1)Cl$_2$] (4)

$K_2[PtCl_4]$ (1.00 g, 2.41 mmol) was dissolved in water (7.5 mL), and was added slowly to a solution of 2-(2-aminoethylamino)ethanol (244 μL, 2.41 mmol) in water (1 mL). The pH was decreased to 7 with 6 M HCl, and then periodically readjusted to 7 with 2 M KOH over the course of 3 h, before leaving to stir at room temperature overnight. Following this the pH was readjusted to 7 once more, stirred for an additional 30 min, and the pale yellow precipitate isolated. Further product could be obtained by adding excess aminoalcohol to the filtrate, adjusting the pH to 7 and again stirring overnight before storage at 277 K. The product was recrystallised from 0.1 M HCl, washed with small quantities of water, ethanol and diethyl ether, and dried under vacuum. Crystals suitable for X-ray diffraction were obtained from a filtrate stored at room temperature.

Yield: 583 mg (65%).

Elemental analysis: Found: C, 12.97; H, 3.19; N, 7.62. $PtC_4H_{12}N_2Cl_2O$ requires: C, 12.98; H, 3.27; N, 7.57%.

^{1}H NMR (800 MHz, DMSO-d_6): δ 6.15 (s, NH, 1H), 5.37 (s, NH_2, 1H), 5.29 (s, NH_2, 1H), 4.74 (t, OH, 1H), 3.69 (m, CH_2, 1H), 3.61 (m, CH_2, 1H), 3.09 (m, CH_2, 1H), 2.78 (m, CH_2, 1H), 2.56 (m, CH_2, 1H), 2.43 (m, CH_2, 1H), 2.36 (m, CH_2, 1H), 2.28 (m, CH_2, 1H).

ESI-MS: $[M + H_2O]^+$ 388, $[M - Cl]^+$ 335 *m/z*.

[Pt(L1)$(N_3)_2$] (5)

[Pt(L1)Cl_2] (450 mg, 1.22 mmol) was suspended in water (20 mL), $AgNO_3$ (407 mg, 2.40 mmol) was added, and the mixture stirred at 328 K in the dark for 16 h. The AgCl precipitate was then filtered off using an inorganic membrane filter. NaN_3 (793 mg, 12.2 mmol) was added, the solution immediately filtered again to remove any AgN_3, and stirred at room temperature in the dark for 4 h. The solvent volume was reduced and the mixture stored at 277 K overnight. A pale yellow precipitate was filtered off and washed with small quantities of water, methanol and diethyl ether, and dried under vacuum. Crystals suitable for X-ray diffraction were obtained from a filtrate stored at 277 K.

Yield: 376 mg (81%).
Elemental analysis: Found: C, 12.52; H, 3.03; N, 29.52. $PtC_4H_{12}N_8O$ requires: C, 12.53; H, 3.16; N, 29.24%.
^{1}H NMR (400 MHz, DMSO-d_6): δ 5.97 (s, NH, 1H), 5.34 (s, NH_2, 1H), 5.24 (s, NH_2, 1H), 4.77 (t, OH, 1H), 3.66 (m, CH_2, 1H), 3.59 (m, CH_2, 1H), 2.88 (m, CH_2, 1H), 2.65 (m, CH_2, 1H), 2.62 (m, CH_2, 1H), 2.39 (m, CH_2, 1H), 2.32 (m, CH_2, 2H).
ESI-MS: $[M + Na]^+$ 406, $[M + H]^+$ 384 *m/z*.

[Pt(L1)$(N_3)_2(OAc)_2$] (6)

[Pt(L1)$(N_3)_2$] (50 mg, 0.13 mmol) was suspended in acetic acid (0.75 mL), acetic anhydride (115 µL, 1.22 mmol) was added and the mixture stirred for 1 min. H_2O_2 (20 µL, 0.19 mmol) was added, after which dissolution of the reagents occurred to give a yellow solution; this was stirred in the dark at room temperature for 4 h. Methanol (1 mL) was added, the mixture stirred for an additional 30 min, then solvent was removed to dryness under vacuum. Very gentle scratching and sonication with diethyl ether yielded a yellow solid, which was washed very sparingly with water, ethanol and diethyl ether, then dried under high vacuum overnight.

Yield: 19 mg (29%).

Elemental analysis: Found: C, 19.46; H, 3.52; N, 21.75. $PtC_8H_{18}N_8O_5Pt$ requires: C, 19.17; H, 3.62; N, 22.35%.

UV-Vis (H_2O): λ_{max} 263 nm, ε 17 500 M^{-1} cm^{-1}.

^{1}H NMR (800 MHz, DMSO-d_6): δ 9.19 (s, NH, 1H), 8.41 (s, NH_2, 1H), 7.48 (s, NH_2, 1H), 5.06 (t, OH, 1H), 3.73 (m, CH_2, 1H), 3.63 (m, CH_2, 1H), 3.23 (m, CH_2, 1H), 2.97 (m, CH_2, 1H), 2.86 (m, CH_2, 1H), 2.80 (m, CH_2, 1H), 2.71 (m, CH_2, 1H), 2.61 (m, CH_2, 1H), 2.00 (s, CH_3, 3H), 1.99 (s, CH_3, 3H).

ESI-MS: $[M + H]^+$ 502, $[M + Na]^+$ 524 *m/z*.

[Pt(L2)Cl_2] (7)

This complex was synthesised by a similar method to [Pt(L1)Cl_2] (**4**), by using 3-(2-aminoethylamino)-1-propanol (L2) in place of L1.

Yield: 32%.

Elemental analysis: Found: C, 15.62; H, 3.59; N, 7.27. $PtC_5H_{14}N_2Cl_2O$ requires: C, 15.63; H, 3.67; N, 7.29%.

^{1}H NMR (400 MHz, DMSO-d_6): δ 6.19 (s, NH, 1H), 5.36 (s, NH_2, 1H), 5.30 (s, NH_2, 1H), 4.52 (t, OH, 1H), 3.41 (m, CH_2, 2H), 2.99 (m, CH_2, 1H), 2.74 (m, CH_2, 1H), 2.50 (m, CH_2, 1H), 2.49 (m, CH_2, 1H), 2.35 (m, CH_2, 1H), 2.27 (m, CH_2, 2H), 1.89 (m, CH_2, 1H), 1.66 (m, CH_2, 1H).

[Pt(L2)(N_3)$_2$] (8)

This complex was synthesised by a method similar to that for [Pt(L1)(N_3)$_2$] (**5**), by using [Pt(L2)Cl_2] (**7**) as the starting material.

Yield: 45%.

Elemental analysis: Found: C, 15.03; H, 3.47; N, 28.07. $PtC_5H_{14}N_8O$ requires: C, 15.12; H, 3.55; N, 28.20%.

^{1}H NMR (400 MHz, DMSO-d_6): δ 6.02 (s, NH, 1H), 5.35 (s, NH_2, 1H), 5.25 (s,

NH_2, 1H), 4.54 (t, OH, 1H), 3.43 (m, CH_2, 2H), 2.80 (m, CH_2, 1H), 2.59 (m, CH_2, 1H), 2.40 (m, CH_2, 1H), 2.25 (m, CH_2, 1H), 2.23 (m, CH_2, 2H), 1.83 (m, CH_2, 1H), 1.66 (m, CH_2, 1H).

[Pt(L3)I_2] (9)

$K_2[PtCl_4]$ (300 mg, 0.72 mmol) was dissolved in water (4 mL), to this was added a solution of KI (1.21 g, 7.2 mmol) in water (3 mL), and the mixture was stirred for 90 min at room temperature. 1,3-diamino-2-propanol (**L3**) (65 mg, 0.72 mmol) was added and the reaction stirred for 3 h, after which volume was reduced and the mixture stored at 277 K overnight. A mustard-yellow solid was filtered off and washed with water, ethanol and diethyl ether, then dried under vacuum.

Yield: 345 mg (89%).
Elemental analysis: Found: C, 6.55; H, 1.74; N, 5.06. $PtC_3H_{10}N_2I_2O$ requires: C, 6.68; H, 1.87; N, 5.20%.
^{1}H NMR (400 MHz, DMSO-d_6): δ 5.63 (s, NH_2, 2H), 5.44 (t, OH, 1H), 5.39 (s, NH_2, 2H), 3.91 (m, CH, 1H), 2.84 (m, CH_2, 1H), 2.76 (m, CH_2, 1H), 2.54 (m, CH_2, 1H) 2.45 (m, CH_2, 1H).

[Pt(L3)Cl_2] (10)

[Pt(L3)I_2] (550 mg, 1.02 mmol) was suspended in water (115 mL), $AgNO_3$ (338 mg, 1.99 mmol) was added, and the mixture stirred in the dark at 328 K for 16 h. The AgI precipitate was filtered off using an inorganic membrane filter. NaCl (596 mg, 10.2 mmol) was added, the solution immediately filtered again to remove any AgCl, and stirred at room temperature in the dark for 4 h. The solvent volume was reduced and the mixture stored at 277 K overnight. The product was recrystallised from 0.1 M HCl, washed with small quantities of water, ethanol and diethyl ether, and dried under vacuum.

Yield: 220 mg (61%).

Elemental analysis: Found: C, 10.07; H, 2.72; N, 8.07. $PtC_3H_{10}N_2Cl_2O$ requires: C, 10.12; H, 2.83; N, 7.87%.

^{1}H NMR (400 MHz, DMSO-d_6): δ 5.20 (d, OH, 1H), 5.03 (s, NH_2, 2H), 4.81 (s, NH_2, 2H), 3.59 (m, CH, 1H), 2.45 (m, CH_2, 2H), 2.29 (m, CH_2, 2H).

[Pt(L3)(N_3)$_2$] (11)

This complex was synthesised by a similar method to [Pt(L3)Cl_2] (**9**), but using NaN_3 in place of NaCl.

Yield: 70%.

Elemental analysis: Found: C, 9.71; H, 2.64; N, 30.13. $PtC_3H_{10}N_8O$ requires: C, 9.76; H, 2.73; N, 30.35%.

^{1}H NMR (400 MHz, DMSO-d_6): δ 5.10 (d, OH, 1H), 4.93 (s, NH_2, 2H), 4.72 (s, NH_2, 2H), 3.54 (m, CH, 1H), 2.44 (m, CH_2, 2H), 2.29 (m, CH_2, 2H).

2-[(2-pyridinylmethyl)amino]ethanol (L4)

A solution of aminoethanol (634 μL, 10.5 mmol) in methanol (15 mL) was cooled in ice. Pyridine-2-carboxaldehyde (1 mL, 10.5 mmol) was added slowly, and the reaction mixture stirred at 298 K for 4 h. $NaBH_4$ (1.19 g, 31.5 mmol) was added in small portions and the mixture stirred for a further two hours. Water (55 mL) was added, the mixture extracted with chloroform (6 x 20 mL), and the combined organic phases dried over $MgSO_4$. Solvent was removed to yield a brown oil, to which water (3 mL) was added, the solution filtered to remove undissolved material, then the water was removed and the product dried under vacuum.

Yield: 958 mg (60%).

UV-Vis (H_2O): λ_{max} 258 nm, ε 3715 M^{-1} cm^{-1}.

^{1}H NMR (400 MHz, $CDCl_3$): δ = 8.55 (d, 1H), 7.65 (td, 1H), 7.27 (d, 1H), 7.18 (td, 1H), 3.95 (s, CH_2, 2H), 3.67 (t, CH_2, 2H), 2.86 (t, CH_2, 2H), 2.44 (s, NH, 1H).

ESI-MS: $[M + H]^+$ 153 *m/z*.

Cis-$[Pt(DMSO)_2Cl_2]$

$K_2[PtCl_4]$ (1.00 g, 2.41 mmol) was dissolved in water (9 mL), and to this was added dimethyl sulfoxide (513 μL, 7.22 mmol). The mixture was stirred for 1 h, then left to stand overnight. A cream solid was filtered off, washed with water, ethanol and diethyl ether, and dried under vacuum.

Yield: 840 mg (83%).
Elemental analysis: Found: C, 11.53; H, 2.52. $PtC_4H_{12}Cl_2O_2S_2$ requires: C, 11.38; H, 2.86%.
^{1}H NMR (400 MHz, DMSO-d_6): δ 2.54 (s, 6H, CH_3).

$[Pt(L4)Cl_2]$ (12)

Cis-$[Pt(DMSO)_2Cl_2]$ (403 mg, 0.96 mmol) was dissolved in dichloromethane (60 mL) and a solution of L4 (146 mg, 0.96 mmol) in dichloromethane (5 mL) was added, upon which the solution became yellow. The mixture was stirred for 3 h, after which all volume was removed to leave a sticky dark yellow residue. Recrystallisation from 0.1 M HCl yielded a fluffy pale yellow solid.

Yield: 80 mg (20%).
Elemental analysis: Found: C, 22.93; H, 2.77; N, 6.69. $PtC_8H_{12}N_2Cl_2O$ requires: C, 22.98; H, 2.89; N, 6.70%.
UV-Vis (H_2O): λ_{max} 263 nm, ε 6020 M^{-1} cm^{-1}.
^{1}H NMR (400 MHz, DMSO-d_6): δ = 9.05 (d, 1H), 8.14 (td, 1H), 7.65 (d, 1H), 7.50 (td, 1H), 7.02 (s, NH, 1H), 4.77 (t, OH, 1H), 4.38 (dd, CH_2, 1H), 4.22 (dd, CH_2, 1H), 3.73 (m, CH_2, 2H), 2.98 (m, CH_2, 1H), 2.81 (m, CH_2, 1H).

N-tert-butoxycarbonyl-1,4-diaminobutane (L5)

1,4-diaminobutane (7.67 g, 87 mmol) was dissolved in dioxane (30 mL). To this, a solution of di-*tert*-butyl dicarbonate (2.45 g, 11 mmol) in dioxane (30 mL) was added dropwise, over the course of 2 h. The resulting mixture was stirred at room temperature for 16 h. All solvent was removed under reduced pressure, and water (50 mL) was added. The mixture was filtered to yield 106 mg of white solid, the diprotected product (3% based on di-*tert*-butyl dicarbonate). The filtrate was then extracted with dichloromethane (3 x 50 mL), and the combined extracts backwashed once with water (30 mL) then dried over Na_2SO_4. Solvent was removed and the product dried under high vacuum to yield a colourless oil.

Yield: 1.42 g (67%).
^{1}H NMR (400 MHz, $CDCl_3$): δ = 4.65 (s, NH, 1H), 3.12 (d, CH_2, 2H), 2.70 (t, CH_2, 2H), 1.50 (m, CH_2, 4H), 1.43 (s, CH_3, 9H), 1.27 (s, NH_2, 2H).

Cis-$[Pt(NH_3)_2I_2]$

$K_2[PtCl_4]$ (1.00 g, 2.41 mmol) was dissolved in water (20 mL), KI (4.00 g, 24.1 mmol) was added, and the mixture stirred at room temperature for 30 min. NH_4Cl (259 mg, 4.88 mmol) was added, and the pH adjusted to 10 with 2 M KOH. The pH was monitored every 5–10 min and readjusted to 10 until no further decrease was observed; the mixture then was stirred for 30 min and left to stand for an additional 30 min. The yellow solid was collected by filtration, washed with small quantities of water, ethanol and diethyl ether, and dried under vacuum.

Yield: 1.10 g (95%).
Elemental analysis: Found: C, 0.00; H, 1.12; N, 5.74. $PtH_6N_2I_2$ requires: C, 0.00; H, 1.25; N, 5.80%.
^{1}H NMR (400 MHz, DMSO-d_6): δ 4.65 (br s, 3H, NH_3).

Cis-[$Pt(NH_3)_2Cl_2$] (Cisplatin)

Cis-[$Pt(NH_3)_2I_2$] (1.05 g, 2.17 mmol) was suspended in water (60 mL), $AgNO_3$ (720 mg, 4.24 mmol) was added, and the mixture stirred at 328 K in the dark for 16 h. The AgI precipitate was filtered off using an inorganic membrane filter. NaCl (2.54 g, 43.4 mmol) was added, the solution immediately filtered again to remove any AgCl, and stirred at room temperature for 3 h. The solvent volume was reduced and the mixture stored at 277 K overnight. A bright yellow precipitate was isolated and recrystallised from 0.1M HCl; the final product was then filtered and washed with small quantities of water, ethanol and diethyl ether, and dried under vacuum.

Yield: 546 mg (84%).
Elemental analysis: Found: C, 0.00; H, 1.90; N, 9.27. $PtH_6N_2Cl_2$ requires: C, 0.00; H, 2.02; N, 9.34%.
^{1}H NMR (500 MHz, DMSO-d_6): δ 3.94 (br s, 3H, NH_3).
ESI-MS: $[M + Na]^+$ 323, $[M – NH_3]^+$ 283, $[M – Cl]^+$ 263 *m/z*.

K[$Pt(NH_3)Cl_3$]

Cis-[$Pt(NH_3)_2Cl_2$] (280 mg, 0.93 mmol) and tetraethylammonium chloride (186 mg, 1.12 mmol) were placed in a two-necked round bottom flask, and dimethylacetamide (58 mL) was added. The mixture was heated, under a nitrogen flow, to 373 K for 6 h. After cooling to room temperature, hexane : ethyl acetate (450 mL, 1:1 v/v) was added and the solution stored at 253 K overnight. The organic solvents were decanted to leave an orange oil, which was dissolved in methanol (10 mL) then filtered to remove any unreacted cisplatin. The methanol was removed under vacuum and the oil redissolved in water (5 mL); this was used directly in the preparation of mixed amine complexes without isolation. Where necessary, the concentration of a methanolic solution of the complex could be

calculated from the absorption spectrum, with reference to a published extinction coefficient.

UV-Vis (MeOH): λ_{max} 345 nm, ε 115 M^{-1} cm^{-1}.
ESI-MS: $[M]^-$ 318, $[M - NH_3]^-$ 301 *m/z*.

Cis-[Pt(L5)(NH_3)Cl_2] (13)

To an aqueous solution of K[Pt(NH_3)Cl_3] was added L5 (351 mg, 1.86 mmol), and the mixture stirred at room temperature for 2 h. A cream precipitate was isolated and washed with water, ethanol and diethyl ether, then dried under vacuum.
Yield: 228 mg (52% based on cisplatin).
Elemental analysis: Found: C, 22.56; H, 4.61; N, 8.86. $PtC_9H_{23}N_3Cl_2O_2$ requires: C, 22.94; H, 4.92; N, 8.92%.
^{1}H NMR (400 MHz, DMSO-d_6): δ = 6.79 (br s, NH, 1H), 4.74 (br s, NH_2, 2H), 3.99 (br s, NH_3, 3H), 2.90 (m, CH_2, 2H), 2.50 (CH_2, 2H, obscured by solvent peak), 1.53 (m, CH_2, 2H), 1.37 (s, CH_3 and CH_2, 11H).

Cis-[Pt(L5)(NH_3)(N_3)$_2$] (14)

Cis-[Pt(L5)(NH_3)Cl_2] (150 mg, 0.32 mmol) was suspended in methanol (35 mL), and to this was added a solution of $AgNO_3$ (105 mg, 0.62 mmol) in water (15 mL). The mixture was stirred at 328 K in the dark for 14 hours. The solvent was evaporated to dryness and the residue re-suspended in water; the AgCl precipitate was then removed by filtration with an inorganic membrane filter. To the filtrate was added NaN_3 (207 mg, 3.18 mmol) and the mixture stirred for three hours, followed by a further filtration. The solvent volume was reduced and the solution stored at 277 K for three hours, after which a yellow precipitate was collected by filtration and washed with water, a small quantity of ethanol and diethyl ether, then dried under vacuum.

Yield: 166 mg (38%).

^{1}H NMR (400 MHz, DMSO-d_6): δ = 6.79 (br s, NH, 1H), 4.61 (br s, NH_2, 2H), 3.86 (br s, NH_3, 3H), 2.89 (m, CH_2, 2H), 2.40 (m, CH_2, 2H), 1.45 (m, CH_2, 2H), 1.38 (s, CH_3 and CH_2, 11H).

***Cis,cis,trans*-[Pt(L5)(NH_3)(N_3)$_2$(OH)$_2$] (15)**

Cis-[Pt(L5)(NH_3)(N_3)$_2$] (35 mg, 0.072 mmol) was suspended in water (20 mL). H_2O_2 (295 µL, 2.88 mmol, 30 % solution) was added and the mixture stirred for 14 h at room temperature in the dark. Following this, additional water (20 mL) and H_2O_2 (295 µL) were added and the mixture stirred for a further 6 h, then filtered through an inorganic membrane filter. The solvent was removed and acetone was added to the residue to isolate a pale yellow precipitate.

Yield: 9 mg (25%).

^{1}H NMR (400 MHz, DMSO-d_6): δ = 6.81 (br s, NH, 1H), 5.63 (br s, NH_2, 2H), 5.06 (br s, NH_3, 3H), 2.91 (m, CH_2, 2H), 2.52 (m, CH_2, 2H), 1.55 (m, CH_2, 2H), 1.38 (s, CH_3 and CH_2, 11H).

3.2.3 Methods

3.2.3.1 X-ray Crystallography

The crystal structure of **3** was solved by Professor Simon Parsons and colleagues at the University of Edinburgh, and that of **4** by Dr Guy Clarkson at the University of Warwick. Data were collected and refined as described in Chapter 2.

3.2.3.2 Stability Studies and Reactions with Glutathione and 5'-GMP

The stability of several Pt^{II} and Pt^{IV} complexes under various biologically relevant conditions was monitored by ^{1}H NMR spectroscopy, with stability under ambient laboratory lighting conditions also investigated. Details for all experiments are given in subsequent sections.

3.2.3.3 Cytotoxicity Testing

The cytotoxicity of several Pt^{II} complexes towards the human ovarian A2780 cancer cell line was investigated. Experiments were performed by Dr Ana Pizarro and Miss Soledad Betanzos Lara at the University of Warwick, according to the procedure outlined in Chapter 2.

3.2.3.4 Photoreactions

Photoreactions of several complexes, both alone in aqueous solutions and in the presence of 5'-GMP, were studied and monitored by ^{1}H NMR and, in certain cases, UV-Visible spectroscopy. Irradiations were performed using a LZC-ICH2 photoreactor equipped with LZC-UVA lamps (λ_{max} = 365 nm, P = 1.7–2.2 mW cm^{-2}) and LZC-VIS UV-Visible light lamps (λ = 400–700 nm, P = 0.27–0.29 mW cm^{-2}); further details and the spectral outputs of these light sources can

be found in Chapter 2. Specific details for each experiment are given in subsequent sections.

3.2.3.5 Phototoxicity Testing

Phototoxicity testing of complexes **2**, **5**, **6**, and **8** was performed using the HaCaT keratinocyte human skin cell line. This was undertaken by Dr Julie Woods and Kim Robinson at the Photobiology Unit in Ninewells Hospital, Dundee, as described in Chapter 2.

3.3 Results

A series of Pt^{II} azido complexes has been synthesised and characterised, containing ligands with a pendant hydroxyl or protected amine group. Two such Pt^{IV} azido complexes were also prepared. The dark stability of one Pt^{II} and one Pt^{IV} azido complex in aqueous and 100 mM chloride solutions was investigated, as well as dark reactions with glutathione and 5'-GMP. The photoreactions of these two complexes upon irradiation with UVA and visible light were monitored, as well as in the presence of 5'-GMP, irradiating with UVA light. Finally the cytotoxicity and phototoxicity of several complexes were determined.

3.3.1 Synthesis and Characterisation

Complexes **1**, **2** and **3**, containing ethylenediamine as a chelating ligand, were prepared according to published methods,[13] and their synthesis will not be discussed here. The following sections describe the synthesis of complexes containing pendant hydroxyl or protected amine functionalities.

3.3.1.1 Platinum Complexes Containing a Pendant Hydroxyl Group

3.3.1.1.1 Pt^{II} Chlorido Complexes

It was not possible to prepare Pt^{II} chlorido complexes of all four aminoalcohol ligands using the same synthetic route; described below are the three different methods used in the preparation of these complexes.

Pt^{II} chlorido complexes of L1 and L2 were prepared in good yields from reaction of the aminoalcohol ligands with $K_2[PtCl_4]$, according to the scheme below:[14]

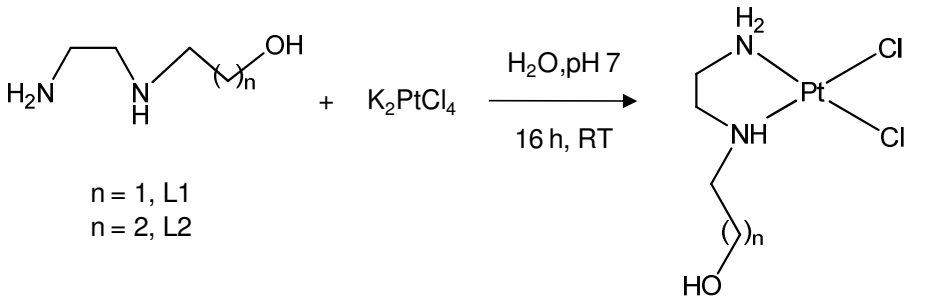

Scheme 3.1 The synthetic route to Pt^{II} chlorido complexes of L1 and L2

It has been previously reported that the reaction of L3 with $K_2[PtCl_4]$ does not yield $[Pt(L3)Cl_2]$, but instead produces the salt $[Pt(L3)_2][PtCl_4]$.[15] Hence an

alternative route was employed, in which the aminoalcohol ligand was first reacted with $K_2[PtI_4]$ to obtain $[Pt(L3)I_2]$ (**9**).[16] The iodides were then abstracted with silver nitrate to yield the aquo species, followed by addition of NaCl to form the required Pt^{II} chlorido complex.

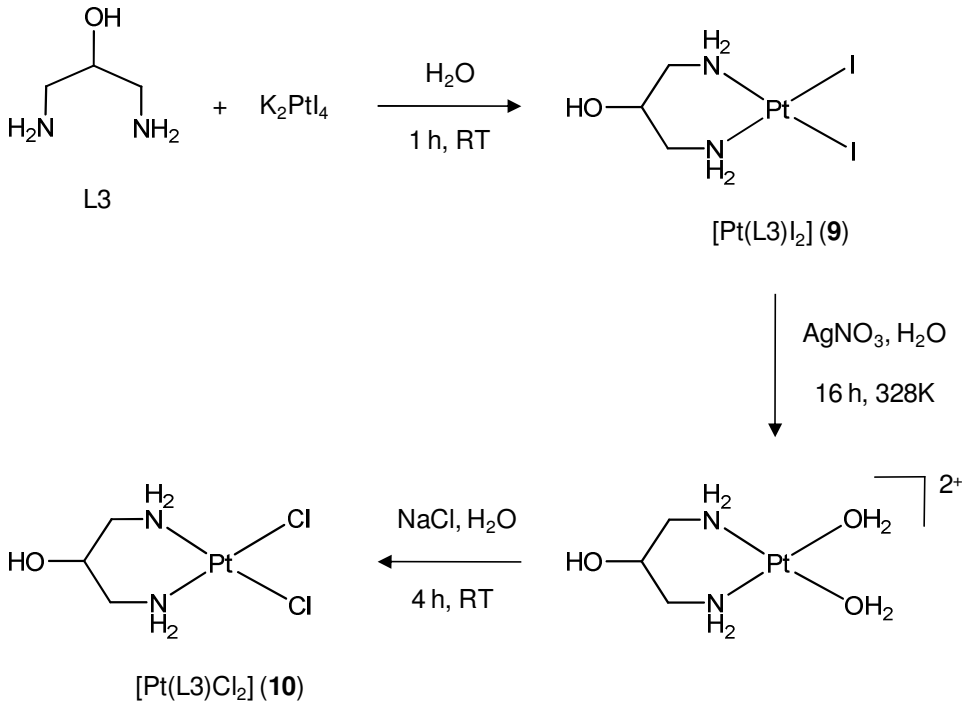

Scheme 3.2 The synthetic route to the Pt^{II} chlorido complex of L3

Attempts to synthesise the new complex $[Pt(L4)Cl_2]$ (**12**) by the method shown in Scheme 3.1 were unsuccessful. The reaction mixture rapidly darkened upon pH adjustment, yet little reaction was apparent when the pH was unaltered. The most successful synthesis of this complex involved reaction of the aminoalcohol ligand L4 with *cis*-$[Pt(DMSO)_2Cl_2]$ in dichloromethane, however yields were still relatively low, and only one suitably pure batch was prepared.

All chlorido complexes were purified by recrystallisation from 0.1 M HCl, and characterised by ^{1}H NMR spectroscopy, CHN analysis and, in the case of complex **4**, X-ray crystallography.

3.3.1.1.2 Pt^{II} Azido Complexes

The corresponding Pt^{II} azido complexes were formed from the chlorido precursors according to published methods for similar complexes.[13] Silver nitrate abstraction of the chlorides forms the aquo species, which react rapidly upon addition of excess NaN_3 to yield the desired Pt^{II} azido complexes, in a similar reaction to that shown in Scheme 3.2. The azido complex of L3 could be formed in this way from either the Pt^{II} chlorido or the iodido precursor.

Recrystallisation was not attempted for the azido complexes due to their sensitivity to temperatures exceeding 313 K. However, purity was confirmed by CHN analysis and NMR spectroscopy, with complex **5** also characterised by X-ray crystallography.

3.3.1.1.3 Pt^{IV} Azido Complexes

Attempts were made to oxidise [Pt(L1)$(N_3)_2$] (**5**), *via* a well documented procedure using hydrogen peroxide in aqueous solution, to yield a Pt^{IV} azido complex containing hydroxyl ligands in the two axial positions.[13] However, although evidence of the required complex was seen by mass spectrometry, impurities were invariably evident in ^{1}H NMR spectra. In addition, the product was very sticky and difficult to isolate and handle; consequently no further work was carried out with this complex.

However, the Pt^{IV} complex containing two axial acetato groups was successfully synthesised, following a published route for oxidation of the Pt^{II} chlorido

precursor,[17] to yield [Pt(L1)$(N_3)_2(OAc)_2$] (**6**). This complex was analysed by ^{1}H NMR spectroscopy, ESI-MS and CHN analysis.

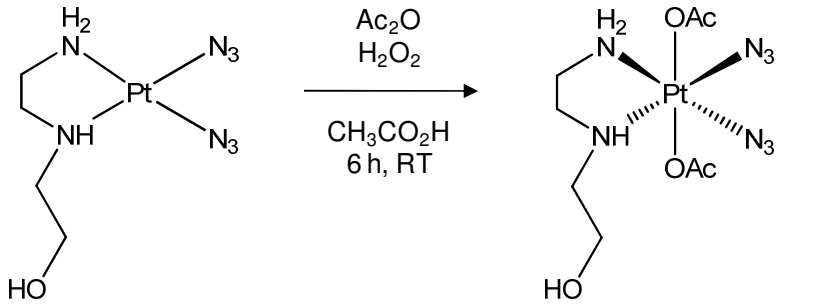

[Pt(L1)$(N_3)_2$] (**5**) [Pt(L1)$(N_3)_2(OAc)_2$] (**6**)

Scheme 3.3 The oxidation of [Pt(L1)$(N_3)_2$] to yield a Pt^{IV} complex with axial acetato groups.

3.3.1.1.4 X-ray Crystallography

The X-ray crystal structures of [Pt(L1)Cl_2] (**4**) and [Pt(L1)$(N_3)_2$] (**5**) were obtained in this work and are discussed below. The structure of **4** has been reported previously,[18] whilst that of **5** is novel.

[Pt(L1)Cl_2] (**4**) crystallised in a monoclinic system with the space group $P2_1/c$, containing two symmetry independent molecules in the asymmetric unit. All data are consistent with the structure previously reported.

Intermolecular hydrogen bonding is observed between the secondary amine hydrogens and the chlorido ligands of complexes stacked vertically in the structure (2.35 Å, Figure 3.2, A). Additionally, the hydroxyl groups are involved in a chain of hydrogen bonds (1.86 Å, Figure 3.2, B), and do not participate in intermolecular interactions with any other groups.

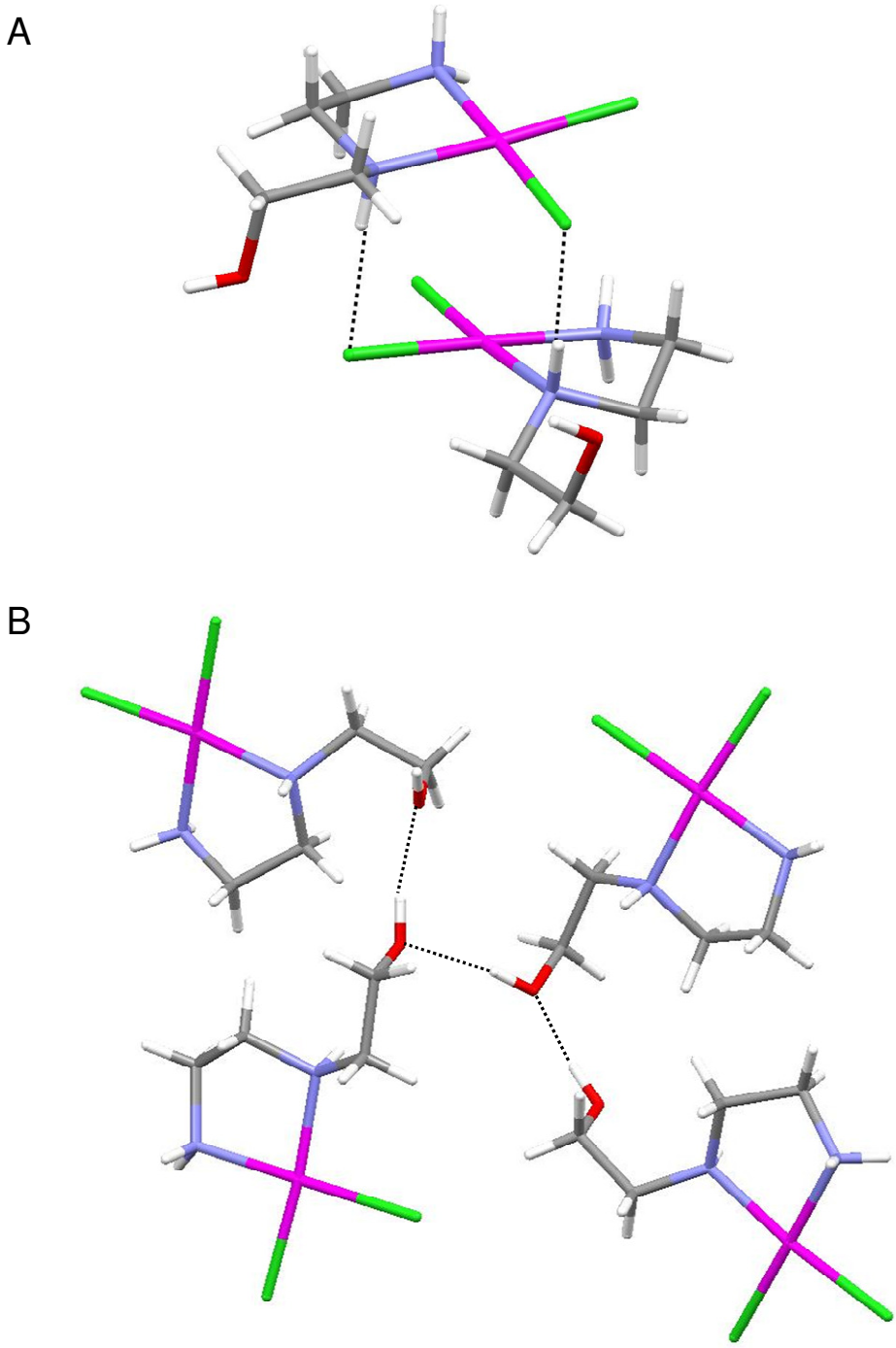

Figure 3.2 A: Intermolecular hydrogen bonding between the secondary amine hydrogens and the chlorido ligands of [Pt(L1)Cl_2] (**4**). B: Hydrogen bonding between the alcohol groups of neighbouring complexes, forming an extended chain.

The structure of $[Pt(L1)(N_3)_2]$ (**5**) is shown in Figure 3.3. This complex also crystallised in the monoclinic system, but with the space group $P2_1/n$. Unlike in the case of **4** there is only one molecule in the asymmetric unit, although four are present in the unit cell. Further crystallographic data and solution refinements are given in Table 3.1.

Table 3.1 Crystallographic data and solution refinements for $[Pt(L1)(N_3)_2]$ (**5**).

Parameters	$[Pt(L1)(N_3)_2]$ (**5**)
Formula	$C_4H_{12}N_8OPt$
Formula Weight	383.31
Crystal Character	Yellow block
Crystal Size (mm)	0.20 x 0.02 x 0.02
Crystal System	Monoclinic
Space Group	$P2_1/n$
Unit Cell Dimensions	a = 8.3389(2), b = 7.9447(2)
	c = 15.2700(4) Å
	α = 90, β = 104.578(2), γ = 90˚
Z	4
Density, calculated (mgM^{-3})	2.600
F(000)	712
Goodness of fit on F^2	0.876
Conventional R	0.0175
Weighted R	0.0260

Selected bond lengths and angles are listed in Table 3.2, with the numbering scheme corresponding to that in Figure 3.3.

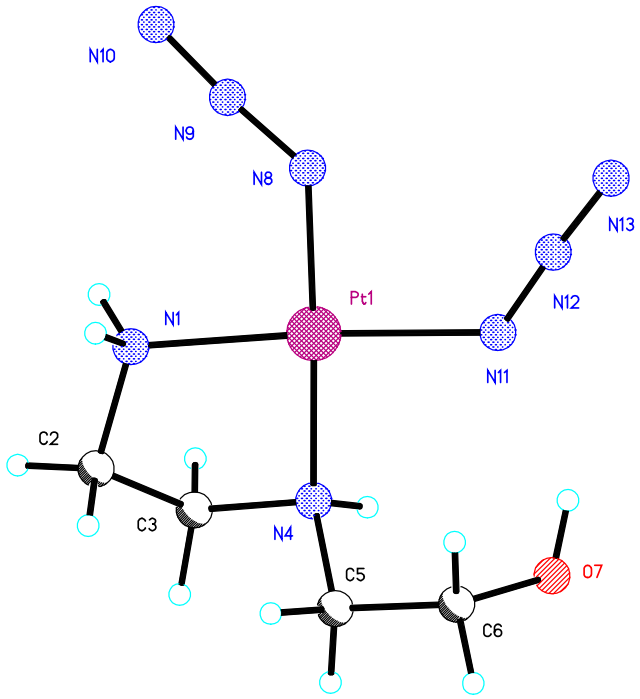

Figure 3.3 X-ray structure and atom numbering scheme for [Pt(L1)(N_3)$_2$] (**5**).

Table 3.2 Selected bond lengths and angles for [Pt(L1)(N_3)$_2$] (**5**).

Bond	Magnitude (Å)	Angle	Magnitude (°)
Pt(1)–N(1)	2.034(3)	N(1)–Pt(1)–N(8)	93.95(11)
Pt(1)–N(4)	2.052(3)	N(1)–Pt(1)–N(11)	175.15(11)
Pt(1)–N(8)	2.035(3)	N(8)–Pt(1)–N(11)	90.77(11)
Pt(1)–N(11)	2.036(2)	N(1)–Pt(1)–N(4)	84.07(11)
N(8)–N(9)	1.221(3)	N(8)–Pt(1)–N(4)	177.99(10)
N(9)–N(10)	1.151(3)	N(11)–Pt(1)–N(4)	91.22(10)
N(11)–N(12)	1.214(3)	N(10)–N(9)–N(8)	175.2(3)
N(12)–N(13)	1.148(3)	N(13)–N(12)–N(11)	176.4(3)
		N(9)–N(8)–Pt(1)	119.6(2)
		N(12)–N(11)–Pt(1)	121.6(2)

The bond lengths are similar to those of previously reported Pt^{II} azido complexes.[22,31] The Pt(1)–N(8) and Pt(1)–N(11) bond lengths, 2.035 and 2.036 Å respectively, are significantly shorter than the analogous Pt–Cl bonds of **4** (2.309 and 2.320 Å); consistent with the fact that azide is a stronger donor ligand towards platinum than is chloride. However, comparing the platinum-amine nitrogen bond lengths, there are no significant differences between complexes **4** and **5**.

The structure of the coordinated azido group can be described as a resonance hybrid in which the bond between bound (α) and central (β) nitrogens has a lower bond order than that between central and terminal (γ). This is reflected by the longer length of the N_α–N_β bonds compared with N_β–N_γ, for example N(8)–N(9) at 1.221 Å, and N(9)–N(10) at 1.151 Å. The azido ligands show N_α–N_β–N_γ angles of 175˚ and 176˚ and as such are essentially linear. The Pt–N_α–N_β angles of 119.6˚ and 121.6˚ are also comparable with those reported for similar Pt^{II} azido complexes.[22,31]

The geometry around platinum is essentially square planar, with the N(8)-Pt(1)-N(11) angle at 90.77˚. The N(1)–Pt(1)–N(4) angle formed within the chelate ring is 84.07˚, smaller than that in the related ethylenediamine complex, which was determined as 95.7˚.[22]

The molecules form many inter- and intramolecular short contacts, more so than those of the chlorido analogue due to the involvement of the azido nitrogens. Of particular interest is an intramolecular hydrogen bond (2.04 Å) between the H of the hydroxyl group and a bound azido nitrogen (Figure 3.4). There is also an intermolecular hydrogen bond (2.05 Å) between a hydrogen of the primary amino group and the hydroxyl oxygen of a neighbouring molecule. Unlike in the chlorido analogue, the hydroxyl groups do not form intermolecular contacts with each other. The nitrogens of the azido groups also form several longer-range intermolecular contacts, involving the primary and secondary amino groups on adjacent molecules.

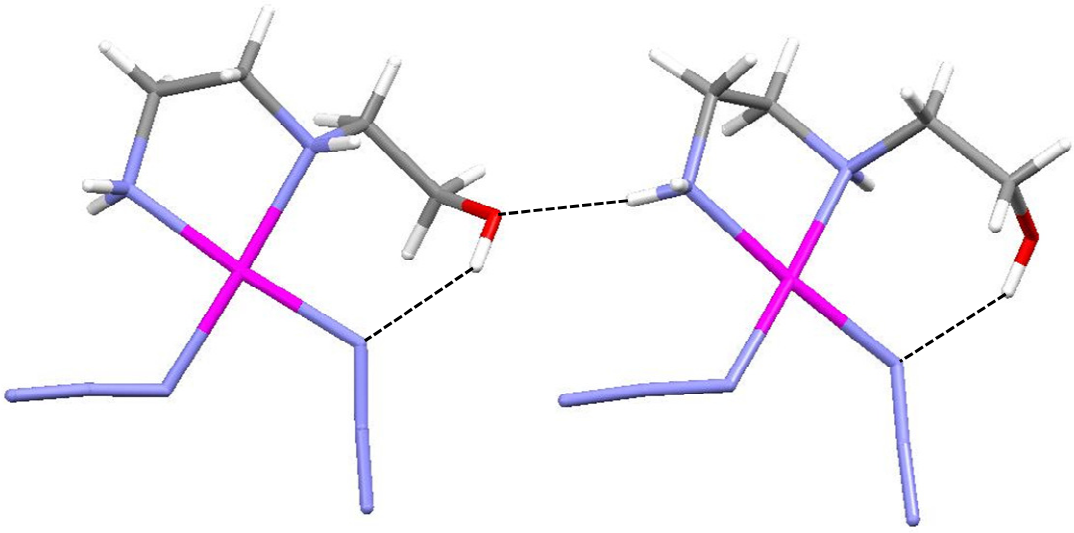

Figure 3.4 Inter- and intramolecular hydrogen bonds formed by $[Pt(L1)(N_3)_2]$ (**5**)

3.3.1.1.5 ^{1}H NMR Spectroscopy

^{1}H NMR experiments were carried out in DMSO-d_6 for all complexes, since spectra generally showed greater clarity in this solvent than in aqueous solutions, where many peaks were found to overlap.

There are several notable features of the spectra of these complexes, which shall be discussed with reference to complexes of L1. Firstly, although peaks resulting from exchangeable protons are typically broad, that of the OH proton is very sharp and presents as a triplet. Evidence for the assignment of this peak is provided by 2D [^{1}H, ^{1}H] COSY NMR experiments, in which cross peaks are seen with the adjacent methylene protons. A D_2O shake results in the disappearance of this peak, confirming it arises from an exchangeable proton. A previous study of $[Pt(L1)Cl_2]$ (**4**) reports this signal to be sharper than those of the amino protons, although it is stated to be a singlet and the spectrum is not shown.[17]

Additionally, as DMSO is a very good ligand, Pt^{II}–Cl bonds readily undergo exchange of the chlorido ligands for this solvent over time.[19] In the case of **4**, the

mono- and bis-DMSO adducts, $[Pt(L1)(DMSO)Cl]^+$ and $[Pt(L1)(DMSO)_2]^{2+}$, are believed to be formed. It is interesting to note that exchange results in a significant shift of the OH peak despite its remoteness from the Pt^{II} centre (Figure 3.5).

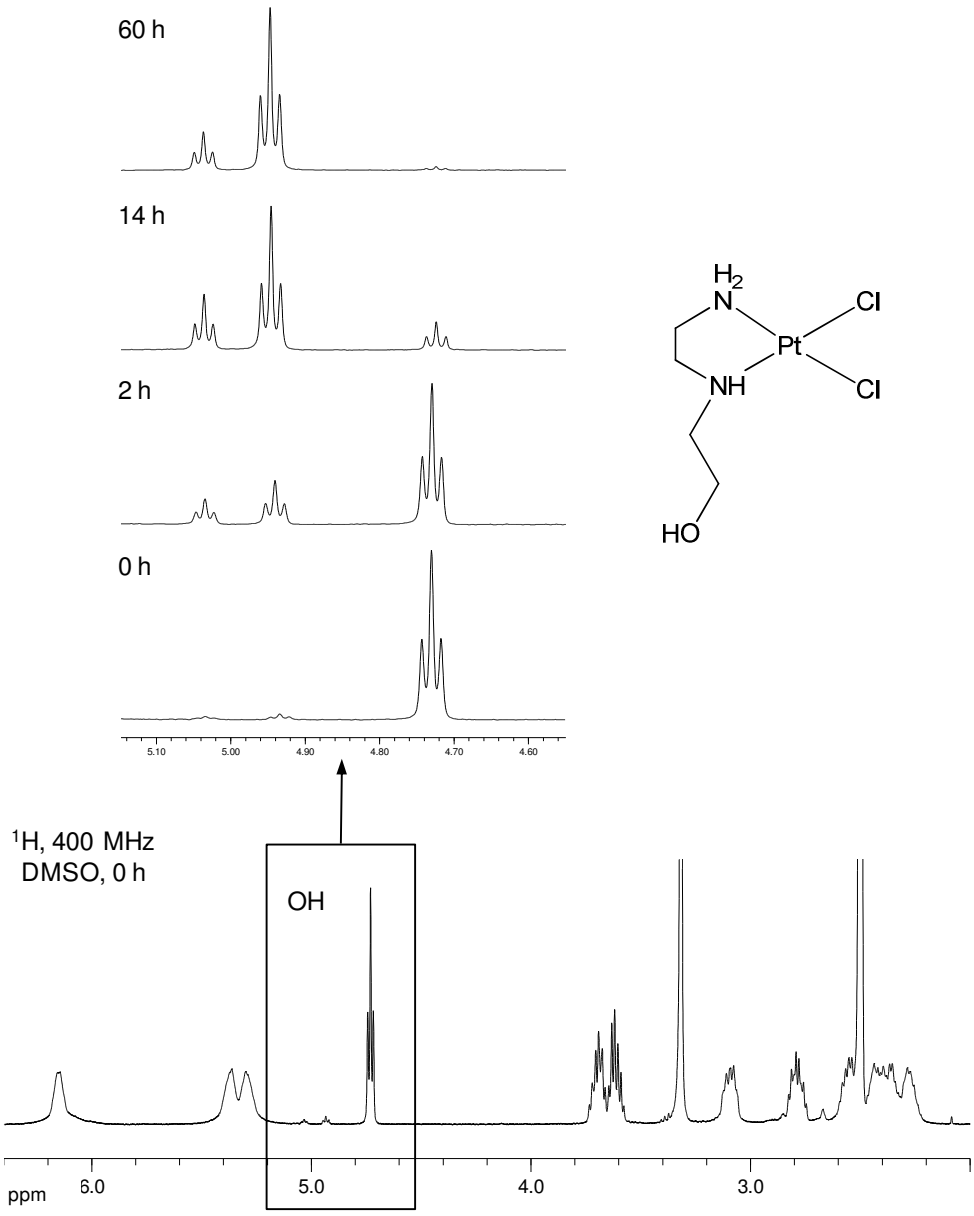

Figure 3.5 ^{1}H NMR spectra of $[Pt(L1)Cl_2]$ (**4**) over time in DMSO-d_6, illustrating the sharp nature of the OH peak, and its significant shift upon exchange of the chlorido ligands for DMSO.

The spectra also reveal the inequivalence of the protons within each methylene pair. At a high magnetic field, it is possible to observe an individual peak for each of the eight methylene protons of [Pt(L1)(N_3)$_2$(OAc)$_2$] (**6**). Through 2D [^{1}H, ^{1}H] COSY and NOESY experiments, these peaks were assigned as shown in Figure 3.6. The two axial acetato groups of this complex are also inequivalent, and their protons give rise to two singlets of equal intensity at 2.00 and 1.99 ppm.

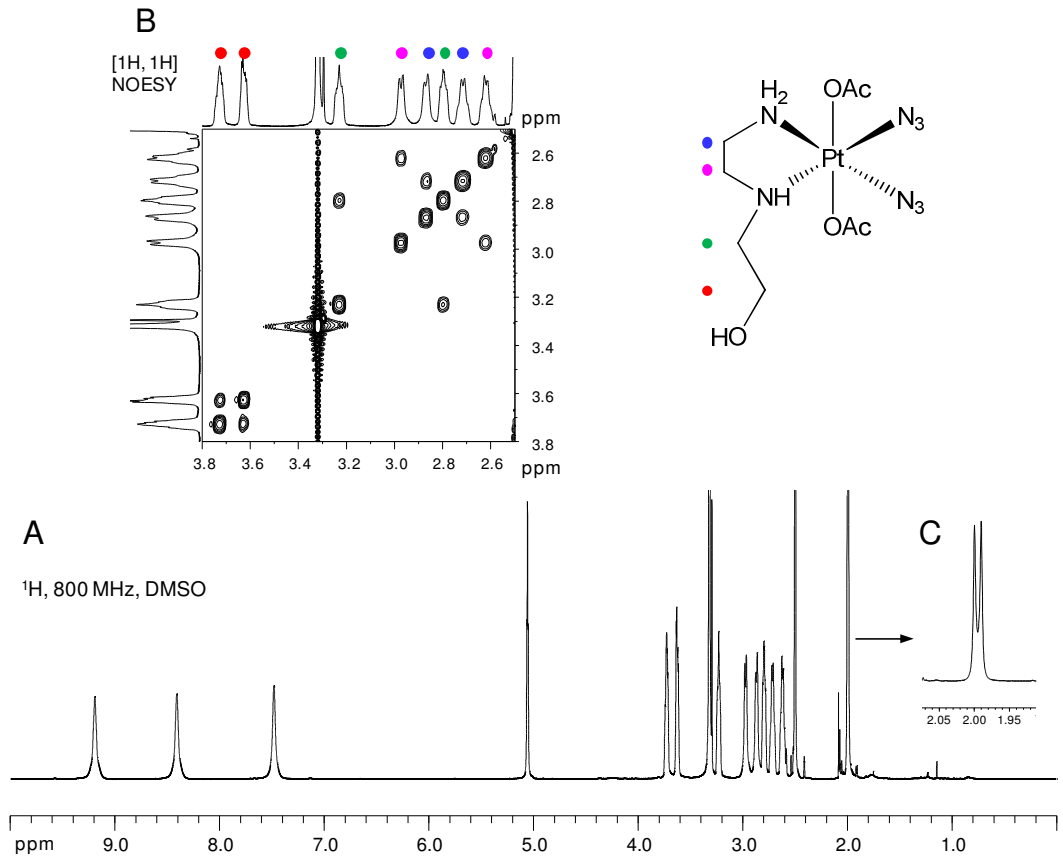

Figure 3.6 A: The ^{1}H NMR spectrum of [Pt(L1)(N_3)$_2$(OAc)$_2$], B: The aliphatic region of the 2D [^{1}H, ^{1}H] NOESY spectrum, showing the assignment of the eight methylene protons. C: The two singlets arise from each inequivalent acetato group.

3.3.1.1.6 UV-Vis and Fluorescence Spectroscopy of 2-[(2-pyridinylmethyl)amino]ethanol (L4)

2-[(2-Pyridinylmethyl)amino]ethanol, (L4), was found to display yellow-white fluorescence upon excitation with UVA light. Emission spectra were recorded in water, with excitation at two different wavelengths (278 nm and 365 nm), with a different emission profile resulting from each.

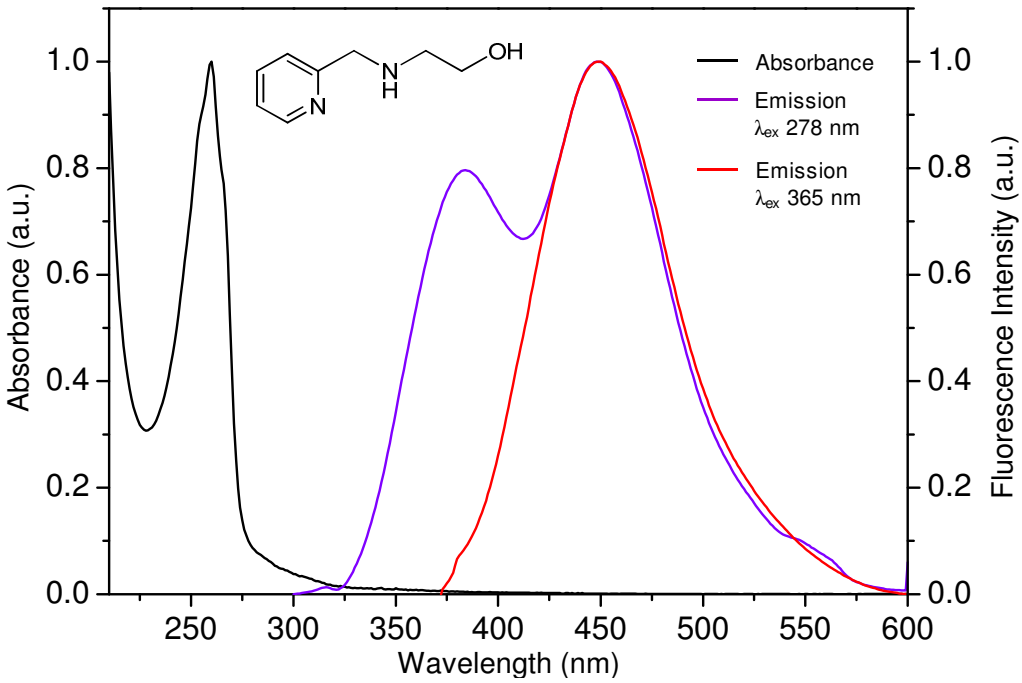

Figure 3.7 Normalised absorption and emission spectra of **L4** in water.

The Pt^{II} chlorido complex of this ligand, $[Pt(L4)Cl_2]$ (**12**), displayed orange fluorescence in the solid state when placed under a UVA light source. However, upon dissolution this fluorescence appeared to be quenched, and emission spectra recorded in water and DMF, again with excitation at 278 nm and 365 nm, revealed the complex to be non-emissive in solution.

3.3.1.2 Platinum Complexes Containing a Protected Amine Group

In addition to complexes containing a pendant hydroxyl group, those containing a protected amine were also investigated. Pt^{II} chlorido and azido complexes, and the Pt^{IV} azido derivative, of the ligand *N-tert*-butoxycarbonyl-1,4-diaminobutane (L5) were prepared according to the scheme below. $K[Pt(NH_3)Cl_3]$[20] and L5[21] were synthesised as previously reported.

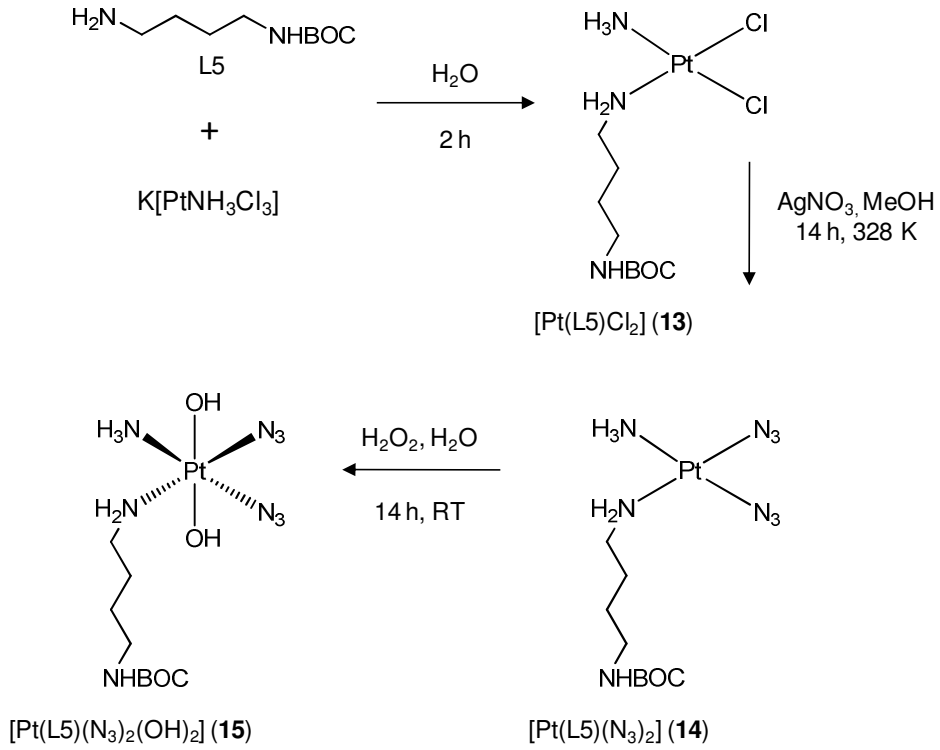

Scheme 3.4 The synthetic route to a Pt^{IV} complex containing a BOC-protected amine.

The mixed amine Pt^{II} chlorido complex **13** was prepared in moderate yield using an excess of L5, and recrystallised where necessary from 0.1 M NaCl. The azido complex **14** was prepared *via* a silver nitrate abstraction of the chlorido ligands, in a similar manner to that reported in Scheme 3.2. However yields were relatively

low as, despite a number of attempts using various conditions, this reaction frequently resulted in the formation of a grey-black solid believed to be Pt^0.

Oxidation to the Pt^{IV} complex was achieved through the use of hydrogen peroxide in aqueous solution, although again was low-yielding due to the formation of a similar dark precipitate. All complexes were characterised by ^1H NMR spectroscopy and, in the case of complex **13**, by CHN analysis.

3.3.2 Stability Studies

3.3.2.1 Stability in Aqueous Solutions

Solutions of **2** and **5** (1.5 mM), and **3** and **6** (3 mM), were prepared in 90% H_2O/10% D_2O, with 0.1 % dioxane (δ = 3.75 ppm) added as an internal calibrant. ^1H NMR spectra were acquired after 0 h, 6 h, 12 h, 24 h, 48 h, 72 h, 5 d, 7 d, 13 d, 22 d and 50 d. Samples were stored at 310 K in the dark between measurements.

a) $[Pt(en)(N_3)_2]$ (**2**)

This complex was found to undergo a degree of oxidation in aqueous solution, forming a Pt^{IV} species identified as $[Pt(en)(N_3)_2(OH)_2]$ (**3**).

Small amounts of this new species were apparent after 6 h, with a new peak at 2.93 ppm accounting for 1% of the total signal in this region. The proportion grew steadily, reaching around 17% after 7 d, after which no further increase was seen. Evidence for the identity of this species was given from comparisons of the chemical shift and coupling constant with those of an authentic sample of **3**.

Quantification of **3** was hindered by the appearance of a broad peak in the spectrum at 72 h, centred around 2.84 ppm, which continued to grow throughout the remainder of the experiment, indicating multiple new species which could not be identified.

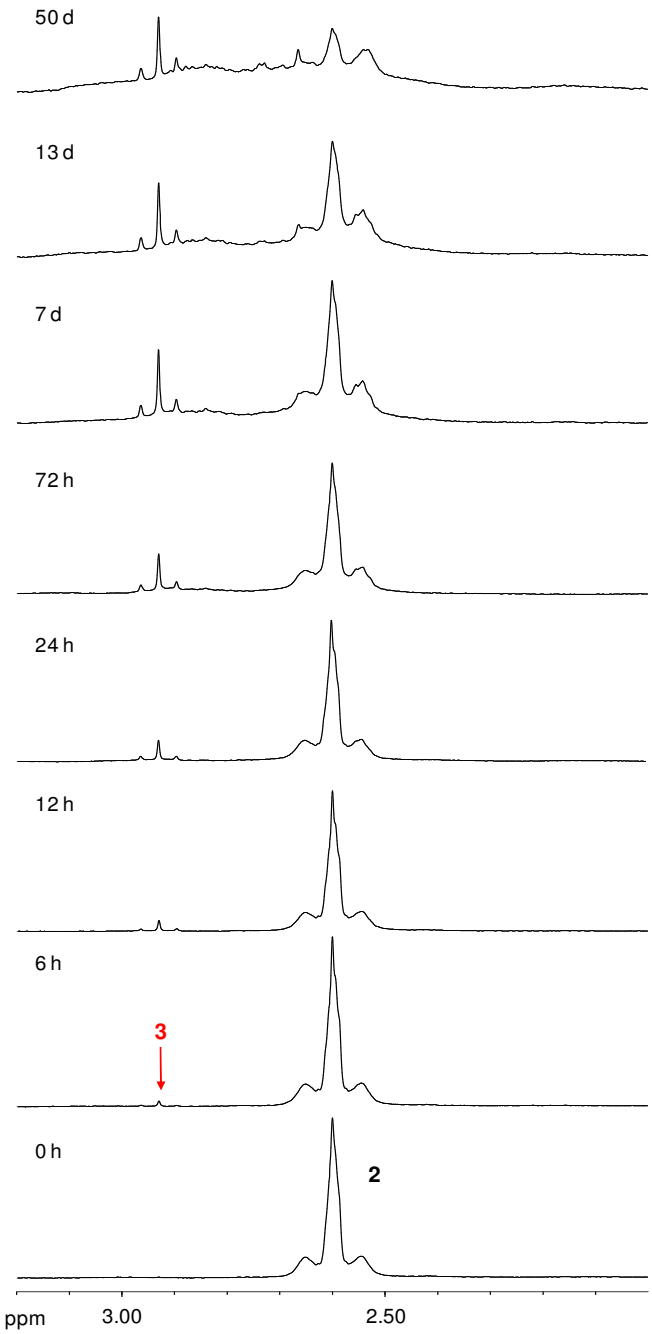

Figure 3.8 ^{1}H NMR spectra of [Pt(en)(N_3)$_2$] (**2**) at various time intervals in aqueous solution, showing formation of the oxidised species [Pt(en)(N_3)$_2$(OH)$_2$] (**3**).

To further investigate the formation of **3**, the experiment was repeated with a degassed sample of $[Pt(en)(N_3)_2]$ (**2**). Oxidation occurred to a lesser extent, with the peak of **3** comprising <5% of the total en-CH_2 signal intensity after 5 d, compared with 15% in the non-degassed sample over the same time period. Evidence of an oxidised product was also found in the spectra of 100 mM NaCl solutions of $[Pt(en)Cl_2]$ (**1**), the signal for which comprised 7% of the total after 5 d. However, despite firm NMR evidence of a Pt^{IV} species, attempts to detect such a complex by mass spectrometry were unsuccessful.

b) $[Pt(en)(N_3)_2(OH)_2]$ (**3**)

The spectrum remained unchanged throughout the course of the 50-day experiment, implying that **3** is stable under these conditions. This is in accordance with previous findings for similar Pt^{IV} azido complexes.[22,31]

c) $[Pt(L1)(N_3)_2]$ (**5**)

Evidence for the formation of new product(s) is seen, however these cannot be readily assigned.

Due to the inequivalence of the eight methylene protons of this complex, the spectrum of **5** in aqueous solutions is inherently more complicated than that of $[Pt(en)(N_3)_2]$ (**2**), rendering any formation of new species harder to follow. After 6 h, two new doublets appeared at 3.48 and 3.51 ppm and increased in intensity until around 48 h, comprising around 10% of the total species. Although it was not possible to identify these peaks, they may result from a hydrolysis product, or a Pt^{IV} species should the complex undergo oxidation as in the case of **2**. Throughout the remainder of the NMR spectrum, a loss of signal resolution and intensity over time indicated the formation of multiple species, which could not be readily assigned.

d) $[Pt(L1)(N_3)_2(OAc)_2]$ (**6**)

Free acetate was released from this complex over time, with a concurrent decrease in pH from 7.92 to 5.03.

A small amount of free acetate (2% of the total acetate signal) was present in the initial spectrum; however the proportion increased to a total of 7% after 50 d. Associated with the decrease in pH was an increase in the chemical shift of free acetate (from 1.90 to 1.97 ppm), and the appearance of peaks corresponding to the amine protons. This is consistent with a previous investigation of the NMR spectra of **3** at various pH values, which found the NH_2 protons to be visible only at pH values below 6.[22] The remainder of the spectrum showed little change throughout the experiment, with a small loss of resolution over time.

3.3.2.2 Stability Towards Chloride

Solutions of **2** and **5** (1.5 mM), and **3** and **6** (3 mM), were prepared in 90% H_2O/10% D_2O containing 100 mM NaCl, with 0.1% dioxane added as an internal calibrant. ^1H NMR spectra were acquired after 0 h, 6 h, 12 h, 24 h, 48 h, 72 h, 5 d, 7 d, 13 d, 22 d and 50 d. Samples were stored at 310 K in the dark between measurements.

a) $[Pt(en)(N_3)_2]$ (**2**)

As in the case of aqueous solutions, this complex was found to undergo oxidation to form a Pt^{IV} species.

The rate and extent of oxidation was found to be similar to that in aqueous solution (14% oxidised species after 7 d), with other changes to the spectrum also similar. The oxidised product was again assumed to be $[Pt(en)(N_3)_2(OH)_2]$ (**3**); it is unlikely that Cl^- could replace an axial hydroxyl group, and such Pt^{IV} azido complexes have previously been found stable to 100 mM NaCl solutions.

c) $[Pt(en)(N_3)_2(OH)_2]$ (**3**)

The spectrum remained unchanged throughout the course of the 50-day experiment, implying that **3** is stable under these conditions. Again, this is in agreement with previous findings for similar complexes.[22,31]

b) $[Pt(L1)(N_3)_2]$ (**5**)

The spectral changes were very similar to those seen for the complex in aqueous solutions, with two new doublets appearing at 3.48 and 3.51 ppm after 6 h, and an overall loss of signal resolution over time.

d) $[Pt(L1)(N_3)_2(OAc)_2]$ (**6**)

Free acetate was again released from this complex over time, with a decrease in pH from 7.84 to 5.42.

The proportion of free acetate again increased from around 2% to 7% over the course of the experiment. The pH change was smaller in this case, resulting in a smaller downfield shift of the free acetate peak (1.90 to 1.93 ppm). Again, peaks corresponding to the amine protons became more visible with the decrease in pH.

3.3.3 Reactions with Glutathione and 5'-GMP

3.3.3.1 Reactions with Glutathione

Samples of $[Pt(en)(N_3)_2]$ (**2**) (1.5 mM) and $[Pt(L1)(N_3)_2(OAc)_2]$ (**6**) (3 mM) were prepared in D_2O, with 2 μL of a 1% acetone solution (δ = 2.22 ppm) added as an internal calibrant. A solution of reduced glutathione (GSH) was degassed under nitrogen, the pH* was altered to 7.0–7.2 with NaOD, degassing was repeated and 2 mol equivalents were added to each sample. The pH* of the samples was then re-recorded as 7.50 and 7.12 respectively, and the samples briefly degassed once more in the NMR tube. ^{1}H NMR spectra were acquired after 0 h, 3 h, 6 h, 12 h, 24 h, 48 h, 72 h, 5 d, 9 d and 16 d. Samples were stored at 310 K in the dark between measurements.

a) $[Pt(en)(N_3)_2]$ (**2**)

Evidence of multiple species was seen, including the sulfur-bridged complex $[\{Pt(en)(\mu_2\text{-}SG)\}_2]^{2+}$.

After 3 h, a new peak was apparent at 2.74 ppm (**2a**). As the en-CH_2 peak (2.60 ppm) was found to overlap with a glutathione resonance, reliable integration was not possible, although the new peak increased in intensity over time with concomitant decrease of the en-CH_2 resonance. This likely corresponds to the monoadduct $[Pt(en)(N_3)(SG)]$. After 48 h a broad peak dominated this region of the spectrum, and much signal intensity in this region was lost thereafter, indicating formation of multiple products. After 12 h, a new peak appeared at 3.36 ppm which increased in intensity throughout the remainder of the experiment (Figure 3.9). This may arise from the cys-β CH_2 protons of a stable Pt-GSH complex (**2b**). Two small doublets at 3.28 and 3.31 ppm, visible after 3 h, arise from a small quantity of oxidised glutathione (GSSG), likely oxidised by air. The pH decreased from 7.50 to 6.68 during the course of the experiment.

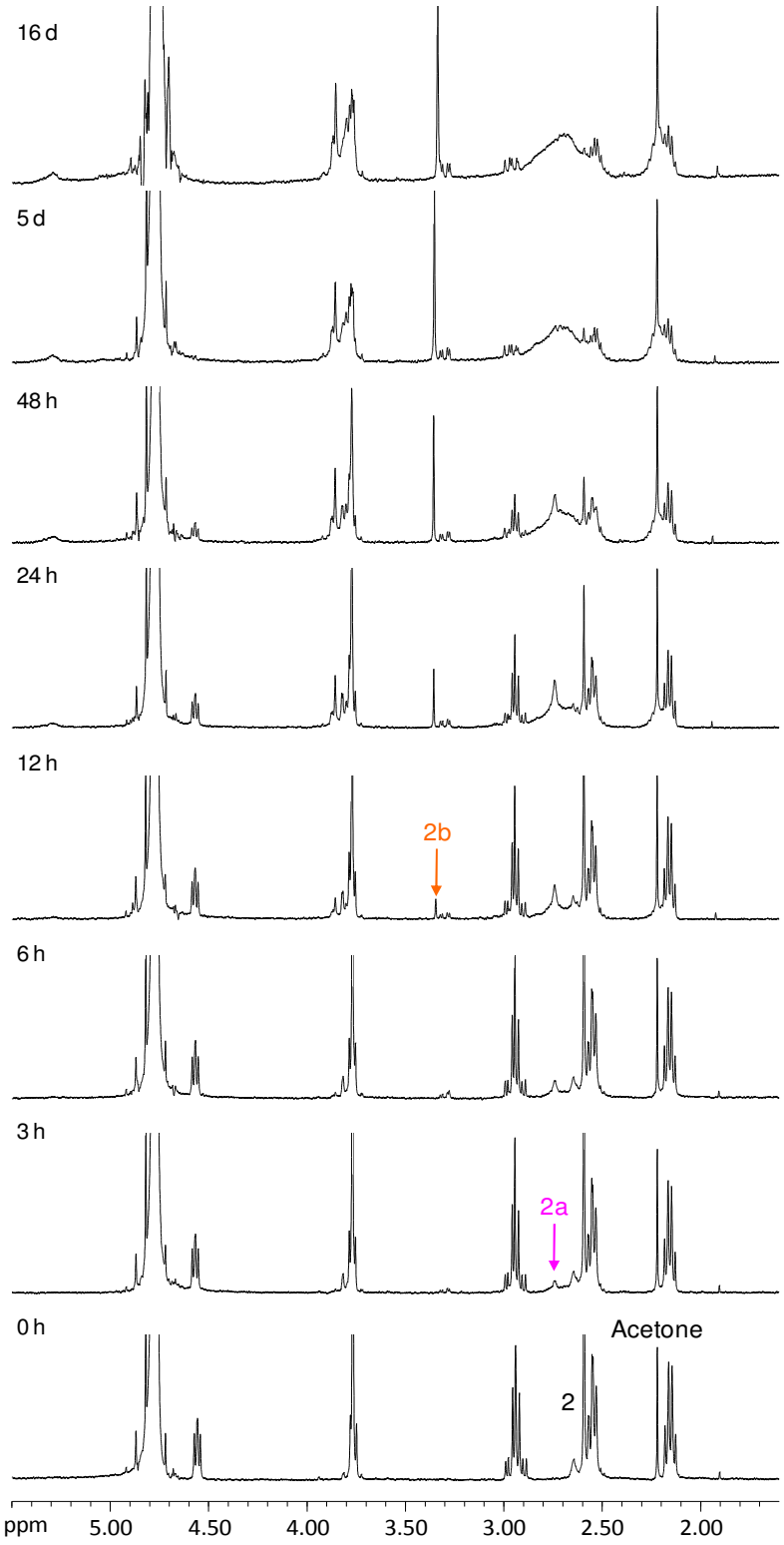

Figure 3.9 ^{1}H NMR spectra recorded at various intervals during the reaction of [Pt(en)(N_3)$_2$] (**2**) with glutathione.

A mass spectrum of the solution showed a peak at *m/z* 561, corresponding to the sulfur-bridged dimer $[\{Pt(en)(\mu_2\text{-}SG)\}_2]^{2+}$, typically the major product of the reaction of glutathione with diam(m)inoplatinum^{II} complexes.[23]

b) $[Pt(L1)(N_3)_2(OAc)_2]$ (**6**)

Little reduction of **6** was seen throughout the course of the reaction with glutathione.

Changes in the spectra were difficult to identify and quantify, since the spectra of both oxidised and reduced glutathione, and Pt^{IV} and Pt^{II} complexes of L1, contained overlapping peaks. However, the appearance of two doublets at 3.28 and 3.31 ppm clearly indicated formation of oxidised glutathione (GSSG). First apparent at 3 h, these peaks increased in intensity slightly throughout the experiment, however their reliable quantification was not possible. It is easier to follow the fate of the Pt^{IV} complex by monitoring the peak of free acetate, which is released upon reduction. Although there was an increase in intensity of this peak (from 2% to 6% of the total acetate region), the magnitude was similar to that seen for the complex alone in aqueous solutions, indicating little reduction had taken place. In the remainder of the spectrum, slight changes to peak shapes were apparent after 5 days, indicative of new species. The pH* was also found to decrease from 7.12 to 5.54.

A mass spectrum of this solution at the end of the experiment revealed peaks corresponding to reduced glutathione at *m/z* 307.08 $[M]^+$, and complex **6** at 524.09 $[M + Na]^+$, with no other platinum containing species found.

3.3.3.2 Reactions with 5'-GMP

Samples of $[Pt(en)(N_3)_2]$ (**2**) (1.5 mM) and $[Pt(L1)(N_3)_2(OAc)_2]$ (**6**) (3 mM) were prepared in D_2O with 2 µL of 1% dioxane added as an internal calibrant. 2 mol equivalents of 5-guanosine monophosphate (5'-GMP) were added to each sample,

and the pH* of the samples was then adjusted to 5.5–5.7 with NaOD. ^{1}H NMR spectra were acquired after 0 h, 3 h, 6 h, 12 h, 24 h, 48 h, 72 h, 5 d, 9 d and 16 d. Samples were stored at 310 K in the dark between measurements.

The interaction of platinum complexes with guanine typically occurs *via* binding to N7,[24] and is followed by the change in chemical shift of the H8 proton. However, this proton can undergo exchange for deuterium over time in D_2O,[25] a process which appears to be accelerated upon platinum binding,[26] and hinders its reliable quantification. To estimate for how long integration of these peaks is reliable, the total integral of the H8 region was compared with that of a non-exchangeable proton, H1', over time. Good agreement was found until 24 hours, after which values differed by >10%, therefore integrals of the H8 region were deemed unreliable after this point and quantification was based, in the case of **2**, on the en-CH_2 peaks.

a) $[Pt(en)(N_3)_2]$ (**2**)

Formation of a 5'-GMP monoadduct was evident after 3h, with detection of the bisadduct at 24 h. Mass spectral evidence of the latter species was obtained. Significant oxidation of **2** was also found.

After three hours a new peak at 8.60 ppm was apparent, the low-field shift of the H8 proton consistent with platinum binding to N7 of 5'-GMP. An additional peak was also present in the aliphatic region at 2.70 ppm arising from the en-CH_2 protons. Both were attributed to a monoadduct of 5'-GMP (**2c**), comprising 12% of the total platinum species after 3h and rising to 17% after 12 h.

After 24 h there was evidence of a new product, assigned as the bisadduct $[Pt(en)(5'\text{-GMP-}N7)_2]^{2+}$ (**2d**) comprising 6.5% of the detectable platinum species. In the H8 region, the new peak (8.57 ppm) showed a characteristic upfield shift from that of the monoadduct,[27] but in the aliphatic region a downfield shift was seen (2.82 ppm). Throughout the remainder of the experiment the proportions of both mono- and bisadducts increased at the expense of $[Pt(en)(N_3)_2]$. However,

whilst the monoadduct appeared to stabilise at 25% after 5 days, the proportion of bisadduct continued to increase, reaching 41% after 16 days (Figures 3.10 and 3.11). Evidence of the bisadduct was provided by mass spectrometry, showing a peak at *m/z* 490.58 $[M]^{2+}$.

A significant amount of a Pt^{IV} species, presumably $[Pt(en)(N_3)_2(OH)_2]$ (**3**), was also formed, as found in the aqueous stability studies. After 24 h this comprised 13% of all platinum species detected, rising to 15% after 16 d. A graph showing the speciation over time can be found in Figure 3.10.

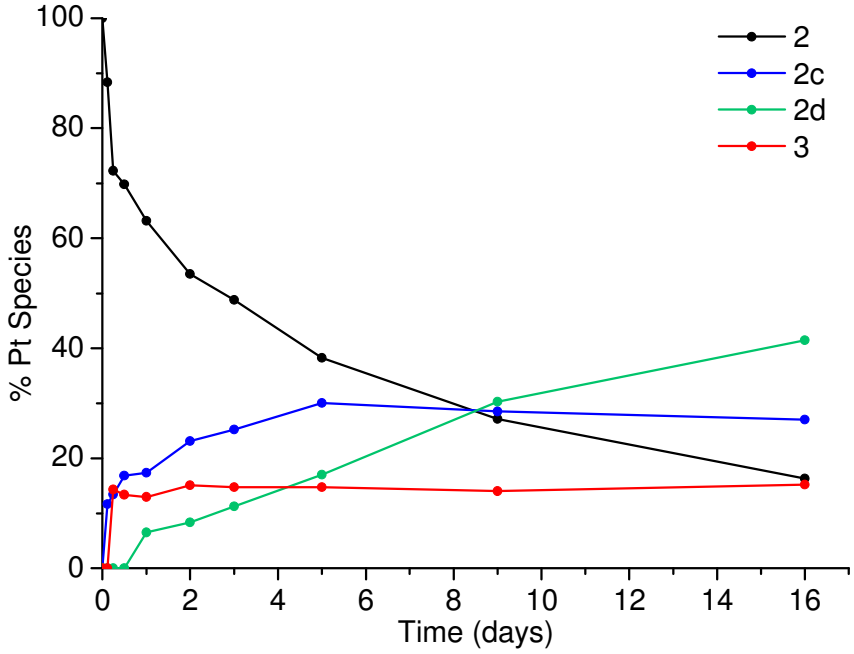

Figure 3.10 The speciation over time during the reaction of **2** with 5'-GMP. **2** $[Pt(en)(N_3)_2]$, **2c** $[Pt(en)(N_3)(5'\text{-GMP-}N7)]^+$, **2d** $[Pt(en)(5'\text{-GMP-}N7)_2]^{2+}$ and **3** $[Pt(en)(N_3)_2(OH)_2]$

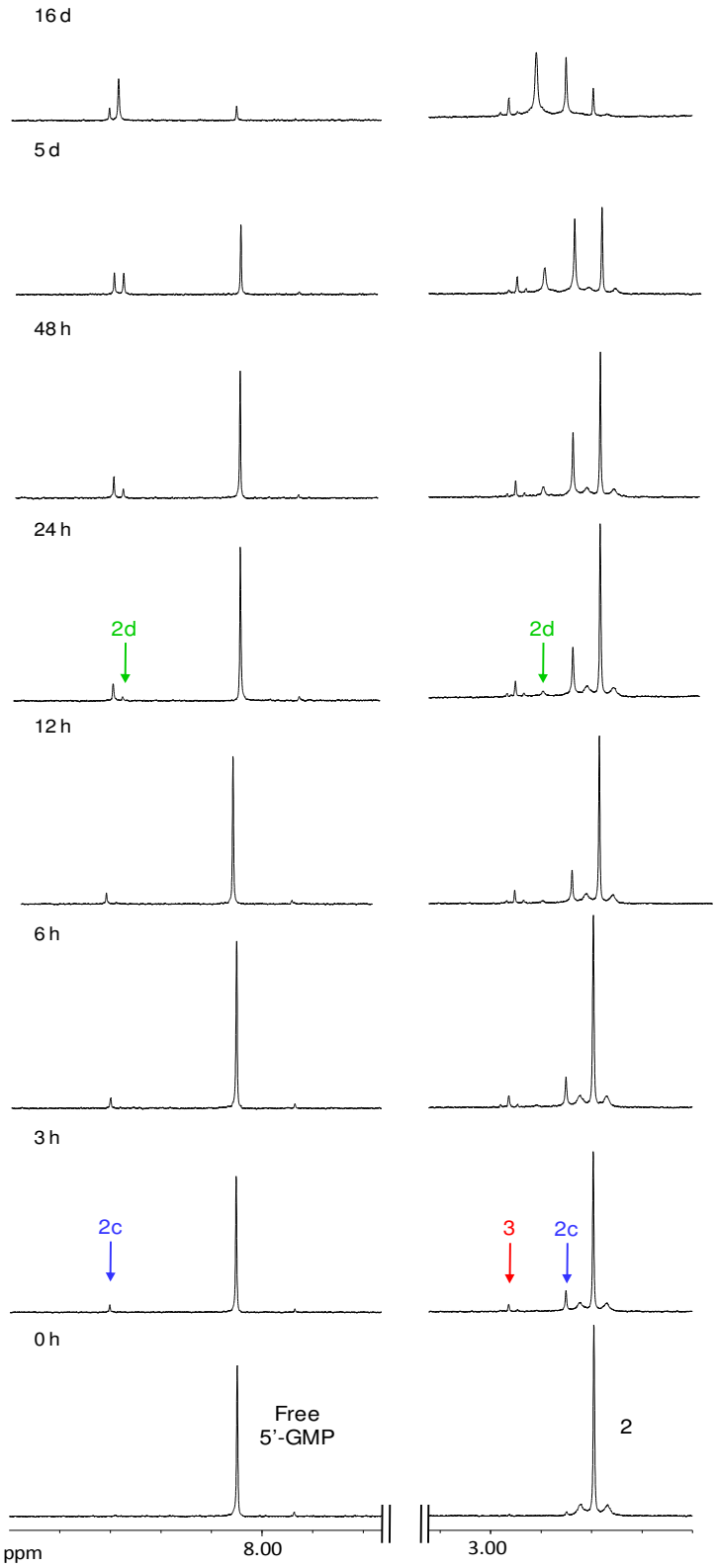

Figure 3.11 Selected regions of the ^{1}H NMR spectra recorded at various timepoints during the reaction of [Pt(en)(N_3)$_2$] (**2**) with 5'-GMP.

b) $[Pt(L1)(N_3)_2(OAc)_2]$ (**6**)

There were no changes in the ^1H NMR spectrum over a period of 16 days, indicating no reaction between complex **6** and 5'-GMP under these conditions.

3.3.3.3 Stability of Pt^{II} Azido Complexes to Ambient Laboratory Lighting

An initial aim of this work was to test a series of Pt^{II} azido complexes for cytotoxic activity against a human cancer cell line. However, these tests are performed in a standard cell culture laboratory with no control over light levels, and many metal azido complexes are known to be photoactive.[8] It was therefore necessary to test the stability of the complexes synthesised under ambient lighting conditions, to which solutions are exposed for approximately twenty minutes during the testing procedure.

Light levels were monitored with a power meter inside the fume hood in which cell testing is carried out, and found to be 0.27 $\mu W/cm^2$ for UV and 950 $\mu W/cm^2$ for visible. Solutions of $[Pt(en)(N_3)_2]$ (**2**) and $[Pt(L1)(N_3)_2]$ (**5**) were prepared and an initial ^1H NMR spectrum acquired. The samples were left in an area of the laboratory with stronger light levels (0.40 $\mu W\ cm^{-2}$ UV and 1150 $\mu W\ cm^{-2}$ visible) and for a longer time period (60 min) than they would experience during testing, after which a final ^1H NMR spectrum was acquired.

No change was detectable in the spectra of either complex following the experiment, suggesting negligible decomposition under these light conditions. Therefore it was concluded that these cytotoxicity experiments are appropriate for this class of complexes. The Pt^{IV} azido complexes were not tested in this way. Their high sensitivity to light, particularly in the presence of biomolecules,[2] plus their sole intended use as photoactivated agents, renders them suitable for controlled phototoxicity testing only.

3.3.4 Cytotoxicity

Several Pt^{II} complexes were tested for cytotoxicity against the A2780 human ovarian cancer cell line. Both Pt^{II} chlorido and azido complexes of each ligand were tested, to investigate the differences upon the change of leaving group.

Table 3.3 IC_{50} values of several Pt^{II} complexes synthesised in this work, against the A2780 human ovarian cancer cell line. The value for cisplatin is included for comparison.

Complex	IC_{50} / μM (A2780)[a]
$[Pt(en)Cl_2]$ (**1**)	3.4
$[Pt(en)(N_3)_2]$ (**2**)	33
$[Pt(L1)Cl_2]$ (**4**)	11
$[Pt(L1)(N_3)_2]$ (**5**)	31
$[Pt(L2)Cl_2]$ (**7**)	11
$[Pt(L2)(N_3)_2]$ (**8**)	47
$[Pt(L3)I_2]$ (**9**)	>100
$[Pt(L3)Cl_2]$ (**10**)	3.3
$[Pt(L3)(N_3)_2]$ (**11**)	21
$[Pt(L4)Cl_2]$ (**12**)	27
Cisplatin	1.3

[a] The IC_{50} value is defined as the concentration required to achieve 50% growth inhibition

All of the Pt^{II} chlorido complexes showed good to moderate cytotoxicity in these tests. The high activity of complexes **1** and **10** is consistent with previous literature reports,[9,28] as is slightly lower activity for complex **4**,[11,18] containing a pendant hydroxyl group. Extending the linker to this hydroxyl group from 2 to 3 carbons apparently has no effect on the cytotoxicity, since the same IC_{50} values are found for complex **4** and the new complex **7**. The previously unreported complex **12**, containing a pyridine ring, shows lower toxicity than the other Pt^{II} chlorido complexes tested.

The Pt^{II} iodido complex, **9**, has an IC_{50} value greater than 100 μM and is therefore deemed inactive; this is consistent with previous findings of such complexes.[3]

It is interesting to note that all of the Pt^{II} azido complexes were moderately cytotoxic at the concentrations tested. From the initial data of this small sample, it appears there is little correlation between the cytotoxicity of the Pt^{II} chlorido complexes and their azido analogues, however this would need to be further investigated with a wider range of complexes.

3.3.5 Photoreactions

The photoactivity of Pt^{II} azido complexes is well documented.[8] It is therefore of interest to explore the photoreactions of the complexes produced in this work, especially with regard to their potential phototoxicity. The light sources and power levels were as described in section 3.2.3.4.

3.3.5.1 Photoreactions of Pt^{II} Chlorido Complexes

Saturated solutions of [Pt(en)Cl_2] (**1**) and [Pt(L1)Cl_2] (**4**) were prepared in 90% H_2O/10% D_2O, with 0.1% dioxane added as an internal calibrant, and the initial pH values recorded. Samples were irradiated in an NMR tube with either UVA or visible light for 120 min, with ^{1}H NMR spectra acquired prior to and immediately following irradiation. pH values were then re-recorded at the end of the experiment.

3.3.5.1.1 [Pt(en)Cl_2] (1)

No changes were seen in the ^{1}H NMR spectrum of this complex following irradiation with either UVA or visible light. The pH also remained effectively constant (7.3 ± 0.1). This complex can therefore be regarded as stable under these conditions.

3.3.5.1.2 [Pt(L1)Cl_2] (4)

Again no changes were seen in either the ^{1}H NMR spectra or the pH values (6.6 ± 0.1) of this complex following irradiation with either UVA or visible light.

3.3.5.2 Photoreactions of Pt^{II} Azido Complexes

Saturated solutions of $[Pt(en)(N_3)_2]$ (**2**) and $[Pt(L1)(N_3)_2]$ (**5**) were prepared in 90% H_2O/10% D_2O, with 0.1% dioxane added as an internal calibrant, and the initial pH values recorded. Samples were irradiated with either UVA or visible light in an NMR tube at 310 K, with ^1H NMR spectra recorded after 0, 5, 10, 15, 20, 25, 30, 45, 60, 90 and 120 min (UVA) and 0, 10, 30, 60 and 120 min (visible). pH values were then re-recorded at the end of the experiment.

3.3.5.2.1 $[Pt(en)(N_3)_2]$ (2)

a) UVA Irradiation

After 5 min irradiation, changes to the en-CH_2 peak at 2.60 ppm were already apparent. The downfield satellite began to broaden, and this increased upon continued irradiation. Concurrently, the main peak at 2.60 ppm decreased in intensity with a new peak forming under the upfield satellite at 2.54 ppm; by 45 min these two peaks were of approximately equal intensity. The loss of signal intensity and resolution throughout the experiment suggested the formation of multiple new species, possibly including hydrolysis products. There was no evidence of free ethylenediamine (2.65 ppm), and no platinum-containing species could be detected by mass spectrometry, The pH decreased significantly over the course of the reaction, from 8.60 to 5.50; such a change will likely traverse the pK_a values for any aqua adducts present, further complicating the spectrum. The spectra can be seen in Figure 3.12.

b) Visible Irradiation

Changes to the spectral profile were similar upon irradiation with visible light; a significant loss in signal intensity and resolution was seen, although at a slower rate than with UVA light. The concomitant decrease in pH was also smaller, from 8.55 to 6.03.

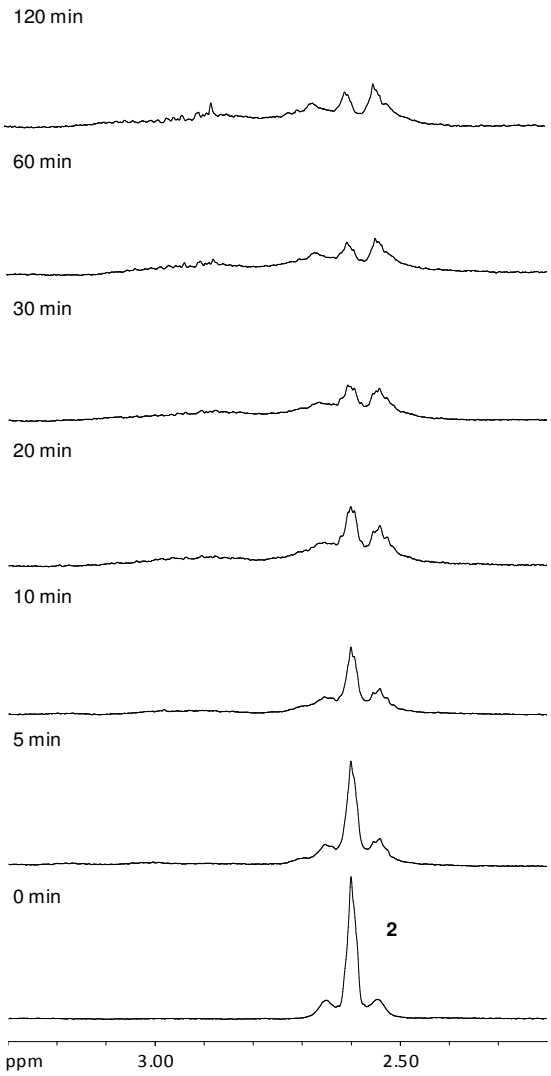

Figure 3.12 ^{1}H NMR spectra recorded at various timepoints during the irradiation of [Pt(en)(N_3)$_2$] (**2**) with UVA light (λ_{max} = 365 nm), in 90% H_2O/10% D_2O at 310 K.

3.3.5.2.2 [Pt(L1)$(N_3)_2$] (5)

a) UVA Irradiation

A loss of signal resolution and intensity was again seen over the course of this experiment. As previously noted, the eight methylene protons of this complex are magnetically inequivalent, resulting in many overlapping ^{1}H NMR peaks in the aliphatic region of the spectrum and rendering the identification of new species difficult. However, two new doublets, at 3.48 and 3.51 ppm, were identified after 10 min irradiation and appeared to grow in intensity slightly throughout the experiment, although reliable integrals could not be obtained. These signals were also seen in the stability study of this complex in aqueous solution (section 3.3.2.2), suggesting they could result from a hydrolysis product, the rate of formation of which is increased upon irradiation. The pH increased slightly during the experiment, from 8.62 to pH 8.97.

b) Visible Irradiation

As for [Pt(en)$(N_3)_2$] (**2**), it appears that similar changes occurred upon irradiation of **5** with visible light as with UVA, although at a slower rate. The pH change was of a similar magnitude, increasing from 8.41 to 8.70.

3.3.5.3 Photoreactions of a Pt^{IV} Azido Complex, [Pt(L1)$(N_3)_2(OAc)_2$] (6)

3.3.5.3.1 ^{1}H NMR Spectroscopy

3 mM solutions of **6** were prepared in D_2O, with 2 μL of a 1% dioxane solution added as an internal calibrant, and the pH recorded. The sample was irradiated in an NMR tube with UVA or visible light at 310 K, with ^{1}H NMR spectra recorded after 0, 1, 2, 3, 5, 7, 10, 15, 20, 30, 45, 60, 90 and 120 min. For the UVA irradiation, the pH value was recorded at the end, whilst for the visible light irradiation the pH was measured after each irradiation timepoint, prior to acquiring the NMR spectrum.

a) UVA Irradiation

The two singlets of the bound acetato groups rapidly decreased in intensity upon irradiation, with the concurrent growth of a peak corresponding to free acetate.

Prior to irradiation, a small peak arising from free acetate (1.90 ppm) was apparent in the spectrum, comprising 4% of the total acetate signal. After just 1 min of UVA irradiation, this had increased to 24% and undergone a significant downfield shift to 1.99 ppm. Upon further irradiation, this peak continued to grow in intensity at the expense of the bound acetato signals, which after 10 min were no longer visible in the spectrum. The downfield shift of the free acetate peak is consistent with the measured decrease in pH*, from 8.30 to 5.01. The large shift after 1 min irradiation, and little change thereafter, suggests the pH* decreases rapidly at the beginning of the experiment. Throughout the remainder of the experiment, signal intensity and resolution is rapidly lost and no further photoproducts could be identified (Figure 3.13).

b) Visible Irradiation

Free acetate was again released, although at a slower rate than upon UVA irradiation. Evidence of an additional complex containing a bound acetato group was also found.

Again the peak of free acetate increased in intensity upon irradiation, comprising 12% of the total acetate signal after 1 min, compared with 24% with UVA light (Figure 3.14). The downfield shift was also less pronounced (δ = 1.93 ppm), although there was a significant pH change after only one minute (7.70 to 5.60). Upon further irradiation the downfield shift and pH decrease continued, stabilising after around 20 minutes with values of 1.99 ppm and 4.75, respectively, despite the intensity of this peak further increasing throughout the experiment.

Evidence of a new acetato complex was also seen with the appearance of a new singlet at 2.14 ppm. First apparent after 5 min, this peak grew in intensity as the two singlets at 2.15 and 2.16 ppm decreased, contributing 12% of the total acetate signal at the end of the experiment. The chemical shift value is in the region of bound acetate, and could potentially arise from a monoacetato intermediate, or a photoisomerisation product in which the two acetate groups are magnetically equivalent; indeed several smaller peaks in this region suggest multiple species may be present. A small peak at 2.14 ppm is also evident following 5 and 10 min of UVA irradiation, however all signals for bound acetate are subsequently lost.

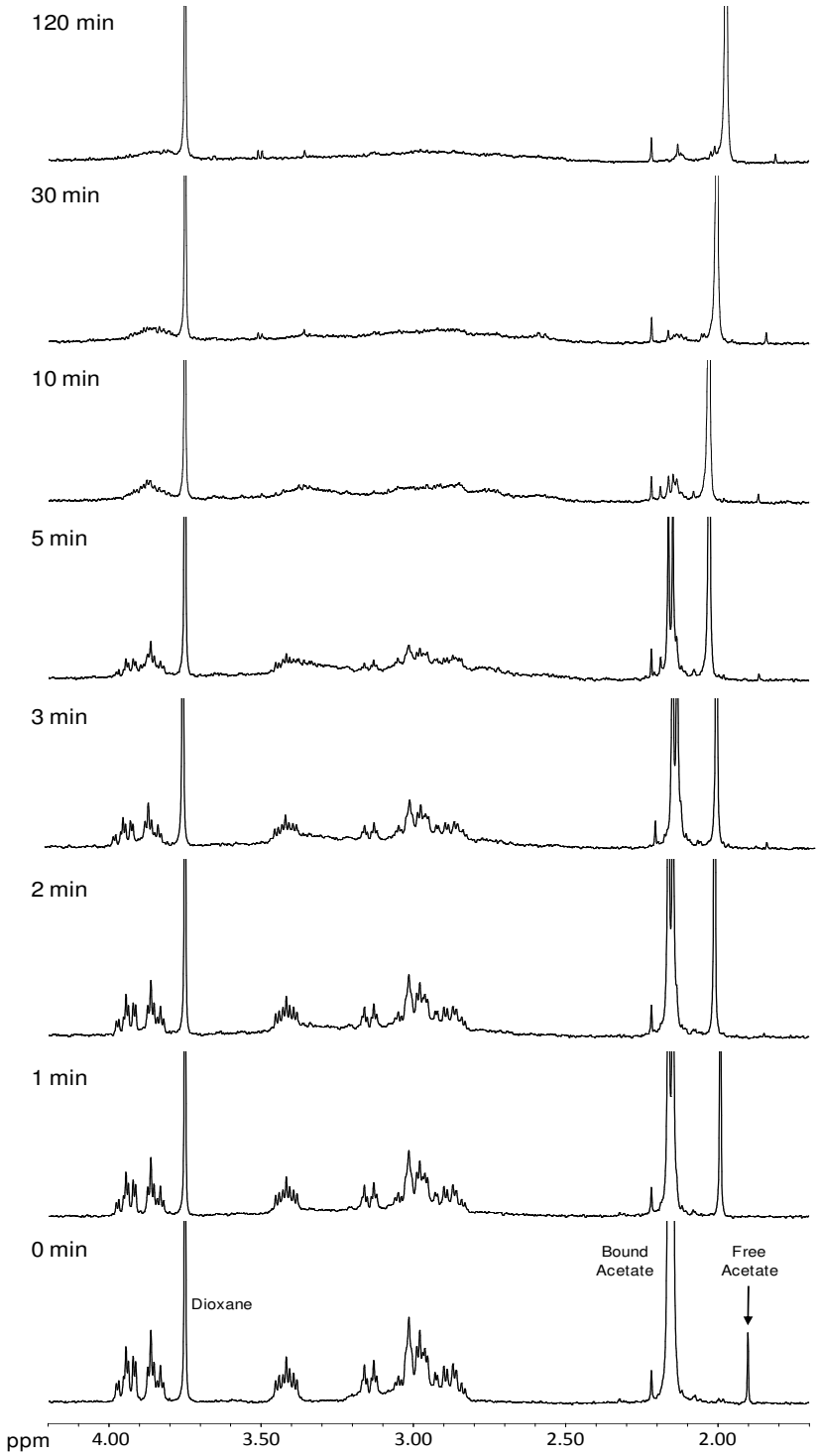

Figure 3.13 ^{1}H NMR spectra recorded at various timepoints during the irradiation of [Pt(L1)$(N_3)_2(OAc)_2$] (**6**) with UVA light (λ_{max} = 365 nm), in D_2O at 310 K.

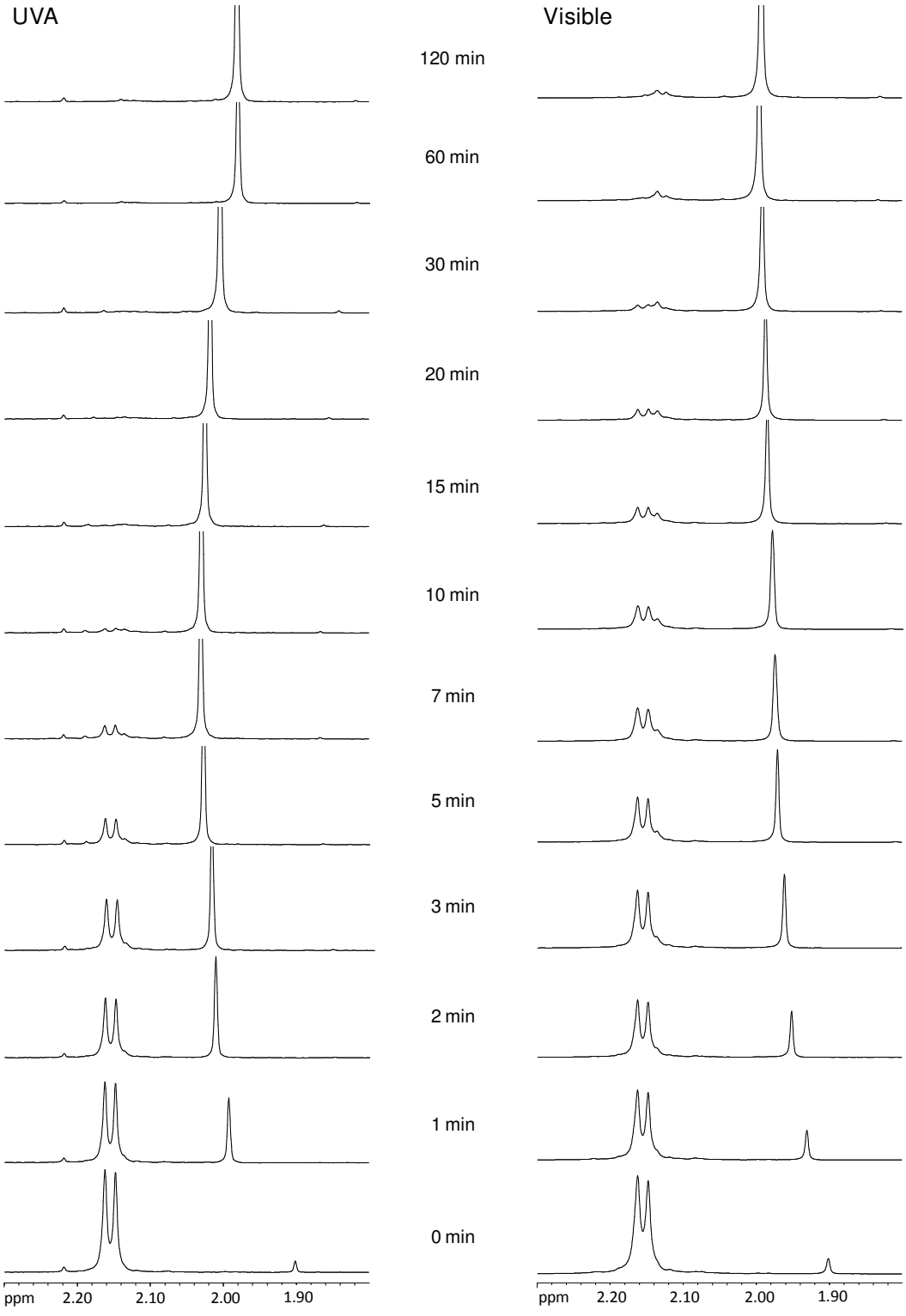

Figure 3.14 Comparison of the acetate region of the ^{1}H NMR spectra of $[Pt(L1)(N_3)_2(OAc)_2]$ (**6**) upon irradiation with UVA and visible light.

3.3.5.3.2 UV-Visible Absorption Spectroscopy

Solutions of **6** (40–50 μM) were prepared in H_2O, and irradiated inside a 3.5 mL Hellma® UV quartz cuvette with either UVA or visible light. UV-visible absorption spectra were acquired after 0, 1, 3, 5, 10, 15, 20, 30, 45, 60, 90 and 120 min of irradiation.

The UV-visible absorption spectrum of **6** contains an intense $N_3 \rightarrow Pt$ ligand-to-metal charge transfer (LMCT) band at 263 nm, as found in similar Pt^{IV} azido complexes.[29,30,31] This band decreases upon irradiation with both UVA and visible light, indicating loss of the azide ligands[32] (Figure 3.15). The rate and extent of decomposition is greater upon UVA irradiation, as can be expected from the greater extinction coefficient at these wavelengths. Indeed, the observation of photoactivity upon visible light irradiation, previously seen for similar complexes,[31,33] is interesting considering the very low absorbance in this region. In both cases, the appearance of bubbles in the UV cuvette indicated the evolution of a gas, presumed to be nitrogen formed from the azide ligands.

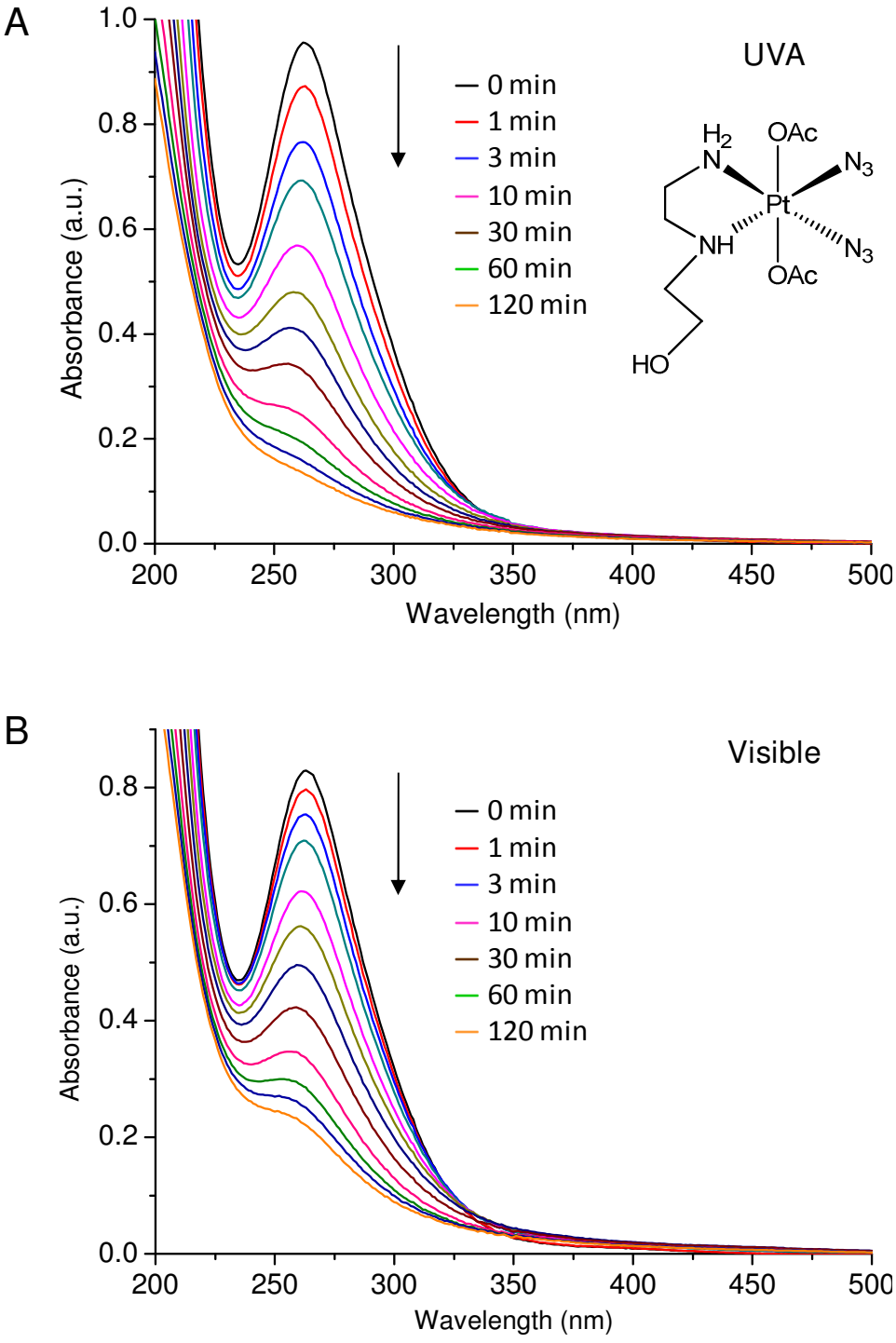

Figure 3.15 UV-visible absorption spectra of aqueous solutions of $[Pt(L1)(N_3)_2(OAc)_2]$ (**6**) following irradiation at 310 K with A: UVA (λ_{max} = 365 nm) and B: visible (λ = 400–700 nm) light.

3.3.5.4 Photoreactions of Pt^{II} and Pt^{IV} Complexes in the Presence of 5'-GMP

Solutions of **2** (1.5 mM) and **6** (3 mM) were prepared in D_2O, with 2 μL of a 1% dioxane solution added as an internal calibrant. 2 mol equivalents of 5'-GMP were added, and the pH* adjusted with dilute NaOD to 5.68 and 5.59 respectively. Samples were irradiated in an NMR tube with UVA light, with ^{1}H NMR spectra recorded after 0, 1, 2, 3, 5, 7, 10, 15, 20, 30, 45, 60, 90 and 120 min. The pH was also recorded prior to obtaining each spectrum.

a) $Pt(en)(N_3)_2$ (**2**)

Rapid binding to 5'-GMP occurs upon irradiation to produce mono- and bisadducts. Two additional species are formed after 10 min, one of which is tentatively assigned to a Pt^{IV} species.

After 1 min of UVA irradiation, a new peak appeared at 8.60 ppm, previously assigned to a 5'-GMP monoadduct (**2c**) (Section 3.3.3.2a). This comprised 10% of the total 5'-GMP signal after 1 min, increasing to 20% after 3 min. After 5 min a new peak was apparent, slightly upfield from that of the monoadduct. This is likely to result from a bisadduct (**2d**), the peaks of which show this characteristic upfield shift. Further evidence was provided from the aliphatic region; the peaks at 2.70 and 2.82 ppm having previously been attributed to **2c** and **2d** respectively (Section 3.3.3.2a). The H8 peaks of both **2c** and **2d** showed a progressive downfield shift during the course of the irradiation, from 8.60–8.68 ppm and 8.61–8.67 ppm respectively. This may result from the gradual increase in pH* throughout the experiment (from 5.68 to 6.75), since an increase in chemical shift value of the H8 proton of 5'-GMP adducts has previously been seen over this pH range.[31]

Two new peaks appear after 10 min, at 8.84 and 9.17 ppm, arising from two new species **2e** and **2f**. These could not be identified, although are likely to be additional Pt–5'-GMP adducts. Over the course of the experiment, clear platinum satellites became apparent on the peak of **2f**, with $^3J(^{195}Pt–^1H)$ = 16 Hz. The high

chemical shift, small ^{3}J value and clarity of the satellites suggest this peak may arise from a Pt^{IV} species; furthermore, a previously reported Pt^{IV}–5'-GMP adduct showed a very similar chemical shift of 9.20 ppm.[34] However, further evidence would be needed to confirm the identity of **2f**. Subsequent irradiation resulted in an increase in the relative proportions of **2d**, **2e**, and **2f**, and a more gradual decrease of the monoadduct **2c**. Since the decline of the monoadduct was not concurrent with a growth in the bisadduct, or a decrease in free 5'-GMP, this suggests it does not undergo further substitution. Indeed, its decline more closely parallels the growth of **2f**, however further evidence would be needed to confirm any relationship between the two. Following 120 min irradiation, the speciation was as follows: free 5'-GMP 77%, **2d** 8%, **2e** 2% and **2f** 13% (Figures 3.16 and 3.17).

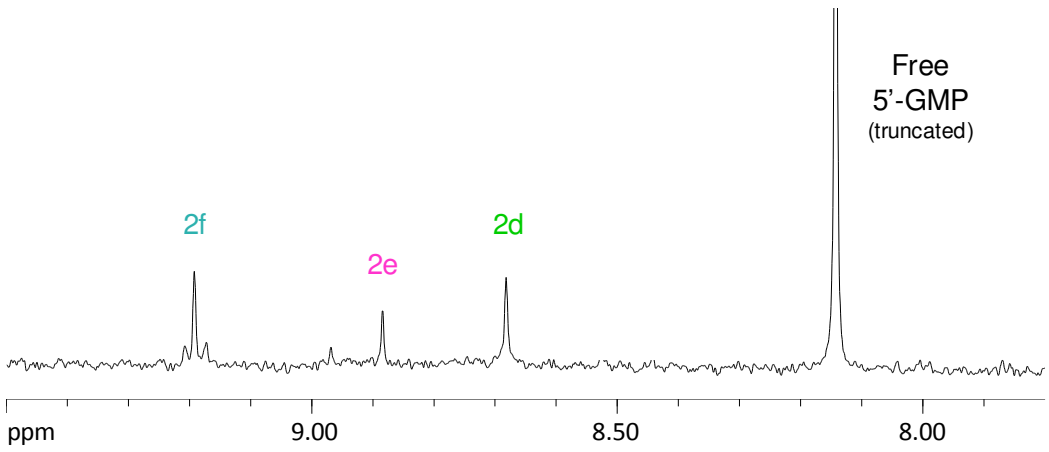

Figure 3.16 The H8 region of the ^{1}H NMR spectrum of $[Pt(en)(N_3)_2]$ (**2**) and 5'-GMP (1:2) in D_2O, following 120 min irradiation with UVA light (λ_{max} = 365 nm) at 310 K.

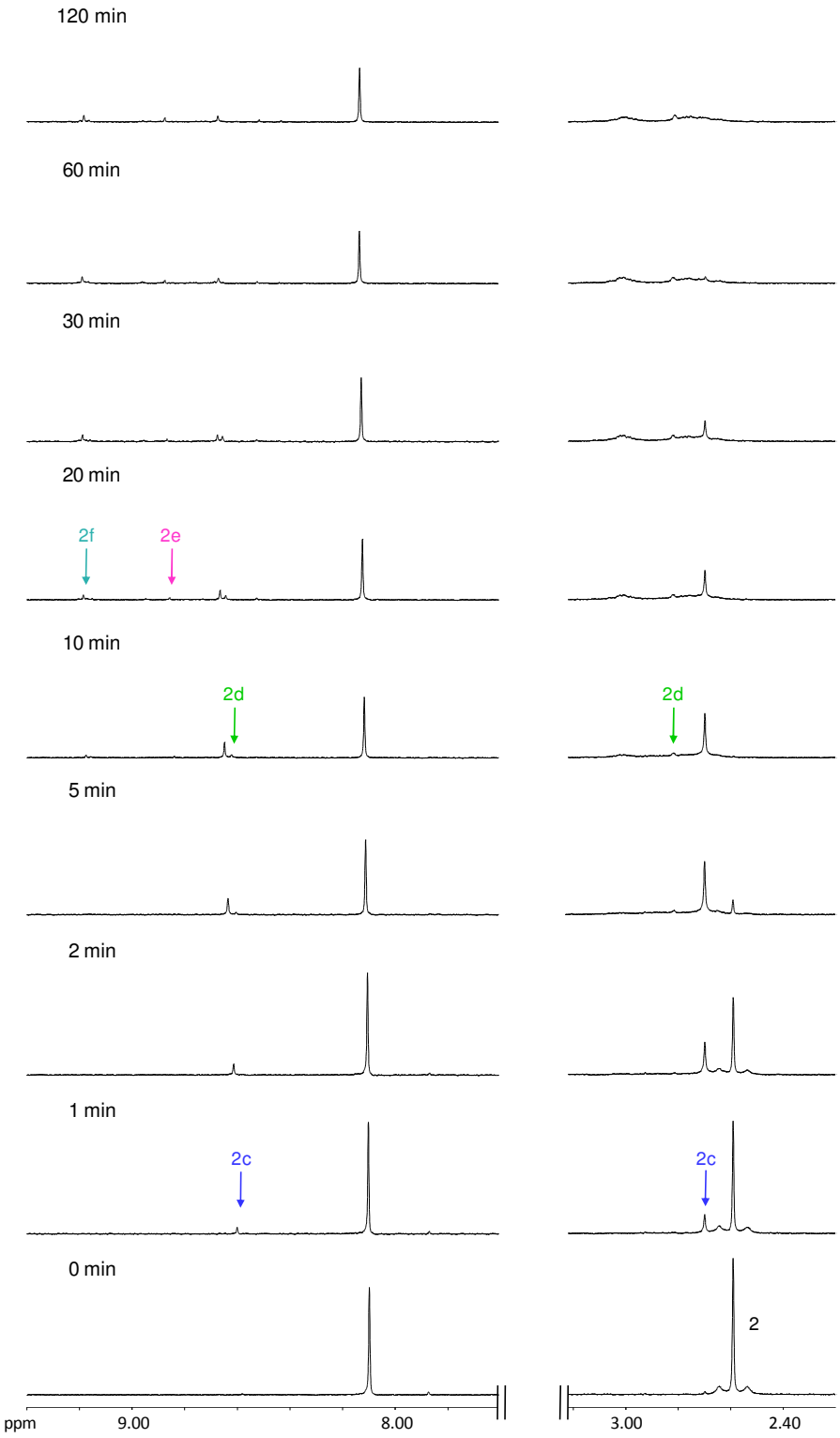

Figure 3.17 ^{1}H NMR spectra recorded at various timepoints during the reaction of [Pt(en)(N_3)$_2$] (**2**) and 5'-GMP (1:2) in D_2O, upon irradiation with UVA light (λ_{max} = 365 nm) at 310 K.

b) $Pt(L1)(N_3)_2(OAc)_2$ (**6**)

Formation of a Pt^{II}–5'-GMP adduct occurs rapidly upon UVA irradiation, however the peak of this species is subsequently lost and no bound 5'-GMP can be detected after 60 min irradiation.

After 1 min irradiation, a new peak was formed at 8.60 ppm, accounting for 3% of the total 5'-GMP signal and believed to result from a Pt–5'-GMP monoadduct (**6a**). Further irradiation resulted in the growth of this peak, reaching 20% by 15 min, followed by a decline and by 60 min no peaks for bound 5'-GMP could be seen.

Little information can be gained from the aliphatic region since, as with the complex alone, signal intensity is rapidly lost and no new species can be identified. The formation of free acetate seems to occur at a similar rate to that in the absence of 5'-GMP, with all signals for bound acetate lost after 15 min irradiation. The small increase in chemical shift of the free acetate peak is consistent with the steady decrease in pH*, from 5.59 to 5.25 over the course of the experiment.

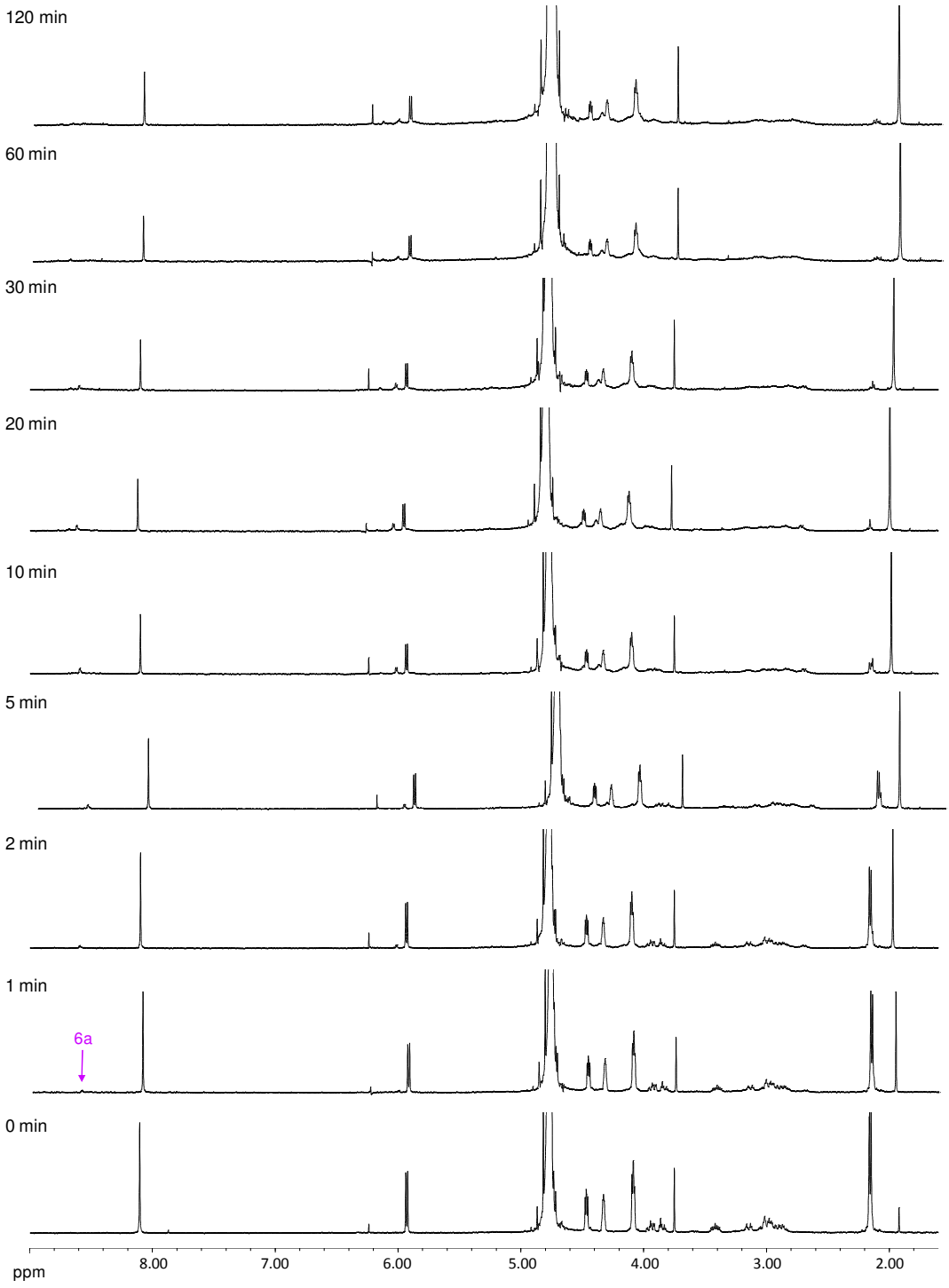

Figure 3.18 ^{1}H NMR spectra recorded at various timepoints during the reaction of [Pt(L1)$(N_3)_2(OAc)_2$] (**6**) and 5'-GMP (1:2) in D_2O, upon irradiation with UVA light (λ_{max} = 365 nm) at 310 K.

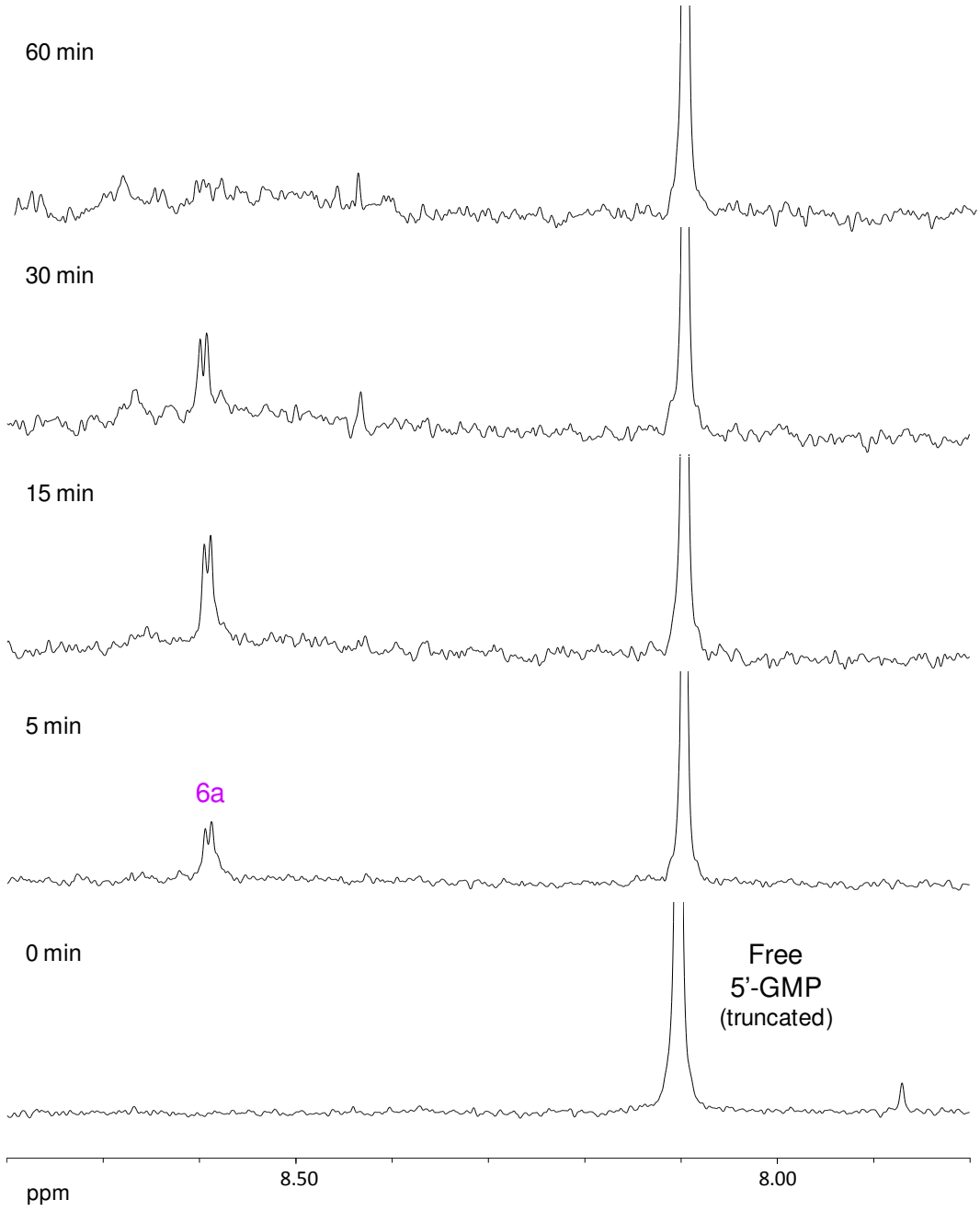

Figure 3.19 The H8 region of the ^{1}H NMR spectra, recorded at various timepoints during the reaction of [Pt(L1)$(N_3)_2(OAc)_2$] (**6**) and 5'-GMP (1:2) in D_2O, upon irradiation with UVA light (λ_{max} = 365 nm) at 310 K.

3.3.6 Phototoxicity

The Pt^{II} azido complexes $[Pt(en)(N_3)_2]$ (**2**), $[Pt(L1)(N_3)_2]$ (**5**) and $[Pt(L2)(N_3)_2]$ (**8**), as well as the Pt^{IV} azido complex $[Pt(L1)(N_3)_2(OAc)_2]$ (**6**), were tested for phototoxicity towards HaCaT keratinocytes upon irradiation with UVA light, as described in Chapter 2.

Complexes **5** and **8** were inactive under these conditions, with IC_{50} values higher than the greatest concentrations tested (260.9 and 251.7 μM, respectively) both upon UVA irradiation and in sham-irradiated (dark) controls. Complex **2** did show a slight increase in activity upon UVA irradiation (IC_{50} = 222.7 μM, compared with >294.8 in the dark), however it is also classified as non-phototoxic in these tests. The Pt^{IV} azido complex **6** was also found to be inactive, with IC_{50} values **>**199.6 μM both upon UVA irradiation and in sham-irradiated controls.

3.4 Discussion

3.4.1 Complex Design

Considering the design of Pt^{II} azido complexes as potential cytotoxic agents, it was decided to first use ethylenediamine (en) as a chelating amine ligand. The chlorido complex, $[Pt(en)Cl_2]$, shows cytotoxicity approaching that of cisplatin[9] and reactions relating to this have been extensively studied, allowing for the possibility of comparisons with the azido analogue.

Aminoalcohol ligands, incorporating hydroxyl groups which would remain uncoordinated (or "pendant") upon complex formation, were also employed. Such groups should aid water solubility of the resulting metal complexes, beneficial since low solubility is often problematic for cisplatin and related compounds. Moreover, platinum complexes of aminoalcohol ligands are of interest due to their hydrogen bonding ability, which could potentially assist DNA binding or stabilise platinated adducts; it has been suggested the hydroxyl substituents could readily hydrogen bond to a phosphate oxygen or the keto oxygen of a platinated guanine

residue.[11] A number of recent studies have focused on such complexes,[11,18,35,36] encouraged by reports of increased activity towards a number of cancer cell lines for aminoalcohol complexes compared with their alkyl analogues.[37]

The Pt^{II} chlorido complex of 2-(2-aminoethylamino)ethanol (L1) has previously been shown to exhibit good to moderate cytotoxicity in a range of cancer cell lines,[11,18,35] hence it was decided to study the azido complex of this ligand. 3-(2-aminoethylamino)-1-propanol (L2) was also chosen, since the increased length of the carbon linker could potentially affect the hydrogen bonding ability of the OH group. Similarly, a ligand with no flexibility of the OH group and a different chelating amine motif was chosen, 1,3-diamino-2-propanol (L3). A recent paper has described the high cytotoxicity of the Pt^{II} chlorido complex of this ligand.[16] Finally, a ligand containing a pyridine ring was synthesised, to investigate the effects of an aromatic, more hydrophobic group in the complex.

As mentioned in the introduction, further motivation to study such complexes arises since the hydroxyl groups provide a handle for functionalisation, for example with targeting agents. In this regard, a complex containing a pendant amine group could also be useful since, given the differing reactivity of the hydroxyl and amine groups, a wider range of targeting compounds could be accessible. Hence a complex containing a protected amine group was also synthesised, which could be deprotected to allow functionalisation. The concept of functionalisation is investigated in Chapter 4.

3.4.2 Synthesis and Characterisation

3.4.2.1 Platinum Complexes Containing Hydroxyl Groups

$[Pt(L1)Cl_2]$ (**4**) and $[Pt(L2)Cl_2]$ (**7**) were synthesised according to a published procedure for similar complexes, in which the pH was maintained near to 7 throughout the reaction.[14] This was found to give slightly greater yields than when the pH remained unaltered. Although the ligands give basic solutions, the

pH decreases during the course of the reaction, to values of 3–4. This is likely to be close to the pK_a of the amino protons; should any unreacted ligand become protonated this would render it unavailable for coordination to platinum. Yields of complex **7** were consistently only around half those of **4**, likely due to the considerably greater water solubility of the former complex, hindering its isolation from the reaction and recrystallisation solutions. It is possible that increasing the length of the carbon linker leads to a significant change in intermolecular interactions, affecting the solubility. The NMR spectra, elemental analyses and, in the case of **4**, crystal structure, confirmed the identities of these complexes. In line with previous observations,[11,18,35] the ligands bind in a bidentate (*N,N*) fashion and the OH group remains uncoordinated. This is consistent with the preference of Pt^{II} for soft donor ligands, with harder donors such as oxygen favoured mainly in the Pt^{IV} state.

$[Pt(L3)Cl_2]$ (**10**) could not be prepared from the reaction of L3 with $K_2[PtCl_4]$, since this is reported to yield $[Pt(L3)_2][PtCl_4]$;[38] presumably formation of a second, stable 6-membered chelate ring drives the coordination of an additional ligand. The use of K_2PtI_4 allows for successful isolation of $[Pt(L3)I_2]$ (**9**), in which a second substitution may be hindered by the more strongly bound iodido ligands; these can then be removed by abstraction with silver nitrate. Reasons behind the problematic synthesis of $[Pt(L4)Cl_2]$ (**12**) are unclear; with decomposition and reduction to Pt^0 seen in both aqueous and organic solvents. No further reactions were carried out with this complex, however the Pt^{II} azido complexes of L1, L2 and L3 were successfully synthesised.

Attempts to oxidise $[Pt(L1)(N_3)_2]$ (**5**) with hydrogen peroxide were unsuccessful, resulting in a sticky solid which showed evidence of impurities and was very difficult to handle. Given the current interest in Pt^{IV} complexes, the oxidation of Pt^{II} chlorido complexes of several aminoalcohol ligands is documented in literature. Although Jolley *et al* reported the successful oxidation of $[Pt(L1)Cl_2]$ (**4**) to form $[Pt(L1)Cl_2(OH)_2]$,[11] others have found this to be problematic. Hambley and co-workers found that, upon heating **4** in an aqueous solution of

hydrogen peroxide, the OH group of L1 was deprotonated and coordinated to the platinum in a tridentate (*N,N,O*) fashion, forming a complex with just one axial hydroxy group, [Pt(L1–H)Cl_2(OH)].[18] Although they suggested the reaction may proceed *via* the trans-dihydroxo complex in the absence of heat, they did not isolate this product. Ren *et al* also failed to achieve the desired product [Pt(L1)$Cl_2(OH)_2$] by oxidation of **4**, although further explanation was not given.[17]. They instead prepared a Pt^{IV} complex with axial acetato groups by oxidation with hydrogen peroxide and acetic anhydride in acetic acid; the OH group of L1 remained uncoordinated, leading to suggestions that its coordination is facilitated by the presence of axial hydroxyl groups.[18] The same method was used in this work, in the oxidation of **5** to produce [Pt(L1)$(N_3)_2(OAc)_2$] (**6**). A previous study has found the pendant hydroxyl group of L1 is slowly acetylated over time (7 d) by acetic anhydride;[11] this was not seen here, although it was found that prolonged reaction times (48 h) gave rise to small impurity peaks in the NMR spectrum of **6**, at 4.40 and 4.25 ppm, which may arise from such a species. Although Pt^{IV} complexes with axial hydroxyl groups are usually preferred due to their greater stability towards reduction,[39] a complex with axial acetato ligands may be beneficial in this case for two reasons. Firstly, the methyl protons of the acetato groups show strong signals in NMR spectra, which enable the fate of the axial ligands upon irradiation to be followed in a way that is not possible with hydroxyl groups. Secondly, interference from the axial ligands will be avoided during any subsequent reaction of the pendant hydroxyl group.

The crystal structures of **4** and **5** reveal that these complexes form many hydrogen bonds, with the pendant hydroxyl groups involved in both cases. This could explain the sharp nature of the OH peaks in the ^{1}H NMR spectrum, since involvement in intermolecular interactions will reduce the tendency to exchange. Additionally, different hydrogen bonds are found in the case of the chlorido and azido complexes **4** and **5**, and this is likely the case for **4** and the DMSO adducts, causing a significant shift on exchange despite the remoteness of this group from the platinum centre. A particularly interesting feature of **5** is the short (2.04 Å)

intramolecular hydrogen bond between the OH and a bound azido nitrogen, N_α. This could have implications for the subsequent functionalisation of the OH, as it may show a reduced tendency to react.

When coordinated to platinum, the protons of each methylene pair in ligands L1–L4 are found to be magnetically inequivalent with each showing a distinct peak in the ^{1}H NMR spectrum. This has been previously noted in spectra of [Pt(L1)Cl$_2$] (**4**).[17] It is likely that the orientation of the ligand, when constrained in the complex, is such that each proton resides in a different environment. The pendant arm may also be constrained to some extent by the hydrogen bonding interactions of the OH group. The two acetato groups of **6** are also inequivalent, with the difference in environment arising since one should be in closer proximity to the pendant arm than the other.

An interesting feature of the fluorescence spectrum of the aminoalcohol ligand L4 is the presence of two distinct bands upon excitation at 278 nm, centered at 370 nm and 450 nm. The presence of two peaks in this case could correspond to the vibrational profile of the ligand. However, whilst the compound was found to be satisfactorily pure by NMR, the presence of a highly fluorescent impurity cannot be ruled out without further investigation by more sensitive techniques. The emission from the platinum complex in the solid state likely arises from a low-lying triplet state, which in solution undergoes non-radiative decay, although this pathway may be minimised in a glass matrix at 77 K. In order to draw any firm conclusions the fluorescence of both the ligand and complex would need to be investigated in further detail; both experimentally, by measuring fluorescence lifetimes, the effect of solvent and excitation wavelength, and theoretically with TD-DFT calculations.

3.4.2.2 Platinum Complexes Containing a Protected Amine

The synthesis of platinum complexes containing pendant amine groups is synthetically more challenging than those with hydroxyl groups, as the high affinity of platinum for amine nitrogens necessitates the use of protecting group chemistry. The ligand employed (**L5**) contained a free amine group for coordination to platinum, separated by a carbon chain linker to a BOC-protected amine. Linker length could thus be varied; in this case 4 carbons was chosen, to give sufficient distance from the platinum centre whilst retaining solubility.

Yields of the mixed amine Pt^{II} chlorido complex $[Pt(L5)(NH_3)Cl_2]$ (**13**) were relatively low, although were found to be slightly higher when the reaction was carried out in water rather than methanol, likely due to the lower solubility of the product in water. The synthesis of the Pt^{II} azido complex (**14**) was found to be more problematic. The typical route to such complexes, involving chloride extraction with silver nitrate in water, gave very low yields, possibly due to the insolubility of the starting material. It had previously been found that, in the case of poorly soluble complexes, yields were increased upon addition of a small quantity (~500 μL) of DMF to the reaction mixture.[31] Here, however, this repeatedly led to the formation of Pt^0. The direct substitution of chlorido for azido ligands in DMF, as described in Chapter 5 and elsewhere,[40] was also unsuccessful in this case; after five days mostly starting material was present with only a small quantity of required product. This method is apparently more suitable for chelating aromatic ligands such as bipyridine or phenylazopyridine (azpy). The most successful synthesis of the Pt^{II} azido complex involved carrying out the silver nitrate reaction in methanol, which was then removed and exchanged for water prior to addition of sodium azide. The oxidation of this complex to yield $[Pt(L5)(NH_3)(N_3)_2(OH)_2]$ (**15**) was readily achieved using an excess of hydrogen peroxide in aqueous solution.

3.4.3 Stability Studies: Aqueous and Chloride Containing Solutions

Stability in aqueous and chloride containing solutions is an important factor to consider in the design of potential platinum anticancer agents. Cisplatin is stable to chloride concentrations found in blood plasma (104 mM), however undergoes hydrolysis upon entering cells where the chloride concentration drops to 4–25 mM. The half-life is fairly short, around 2 h, and it is the hydrolysed species which are reactive towards DNA. Azide is known to form stronger bonds to platinum than does chloride, hence a slower hydrolysis rate would be expected, which may have implications for the cytotoxicity of Pt^{II} azido complexes. Stability in chloride solutions is also important in order to determine if the complex could undergo substitution prior to entering the cell, especially considering azide loss may result in a loss of photoactivity.

Additionally, since work in the area of photoactivated Pt^{IV} azido anticancer agents has thus far focused upon complexes with axial hydroxyl groups, there have been no stability studies involving complexes with axial acetato groups, despite the synthesis of several[22,31,40] and recent interest in those containing chelating aromatic ligands.[40] Therefore, the stability of **6** to aqueous and chloride solutions was also examined.

a) $[Pt(en)(N_3)_2]$ (**2**)

The tendency of **2** to undergo oxidation in aqueous and chloride-containing solutions is surprising. The involvement of oxygen is suggested, since a reduction in the rate and extent of oxidation is seen in degassed solutions. There appear to be few previous reports of such a process. *Trans*-$[Pt(MeNH_2)(NH_3)Cl_2]$ was found to undergo oxidation in air during synthesis, which was prevented by performing the reaction under nitrogen, although a similar effect was not seen for the ethylamine complex.[31] Hydrolysis was found to trigger the oxidation of *trans*-diamine Pt^{II} complexes, and was found to be suppressed in an argon medium but accelerated in the presence of oxygen.[41] Here, however, oxidation of

$[Pt(en)Cl_2]$ (**1**) was found to occur in 100 mM NaCl solution (in which hydrolysis would be suppressed), although to a lesser extent than for **2**. This suggests that hydrolysis is not necessary for oxidation, although it may accelerate the process. However, a lesser extent of oxidation may be expected for complex **1** compared with **2** in any case; azide is more electron donating than chloride, resulting in greater electron density on platinum and rendering it more susceptible to oxidation. There was no evidence of oxidation over time in DMSO solutions of **2,** in which oxygen is poorly soluble and hydrolysis would be suppressed.

Over increasing time in both aqueous and chloride containing solutions there was evidence of a mixture of species in the spectra of **2**, believed to be multiple hydrolysis and degradation products. However, there was little evidence of this change in the first five days. A previous investigation of the stability of $[Pt(NH_3)_2(N_3)_2]$ in 100mM NaCl solution showed substitution of one azido ligand by chloride.[22] In this case, such a species may not be detectable by ^1H NMR spectroscopy since the en-CH_2 protons of both **1** and **2** have very similar chemical shifts. Further evidence could be provided from 2D [^1H, ^{15}N] experiments with a ^{15}N-labelled complex.

b) $[Pt(en)(N_3)_2(OH)_2]$ (**3**)

The stability of this complex over time is in accordance with that of similar Pt^{IV} azido complexes.[22,31] A previous investigation of c*is,trans,cis*- and *trans,trans,trans*-$[Pt(NH_3)_2(N_3)_2(OH)_2]$ in 100 mM chloride solution found evidence of free ammonia after 12 d and 6 d respectively,[31] however amine loss would be less likely in this case due to the stability of the ethylenediamine chelate ring, and no evidence of this was seen.

c) $[Pt(L1)(N_3)_2]$ (**5**)

Any reactions of these complexes are inherently difficult to follow due to the inequivalence of the eight methylene protons. As a result, new peaks in the

spectrum could not be identified, although it appears the same reaction is occurring in both aqueous and chloride containing solutions. From analogies with complex **2** an oxidised product may be expected. A multiplet at the same chemical shift as these new peaks is found in the spectrum of $[Pt(L1)(N_3)_2(OH)_2]$, however this does not give conclusive evidence of an oxidised product, and no evidence was seen in the mass spectrum.

d) $[Pt(L1)(N_3)_2(OAc)_2]$ (**6**)

Free acetate was released from this complex over time. The reduction of **6** to a Pt^{II} species would likely liberate acetate; however the lack of a suitable reducing agent in solution renders this improbable. The starting solution was slightly basic, therefore it may be possible that the Pt–OR ester bond undergoes a slow base-catalysed hydrolysis, forming a Pt–OH species and the observed free acetate.

3.4.4 Reactions with Glutathione and 5'-GMP

The fairly rapid hydrolysis of cisplatin enables binding to DNA, however its severe toxicity is attributed to side reactions with other biomolecules. In particular, it is highly reactive towards intracellular thiols such as glutathione, which can deactivate much of the drug before it reaches its intended site. The rationale behind the use of more stable leaving groups is that side reactions may be reduced, so it is of interest to investigate the reaction of Pt^{II} azido complexes such as **2** with molecules such as glutathione. However, it may be important that the leaving group is not so stable that it is inactive towards nucleobases.

Pt^{IV} azido complexes containing axial hydroxyl groups were previously shown to be unreactive to both glutathione and nucleobases in the dark,[22,31] however acetato complexes such as $[Pt(L1)(N_3)_2(OAc)_2]$ (**6**) have not been investigated. It is known that similar Pt^{IV} acetato complexes are less stable towards reducing agents than their hydroxyl analogues;[42] additionally, certain Pt^{IV} complexes have

been shown to interact with nucleotides without prior reduction.[34] Since **6** is designed to be reduced and bind to DNA only upon irradiation, it is important such reactions are investigated.

3.4.4.1 Reactions with Glutathione

a) $[Pt(en)(N_3)_2]$ (**2**)

Reaction was apparent within the first three hours, with the initial product formed likely to be the monoadduct $[Pt(en)(N_3)(SG)]$. However, after 12 hours a new singlet at 3.36 ppm appeared in the spectrum, which appeared to grow in intensity thereafter whilst that of other peaks was lost. Sulfur ligands show a strong *trans*-labilising effect and are known to induce the release of amine ligands *trans* to them, as has been recently noted in reactions of cisplatin with cell extracts.[43] Although the release of ethylenediamine should be less favourable than ammonia due to the stability of the chelate ring, this has been observed in the reaction of $[Pt(en)(H_2O)_2]^{2+}$ with L-cysteine based ligands, shown by a peak also at 3.36 ppm.[44] However the pH* of the reaction solution was 1.6, hence ethylenediamine (pK_a 3.92) was protonated; in this case the final pH* was 6.68, at which pH* the peak of ethylenediamine would appear at 2.65 ppm and was not seen in the spectrum. Additionally, in the 2D [^{1}H, ^{1}H] COSY NMR experiment the signal at 3.36 ppm showed cross peaks to other regions of the spectrum, where signals were weak. It is therefore likely that this peak arises from a stable Pt–GSH adduct, likely the sulfur-bridged dimer $[\{Pt(en)(\mu_2\text{-}SG)\}_2]^{2+}$, a major product in reactions of Pt-diamine species with glutathione, and the presence of which was confirmed here by mass spectrometry. A previous study[23] concerning the reaction of $[Pt(en)Cl_2]$ (**1**) with glutathione identified not only the sulfur-bridged dimer but also a novel macrochelate, a di-Pt(en) complex containing one glutathione ligand. There was no evidence of such a species in this reaction, however further NMR studies and HPLC analysis could confirm this.

Although some reaction of **2** with glutathione was apparent within three hours, it is shown to proceed at a much slower rate than with Pt^{II} chlorido complexes: the half-life for the reaction of $[Pt(en)Cl_2]$ (**1**) with glutathione has previously been determined as 0.9 hours.[23] A half-life could not be determined from this ^1H NMR experiment, since the en-CH_2 peak was found overlapping with peaks from glutathione and its disappearance could not be quantified. However, it can be estimated that the half-life is at least 12 hours; for comparison, the half-life of the reaction of carboplatin with glutathione has been calculated as 24.5 hours.[45]

b) $[Pt(L1)(N_3)(OAc)_2]$ (**6**)

The reduction of Pt^{IV} complexes generally involves the liberation of the axial ligands,[42] with the free acetate formed here providing a useful way of following the reaction. The small increase in free acetate observed suggests complex **6** is remarkably stable to glutathione, with very little reduction seen over 16 days. Although some evidence of oxidised glutathione (GSSG) is seen in the NMR spectrum, it is unclear whether this results from autoxidation in air or interaction with complex **6**. More conclusive evidence of the fate of the Pt^{IV} complex could be gained from 2D [^1H, ^{15}N] NMR experiments, since nitrogens bound to Pt^{II} and Pt^{IV} give signals in distinct regions of the spectrum, although for this purpose a complex containing a ^{15}N-labelled ligand would be required.

The biological reduction of Pt^{IV} complexes containing axial acetato groups is currently under debate. Reports have shown that *cis,trans,cis*-$[Pt(NH_3)_2Cl_2(OAc)_2]$ is rapidly reduced in cancer cells, with only 33% remaining in the Pt^{IV} state after two hours;[46] however, questions are raised as to the role of glutathione in this process. Whilst one report correlates the reduction of Satraplatin with intracellular GSH levels,[47] two papers have indicated the stability of Pt^{IV} acetato complexes to glutathione,[48,49] with another suggesting the majority of the reduction is carried out by the high molecular weight fractions of cell extracts.[50] In addition, other biomolecules such as cysteine and methionine

are also capable of reducing such complexes,[51] indicating their stability in cells cannot be easily predicted.

3.4.4.2 Reactions with 5'-GMP

a) $[Pt(en)(N_3)_2]$ (**2**)

The binding of 5'-GMP to **2** is apparent after three hours, however is relatively slow with the half-life for the disappearance of **2** estimated at around 3 days. As an approximate comparison, that for the reaction of cisplatin with 5'-GMP has been calculated as 8 hours under similar conditions.[52] The slower rate is to be expected given the stronger binding to platinum of azide compared with chloride, however would not necessarily imply a lack of cytotoxicity. A much reduced rate is also seen in the case of carboplatin, for which the half-life of this reaction is 420 hours (17.5 days),[52] yet this complex still shows good antitumour efficacy along with the desired reduced toxicity. The appearance first of the monoadduct followed by the bisadduct of 5'-GMP is consistent with that observed for cisplatin and related complexes. The platination site is suggested to be N7 from the shift of the H8 peak upon binding, however this could be further confirmed by a ^{1}H NMR pH titration. The H8 chemical shift change associated with protonation of N7 of free 5'-GMP, at around 2.5, should be absent for the platinum adduct.[31]

As seen in aqueous solutions of **2**, a significant proportion of the oxidised product $[Pt(en)(N_3)_2(OH)_2]$ (**3**) was formed over time, comprising 13% of the total platinum species after 24 h with a slight rise thereafter. Although oxidation renders a proportion of platinum unable to bind to 5'-GMP, it would be unlikely to occur inside cells which typically maintain a reducing environment.

b) $[Pt(L1)(N_3)_2(OAc)_2]$ (**6**)

The observed stability of **6** to 5'-GMP is important, since the complex is intended not to undergo reduction or reactions with biomolecules until photoactivated. The

reactivity of Pt^{IV} complexes to nucleobases has been shown to increase with their reduction potential.[34] During the reaction of $[Pt(en)Cl_2(OAc)_2]$ with 5'-GMP, Choi *et al* found evidence of a Pt^{II}-GMP adduct after 7 days;[34] whilst Galanski and Keppler detected a stable Pt^{IV} adduct in the reaction of $[Pt(en)(OAc)_4]$ with 5'-GMP.[53] However, no such reactions are observed in the case of **6** up to 16 days. The reduction potentials of these Pt^{IV} azido complexes have not been measured, however the greater donating ability of azide compared with chloride suggests they may have a lower reduction potential than their chlorido analogues.

3.4.5 Cytotoxicity

All of the Pt^{II} chlorido complexes tested showed good to moderate cytotoxicity (IC_{50} 3.3–27 μM), which can be expected given their similarities to cisplatin. The moderate toxicity of $Pt(L1)Cl_2$ (**4**) (11 μM) is consistent with previous reports.[11,18,54] It was believed the additional methylene group of $[Pt(L2)Cl_2]$ (**7**) may affect the cytotoxicity, possibly by affecting the hydrogen bonding capability suggested to be important for such complexes; indeed one report suggests flexibility in this linker may influence cytotoxicity.[54] However, the effect appeared to be minimal at least in the Pt^{II} chlorido case, since the IC_{50} values of **4** and **7** are the same. The new complex $[Pt(L4)Cl_2]$ (**12**), containing a pyridine ring, is the least cytotoxic of all Pt^{II} chlorido complexes tested (27 μM). An imine analogue of this complex has been prepared and showed high levels of binding to both single- and double-stranded DNA,[55] however no cytotoxicity data was reported.

The moderate cytotoxicity of the Pt^{II} azido complexes (21–47 μM) is especially interesting. No previous examples of the testing of such complexes could be found; they were probably believed to be inactive based upon the known stability of the $Pt–N_3$ bond and the observed inactivity of Pt^{II} iodido complexes;[3] indeed, the Pt^{II} iodido complex $[Pt(L3)I_2]$ was tested for comparison and found to be inactive. There appears to be little correlation between the cytotoxicity of the Pt^{II}

chlorido complexes and their azido analogues, although the sample size is too small to draw any accurate conclusions.

The mechanism of action of these azido complexes would need to be further investigated. Although the rate and extent of nucleobase binding is low in comparison to that of Pt^{II} chlorido complexes, the cytotoxicity of metal complexes often does not correlate with nucleotide binding ability. In the one example of metal-azido complexes previously tested, hydrolysis and DNA binding rates were also low yet a complex with high cytotoxicity (5 μM) was obtained.[7] Furthermore, nucleobase binding studies *in vitro* cannot accurately mimic conditions *in vivo*. Whilst a 100-fold greater concentration of carboplatin is required to achieve the same rate of DNA platination as cisplatin *in vitro*, only a 4–20 fold increase is required to achieve the same platination rates in patients.[5] This can be attributed to the reduced deactivation of carboplatin by side reactions, as a result of its increased stability.

Additionally, these complexes release azide anions upon hydrolysis. This anion is itself cytotoxic by inhibition of cytochrome c oxidase and subsequent disruption of cellular respiration,[56] so it is possible this has an effect on the cytotoxicity of these complexes and could be further investigated.

3.4.6 Photoreactions

The photochemistry of metal azido complexes is well established, with several reports concerning Pt^{II} and Pt^{IV} complexes.[8] Since the hydrolysis of the Pt–N_3 bond has been observed upon irradiation of Pt^{II} complexes, it was hypothesised that this may lead to an increase in nucleobase binding and cytotoxicity upon irradiation. On the other hand, the Pt^{IV} diazido analogues are intended to be stable and unreactive towards biomolecules in the dark but become activated upon irradiation, as is the case for many Pt^{IV} complexes previously reported.[2,22,31] Hence the photoreactions of $[Pt(en)(N_3)_2]$ (**2**) and $[Pt(L1)(N_3)_2(OAc)_2]$ (**6**) were

investigated both alone and in the presence of 5'-GMP. The Pt^{II} chlorido complexes were also included for comparative purposes.

3.4.6.1 Photoreactions in Aqueous Solution

a) $[Pt(en)Cl_2]$ (**1**) and $[Pt(L1)Cl_2]$ (**4**)

The lack of change in the ^1H NMR spectra and pH values following UVA and visible light irradiation indicated that the Pt^{II} chlorido complexes **1** and **4** were stable under these conditions. Although it has been previously suggested that cisplatin is unstable upon irradiation with UVA and prolonged exposure to daylight,[57] it has been found to show no change in toxicity upon irradiation with UVA light.[2]

b) $[Pt(en)(N_3)_2]$ (**2**)

The decomposition of complex **2** was apparent after 5 min of UVA irradiation, however the photoproducts could be not identified. This was also the case in a previous study into the photoactivity of this complex in water;[22] although a new species was seen by 2D [^1H, ^{15}N] NMR experiments, its identity was unknown. The same reaction performed in 100 mM NaCl solution gave rise to $[Pt(en)Cl(N_3)]$, indicating an azido ligand can be substituted upon irradiation. Further irradiation resulted in the loss of intensity of peaks in the spectrum and formation of a small amount of yellow precipitate. The former was observed in the experiment performed in this work, although a precipitate was not observed.

The photochemistry of coordinated azides is rich and varied, and can involve the formation of nitrene intermediates, nitrido complexes and azide radicals, among others,[8] hence the identification of photoproducts is not trivial. Furthermore, certain photoproducts may not be amenable to NMR observation; for example the formation of paramagnetic species would result in significant broadening of NMR

signals. This experiment is nevertheless useful to gain an idea of the rate of decomposition of the starting material.

c) $[Pt(L1)(N_3)_2(OAc)_2]$ (**6**)

Very rapid photoreduction of this complex is seen as monitored by the increase in free acetate, which comprised 24% of the total acetate signal by ^1H NMR after just 1 min of UVA irradiation. The rate was reduced somewhat upon irradiation with visible light, with 12% free acetate after 1 min. Two previous irradiation studies followed by NMR have been carried out with Pt^{IV} azido complexes containing axial acetato groups, both using visible light. The first involved irradiation of $[Pt(NH_3)_2(N_3)_2(OAc)_2]$ with blue light (457.9 nm, 15 mW)[22] where the photoreduction proceeded much more slowly, with over half of the acetate still bound after 4.1 h. The second involved irradiation of three pyridyl complexes with green light (514 nm, 60 mW cm^{-2}),[40] in which the percentage of bound acetate after 15 min irradiation was 15%, 65% and 76%, highlighting dependence upon the nature of the amine ligands. In the present case, 34% of acetate was bound after this time. There appears to be little information on the reduction rate of Pt^{IV} azido complexes containing axial hydroxyl groups, however it appears that the reduction proceeds faster with acetato groups. Such complexes have increased reduction potentials; however this factor may not be so relevant in the case of photochemical reductions.

Photoreduction was also monitored by UV-visible spectroscopy, following the decrease in intensity of the $N_3 \rightarrow Pt$ ligand-to-metal charge transfer (LMCT) band; again this indicated a decrease in rate with visible compared with UVA light. It is interesting that visible light can induce such a reaction given the very small extinction coefficients at these wavelengths; however a computational study has indicated low-energy transitions of a highly dissociative nature, which can clearly induce ligand dissociation.[40]

It is evident that the major photoproduct(s) do not contain acetate. A previous study of $[Pt(bipy)(N_3)_2(OAc)_2]$ (bipy = bipyridine) suggested the products of UVA irradiation included $[Pt(bipy)(OH)_2]$ and $[\{Pt(bipy)(\mu\text{-}OH)\}_2]$, by comparison with their UV-visible absorption spectra.[40] However solutions of **6** rapidly become acidic upon irradiation, in such conditions dimer formation does not occur and any hydroxy species would be protonated. Upon visible irradiation of **6** a new peak was seen by ^{1}H NMR in the region of bound acetate (2.14 ppm); this could potentially arise from a monoacetato intermediate, or an isomerisation product in which the two acetato groups are chemically equivalent. This product was not observed upon UVA irradiation; the much faster rate of photoreduction could render any intermediates difficult to distinguish.

3.4.6.2 Photoreactions with 5'-GMP

a) $[Pt(en)(N_3)_2]$ (**2**)

UVA irradiation initially appeared to accelerate the reaction of 5'-GMP with **2**, with the formation of monoadducts after 1 min and bisadducts after 5 min. However, after 10 min there was little change in the proportion of free 5'-GMP, and by the end of the reaction, 77% of the total remained unbound.

The proportion of monoadduct reached a peak at 7 min (22%) and began to decrease thereafter, but the concomitant increase in bisadduct was small and did not parallel this, suggesting further substitution did not occur. In fact, the decline of monoadduct seems to more closely parallel the growth of the new species **2f**, however this was not confirmed. Although **2f** was not identified, it is tentatively suggested to arise from a Pt^{IV} species, on account of its high chemical shift, small coupling constant ($^3J(^{195}Pt–^1H)$ = 16 Hz) and clearly visible satellites. Choi *et al* have reported a Pt^{IV}–5'-GMP adduct with a very similar chemical shift.[34] However, in that case the species was an intermediate in the reaction of a Pt^{IV} complex with 5'-GMP, and subsequently underwent reduction. In this reaction of a Pt^{II} complex it is not clear how an oxidised species would arise, since there is no

oxidant present in the reaction solution; an additional question is whether oxidation would take place before or after binding. There is no evidence to suggest formation of a Pt^{IV} species upon the irradiation of **2** alone, although the oxidation of **2** over time in solution has been observed. Should the suggested relationship between the monoadduct and this species be confirmed, it would indicate oxidation taking place when the platinum was bound. Further experiments would be needed in order to investigate this.

Complex **2** appeared to be less reactive towards 5'-GMP on irradiation than are the Pt^{IV} analogues previously studied.[31] This could be due to the decomposition into photoproducts to which 5'-GMP cannot bind. However, little further reaction towards 5'-GMP was seen after 10 min, whilst irradiation studies in water alone suggest a significant proportion of **2** remains at this time.

b) $[Pt(L1)(N_3)_2(OAc)_2]$ (**6**)

Although formation of a Pt^{II}–5'-GMP adduct was initially seen, reaching 20% of the total 5'-GMP intensity after 15 min of irradiation, signals began to decrease thereafter and by 60 min there was no evidence of bound 5'-GMP. This is in contrast to other Pt^{IV} azido complexes studied. For example upon UVA irradiation of *trans,trans,trans*-$[Pt(NH_3)_2(N_3)_2(OH)_2]$ with 5'-GMP, the bisadduct accounted for 50% of the total 5'-GMP intensity after 20 min and rose to 70% after 60 min.[31] The reason for the lack of reactivity here is unclear. As also suggested for **2**, it may be that the photoproducts of this irradiation are unable to bind significantly to 5'-GMP. A similar rate of reduction and loss of aliphatic signal intensity is seen here compared with the irradiation of **6** alone, indicating that the decomposition pathway is similar. It is also unclear as to why the adduct formed should be unstable to further irradiation.

3.4.6.3 Phototoxicity

As stated before, the Pt^{II} azido complexes $[Pt(en)(N_3)_2]$ (**2**), $[Pt(L1)(N_3)_2]$ (**5**) and $[Pt(L2)(N_3)_2]$ (**8**), and the Pt^{IV} complex $[Pt(L1)(N_3)_2(OAc)_2]$ (**6**), were all found to be non-phototoxic towards HaCaT keratinocytes upon UVA irradiation. A contributing factor to this may be the lack of adduct formation with nucleobases, as discussed in section 3.4.6.2. Complex **2**, which shows a small degree of adduct formation, does show slightly greater toxicity upon irradiation than in the dark, however with an IC_{50} of 222.7 μM it is classified as inactive in these tests. Complexes **5** and **8** are inactive at all concentrations tested, and it would be interesting to see if any 5'-GMP adducts are formed with these complexes upon irradiation.

The Pt^{IV} azido complex **6** showed no evidence of phototoxicity at concentrations up to 200 μM. Although a small degree of 5'-GMP binding is seen, the adduct formed appears to be unstable and by 60 min irradiation is no longer detected by NMR. Since the irradiation time during testing is 50 min, it is possible that any adduct that does form would be decomposed upon subsequent irradiation. This is the only Pt^{IV} azido complex with axial acetato groups tested for phototoxicity, so it would be interesting to see if the lack of activity is common to all acetato complexes, or if those with a different amine ligand may show different results.

It is important to consider that DNA binding would not be the only factor governing phototoxicity; for example cell uptake and distribution and reactions with other biomolecules would also be of great importance.

3.5 Conclusions

A series of Pt^{II} azido complexes with a pendant hydroxyl group was synthesised and characterised, along with one Pt^{IV} complex with acetato groups in the axial positions. The X-ray crystal structure was obtained for one Pt^{II} complex and indicates the hydroxyl group is involved in intra- and intermolecular hydrogen

bonding. In addition, Pt^{II} and Pt^{IV} azido complexes of a ligand containing a protected amine group were also prepared.

Stability studies were carried out on the Pt^{II} azido complex $[Pt(en)(N_3)_2]$ (**2**), which was found to undergo slow reaction in aqueous and 100 mM chloride solutions, yielding hydrolysis products and also a significant proportion of a Pt^{IV} species. Complex **2** was reactive towards glutathione in the dark, although at a much reduced rate compared with the Pt^{II} chlorido analogue, and also reacted with 5'-GMP in the dark forming mono and bisadducts, at a rate approximately an order of magnitude lower than that of cisplatin. All four Pt^{II} azido complexes tested showed moderate cytotoxicity against the A2780 human ovarian cancer cell line, with IC_{50} values ranging from 21–47 μM. Similar stability studies were performed with the Pt^{IV} azido complex $[Pt(L1)(N_3)_2(OAc)_2]$ (**6**), and showed that this complex was stable in aqueous and chloride solutions, and unreactive towards glutathione and 5'-GMP in the dark.

Complex **2** was found to be photoactive in aqueous solution upon irradiation with both UVA and visible light, although the identity of the photoproducts could not be ascertained, whilst complex **6** underwent a rapid photoreduction with release of acetate. The extent of binding to 5'-GMP upon UVA irradiation was low for both complexes. In addition to mono and bis Pt^{II}–5'-GMP adducts, **2** gave rise to a species tentatively assigned as a Pt^{IV}–5'-GMP adduct, whilst the small quantity of a Pt^{II}–5'-GMP adduct produced in the reaction of **6** decomposed upon further irradiation. The lack of formation of stable adducts with nucleobases could explain the observed lack of phototoxicity of these complexes.

This Chapter reports the first example of Pt^{II} azido complexes investigated for anticancer activity. Although such complexes were expected to be inactive due to the stability of the $Pt–N_3$ bond, moderate activity was found in all complexes tested. These results further support the investigation of poor leaving groups in the search for complexes that undergo minimal deactivation reactions but still retain cytotoxic activity.

3.6 References

[1] P. J. Bednarski, F. S. Mackay and P. J. Sadler, *Anti-Cancer Agents Med. Chem.*, 2007, **7**, 75.

[2] F. S. Mackay, J. A. Woods, P. Heringová, J. Kašpárková, A. M. Pizarro, S. A. Moggach, S. Parsons, V. Brabec and P. J. Sadler, *Proc. Natl. Acad. Sci. U. S. A.*, 2007, **104**, 20743.

[3] M. J. Cleare and J. D. Hoeschele, *Bioinorg. Chem.*, 1973, **2**, 187.

[4] F. Basolo, H. B. Gray and R. G. Pearson, *J. Am. Chem. Soc.*, 1960, **82**, 4200.

[5] M. A. Jakupec, M. Galanski, B. K. Keppler, H. G. Koch, M. Muller, B. C. Burckhardt and G. Burckhardt, *Rev. Physiol. Biochem. Pharmacol.*, 2003, **146**, 1.

[6] A. M. Pizarro and P. J. Sadler, in *Nucleic Acid-Metal Ion Interactions*, ed. N. V. Hud, Royal Society of Chemistry, Cambridge, England, 2008, ch. 10, pp 350–398.

[7] F. Wang, A. Habtemariam, E. P. L. van der Geer, R. Fernández, M. Melchart, R. J. Deeth, R. Aird, S. Guichard, F. P. A. Fabbiani, P. Lozano-Casal, I. D. H. Oswald, D. I. Jodrell, S. Parsons and P. J. Sadler, *Proc. Natl. Acad. Sci. U. S. A.*, 2005, **102**, 18269.

[8] J. Šima, *Coord. Chem. Rev.*, 2006, **250**, 2325.

[9] B. Rosenberg, L. Van Camp, J. E. Trosko and V. H. Mansour, *Nature*, 1969, **222**, 385.

[10] J. Kašpárková, F. S. Mackay, V. Brabec and P. J. Sadler, *J. Biol. Inorg. Chem.*, 2003, **8**, 741.

[11] J. N. Jolley, A. I. Yanovsky, L. R. Kelland and K. B. Nolan, *J. Inorg. Biochem.*, 2001, **83**, 91.

[12] P. Urban and L. Bretherick, *Bretherick's Handbook of Reactive Chemical Hazards Volume 2*, Butterworth-Heinemann, Oxford, 6th edn., 1999.

[13] P. Muller, B. Schroder, J. A. Parkinson, N. A. Kratochwil, R. A. Coxall, A. Parkin, S. Parsons and P. J. Sadler, *Angew. Chem. Int. Ed.*, 2003, **42**, 335.

[14] M. Galanski, W. Zimmermann, M. Berger, C. Baumgartner, G. Giester, and B. K. Keppler, *Eur. J. Inorg. Chem.*, 2002, 417.

[15] T. G. Appleton and J. R. Hall, *Inorg. Chem.*, 1972, **11**, 112.

[16] W. Liu, X. Chen, M. Xie, L. Lou, Q. Ye, Y. Yu and S. Hou, *J. Inorg. Biochem.*, 2008, **102**, 1942.

[17] S. Ren, L. Cai and B. M. Segal, *J. Chem. Soc. Dalton Trans.*, 1999, 1413.

[18] M. S. Davies, P. N. Wong, A. R. Battle, G. Haddad, M. J. McKeage and T. W. Hambley, *J. Inorg. Biochem.*, 2002, **91**, 205.

[19] H. C. Fry, C. Deal, E. Barr and S. D. Cummings, *J. Photochem. Photobiol. A*, 2002, **150**, 37.

[20] M. J. Abrams, C. M. Giandomenico, J. F. Vollano and D. A. Schwartz, *Inorg. Chim. Acta*, 1987, **131**, 3.

[21] A. P. Krapcho and C. S. Kuell, *Synth. Commun.*, 1990, **20**, 2559.

[22] P. Müller, Ph.D. Thesis, The University of Edinburgh, 2002.

[23] P. del Socorro Murdoch, N. A. Kratochwil, J. A. Parkinson, M. Patriarca and P. J. Sadler, *Angew. Chem. Int. Ed.*, 1999, **38**, 19.

[24] E. R. Jamieson and S. J. Lippard, *Chem. Rev.*, 1999, **99**, 2467.

[25] J.-P. Girault, J.-C. Chottard, E. R. Guittet, J. Y. Lallemand, T. Huynh Dinh and J. Igolen, *Biochem. Biophys. Res. Commun.*, 1982, **109**, 1157.

[26] J. L. van der Veer, H. van den Elst and J. Reedijk, *Inorg. Chem.*, 1987, **26**, 1536.

[27] A. T. M. Marcelis, C. G. van Kralingen and J. Reedijk, *J. Inorg. Biochem.*, 1980, **13**, 213.

[28] W. Liu, X. Chen, M. Xie, L. Lou, Q. Ye, Y. Yu and S. Hou, *J. Inorg. Biochem.*, 2008, **102**, 1942.

[29] A. Vogler, A. Kern and J. Hüttermann, *Angew. Chem. Int. Ed. Engl.*, 1978, **17**, 524.

[30] A. Vogler and J. Hlavatsch, *Angew. Chem. Int. Ed. Engl.,* 1983, **22**, 154.

[31] F. Mackay, Ph.D. Thesis, The University of Edinburgh, 2006.

[32] H. Knoll, R. Stich, H. Hennig and D. J. Stufkens, *Inorg. Chim. Acta*, 1990, **178**, 71.

[33] F. S. Mackay, J. A. Woods, P. Heringová, J. Kašpárková, A. M. Pizarro, S. A. Moggach, S. Parsons, V. Brabec and P. J. Sadler, *Proc. Natl. Acad. Sci. U. S. A.*, 2007, **104**, 20743.

[34] S. Choi, S. Mahalingaiah, S. Delaney, N. R. Meale and S. Masood, *Inorg. Chem.*, 1999, **38**, 1800.

[35] M. S. Robillard, M. Galanski, W. Zimmermann, B. K. Keppler and J. Reedijk, *J. Inorg. Biochem.*, 2002, **88**, 254.

[36] M. Galanski, C. Baumgartner, V. Arion and B. K. Keppler, *Eur. J. Inorg. Chem.*, 2003, 2619.

[37] A. R. Khokhar, Q. Xu, R. A. Newman, Z. Kido and Z. H. Siddik, *J. Inorg. Biochem.*, 1992, **45**, 211.

[38] A. Oksanen, R. Kivekäs and P. Lumme, *Acta Cryst.*, 1991, **C47**, 719.

[39] L. T. Ellis, H. M. Er and T. W. Hambley, *Aust. J. Chem.*, 1995, **48**, 793.

[40] F. S. Mackay, N. J. Farrer, L. Salassa, H.-C. Tai, R. J. Deeth, S. A. Moggach, P. A. Wood, S. Parsons and P. J. Sadler, *Dalton Trans.*, 2009, 2315.

[41] A. M. Pizarro, V. P. Munk, C. Navarro-Ranninger and P. J. Sadler, *Angew. Chem. Int. Ed.*, 2003, **42**, 5339.

[42] M. D. Hall and T. W. Hambley, *Coord. Chem. Rev.*, 2002, **232**, 49.

[43] Y. Kasherman, S. Sturup and D. Gibson, *J. Biol. Inorg. Chem.*, 2009, **14**, 387.

[44] T. Rau, R. Alsfasser, A. Zahl, and R. van Eldik, *Inorg. Chem.*, 1998, **37**, 4223.

[45] D. Hagrman, J. Goodisman and A.-K. Souid, *J. Pharmacol. Exp. Ther.*, 2004, **308**, 658.

[46] M. D. Hall, C. T. Dillon, M. Zhang, P. Beale, Z. H. Cai, B. Lai, A. P. J. Stampfl and T. W. Hambley, *J. Biol. Inorg. Chem.*, 2003, **8**, 726.

[47] F. I. Raynaud, D. E. Odell and L. R. Kelland, *Br. J. Cancer,* 1996, **74**, 380.

[48] N. A. Kratochwil and P. J. Bednarski, *Arch. Pharm.*, 1999, **332**, 279.

[49] J. Kašpárková, O. Novakova, O. Vrana, F. Intini, G. Natile and V. Brabec, *Mol. Pharmacol.*, 2006, **70**, 1708.

[50] A. Nemirovski, Y. Kasherman, Y. Tzaraf and D. Gibson, *J. Med. Chem.*, 2007, **50**, 5554.

[51] L. Chen, P. F. Lee, J. D. Ranford, J. J. Vittal and Y. S. Wong, *J. Chem. Soc. Dalton Trans.*, 1999, **8**, 1209.

[52] A. Küng, D. B. Strickmann, M. Galanski and B. K. Keppler, *J. Inorg. Biochem.*, 2001, **86**, 691.

[53] M. Galanski and B. K. Keppler, *Inorg. Chim. Acta.*, 2000, **300–302**, 783.

[54] L. Cai, K. Lim, S. Ren, R. S. Cadena and W. T. Beck, *J. Med. Chem.*, 2001, **44**, 2959.

[55] L. G. Nikolcheva, C. M. Vogels, R. A. Stefan, H. A. Darwish, S. J. Duffy, R. J. Ireland, A. Decken, R. H. E. Hudson and S. A. Westcott, *Can. J.*

Chem., 2003, **81**, 269.

[56] K. Inomata and H. Tanaka, *J. Pharmacol.*, 2003, **93**, 163.

[57] M. Macka, J. Borák, L. Seménková and F. Kiss, *J. Pharm. Sci*., 1994, **83**, 815.

Chapter 4

Functionalisation of Platinum Complexes

4.1 Introduction

An increasingly popular strategy in the development of metal-based anticancer complexes is their functionalisation with biologically-active species. This offers the possibility to address several major challenges in drug design; including selectivity, either for cancer cells over healthy cells or for specific intracellular targets, and the understanding of drug distribution and mechanism of action. There have been many examples of this approach, involving a variety of biologically-active species for different purposes; some examples are given in Figure 4.1.

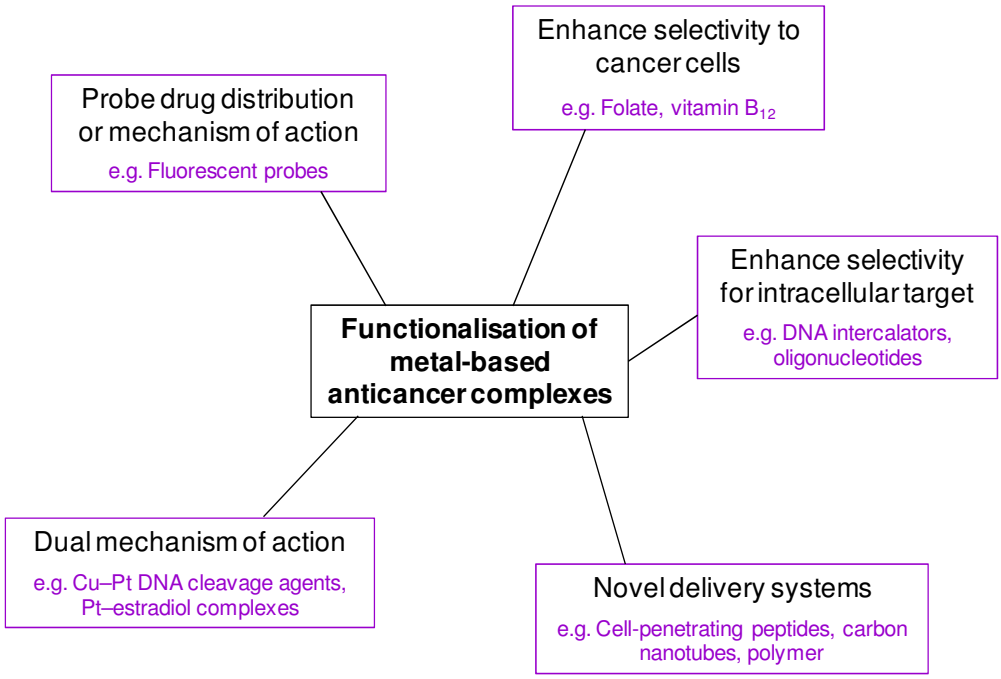

Figure 4.1 Examples of the functionalisation of metal-based anticancer complexes with biologically-active species.

Several approaches selectively target cancer cells by exploiting their differences compared with healthy cells. For example, the rapid proliferation of cancer cells

elevates their nutritional requirements, and as such the receptors for many nutrients are overexpressed on their surfaces. Platinum complexes of folic acid[1] and vitamin B_{12}[2] were thus designed to be selectively taken up into cancer cells. In addition, as a result of compromised vasculature, tumour tissue can often accumulate large macromolecules and this has been exploited in the use of novel drug delivery methods, such as polymers and liposomes. Several examples of this strategy were given in the introduction to this thesis (Chapter 1).

Also discussed in Chapter 1 were several complexes with a dual mode of action – for example, Pt^{IV}–estradiol complexes designed to sensitise ER(+) cells to the cytotoxic platinum species released upon reduction.[3] An additional example is that of a Cu–Pt complex with the ability to cleave DNA as well as form cross-links; the platinum moiety also serves to anchor the complex, resulting in a different DNA cleavage profile to that of the copper complex alone.[4]

Monitoring the cellular distribution and elucidating the mechanism of action of potential metal-based drugs is of particular interest, since their biochemistry is often rich and varied. Many organic drug molecules are designed to interact with a specific receptor or enzyme, however for some metal complexes the mechanism is less well defined, and even their intracellular target can be unclear.[5] Functionalisation with a fluorescent probe or incorporation of a fluorescent ligand can therefore be of great benefit, both in visualising the distribution and in monitoring changes in fluorescence to give an indication of possible intracellular transformations.[6]

This Chapter is concerned with the functionalisation of Pt^{II} and Pt^{IV} azido complexes, and is divided into three sections. The first investigates the derivatisation of Pt^{II} and Pt^{IV} azido complexes with organic fluorescent probes. The second involves the synthesis of quantum dots, semiconductor nanocrystals with superior fluorescent properties, and their functionalisation with platinum complexes. The final part of the Chapter is concerned with the synthesis of Pt^{II} chlorido and azido complexes containing a porphyrin ligand, a moiety which shows well established photochemical behaviour.

4.2 Platinum Complexes Containing Organic Fluorescent Probes

4.2.1 Introduction

As discussed in section 4.1, the attachment of a fluorescent probe to a potential drug molecule can aid in monitoring cellular distribution and elucidating the mechanism of action. Although this strategy has been widely used in the study of organic drugs,[7] it has only recently begun to receive interest in application to platinum complexes. Reedijk *et al* reported the cellular distribution and processing pathways of cisplatin analogues derivatised with fluorescent probes,[8] visualised by digital fluorescence microscopy, as well as a series of monofunctional platinum complexes for use as nucleic acid labelling reagents.[9] In addition, complexes have been studied in which the fluorescent species are directly bound to platinum. Very recently, Hambley *et al* described a series of complexes containing coumarin, in which the fluorescence is sensitive to the oxidation state of the platinum and could thus act as a sensor for the Pt^{IV} to Pt^{II} reduction event.[6] Similarly, a complex of 7-azaindole was reported in which the fluorescence of the ligand is quenched upon coordination to platinum, but increases upon reaction of the complex with sulfur-containing biomolecules due to *trans*-labilisation, and could thus be of use in monitoring intracellular transformations of such complexes.[10]

Chapter 3 of this thesis described the synthesis of Pt^{II} and Pt^{IV} azido complexes containing pendant functional groups suitable for derivatisation, and incorporation of fluorescent probes into these complexes could provide valuable knowledge of the photoproducts formed upon irradiation and, potentially, the fate of the complexes within cells. Previous studies have indicated the Pt^{IV} complexes have a complicated photodegradation pathway,[11] and a potentially different cytotoxic mechanism to cisplatin.[12] Furthermore, the Pt^{II} azido complexes are novel and their mechanism of action has not yet been investigated.

Two organic fluorescent probes were chosen for conjugation to the Pt^{II} and Pt^{IV} azido complexes. The first, *N*-methylisatoic anhydride (MIA), reacts readily with

alcohol groups to form fluorescent esters, and has found many applications in biochemistry ranging from the labelling of nucleotides[13] and small-molecule protein inhibitors[14] to proteins and large enzymes such as kinases;[15] however only one previous example of its use in the labelling of metal complexes can be found.[16] The small size of the probe should minimise any change in properties of the complex arising from conjugation; it has previously been found that conjugation of a large fluorophore such as fluorescein can affect cellular uptake and diffusion rates of labelled complexes.[17] MIA was therefore selected for conjugation to the pendant hydroxyl group of the Pt^{II} azido complex $[Pt(L1)(N_3)_2]$ (**5**), and the axial hydroxyl groups of the Pt^{IV} complex $[Pt(en)(N_3)_2(OH)_2]$ (**3**).

The second probe, dansyl chloride (DnCl), was chosen for the derivatisation of the Pt^{II} and Pt^{IV} complexes containing a protected amine group, $[Pt(L5)(NH_3)(N_3)_2]$ (**14**) and $[Pt(L5)(NH_3)(N_3)_2(OH)_2]$ (**15**). Dansyl chloride itself is non-fluorescent, but readily reacts with amine groups to produce fluorescent dansyl sulfonamides. It is widely used in protein sequencing, in the determination of the N-terminal amino acid residue.[18]

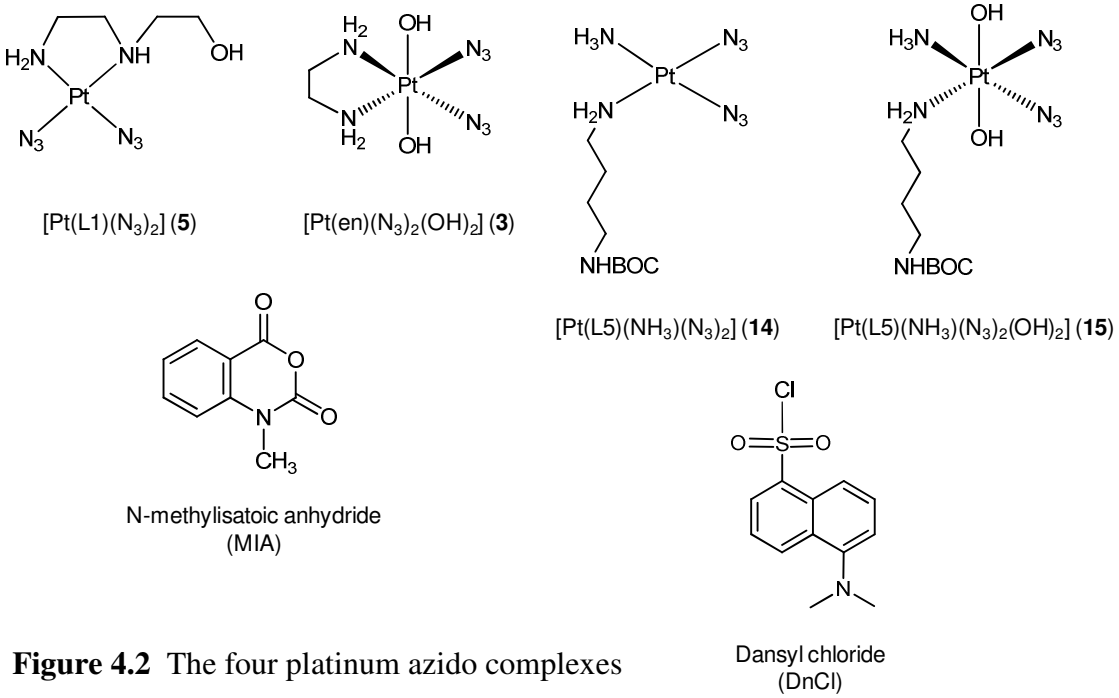

Figure 4.2 The four platinum azido complexes investigated for derivatisation and two fluorescent probes.

4.2.2 Experimental

4.2.2.1 Materials

[Pt(L1)$(N_3)_2$] (**5**), *cis,trans*-[Pt(en)$(N_3)_2(OH)_2$] (**3**), *cis*-[Pt(L5)$(NH_3)(N_3)_2$] (**14**) and *cis,cis,trans*-[Pt(L5)$(NH_3)(N_3)_2(OH)_2$] (**15**) were synthesised as described in Chapter 3. *N*-Methylisatoic anhydride (MIA, 90%) was obtained from Acros Organics, and 4-dimethylaminopyridine (DMAP) and dansyl chloride (DnCl) were from Sigma-Aldrich. Anhydrous grade *N,N*-dimethylformamide (DMF, 99.8 %) was purchased from Aldrich, and triethylamine from Fisher.

4.2.2.2 Synthesis

[Pt(L1-OMIA)$(N_3)_2$] (16)

[Pt(L1)$(N_3)_2$] (**5**) (50 mg, 0.13 mmol) was dissolved in anhydrous DMF (1.5 mL). Triethylamine (18 µL, 0.13 mmol) and DMAP (3.2 mg, 0.03 mmol) were added, followed by MIA (92 mg, 0.52 mmol), and the solution was placed under nitrogen and stirred at room temperature for 40 h in the dark. The addition of diethyl ether yielded a sandy coloured precipitate, which was isolated by centrifugation and washed extensively with diethyl ether to remove excess MIA, until the supernatants were non-fluorescent. The precipitate was then dried under vacuum overnight.

Yield: 20 mg (30%).

^{1}H NMR (400 MHz, DMSO-d_6): δ = 7.90 (d, arom-CH, 1H), 7.54 (d, NH, 1H), 6.72 (d, arom-CH, 1H), 6.59 (t, arom-CH, 1H), 6.33 (br s, NH, 1H), 5.40 (br s, NH_2, 1H), 5.24 (br s, NH_2, 1H), 4.51 (m, CH_2, 1H), 4.38 (m, CH_2, 1H), 3.16 (d, CH_3, 3H), 2.98 (m, CH_2, 1H), 2.67 (m, CH_2, 1H), 2.65 (m, CH_2, 1H), 2.41 (m, CH_2, 1H), 2.32 (m, CH_2, 2H).

ESI-MS: 539.1203 $[M + Na]^+$, $NaPtC_{12}H_{19}N_9O_2$ requires 539.1202 *m/z*.
Fluorescence (DMF): λ_{em} 421 nm.

Cis,trans-[Pt(en)$(N_3)_2$(OH)(OMIA)] (17)

Cis,trans-[Pt(en)$(N_3)_2(OH)_2$] (**3**) (50 mg, 0.14 mmol) was suspended in anhydrous DMF (1 mL). MIA (95 mg, 0.54 mmol) was added and the mixture stirred at 310 K in the dark for 48 h. A small quantity of yellow-grey solid was removed by filtration, and to the brown filtrate was added diethyl ether. A yellow solid precipitated, which was isolated by centrifugation and washed extensively with diethyl ether, then dried under vacuum overnight.

Yield: 18 mg (25%).
^{1}H NMR (400 MHz, DMSO-d_6): δ = 7.92 (d, arom-CH, 1H), 7.69 (br s, NH_2, 2H), 7.63 (d, arom-CH, 1H), 7.27 (t, arom-CH, 1H), 6.74 (br s, NH_2, 2H), 6.58 (d, arom-CH, 1H), 6.48 (t, arom-CH, 1H), 2.79 (d, CH_3, 3H), 1.59 (s, CH_2, 2H).
ESI-MS: 529.0994 $[M + Na]^+$, 507.1176 $[M + H]^+$, $NaPtC_{10}H_{17}N_9O_3$ requires 529.0990, $PtC_{10}H_{18}N_9O_3$ requires 507.1177 *m/z*.
Fluorescence (DMF): λ_{max} 414 nm.

Cis-[Pt(L5-NDn)$(NH_3)(N_3)_2$]

Cis-[Pt(L5)$(NH_3)(N_3)_2$] (**14**) was suspended in 0.1 M HCl (2 mL) and stirred at 310 K in the dark for 16 h, after which all solid had dissolved to give a yellow solution. The pH was then adjusted to 9.5, the solution cooled to 273 K and dansyl chloride (7.7 mg) was added, after which the solution was stirred for 4 h in the dark. Work-up attempts included removal of solvent and re-suspension in water, and precipitation with various solvents, however it was not possible to isolate a clean sample of this complex despite mass spectral evidence of its formation.
ESI-MS: 616.15 $[M – H]^+$, $PtC_{16}H_{25}N_{10}O_2S$ requires 616.15 *m/z*.
Fluorescence (H_2O): λ_{max} 493 nm.

***Cis,trans,cis*-[Pt(L5-NDn)(NH_3)(N_3)$_2$(OH)$_2$]**

The synthetic procedure was as for [Pt(L5-NDn)(NH_3)(N_3)$_2$], but starting from the Pt^{IV} complex [Pt(L5)(NH_3)(N_3)$_2$(OH)$_2$] (**15**). Again, a clean sample of the desired complex could not be obtained, and mass spectral evidence could not be found.

Fluorescence (DMF): λ_{max} 491 nm.

4.2.2.3 Methods

4.2.2.3.1 Fluorescence Spectroscopy

Fluorescence emission spectra of 7 µM solutions of **16**, **17** and MIAH were recorded at 298 K in DMF, with λ_{ex} = 316 nm. MIAH was obtained from the addition of 5 eq HCl to a 7 µM solution of MIA. Emission spectra of **18** and **19** were recorded at 298 K in water, with λ_{ex} = 337 nm.

4.2.2.3.2 Photoreactions

The change in the fluorescence spectra of **17** upon irradiation with visible light was monitored over a 10 min period. A 7 µM solution of **17** in DMF was irradiated in a LZC-ICH2 photoreactor equipped with LZC-VIS UV-Visible light lamps (λ = 400–700 nm, P = 0.27 mW cm^{-2}), and fluorescence emission spectra were recorded every 1 min for a total of 10 min, with λ_{ex} = 316 nm.

4.2.3 Results

This section has investigated the conjugation of fluorescent probes to Pt^{II} and Pt^{IV} azido complexes synthesised in Chapter 3. The pendant hydroxyl group of a Pt^{II} azido complex was derivatised with N-methylisatoic anhydride (MIA); this fluorophore was also used in the functionalisation of an axial hydroxyl group of a

Pt^{IV} azido complex. The fluorescence emission spectra of both complexes were obtained and compared with that of an equimolar solution of the fluorophore. The change in fluorescence intensity of the Pt^{IV} complex upon irradiation with visible light was monitored. Attempts were also made to functionalise Pt^{II} and Pt^{IV} azido complexes containing protected amine ligands, *via* deprotection followed by reaction with dansyl chloride to form fluorescent sulfonamides.

4.2.3.1 Functionalising Platinum Complexes with N-methylisatoic anhydride

4.2.3.1.1 Synthesis and Characterisation

a) Functionalisation of a Pt^{II} complex

The Pt^{II} complex $[Pt(L1)(N_3)_2]$ (**5**), containing a pendant hydroxyl group, was reacted with excess *N*-methylisatoic anhydride (MIA) to form a fluorescent ester (Scheme 4.1). The reaction was carried out in DMF, since it is reported that the derivatisation of low molecular weight alcohols with this fluorophore proceeds best in aprotic organic solvents,[19] with DMAP and triethylamine used as a catalyst and auxiliary base, respectively.[20] The product was obtained in a low yield, and characterised by NMR and mass spectrometry.

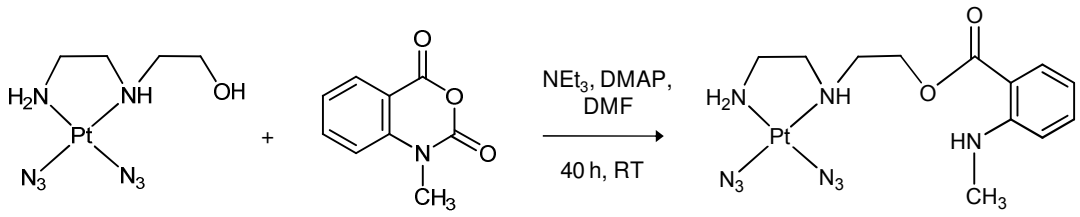

$[Pt(L1)(N_3)_2]$ (**5**) MIA $[Pt(L1\text{-}OMIA)(N_3)_2]$ (**16**)

Scheme 4.1 The functionalisation of the pendant hydroxyl group of a Pt^{II} azido complex with the fluorescent probe N-methylisatoic anhydride (MIA).

b) Functionalisation of a Pt^{IV} complex

$[Pt(en)(N_3)_2(OH)_2]$ (**3**) was reacted with excess MIA in DMF, following a well documented procedure for derivatisation of the axial hydroxyl groups of Pt^{IV} complexes.[21] However, lower temperatures were used in this case due to the sensitivity of azido complexes to temperatures exceeding 313 K. Interestingly, this reaction formed a complex in which only one hydroxyl group was esterified. The ^1H NMR spectrum gives integrals consistent with the mono-esterified complex; in addition, a separate peak was seen for the protons of each NH_2 group, their inequivalence resulting from asymmetry at the platinum centre. Mass spectrometry showed peaks corresponding only to the mono-esterified product and its sodium adduct, with no evidence of the bis product.

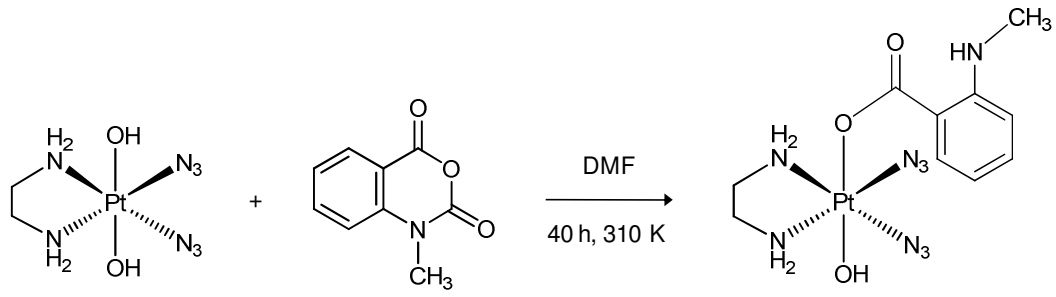

$[Pt(en)(N_3)_2(OH)_2]$ (**3**) MIA $[Pt(en)(N_3)_2(OH)(OMIA)]$ (**17**)

Scheme 4.2 The functionalisation of the axial hydroxyl groups of a Pt^{IV} complex with *N*-methylisatoic anhydride (MIA).

4.2.3.1.2 Fluorescence Spectroscopy

The fluorescence emission spectra of equimolar solutions of [Pt(L1-OMIA)$(N_3)_2$] (**16**) and [Pt(en)$(N_3)_2$(OH)(OMIA)] (**17**) were recorded in DMF, along with that of the free fluorophore MIAH (Figure 4.3). The ring-opened carboxylic acid MIAH was formed from the anhydride MIA by addition of acid, to allow for comparison with the fluorescence spectra of the complexes, in which this is the emissive species.

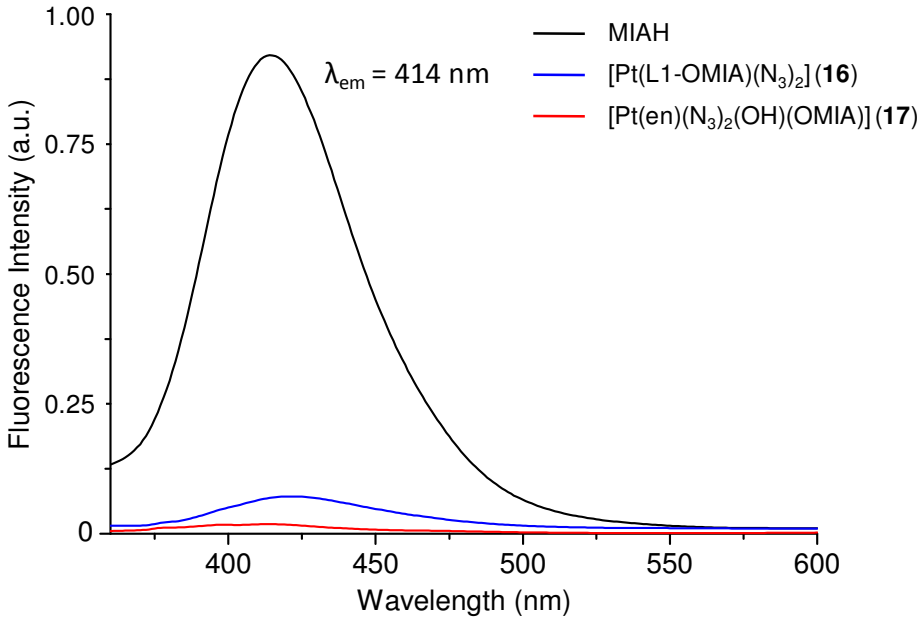

Figure 4.3 Fluorescence emission spectra (λ_{ex} = 316 nm) of 7 µM solutions of MIAH, [Pt(L1-OMIA)$(N_3)_2$] (16) and [Pt(en)$(N_3)_2$(OH)(OMIA)] (**17**) in DMF.

MIAH shows relatively broad emission in the blue region, centred at 414 nm. As expected, quenching of the fluorescence is observed in the spectra of the platinum complexes, due to the internal heavy-atom effect.[22] The Pt^{II} complex (**16**) shows a small red shift (~7 nm) and an approximately 12-fold decrease in fluorescence intensity compared with MIAH; a similar degree of quenching was also observed in the Ru^{II} complex of L1-OMIA.[16] The quenching is more pronounced for the

Pt^{IV} complex (**17**), for which fluorescence is almost undetectable at this concentration, due to the closer proximity of the fluorophore to the metal centre in this complex compared with **16**; furthermore the quenching ability of metals is also affected by their oxidation state, and it has been previously shown that Pt^{IV} appears to exert a greater quenching effect than does Pt^{II}.[6] However, in order to draw quantitative conclusions regarding the reduction in quantum yield, it would be necessary to ensure the solutions were of equal optical density (isoabsorbant).

4.2.3.1.3 Photoreactions of [Pt(en)$(N_3)_2$(OH)(OMIA)] (17)

The fluorescence spectra of [Pt(en)$(N_3)_2$(OH)(OMIA)] (**17**) upon irradiation with visible light in DMF solution was measured over a ten minute period, with spectra acquired every one minute. The fluorescence intensity was found to dramatically increase after only very short irradiation times.

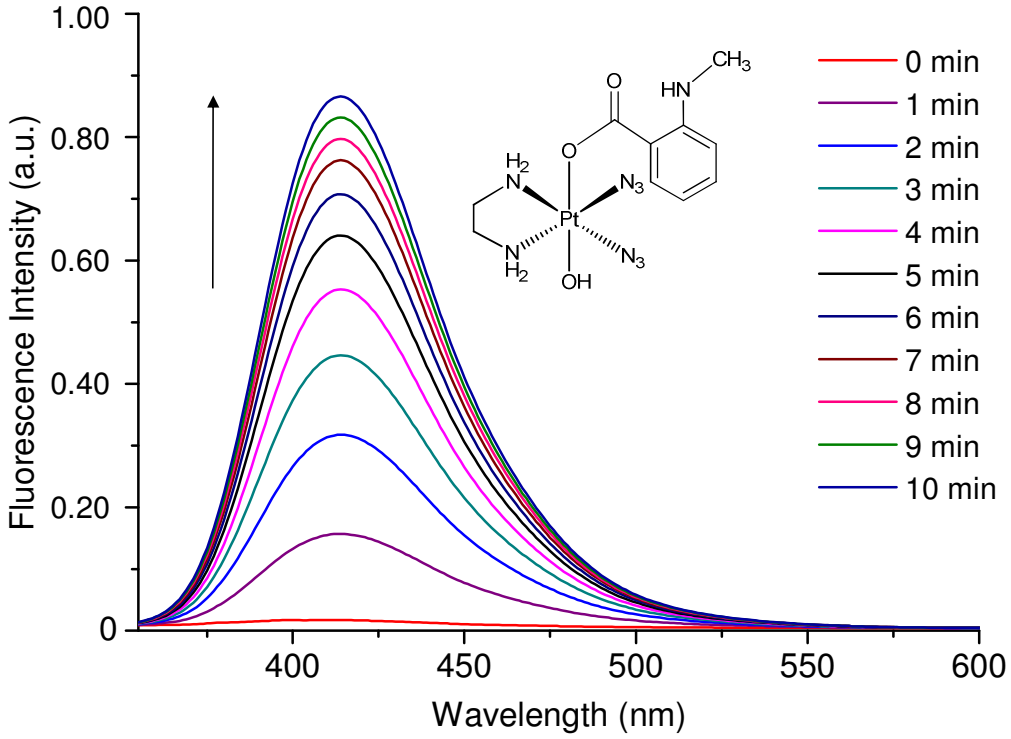

Figure 4.4 The increase in fluorescence observed upon irradiating a sample of (en)$(N_3)_2$(OH)(OMIA)] (**17**) with visible light in DMF.

The increase in intensity upon irradiation indicates the release of MIAH, as the axial ligands are lost upon photoreduction to Pt^{II}. The rapid increase in intensity at the beginning of the experiment indicates that reduction occurs very quickly, and the majority of the Pt^{IV} complex is reduced after only a few minutes of irradiation.

4.2.3.2 Functionalising Platinum Complexes with Dansyl Chloride

4.2.3.2.1 Synthesis and Characterisation

Both the Pt^{II} and Pt^{IV} azido complexes containing a BOC-protected amine were investigated for functionalisation with a dansyl group, with the same reaction scheme followed for both (Scheme 4.3). Deprotection of the BOC group was first carried out by stirring in strong acid; the resulting protonated amine species was not isolated, although reaction was evident, especially in the case of the Pt^{II} complex, by the dissolution of the starting material and formation of a yellow solution. The pH was then increased and dansyl chloride added in order to form the fluorescent sulfonamide; this latter step was carried out at 273 K to minimise the competing hydrolysis of dansyl chloride.

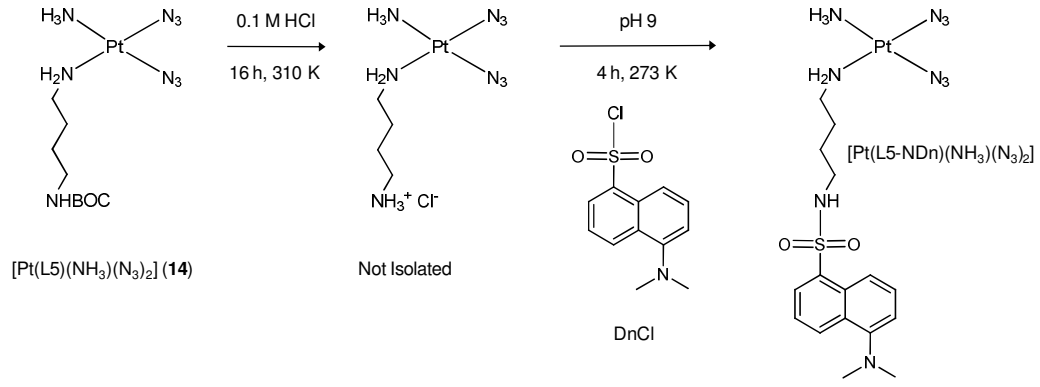

Scheme 4.3 The synthetic procedure for the attempted formation of dansyl sulfonamide complexes, demonstrated for the Pt^{II} complex [Pt(L5-NDn)$(NH_3)(N_3)_2$].

It was not possible to isolate a clean sample of either the Pt^{II} or the Pt^{IV} target complex. Attempts to precipitate the product gave only very small amounts which were found to be impure. However, mass spectral evidence of the Pt^{II} complex $[Pt(L5\text{-}NDn\text{-}H)(N_3)_2]^+$ was obtained. The apparent formation of the ion $[Pt(L5\text{-}NDn\text{-}H)(N_3)_2]^+$, in which the target complex appears to have ionised *via* loss of a hydride, is unexpected, although the mass and isotope pattern match this species well. It is postulated that this ion could be formed by loss of hydride at the dimethylamino group, forming an imine-type species. However, the dimethylamino group is a prime site for protonation under mass spectrometry conditions, and this would have been expected preferentially to give a complex with *m/z* two units higher.

4.2.3.2.2 Fluorescence Spectroscopy

Dansyl chloride itself is not fluorescent, however blue-green fluorescent sulfonamides are generated upon its reaction with amines. The fluorescence spectra of the reaction solutions were therefore measured, in order to determine if there was any evidence of fluorophore formation (Figure 4.5).

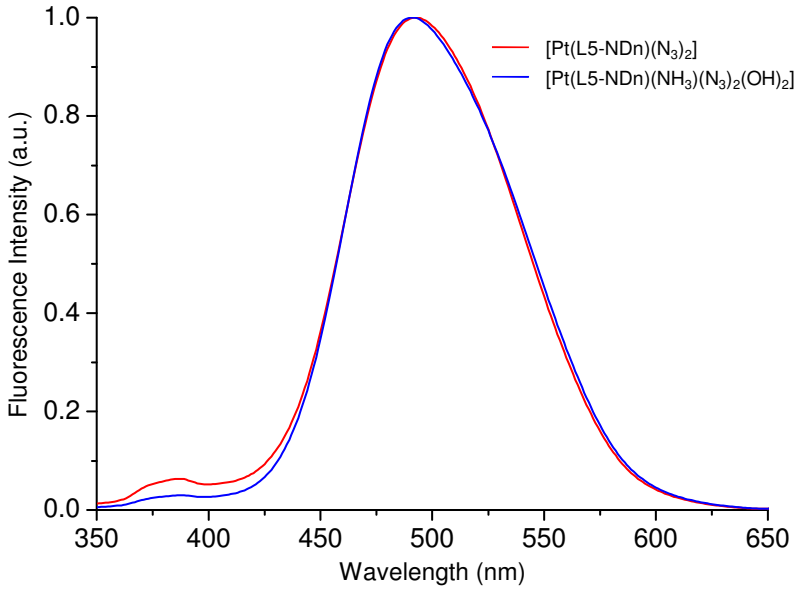

Figure 4.5 The fluorescence emission spectra of the reaction solutions of the Pt^{II} and Pt^{IV} complexes **14** and **15** with dansyl chloride.

The broad band centred upon 492 nm is indicative of sulfonamide formation, and suggests that the reaction was to some degree successful in functionalising the pendant amine group of both Pt^{II} and Pt^{IV} complexes. However, no further information can be gained from the fluorescence spectra, and it cannot be ascertained that this fluorescence arises from the target species. For example, the dissociation of an amine ligand from the platinum centre under strongly acidic conditions, and its subsequent reaction with dansyl chloride, would also generate a species with such an emission spectral profile.

4.2.4 Discussion

4.2.4.1 Functionalisation Strategies

The motivation for the attachment of fluorescent probes to platinum azido complexes was discussed in the introduction: monitoring the fluorescence could provide information on cellular distribution and the mechanism of action of such complexes, as well as their fate upon irradiation. Despite this, however, there have been relatively few examples in the literature of fluorescent probes conjugated to platinum anticancer complexes. An early paper by Lippard *et al* reported a Pt^{II} chlorido complex containing an ethylenediamine unit, to which a fluorescent dansyl group was tethered.[23] In this case, the organic framework was constructed first, followed by the simple addition of a platinum salt to coordinate to the ethylenediamine unit and generate the required, functionalised Pt^{II} complex. Such a strategy has also been employed, for example, in the synthesis of platinum species tethered to intercalators.[24] However, in the case of the Pt^{II}, and particularly Pt^{IV} azido complexes studied in this work, this functionalisation strategy is not feasible. Following synthesis of a Pt^{II} chlorido complex, the Pt^{II} azido species is prepared by chloride extraction with silver nitrate, and the Pt^{IV} complex by oxidation with hydrogen peroxide. The organic framework of many fluorescent probes or other biologically active species would be incompatible with such reagents, as has been recently demonstrated: the oxidation of Pt^{II} chlorido complexes containing fluorescent coumarin ligands was reported to be problematic and low yielding, and in some cases involved oxidation or labilisation of the coumarin moiety.[6] Instead, the preferred functionalisation strategy for Pt^{II} and Pt^{IV} azido complexes involved the preparation of complexes containing a reactive functional group, to which biologically active species could then be attached. Complexes were chosen to contain either a pendant hydroxyl or a protected amine group; the differing chemistries of these two groups allowing for a wide range of biologically active species with which to functionalise. Chapter 3

of this thesis described the synthesis and characterisation of several Pt^{II} and Pt^{IV} azido complexes of this type.

4.2.4.2 Functionalisation of [Pt(L1)(N_3)$_2$] (5) with N-methylisatoic anhydride, and Reactivity of the Pendant Hydroxyl Group

The functionalisation of Pt(L1)(N_3)$_2$ (**5**), containing a pendant hydroxyl group, with a fluorescent probe was thus investigated. A probe was required which would react with the hydroxyl group under mild conditions, hence N-methylisatoic anhydride (MIA) was chosen, since anhydrides react readily with alcohols at room temperature. An additional advantage of this compound is its small size, as discussed in section 4.2.1.

Several observations had led to the suggestion that the pendant hydroxyl group of **5** may show a reduced reactivity compared with organic primary aliphatic alcohols. The NMR spectra of all complexes of L1 synthesised in this work showed a sharp triplet arising from the OH proton, indicating that it is not readily exchangeable, likely due to involvement in inter- or intramolecular interactions. Indeed, the crystal structures of both the Pt^{II} chlorido and azido complexes of L1 (Chapter 3, Section 3.3.1.1.4) showed heavy involvement of the OH group in hydrogen bonding: intermolecular in the case of the chlorido complex, and intramolecular, involving a nitrogen of the azido group, in the azido complex. Such interactions may mask the reactivity of the hydroxyl group and decrease its tendency to participate in typical nucleophilic attack. In addition, there have been previous reports of the inactivity of the hydroxyl group of this ligand in metal complexes,[25] and the functionalisation of a Ru^{II} arene complex of L1 with MIA was reported to be unsuccessful *via* derivatisation of the hydroxyl group.[16]

However, Segal *et al* performed a successful phosphoramidite coupling with the hydroxyl group of a Pt^{II} chlorido complex of L1,[26] and Nolan *et al* reported that, during the acetylation of the axial hydroxyl groups of a Pt^{IV} complex, the pendant

hydroxyl group of L1 was acetylated also; however, the yield of this species was low (14%) and the reaction time long (7 days).[27] In this work, the use of higher temperatures to accelerate the reaction was restricted by the sensitivity of the Pt^{II} azido complex to temperatures exceeding 313 K. Hence DMAP was used as an esterification catalyst with triethylamine as the auxiliary base, and the reaction to form [Pt(L1-OMIA)$(N_3)_2$] (**16**) was successful, although fairly low yielding. This therefore demonstrates the ability to functionalise this hydroxyl group, and the concept could be extended to other bioactive species.

The significant decrease in fluorescence intensity of MIAH upon complex formation results from quenching due to the internal heavy-atom effect.[22] The presence of a heavy metal within the same compound as the fluorophore increases the spin-orbit coupling in the system, and as a result the excited states are not purely singlet or triplet in character. Hence the spin selection rules are relaxed somewhat, allowing for an increased rate of (formally forbidden) intersystem crossing from a singlet to a triplet excited state. This non-radiative transition competes effectively with the emissive $S_1 \rightarrow S_0$ relaxation pathway, and results in a decrease of the fluorescence quantum yield. However, the fluorescence of this Pt^{II} complex would still be sufficient to allow for the observation of cellular uptake and distribution, and potential monitoring of intracellular reactions. For example, the binding of sulfur-containing biomolecules to Pt^{II} complexes has been shown to induce *trans*-labilisation of the amine ligands; should this occur in this case, an increase in fluorescence intensity would be expected. This strategy has already been demonstrated with Pt^{II} complexes containing the fluorescent 7-azaindole ligand.[10]

However, in the case of **16** an increase in fluorescence could also result from other intracellular transformations, for example hydrolysis of the ester bond linking the fluorophore to the ligand L1, which would limit the usefulness of the complex for tracking the fate of the platinum moiety. The cytosol contains many esterases capable of catalysing such a hydrolysis reaction, and a Ru^{II} arene complex, containing MIA conjugated to L1, was recently tested for its ability to act as a

substrate for one such enzyme.[16] The half-life of hydrolysis was approximately 40 h indicating that, although slow, ester hydrolysis would likely occur inside cells and may lead to misrepresentation of the cellular distribution of the complex. A similar experiment would need to be performed to assess if this is also the case for the Pt^{II} azido complex **16**.

However, hydrolysis by esterases is exploited in the activation of several organic-based prodrugs, such as capecitabine, which upon hydrolysis releases the anticancer agent 5-deoxy-5-fluorouridine.[28] The application of this strategy to platinum drugs has been suggested,[29] however no examples have yet been published. Therefore, now the functionalisation of $[Pt(L1)(N_3)_2]$ (**5**) has been demonstrated, it may be of interest to further explore this in the design of an esterase-activated prodrug delivery system.

4.2.4.3 Functionalisation of the Axial Hydroxyl Groups of $[Pt(en)(N_3)_2(OH)_2]$ (3)

It was discussed in Chapter 1 that the photodegradation pathways and phototoxic mechanism of action of Pt^{IV} azido complexes are not trivial to establish, although it is known that reduction to Pt^{II} is necessary for phototoxicity. NMR and UV-visible absorption experiments indicate that photoreduction of such complexes is rapid, particularly in the presence of biomolecules. However it would be of use to follow such reactions intracellularly, for example by a change in fluorescence intensity of the complex upon reduction.

Hambley *et al* have very recently explored this idea with the use of fluorescent coumarin ligands as probes of Pt^{IV} to Pt^{II} reduction, and have monitored such reactions in cells using confocal microscopy.[6] Since the fluorescence of these ligands is quenched more efficiently by Pt^{IV} than by Pt^{II}, an increase in fluorescence intensity following treatment with a Pt^{IV} complex is indicative of reduction. However, the ligands must be carefully chosen to ensure the difference

of fluorescence intensity between the Pt^{II} and Pt^{IV} complexes is sufficiently large to be visualised by microscopy. An alternative strategy was considered in this work, involving the functionalisation of the axial groups with a fluorescent probe. The loss of the axial ligands upon reduction is well known and has been exploited previously,[3] and NMR experiments on Pt^{IV} azido complexes with axial acetato groups confirm these ligands are rapidly released upon photoreduction.[30] Furthermore, the difference in fluorescence intensity of a probe when bound to Pt^{IV} or unbound following reduction should be very large. However, more suitable still would be a system utilising ratiometric imaging, involving a change of emission energy upon reduction. The advantage of such a method is the ability to normalise for changes in fluorescence intensities which are unrelated to changes in concentration of the target species.

The functionalisation of axial hydroxyl groups of Pt^{IV} complexes is well established, and has been employed in the synthesis of novel carboxylato complexes as potential anticancer agents,[31,32] or for the introduction of bioactive species into a Pt^{IV} complex.[3,33] Since many synthetic routes use anhydrides in the formation of carboxylates, it was believed reaction with MIA may be feasible. However, despite the use of excess anhydride, the reaction gave rise solely to the mono-esterified Pt^{IV} complex, in which only one hydroxyl group was functionalised. The reasons for this are not clear, and only a few examples of Pt^{IV} complexes containing different axial ligands can be found in literature. Lippard *et al* prepared *cis,cis,trans*-$[Pt(NH_3)_2Cl_2(OH)(OEt)]$, however this was *via* the oxidation of cisplatin in dilute ethanolic hydrogen peroxide; the hydroxyl group was then found to undergo subsequent reaction with an anhydride whilst the ethoxy group remained intact.[34] Mixed carboxylates have also been formed from complexes such as $[Pt(dach)(OH)_4]$, with the functionalisation of one OH group achieved by addition of one equivalent of anhydride, however, this resulted in mixtures that required chromatographic separation.[35] The carboxylation of $[Pt(dach)(OH)_4]$ with an excess of carboxylic acid formed the tris-carboxylate cleanly, where one OH group remained intact, however this could be attributed to

the differing mechanism of reaction in acidic conditions, in which protonation of the OH groups occurs prior to substitution.[36] Functionalisation with bulky aromatic anhydrides has been achieved before, so steric constraints are unlikely.[32] It is possible that the second hydroxyl ligand is harder to functionalise one the first is carboxylated, and the elevated temperatures usually employed in such reactions are necessary to ensure reaction of both hydroxyl groups.

4.2.4.4 Irradiation of [Pt(en)(N_3)$_2$(OH)(OMIA)] (17)

The increase in fluorescence intensity upon irradiation is indicative of photoreduction and release of MIAH, and is in accordance with previous evidence of the release of axial ligands upon reduction. The large contrast in fluorescence intensity between that of the free probe and the essentially non-fluorescent Pt^{IV} complex demonstrates that such a system could be useful in following the photoreduction in cells by fluorescence microscopy.

The large increase in intensity after very short irradiation times indicates that the majority of the complex is reduced after only a few minutes, even upon irradiation with visible light; this was also the case for the Pt^{IV} complex [Pt(L1)(N_3)$_2$(OAc)$_2$] (**6**), as shown in Chapter 3. It is known that complexes with axial carboxylates are more readily chemically reduced than those containing hydroxyl groups, however the extrapolation of this to photochemical reductions may not be valid. The high reduction rate in the case of **17** may result in part from the bulky nature of the axial ligand, since this is known to destabilise the Pt^{IV} state. In any case, rapid photoactivation is a desirable quantity for potential drug candidates, however the Pt^{IV} state must not be so unstable as to undergo spontaneous reduction or reactions in the dark.

Since the rapid release of the axial groups upon irradiation has been demonstrated, it may also be of interest to explore the attachment of other bioactive species to the hydroxyl group, which could then be selectively released upon irradiation.

4.2.4.5 Functionalising Platinum Complexes with Dansyl Chloride

In addition to complexes containing a free hydroxyl group, it was believed that a complex with a free amine group would allow access to a wider range of functionalising species, given their differing chemistries. Furthermore, the amide linkages formed upon reaction are more stable than ester bonds, and do not undergo hydrolysis under mild conditions.

The reactivity of platinum towards amines necessitates the use of protecting group chemistry in the formation of such a complex. A ligand was chosen in which the protected amine to be functionalised was separated from the coordinating amine by four carbons; it has previously been shown that this distance is sufficient to minimise quenching from the platinum centre upon attachment of a fluorophore.[23]

There are several functional groups that can react with free amines at room temperature, for example isothiocyanate, and fluorescein isothiocyanate is widely used in biochemical applications. However, this probe could not be used in this case, since metal azido complexes can undergo cycloaddition reactions of the coordinated azide with isothiocyanate groups, to give complexes containing S-coordinated, tetrazole-thiolate ligands.[37] Hence dansyl chloride was chosen, which forms fluorescent, stable sulfonamides upon reaction with amines.

Unfortunately, it was not possible to isolate a clean sample of either the Pt^{IV} or the Pt^{II} sulfonamide complex. The deprotection of the BOC group appeared to be successful, however, and provides validation of this functionalisation route. Upon addition of dansyl chloride, fluorescent sulfonamide species were clearly formed, and in the case of the Pt^{II} complex there was evidence of the required product. However, the formation of other fluorescent sulfonamides cannot be ruled out, for example if the amine ligand L5 were to dissociate from the platinum under the strongly acidic conditions of the reaction, this could also combine with dansyl chloride to form a product with a similar emission profile.

4.3 Attachment of Platinum Complexes to Quantum Dots

4.3.1 Introduction[38,39]

Quantum dots are a class of fluorophore receiving increasing interest for biological sensing and imaging purposes, as a result of their superior optical and electronic properties compared with traditional organic dyes. They are approximately spherical particles of semiconductor materials, typically of the II-VI group such as CdSe, vary between 2–10 nm in size and contain around 200–10 000 atoms; hence they are often termed "semiconductor nanocrystals".

In such materials, excitons (electron-hole pairs) are confined in all three spatial dimensions, giving rise to the term "dot", and energy levels are discrete and quantised, unlike the continuum of a bulk material. The optical properties result from transitions between the valence and conduction bands and are thus dependent upon the band gap energy; in such nanocrystals this is a function of their size ($E \alpha 1/r^2$), the variation of which allows the optical properties to be tuned. With increasing size, the energy levels are greater in number and more closely spaced (i.e. more similar to a bulk material), resulting in a red shift in absorption and emission. In the case of CdSe dots, emission throughout the entire visible spectrum can be obtained by variation of the size, which is readily achieved during the synthetic pathway.

Readily tunable emission is one of many benefits quantum dots show over traditional organic fluorophores. When coated with a "shell" of a higher band gap material, such as ZnS, CdSe quantum dots are also around 10–100 times brighter, due to a larger absorption cross section, and 100–1000 times more resistant to photobleaching than organic dyes. Their broad absorbance in the UV-visible region allows for a wide range of excitation wavelengths, however they show very narrow and tunable emission profiles. Quantum dots have thus found application in many areas such as electronics, optics and OLEDs, and are becoming increasingly important for biological applications.[40] Although early work in this

field produced quantum dots which were insoluble in aqueous media, it is now possible to modify their surface to impart biocompatibility, generally through exchange of the organic ligands with hydrophilic alternatives, or through encapsulation of the dots in an amphiphilic polymer. Subsequent conjugation to biomolecules can then be performed and is becoming an increasingly popular strategy, allowing for targeting of the dots and increasing their potential for application in areas such as cellular imaging and diagnostics, and for dual imaging and therapy purposes.

There are numerous examples of the conjugation of biomolecules or biologically active species to quantum dots. Several species, such as the TAT peptide, have been used to aid the internalisation of quantum dots into cells.[41] Conjugation of streptavidin is particularly useful in targeting since the resultant dots readily bind to specifically biotinylated molecules,[42] and many small organic ligands have been utilised to interact with different cellular receptors and targets.[43] The conjugation of photosensitisers has also been explored, using both organic compounds[44] and metal complexes;[45] such conjugates represent a dual imaging and therapy strategy, having the potential for both singlet oxygen generation and fluorescence imaging. Additionally, a very recent report describes the reduction of a Pt^{IV} complex *via* photoinduced electron transfer upon irradiation in the presence of CdSe–ZnS quantum dots; such a method may have application in the field of photoactivated anticancer agents.[46]

However, there are no reported examples of the covalent conjugation of a platinum complex to quantum dots. It was believed that such a conjugate could form a novel example of a potential dual imaging and therapy agent, allowing for the monitoring of uptake and distribution of a cytotoxic moiety. Furthermore, the incorporation of a photoactivated platinum complex could allow for potentially novel methods of activation, for example by irradiation at the visible wavelengths at which the quantum dots absorb. This section involves the synthesis and characterisation of water soluble quantum dots and subsequent investigations into the conjugation of a platinum complex.

4.3.2 Experimental

4.3.2.1 Materials

Cadmium oxide (CdO, ~1 micron, 99.5%), trioctylphosphine (TOP, 90%), trioctylphosphine oxide (TOPO, 99%), tributylphosphine (TBP, 97%), hexamethyldisilathiane ($(TMS)_2S$, synthesis grade), N,N-diethyldiethylenetriamine (L6, 98%), D-(+)-glucosamine hydrochloride (≥ 99%) and human apo-Transferrin (apo-hTf, ≥ 97%) were purchased from Aldrich. Stearic acid (≥ 98.5%), hexadecylamine (HDA, ≥ 90%), potassium *tert*-butoxide (≥ 97%), diethylzinc solution (~1 M in hexane), (±)-α-lipoic acid (≥ 98%), N-(3-dimethylaminopropyl)-N'-ethylcarbodiimide hydrochloride (EDC, ≥ 98%) and *N*-hydroxysulfosuccinimide sodium salt (sulfo-NHS, ≥ 98.5%) were obtained from Fluka. Selenium powder (~200 mesh, 99.8%) was purchased from Chempur, Germany. apo-hTf was purified on a Sephacryl 200 column prior to use, with 1 X phosphate buffered saline solution (PBS) prepared as previously described,[47] and all other reagents were obtained from commercial sources and used as received.

4.3.2.2 Synthesis

The syntheses of CdSe and CdSe-ZnS quantum dots, and preparation of ZnS stock solution, were carried out under an argon atmosphere using standard Schlenk techniques; all other syntheses were carried out in air unless otherwise stated.

CdSe Quantum Dots (CdSe QDs)

CdO (39 mg) and stearic acid (780 mg) were placed in a 50 mL two-necked round-bottomed flask equipped with a magnetic stirring bar. The mixture was heated to 473 K with stirring until dissolution of CdO was complete (~ 15 min), then allowed to cool to room temperature. HDA (3 g) and TOPO (9 g) were

added, and the mixture heated to 573 K on a heating mantle. A fresh solution of Se (240 mg) in TOP (2.5 mL) was then added rapidly by injection. After 30 sec, the flask was transferred to a hotplate at 533 K, where it was stirred for another 2 min before cooling in ice. Once at 333 K chloroform (50 mL) was added, followed by methanol (250 mL). The precipitated dots were collected by centrifugation (7500 rpm, 8 min) and washed once more with 1:4 $CHCl_3$:MeOH prior to drying in air.

CdSe-ZnS Quantum Dots (CdSe–ZnS QDs)

CdSe QDs (prepared as described) and TOPO (16 g) were placed in a 50 mL two-necked round-bottomed flask, equipped with a magnetic stirring bar, and heated to 483 K. Meanwhile, a ZnS stock solution was freshly prepared by mixing 3.5 mL of a $Zn(Et)_2$ solution with 6 mL TOP and 0.52 mL $(TMS)_2S$. This was injected into the former solution at 483 K, dropwise over a period of 15 min. Following injection, the flask was cooled to 383 K by blowing with compressed air for around 10 min, and then heated at 383 K for 5 h. The solution was allowed to cool to room temperature, after which $CHCl_3$ (30 mL) and methanol (120 mL) were added. The precipitated dots were collected by centrifugation (7500 rpm, 8 min) and washed with a 1:4 $CHCl_3$:MeOH mixture, to yield 1.79 g of CdSe-ZnS dots.

It was also possible to perform the ZnS coating immediately following the preparation of CdSe dots. In such syntheses, following the growth of CdSe dots at 533 K, the flask was transferred to a hotplate preheated to 483 K, and the ZnS stock solution added as described.

Dihydrolipoic Acid (DHLA)

A solution of lipoic acid (3.01 g, 14.5 mmol) in 0.25 M $NaHCO_3$ (70 mL) was placed under nitrogen and cooled in an ice bath to 273 K. $NaBH_4$ (2.21 g,

58.4 mmol) was added in small portions over the course of 1 h; the solution was then stirred at 273 K for a further 2 h. The reaction mixture was acidified to pH 1, extracted with toluene (3 x 30 mL), and the combined organic phases were dried over $MgSO_4$. Solvent was removed to yield a colourless oil, which was stored at 277 K under nitrogen.

Yield: 2.72 g (90%).
^{1}H NMR (500 MHz, $CDCl_3$): δ = 10.64 (br s, 1H), 2.92 (m, 1H), 2.69 (m, 2H), 2.37 (m, 2H), 1.89 (m, 1H), 1.78-1.42 (m, 5H), 1.35 (t, 1H), 1.31 (d, 1H).

CdSe–ZnS/DHLA Quantum Dots (CdSe-ZnS/DHLA QDs)

Freshly synthesised and air-dried CdSe–ZnS dots (1.79 g) were placed in a sealed vessel, followed by addition of DHLA (2.2 mL), and the mixture heated to 348 K for 3.5 h under nitrogen. Upon cooling to room temperature, DMF (20 mL) was added and the mixture centrifuged (6500 rpm, 7 min). The dark brown/red supernatant was retained, and the precipitate washed twice with additional DMF, after which all supernatants were combined and filtered through a 0.2 μm hydrophobic syringe filter (Millex-FG), to remove any insoluble impurities or non cap-exchanged dots. Potassium *tert*-butoxide (1.5 g) was then added, the mixture stirred for 10 min, and the precipitated dots collected by centrifugation (8400 rpm, 7 min) and washed with DMF. Water (35 mL) was added to dissolve the dots; the solution was then filtered through a 0.2 μm hydrophilic syringe filter (Sartorius Minisart®), and this stock solution was stored at 278 K under argon. Prior to further use, the dots were purified on a Sephacryl 200 column, eluting with 100 mM PBS solution at pH 7.4.

QD–L6

To 6 mL of an 8.3 μM solution of CdSe–ZnS/DHLA QDs in 1 X PBS (pH 7.4) was added EDC (58 mg, 50 mM) and sulfo-NHS (6.5 mg, 5 mM), and the

solution mixed for 20 min at room temperature. 2-Mercaptoethanol (10 µL) was added, the mixture shaken for 10 min, then L6 (1 µL, 0.9 mM) was added and the solution placed on a shaker at room temperature for 12 h. Most of the QDs had precipitated after this time; these were isolated by centrifugation, washed twice with water, and redissolved in 0.1 M NaOD solution with the aid of sonication.

QD–L6–Pt (18)

1 mL of a 2 µM QD–L6 solution in 0.1 M NaOD/NaCl was added to $Pt(DMSO)_2Cl_2$ (0.1 mg), and the mixture placed on a shaker for 5 h. The solution was exchanged for 0.1 M NaCl in D_2O in a 30 kDa molecular weight cut-off (MWCO) filter, upon which some precipitation of dots occurred; further precipitation was seen upon storage at 278 K. Some solubility could be regained upon addition of 0.1 M NaOH.

QD–Glu

To 3 mL of a 10 µM solution of CdSe–ZnS/DHLA QDs in 1 X PBS (pH 7.4) was added EDC (30 mg, 64 mM) and glucosamine (10 mg, 15 mM). The solution was stirred gently for 4 h, and washed over a 30 kDa MWCO filter three times with 1 x PBS.

QD–Tf

EDC (1 mg) and sulfo-NHS (2.5 mg) were dissolved in 1 mL of 0.1 M MES activation buffer (pH 6.0), and added to 400 µL of a 10 µM solution of QDs in 1 X PBS (pH 7.6). The mixture was placed on a shaker at room temperature for 30 min. 2-Mercaptoethanol (2.5 µL) was added followed by further shaking for 10 min. The pH was adjusted to 7.0 with 1M NaOH, apo-hTf (58 µL of a 150 µM

solution in 1 x PBS) was added, and the pH increased to 7.8 before placing on a shaker at room temperature for 2.5 h. The solution was washed with 1 X PBS three times through a 100 kDa MWCO filter, and the product purified on a Sephacryl 200 column, eluting with 100 mM PBS solution at pH 7.4.

QD–Tf–L6

To 1 mL of a 1 μM solution of QD–Tf in 1 X PBS was added EDC (9.6 mg) and sulfo-NHS (1.1 mg), and the reaction mixture acidified with dilute HCl to pH 6.5 and shaken for 10 min. L6 (1 μL) was added, upon which the pH rose to 8.5, and the mixture was placed on a shaker for 5 h at room temperature. The solution was then washed three times in a 30 kDa MWCO filter with 100 mM PBS at pH 8.5.

QD–Tf–L6–Pt (19)

To 2 mL of a 0.6 μM solution of QD–Tf–L6 was added K_2PtCl_4 (0.5 mg), and the reaction shaken at room temperature for 2 h. Following storage at 277 K for 48 h the mixture was washed three times in a 30 kDa MWCO filter with 100 mM PBS at pH 8.5.

QD–Tf–Pt

To 400 μL of a 0.4 μM solution of QD–Tf in 1 X PBS was added 20 μL of a 0.7 mM K_2PtCl_4 solution in H_2O. The solution was placed on a shaker for 2 h, then washed three times in a 30 kDa MWCO filter with 1 X PBS at pH 7.4.

4.3.2.3 Methods

4.3.2.3.1 ICP–MS

The concentrations and relative ratios of Cd, Se, Zn and S were determined for CdSe, CdSe-ZnS and CdSe–ZnS/DHLA QDs. Cd and Pt concentrations were determined for CdSe–ZnS/DHLA QDs, QD–L6–Pt, QD–Tf, QD–Tf–Pt, QD–Tf–L6 and QD–Tf–L6–Pt. Samples of water-soluble products were prepared to a concentration of ~0.1 μM in 3% nitric acid, and digested for 48 h at 343 K. For all other products, a sample of the solid was digested in aqua regia, again for 48 h at 343 K, prior to dilution to give a final acid concentration of 3%. Standard solutions (3200–5 ppb) were prepared from stock 1000 ppm solutions of Cd, Se, P, S, Zn and Pt (Sigma-Aldrich), and were run to give a calibration curve from which unknown concentrations of the elements could be determined. The isotopes observed were ^{111}Cd, ^{82}Se, ^{32}S, ^{66}Zn and ^{195}Pt.

4.3.2.3.2 Iron Uptake by QD–Tf

500 μL of a 0.4 μM solution of QD–Tf was placed in a cuvette, the UV-visible absorption spectrum recorded and the value at 470 nm set to zero. To this was added 6 μL of an 800 mM $NaHCO_3$ solution, followed by 10 μL of a 4 mM Fe^{III} citrate solution, and the solution gently mixed for 2 min. The change in absorbance at 470 nm was then followed, with a reading taken every 30 sec for 90 min, with the temperature set to 298 K. The experiment was repeated with CdSe-ZnS/DHLA QDs to act as a control.

4.3.2.3.3 Cytotoxicity Testing

The cytotoxicity of QD, QD–Tf and QD–Tf–L6–Pt (**19**) towards the human ovarian A2780 cancer cell line was assessed by Dr Ana Pizarro at the University of Warwick, according to the procedure outlined in Chapter 2.

4.3.3 Results

CdSe–ZnS quantum dots were synthesised, and rendered water soluble by the incorporation of an amphiphilic thiol ligand. The carboxylate groups of these ligands were then subject to an amide coupling to incorporate a platinum binding chelating amine moiety; subsequent reaction with a platinum complex formed a platinum conjugate, with evidence from ICP-MS data. Attempts were then made to increase the water solubility and potential tumour targeting properties by initial functionalisation of the quantum dots with glucosamine and transferrin; amide coupling and platinum binding were then achieved with the transferrin conjugate. The water soluble quantum dots, the transferrin conjugate and its platinated analogue were tested for cytotoxicity against the human A2780 ovarian cancer cell line.

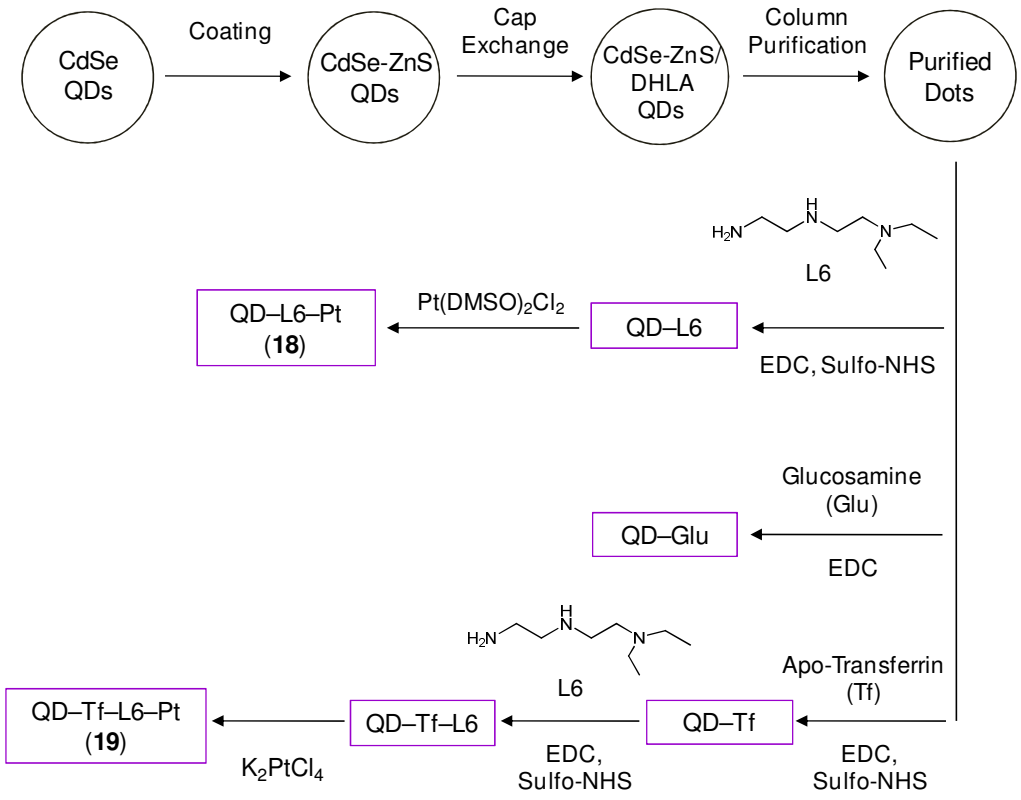

Figure 4.6 A diagram illustrating the reactions performed with quantum dots.

4.3.3.1 Synthesis of CdSe–ZnS/DHLA Quantum Dots

The reaction scheme for the synthesis of water soluble quantum dots is displayed below in Scheme 4.4. These are synthesised *via* the initial preparation of organic soluble dots, followed by exchange with an amphiphilic thiol ligand to impart water solubility.

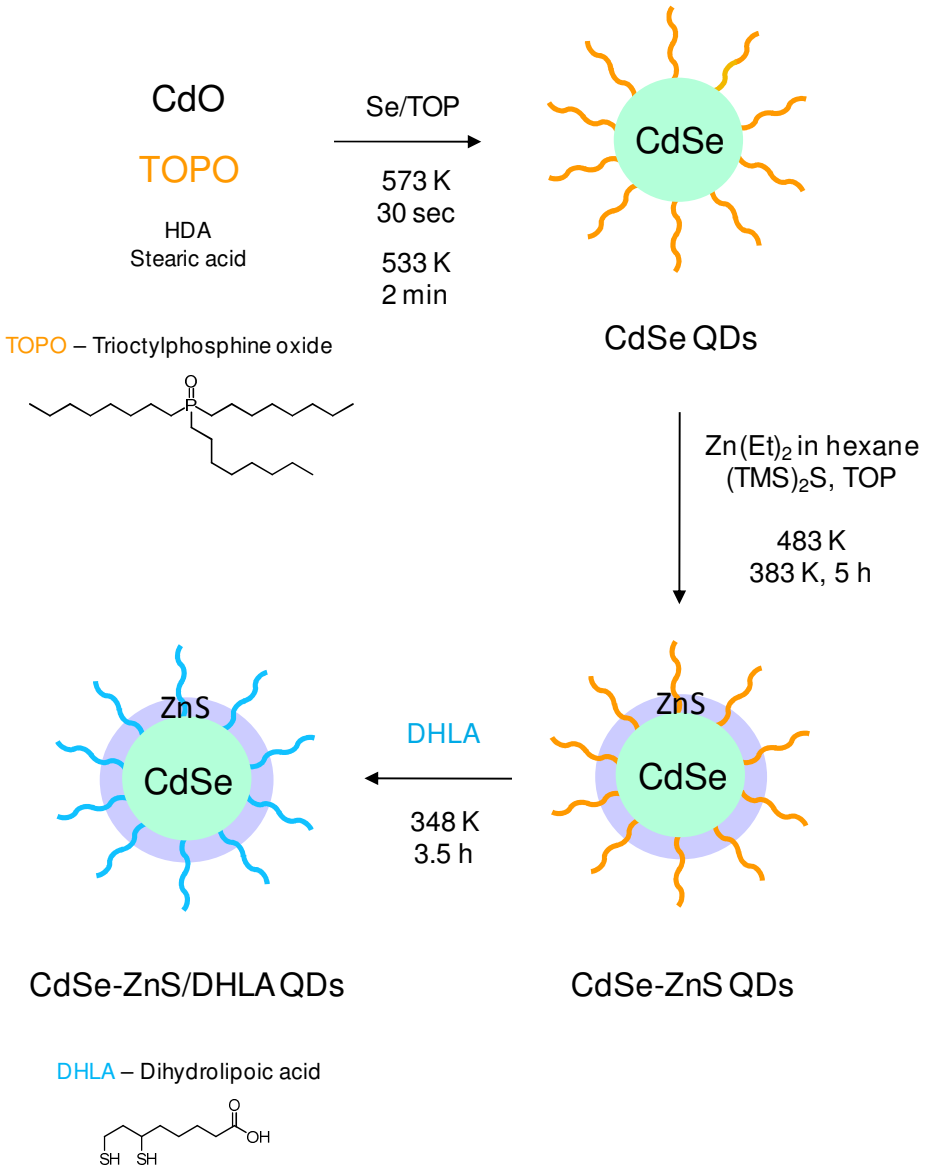

Scheme 4.4 The synthetic route to CdSe-ZnS/DHLA quantum dots. HDA = hexadecylamine, TOP = trioctylphosphine, $(TMS)_2S$ = hexamethyldisilathiane.

CdSe quantum dots (CdSe QDs) were synthesised with minor modifications to a literature method,[48] by the high-temperature reaction of Cd and Se precursors in the presence of a high-boiling organic solvent, TOPO. These dots were typically isolated and characterised by UV-visible absorption and fluorescence spectroscopy prior to coating with a ZnS shell; however, it was also possible to perform the coating directly following CdSe quantum dot growth *in situ*, without prior isolation. Coating was accomplished by addition of appropriate Zn and S precursors and allowing growth of the shell for 5 h at a lower temperature than that required for nanocrystal growth;[48] this coating yields quantum dots with improved photochemical stability and luminescence properties compared with their non-coated CdSe precursors.

The resultant CdSe–ZnS quantum dots are soluble only in organic solvents on account of the highly hydrophobic capping ligand TOPO; hence in order to obtain aqueous solubility these ligands must be exchanged for more hydrophilic alternatives. The commonly-used dihydrolipoic acid (DHLA) was chosen in this case, containing two thiol groups to allow for bidentate interactions with the quantum dot surface, and a carboxylate group to confer solubility in aqueous solutions. Ligand exchange was accomplished by stirring CdSe–ZnS QDs in neat DHLA with moderate heating.[49] The resultant CdSe–ZnS/DHLA QDs were then purified on a Sephacryl-200 column eluting with 100mM PBS at pH 7.4, with the chromatogram shown in Figure 4.7. The first eluted peak consisted of the required quantum dots, with a second species eluting at a later timepoint and thus of a lower molecular weight. These fractions were neither coloured nor fluorescent, and were slightly malodorous; they were thus presumed to arise from high molecular weight polymeric thiol species.

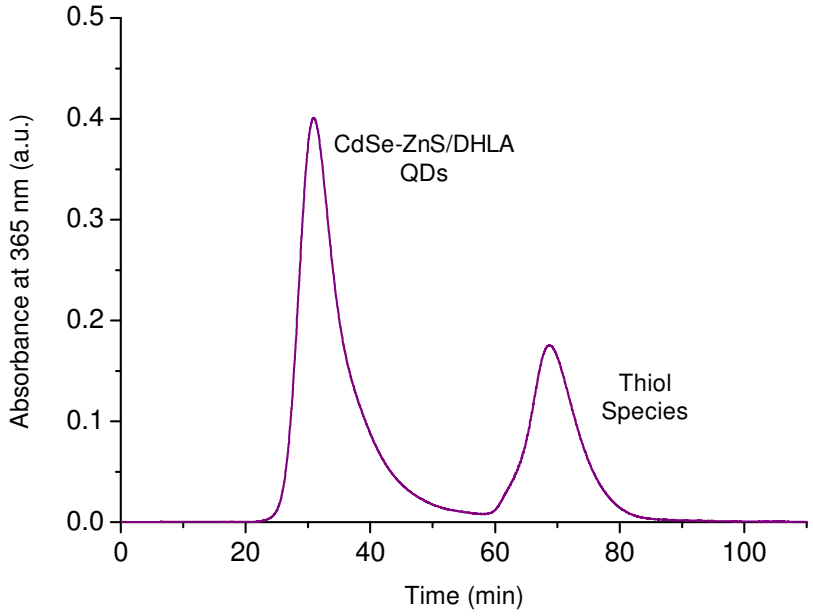

Figure 4.7 Chromatogram obtained upon purification of CdSe–ZnS/DHLA QDs, using a Sephacryl-200 size-exclusion column eluting with 100 mM PBS (pH 7.4).

4.3.3.2 Characterisation of Quantum Dots

4.3.3.2.1 UV-Visible Absorption Spectroscopy

CdSe QDs, CdSe–ZnS QDs and CdSe–ZnS/DHLA QDs were characterised by UV-visible absorption spectroscopy, and showed an absorption profile typical of quantum dots. The red shift of λ_{max} upon ZnS coating results from the partial leaking of the exciton into the ZnS matrix, leading to a reduction in quantum confinement.[50] There is no change in λ_{max} upon exchange of the capping ligand to form water soluble dots, since the core of the dots giving rise to the absorption in this region is unaffected.

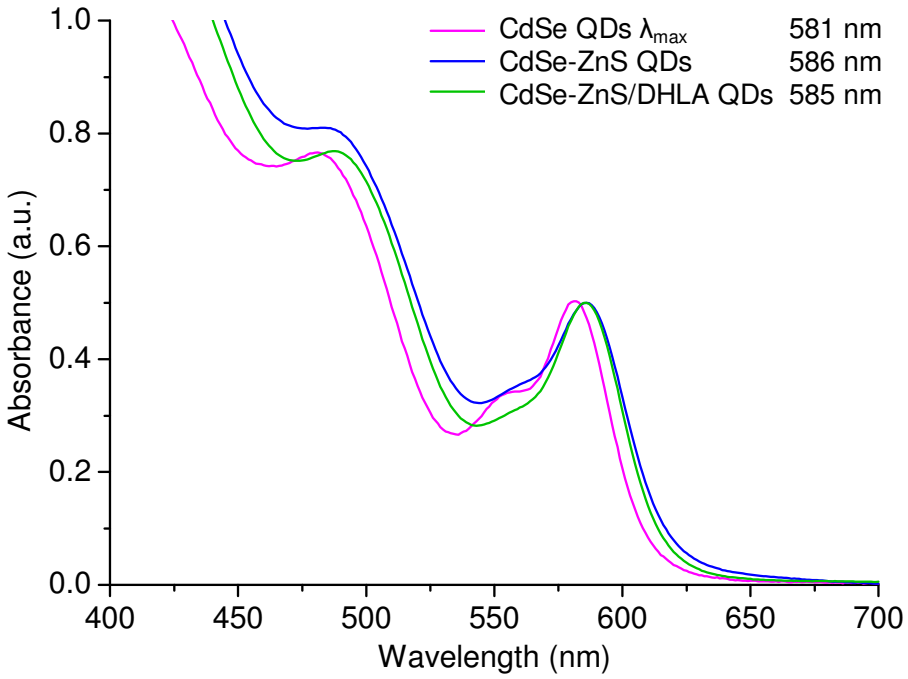

Figure 4.8 Normalised UV-visible absorption spectra of CdSe QDs and CdSe–ZnS QDs in chloroform, and of CdSe–ZnS/DHLA QDs in aqueous solution.

Several parameters can be obtained from the absorption spectra of the dots; these are calculated below for the water soluble CdSe–ZnS/DHLA QDs.

a) Size

The band gap (and thus the energy required for the transition) is related to the size of the emissive core of the quantum dots; thus from the position of the first absorption peak, the size can be calculated according to the following polynomial equation (where D = diameter and $\lambda = \lambda_{max}$).[51]

$$\text{CdSe: } D = (1.6122 \times 10^{-9})\lambda^4 - (2.6575 \times 10^{-6})\lambda^3 + (1.6242 \times 10^{-3})\lambda^2 - (0.4277)\lambda + 41.57.$$

Inputting the value of 581 nm as λ yields **D = 4.0 nm.**

b) Concentration

The extinction coefficient per mole of nanocrystals can be calculated from their diameter as follows:[51]

CdSe: $\varepsilon = 5857(D)^{2.65}$

Inputting the value of 4.1 nm yields $\boldsymbol{\varepsilon = 230\ 750\ M^{-1}\ cm^{-1}}$

The absorption spectrum is also an indication of the size distribution of the dots, with a broad peak, or more than one maximum, indicative of a broad distribution. However, as the dots increase in size and move towards the properties of the bulk material the spectra become inherently more structured,[38] and a much more reliable way to assess the size distribution is by analysis of the fluorescence emission spectrum.

4.3.3.2.2 Fluorescence Spectroscopy

Fluorescence emission spectra were obtained for CdSe QDs, CdSe–ZnS QDs and CdSe–ZnS/DHLA QDs, and show narrow bands with low full-width half-maximum (FWHM) values (32 nm, 38 nm and 42 nm respectively), indicative of a narrow size distribution. Again a red-shift is seen upon ZnS coating, with no change upon exchange of the capping ligands.

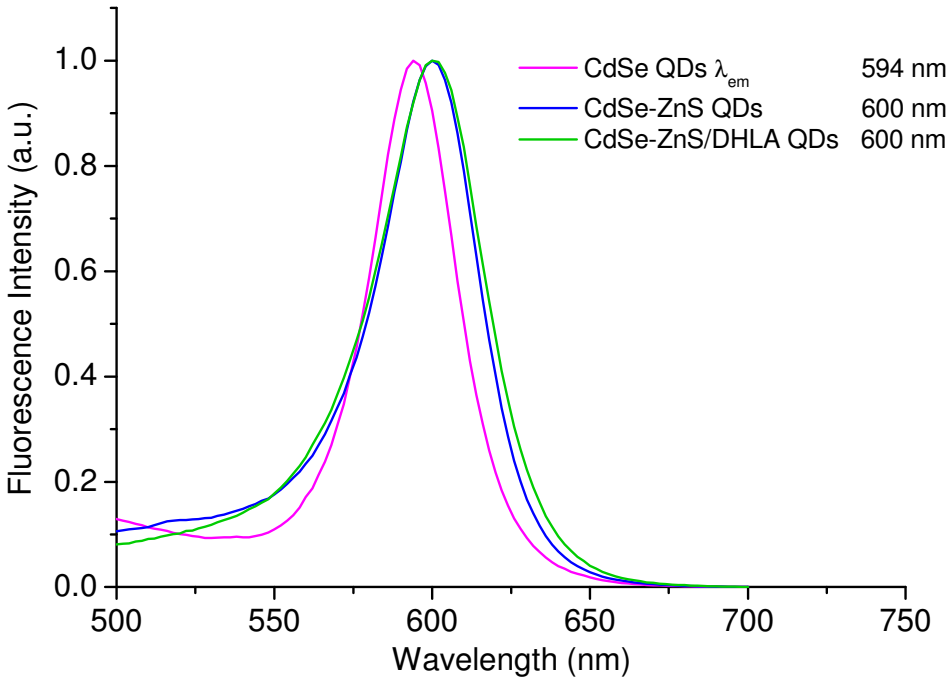

Figure 4.9 Normalised fluorescence emission spectra of CdSe QDs and CdSe–ZnS QDs in chloroform, and CdSe–ZnS/DHLA QDs in aqueous solution, with excitation at 365 nm.

4.3.3.3 Functionalisation of CdSe-ZnS/DHLA QDs with an Organic Amine

4.3.3.3.1 Binding of an Organic Amine Ligand (QD–L6)

The carboxylate group of DHLA is amenable to derivatisation by standard coupling techniques; such reactions of the capping ligands are a common route to the functionalisation of quantum dots.[40] In this case, it was necessary to incorporate a ligand capable of binding a platinum moiety. A ligand was chosen containing a primary, secondary and tertiary amine group separated by ethylene units (L6, Figure 4.6); the primary amine can selectively participate in amide coupling reactions, leaving the secondary and tertiary groups available for chelation to platinum.

Amide coupling was thus performed in 1 X PBS at pH 7.4, using an excess of amine and the coupling reagents EDC and sulfo-NHS.

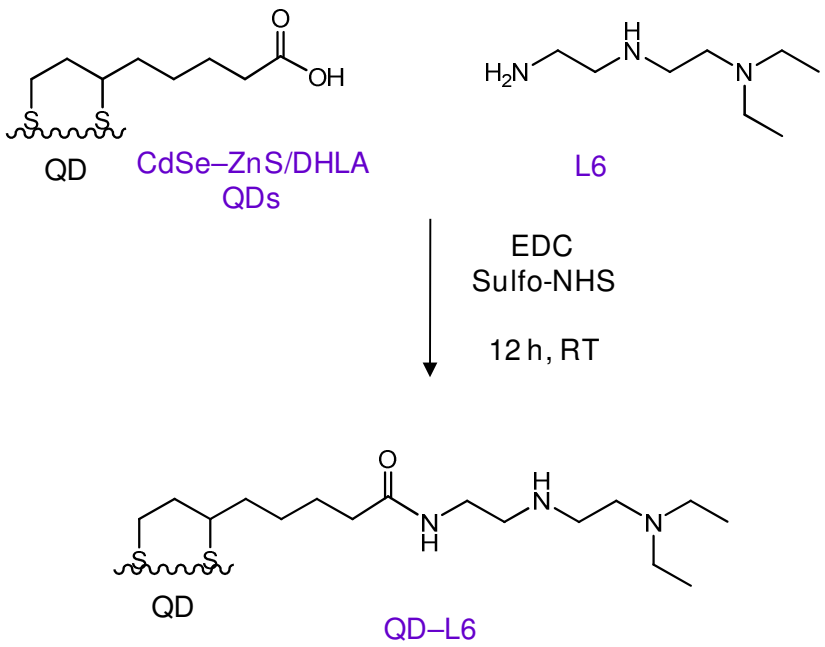

Scheme 4.5 The coupling of L6 to the carboxylate groups of DHLA.

The quantum dots precipitated to some extent during the course of the reaction, likely resulting from the reduced solubility of the amine capping ligand in the buffered reaction medium (pH 7.4); solubility could be restored upon sonication of the precipitated dots in a 0.1 M NaOH solution. The solubility change provides some evidence of reaction; a ^{1}H NMR spectrum in 0.1 M NaOD in D_2O was also obtained and compared with that of the ligand alone to obtain further evidence. The expected peaks for the ligand appear to be present in the product (QD–L6), including the triplet of the two methyl groups which does not appear in DHLA.

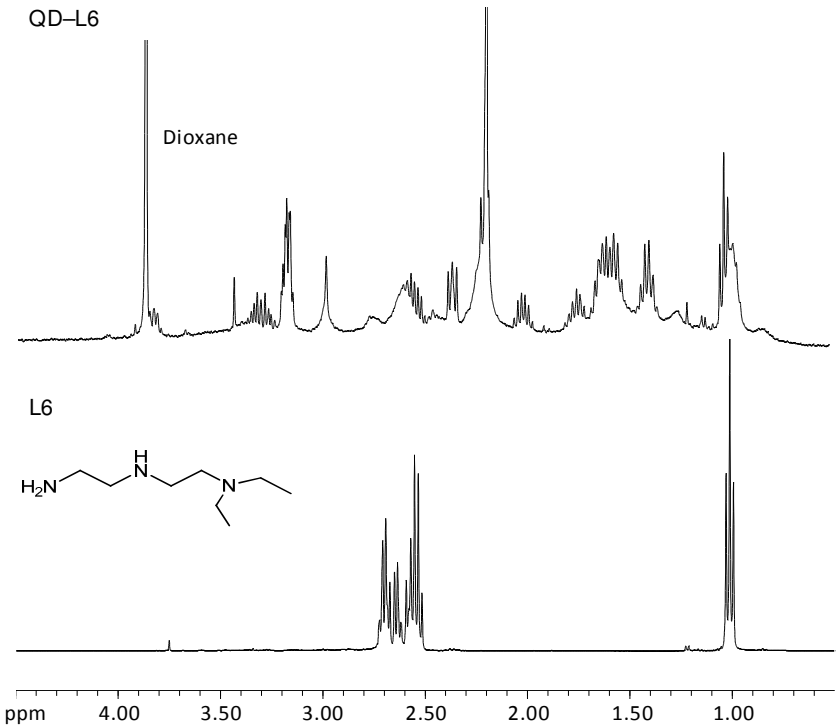

Figure 4.10 ^{1}H NMR spectra in 0.1 M NaOD/D_2O of the ligand L6 and the functionalised quantum dots, QD–L6.

4.3.3.3.2 Binding of Platinum (QD–L6–Pt, 18)

The platination of QD–L6 was carried out using an excess of $Pt(DMSO)_2Cl_2$ in 0.1 M NaOH solution, however during removal of excess starting material and exchange for 0.1 M NaCl in D_2O in a MWCO filter, the dots began to precipitate, with further precipitation seen upon storage. Addition of 0.1 M NaOH dissolved the solid to some extent, although not all could be resolubilised.

Immediately following the reaction, visual observation of the solution under a UVA lamp indicated a large degree of fluorescence quenching upon reaction with the platinum complex; presumably due to the heavy-atom effect.[22] An attempt was made to measure the degree of quenching in the product, QD–L6–Pt (**18**), by

recording fluorescence emission spectra of isoabsorbant solutions of QD–L6–Pt and CdSe-ZnS/DHLA.

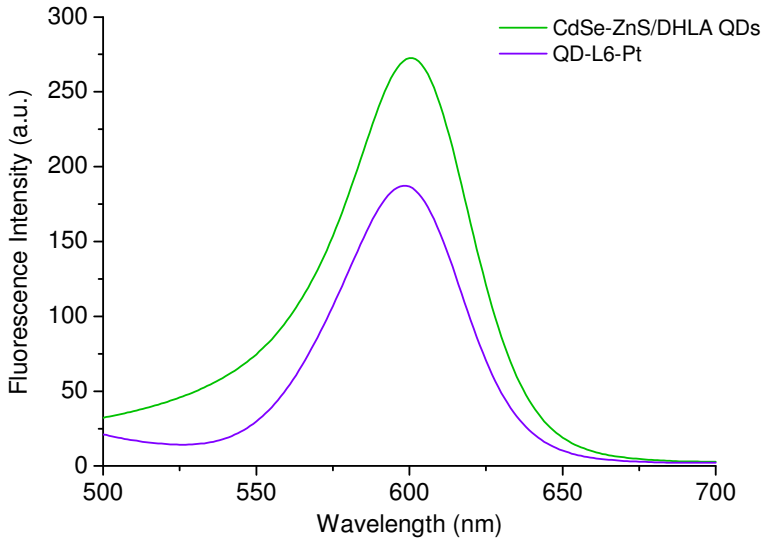

Figure 4.11 Fluorescence emission spectra of isoabsorbant solutions of CdSe–ZnS/DHLA QDs in 1 X PBS, and QD–L6–Pt (**18**) in 0.1 M NaOH.

The spectra show a decrease in fluorescence intensity for QD–L6–Pt compared with the non-platinated dots, however this spectrum may be unlikely to reflect the true degree of quenching in the product. To obtain the spectrum it was necessary to resolubilise the precipitated QD–L6–Pt in alkaline solution, however as mentioned this did not solubilise the entire product. It is likely the dots that were solubilised were those that did not react with platinum, or those that were platinated to a lesser extent, since the free amines of QD–L6 would be expected to show greater solubility than when platinated in QD–L6–Pt. Platination was, however, confirmed by ICP–MS, the results of which are discussed in Section 4.3.3.6.

The aqueous insolubility and quenching of fluorescence observed for QD–L6–Pt render these dots unsuitable for biological imaging purposes. It was therefore decided to investigate the functionalisation of quantum dots with biomolecules prior to platination; to gain the dual benefit of imparting aqueous solubility and distancing the platinum from the fluorophore, thereby minimising the degree of quenching.

4.3.3.4 Functionalising Quantum Dots with Glucosamine (QD–Glu)

Glucosamine is a naturally occurring amino monosaccharide, which can be derivatised through reactions of the amino group.[52] Attempts were made to conjugate glucosamine to CdSe–ZnS/DHLA quantum dots *via* the coupling of this amine to the carboxylate group of DHLA.

Successful coupling was achieved using an excess (~20 fold) of glucosamine in the presence of EDC; a larger excess was found to induce precipitation of the quantum dots. The UV-visible absorption and fluorescence spectra of the resultant conjugate QD–Glu were unchanged from those of CdSe–ZnS/DHLA quantum dots, as expected, and evidence for successful conjugation was provided from the NMR spectrum of QD–Glu in comparison with that of glucosamine alone (Figure 4.12). The presence of a peak at 5.37 ppm, corresponding to the proton on the anomeric carbon, was particularly indicative of successful binding.

Subsequent attempts to derivatise the OH groups were unsuccessful. Reaction with bromoacetic acid, to provide carboxylate groups available for subsequent amide coupling, led to precipitation of the quantum dots. Although it was believed successful derivatisation could be achieved, attention was then turned to alternative biomolecules and no further work was carried out with the glucosamine conjugate.

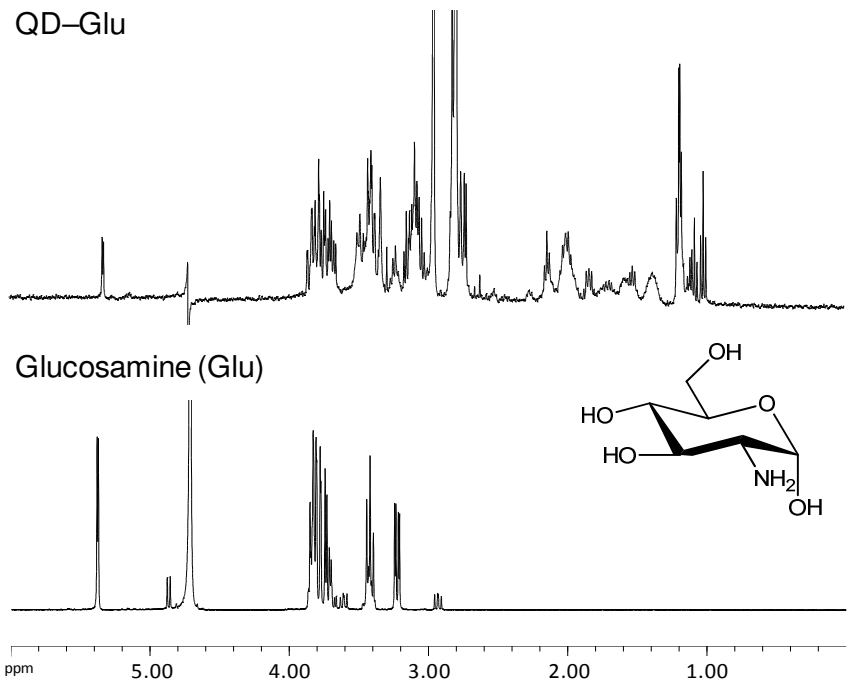

Figure 4.12 ^{1}H NMR spectra of glucosamine (in D_2O) and QD–Glu (in D_2O with water suppression).

4.3.3.5 Functionalising Quantum Dots with Transferrin (QD–Tf)

Human transferrin is an 80 kDa protein involved in the binding and transportation of iron *in vivo,* with cellular delivery of iron achieved upon interaction of transferrin with the transferrin receptor (TfR1) and subsequent internalisation by endocytosis. TfR1 is overexpressed on rapidly dividing cells, with low expression in non-proliferating cells; thus it has become an attractive target for the selective delivery of drugs to tumours.[53] It was believed the conjugation of transferrin to quantum dots prior to platinum binding would aid water solubility and internalisation specifically into tumour cells, and distance the platinum from the fluorophore such that quenching of fluorescence is minimised.

Attempts were made to conjugate human apo-transferrin (metal-free, hereby abbreviated Tf) to the carboxylate ligands of DHLA, *via* the amino groups of lysine residues on the protein. Attempts at coupling using EDC alone were

unsuccessful, leading to precipitation of the protein. The use of EDC and sulfo-NHS, previously reported for the conjugation of biomolecules to quantum dots,[54] led to successful preparation of a conjugate denoted QD–Tf. This product was purified on a Sephacryl-200 column, eluting with 100mM PBS at pH 7.4 (Figure 4.13), allowing for separation of the conjugate from both unmodified quantum dots and free apo-hTf.

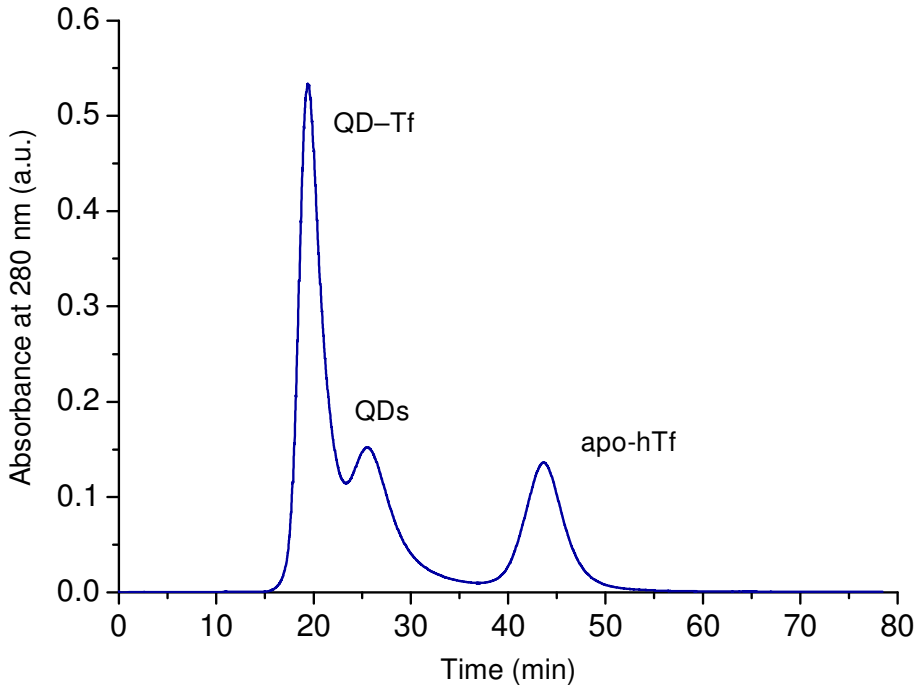

Figure 4.13 The chromatogram obtained upon purification of QD–Tf, using a Sephacryl-200 size-exclusion column eluting with 100 mM PBS (pH 7.4).

4.3.3.5.1 Iron Uptake by QD–Tf

Upon addition of an Fe^{III} source to apo-transferrin, along with HCO_3^- to act as a synergistic anion, the binding of Fe^{III} can be monitored by the increase in absorbance at 470 nm, the λ_{max} of the tyrosine oxygen–Fe^{III} ligand-to-metal charge transfer (LMCT) band. This experiment was performed with QD–Tf, to confirm conjugation of Tf to the quantum dots. The observed increase in absorbance, up to

a saturation point of around 20 min, is indicative of such an iron uptake reaction and provides evidence of the successful conjugation of Tf. As a control, the experiment was performed with CdSe–ZnS/DHLA QDs, where no such change was seen.

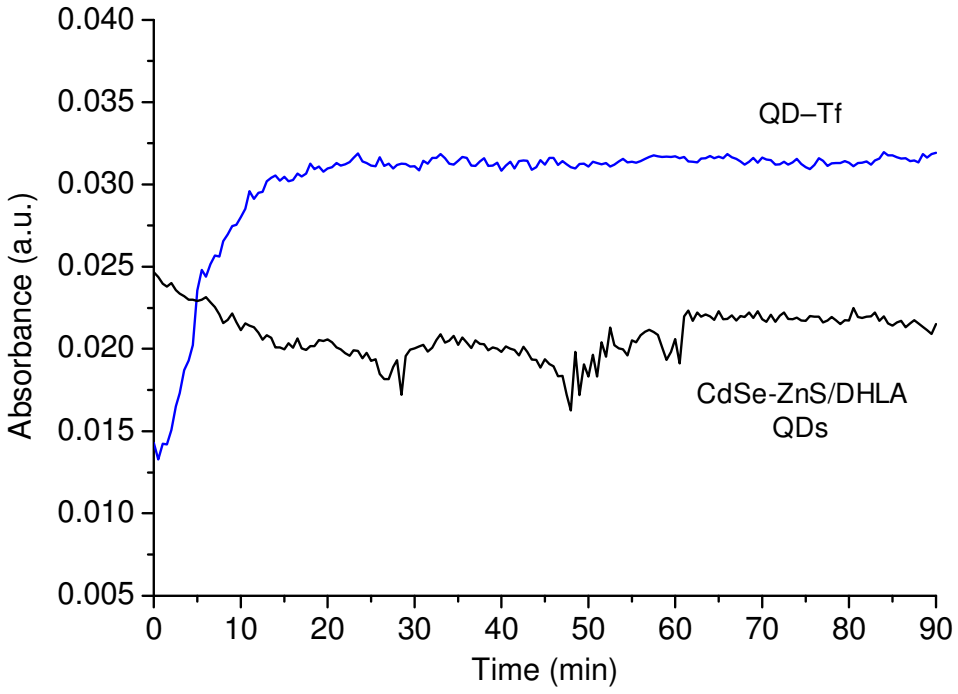

Figure 4.14 The change in absorbance at 470 nm following addition of Fe^{III} to QD–Tf and CdSe–ZnS/DHLA, as a monitor of iron uptake.

4.3.3.5.2 QD–Tf–L6 and QD–Tf–L6–Pt (19)

The ligand L6 was conjugated to QD–Tf *via* an amide coupling reaction involving the primary amino group of the ligand and accessible free carboxylates of the transferrin. In this case, no precipitation was seen; the transferrin clearly imparting enhanced water solubility on the conjugate.

Platination was accomplished by addition of an excess of K_2PtCl_4. Fluorescence spectra of equimolar solutions of QD–Tf–L6–Pt (**19**) and CdSe–ZnS/DHLA QDs indicate that platination has very little effect on the fluorescence of the quantum dot (Figure 4.15), there is essentially no contact between the two as a result of the distance imposed by the conjugation of transferrin.

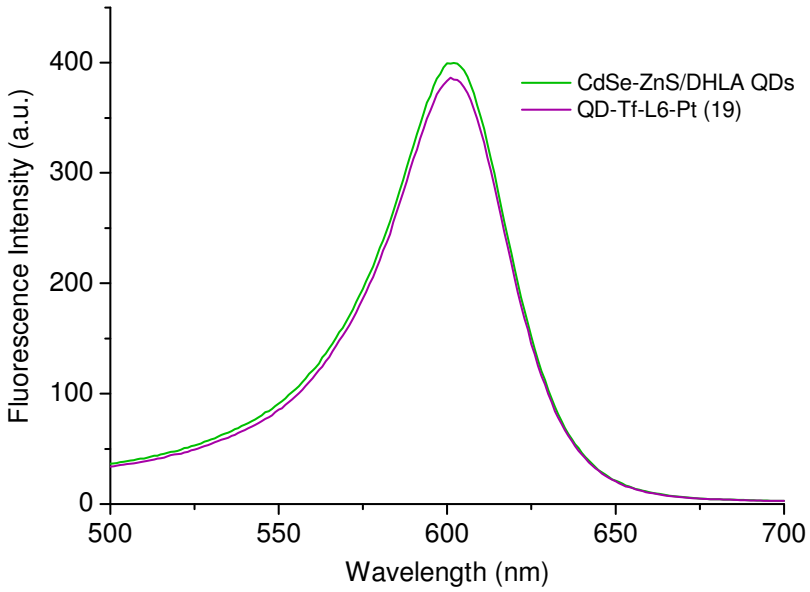

Figure 4.15 Fluorescence emission spectra of isoabsorbant solutions of CdSe–ZnS/DHLA QDs in 1 X PBS, and QD–Tf–L6–Pt (**19**) in 100 mM PBS pH 8.4.

To ensure platination was occurring at L6 with minimal non-specific binding to amino acid residues on transferrin, QD–Tf was treated with K_2PtCl_4 in the same way as QD–Tf–L6, and the resulting conjugate assessed for platinum content by ICP-MS.

4.3.3.6 ICP-MS of Quantum Dots and Conjugates

The concentrations and relative ratios of Cd, Se, Zn and S were determined for CdSe, CdSe–ZnS and CdSe–ZnS/DHLA QDs by ICP-MS.

Table 4.1 ICP-MS data for CdSe, CdSe–ZnS and CdSe–ZnS/DHLA QDs

	Element	Concentration (μM)	Cd:Se	Zn:S
CdSe	Cd	2.94	1	
	Se	22.55	7.66	
	Zn	0		–
	S	2.97		–
CdSe–ZnS	Cd	3.31	1	
	Se	3.33	1.01	
	Zn	5.55		1
	S	5.10		0.92
CdSe–ZnS/DHLA	Cd	4.61	1	
	Se	6.41	1.39	
	Zn	2.36		1
	S	7.57		3.21

These results indicate a large excess of selenium in the CdSe quantum dots, when more equal concentrations of cadmium and selenium would be expected. Excess selenium is no longer present, however, in the CdSe–ZnS dots, and approximately equal proportions of Zn and S are seen as expected. The exchange of TOPO for the thiol ligand DHLA can also be evidenced by the increase in the proportion of sulfur in the CdSe–ZnS/DHLA quantum dots.

To monitor the platination reactions of several quantum dots and conjugates, Cd and Pt concentrations were determined for CdSe–ZnS/DHLA QDs, QD–L6–Pt (**18**), QD–Tf, QD–Tf–Pt, QD–Tf–L6 and QD–Tf–L6–Pt (**19**).

Table 4.2 ICP-MS data for several quantum dot-platinum conjugates and their precursors.

	Element	Concentration (μM)	Cd:Pt
CdSe–ZnS/DHLA	Cd	7.23	–
	Pt	0	
QD–L6–Pt (**18**)	Cd	2.14	1
	Pt	1.01	0.47
QD–Tf	Cd	4.47	–
	Pt	0	
QD–Tf–Pt	Cd	5.79	1
	Pt	1.10	0.19
QD–Tf–L6	Cd	4.74	–
	Pt	0	
QD–Tf–L6–Pt (**19**)	Cd	1.50	1
	Pt	4.10	2.73

These results indicate the successful platination of QD–L6, with the platinum concentration approximately half that of cadmium. It is evident that some platination of transferrin occurred in QD–Tf, however the degree of platination is smaller than for conjugates containing the platinum-binding ligand L6. Surprisingly, the conjugate QD–Tf–L6–Pt (**19**) contained a very large proportion of platinum compared with cadmium, and compared with QD–L6–Pt (**18**) in

which the platinum binding ligand L6 is also present. This could indicate the non-specific platination of transferrin to some extent, and will be further discussed in Section 4.3.4.2.3.

4.3.3.7 Cytotoxicity

CdSe–ZnS/DHLA QDs, QD–Tf and QD–Tf–L6–Pt (**19**) were tested for cytotoxicity against the A2780 human ovarian cancer cell line, as described in section 4.3.2.3.3. The concentrations were calculated based on the results of the ICP-MS measurements, and chosen such that the concentrations of Pt administered during the testing of **19** were 100, 50 and 5 μM, in line with the standard protocol for the screening of platinum complexes. The corresponding concentrations of cadmium were determined and, in order to draw comparisons, CdSe-ZnS/DHLA QDs and QD–Tf were tested at these cadmium concentrations also.

Screening indicated that both CdSe–ZnS/DHLA QDs and QD–Tf were cytotoxic at the concentrations tested, with IC_{50} values estimated to be in the range of 20–40 μM (cadmium concentration). However, QD–Tf–L6–Pt (**19**) was non-toxic, with cell survival ≥ 100% at all concentrations tested.

4.3.4 Discussion

4.3.4.1 Synthesis of CdSe–ZnS/DHLA dots

Interest in semiconductor quantum dots has grown rapidly in recent years with the emergence of numerous potential applications, many of which require a narrow fluorescence emission profile and thus a narrow size distribution of dots. Despite this, it was found that detailed synthetic information on the preparation of quantum dots is somewhat sparse, and literature preparations are not always trivial to reproduce. The discussion below includes several observations made during the

synthesis of quantum dots, some of which are apparently scarcely documented in literature.

Many experimental factors affect the size and size distribution of quantum dots, including the Cd:Se ratio, temperature and growth time. In this work, the optimal synthesis of quantum dots was achieved *via* minor modifications to a literature method,[48] resulting in orange fluorescent CdSe quantum dots with a narrow size distribution, as evidenced from the absorption and fluorescence spectra. This method uses a small Cd:Se ratio of 1:10, which is reported to increase the quantum yield of fluorescence. A large excess of Se was observed in the CdSe QDs by ICP-MS (1:8) when a ratio closer to 1:1 may be expected, or indeed excess cadmium,[55] and this may arise from insufficient washing of the product, resulting in an excess of Se starting material (or its oxide) in the CdSe quantum dots tested.

Varying the growth time is the simplest way to prepare CdSe quantum dots of different sizes; however, since at longer growth times a wider range of sizes will be present statistically, it is more difficult to obtain larger dots in a narrow size distribution. It was also observed that further growth of CdSe dots following their isolation is not possible: an attempt was made to encourage the growth of a batch of dots with an uneven size distribution by reheating to 493 K in TOPO, however this was unsuccessful and resulted in a loss of fluorescence after heating.

The solubility of CdSe quantum dots appeared to vary with their size; with smaller dots requiring a more polar solvent mixture for solubilisation. In addition, it was observed that the total drying of quantum dots renders them insoluble, with only extensive sonication aiding redissolution. This is seemingly poorly documented in literature and yet was found to be true for all dots synthesised, including the water soluble CdSe–ZnS/DHLA QDs; it is likely to result from aggregation of the surface ligands upon drying. Therefore, care was taken not to completely dry samples of solid dots prior to further use; alternatively they were stored in solution under an inert gas.

The coating of the CdSe core with a "shell" of a higher bandgap material, typically ZnS, greatly enhances the luminescence properties and photochemical stability of the quantum dot.[56] The shell acts to saturate surface defects, thus preventing oxidation or interactions of exposed Se core atoms, and also minimises non-radiative recombination of electron-hole pairs, thereby increasing the fluorescence quantum yield approximately three-fold.[57] In this work, coating was typically performed on pre-isolated samples of CdSe, although coating *in situ* immediately following CdSe growth was also possible. A number of observations were made during coating attempts in this work; firstly, it is best to prepare fresh solutions of the Zn and S precursors, since storage leads to formation of a white film, presumably of ZnS, and the solution becomes ineffective. Secondly, the literature description for the reduction in temperature between injection of the coating solution (483 K) and growth phase (383 K) is ambiguous. It was found that altering the temperature of the hotplate and allowing the flask to cool slowly resulted in a loss of fluorescence, whereas rapid cooling with compressed air followed by transfer to a hotplate preset to 383 K yielded much better results. Additionally, several literature preparations report the use of tributylphosphine (TBP) rather than trioctylphosphine (TOP) as the solvent for the ZnS solution;[58] attempts in this case found that the viscous liquid TBP persisted and was very difficult to remove, preventing precipitation of the dots from the reaction solution and, furthermore, quenching the fluorescence. It was believed TOP is a better solvent for this reaction since it is readily oxidised to TOPO, which is already present in the reaction as the capping ligands for the quantum dots.

Aqueous solubility is achieved by exchange of the organic capping ligand TOPO for amphiphilic alternatives, typically thiols which show a high affinity for the ZnS shell. Dihydrolipoic acid (DHLA) is a common choice due to the stability provided by its bidentate mode of coordination; in this case exchange was achieved by the stirring of TOPO-capped CdSe–ZnS QDs in neat DHLA. However, whilst imparting aqueous solubility, thiols such as DHLA are known to quench the fluorescence of quantum dots to some degree,[49] hence a balance is

necessary. However, even in a large excess of DHLA a small proportion of dots was found to undergo minimal cap-exchange, as evidenced by their insolubility in water at the end of the experiment.

Sephacryl S-200 was found to be a suitable medium for purification of water-soluble quantum dots by FPLC, enabling their isolation from what were believed to be polymeric thiol species. Such species may have a quenching effect on the fluorescence of the quantum dot, or could potentially participate in side reactions upon attempts to functionalise CdSe–ZnS/DHLA QDs. Gel filtration chromatography is common for the purification of bioconjugates of quantum dots,[59] however there appears to be little precedence for the purification of CdSe–ZnS/DHLA QDs in this way.

4.3.4.2 Functionalisation Techniques and Platination

4.3.4.2.1 Small-molecule Amine Ligand

The carboxylate groups of DHLA are known to participate in common cross-linking reactions to enable functionalisation of quantum dots.[60] In this work, an amide coupling with a small-molecule primary amine was attempted and evidence of functionalisation was obtained, although the resulting conjugate showed poor aqueous solubility, requiring a strong base for dissolution. It has been previously reported that EDC couplings with CdSe–ZnS/DHLA QDs typically result in aggregate build-up, due to a lack of affinity for water once the carboxylate groups are reacted.[49] Platination was successful as evidenced by ICP-MS, and further reduced the solubility; perhaps unsurprisingly so since neutral Pt^{II} complexes often show poor water solubility, and this rendered the conjugate unsuitable for any further testing. It was therefore decided to investigate functionalisation with biomolecules, to impart aqueous solubility to the conjugates, to introduce distance between the platinum and the fluorophore in order to minimise quenching by the metal, and to allow the possibility of selective tumour targeting.

4.3.4.2.2 Glucosamine

Conjugation of glucosamine to CdSe–ZnS/DHLA QDs *via* an EDC-mediated amide coupling was successful, as evidenced by ^{1}H NMR spectroscopy. Formation of a quantum dot conjugate with monomeric glucosamine is apparently unreported, although coupling to chitosan, a glucosamine-based polysaccharide, has been previously described.[61] The OH groups of QD–Glu are thus free for further derivatisation if required. An initial attempt using bromoacetic acid was unsuccessful and led to precipitation of the quantum dots, although it may be possible to derivatise these groups successfully *via* a different route.

4.3.4.2.3 Transferrin

The conjugation of quantum dots to proteins is of increasing interest in biosensing and imaging applications. One strategy exploits electrostatic self-assembly, whereby positively charged His-tagged proteins can interact with negatively charged DHLA-capped quantum dots, whilst another common approach involves binding of biotinylated proteins to streptavidin-coated quantum dots.[49,54] Transferrin has been conjugated to quantum dots *via* the latter method,[42] and found to internalise into cells *via* endocytosis in a manner similar to that of transferrin alone. Additionally, covalent binding of the protein to lysine-coated CdSe/CdS/ZnS quantum dots has also been reported for the imaging of pancreatic cancer.[62] It was believed in this case that the conjugation of transferrin to quantum dots, with subsequent derivatisation to incorporate a platinum binding ligand, would provide a more successful route to a platinated quantum dot, and furthermore aid the internalisation of a platinum-dot conjugate; it has been demonstrated previously that the reactivities of many types of biomolecules have been found to remain after conjugation to quantum dots.[40]

Initial attempts to conjugate the lysine amino groups of transferrin with DHLA employed EDC as a carboxyl-activating reagent and resulted in the precipitation of protein. The addition of sulfo-NHS was beneficial; this reagent is typically employed to increase the efficiency of the coupling reaction, however in this case, and in the case of the organic amine ligand, it was found to circumvent the problem of precipitation during the coupling reaction with EDC alone.

Evidence of transferrin binding was provided by the titration with Fe^{III} resulting in the growth of an absorption band arising from the tyrosine oxygen-Fe^{III} LMCT transition; this was found to be a simple way to determine conjugation. Other methods, such as iron supplementation followed by ICP-MS determination of iron content, could be unreliable due to the potential loss of iron from the protein and the ubiquitous nature of the metal.

It was observed that the conjugation of transferrin to form QD–Tf, and all subsequent reactions with the product, were best performed at low concentrations (1–2 μM) to avoid precipitation of the quantum dots. In particular, the addition of sulfo-NHS and EDC led to a fall in pH often sufficient to induce precipitation of the dots on larger scales. This was partially overcome by the use of a higher strength buffer, however reactions were typically more reliable on smaller scales. The decreased stability of the dots once biomolecules were bound was evident, necessitating more gentle conditions, such as centrifuging at lower speeds or alternatively the use of dialysis.

The subsequent reaction with the primary amino group of L6 proceeded via a sulfo-NHS/EDC coupling as described, followed by platination with an excess of K_2PtCl_4. ICP-MS data indicated a very large degree of platinum binding, the reason for which is unclear. The control reaction, in which the platinum salt was reacted with QD–Tf directly, showed much lower levels of platinum indicating a reduced degree of non-specific binding to transferrin. However it could be possible that such binding occurred to a greater extent in the reaction of QD–Tf–L6; there are typically many potential platination sites available on proteins, and

binding of platinum to transferrin has previously been established.[63] Further work would be necessary in order to confirm this.

4.3.4.3 ICP-MS of Quantum Dots and Conjugates

The use of ICP-MS to determine elemental concentrations of quantum dots and their conjugates was unreported until very recently,[55] but is a very useful method for determining not only the ratios of elements comprising the dot, but also, in this case, as evidence for and quantification of the conjugation of platinum, which would be difficult to determine by alternative analytical techniques.

4.3.4.4 Cytotoxicity of Quantum Dot Conjugates

The cytotoxicity of quantum dots is a matter of much interest, since it hinders at present any potential *in vivo* application. Toxicity is seen at micromolar levels, and although the exact mechanisms are yet to be established, it has been related to free cadmium ions and to the generation of reactive oxygen species.[64] It was therefore of interest to assess the cytotoxicity of the water soluble CdSe–ZnS/DHLA QDs alone, as well as QD–Tf, to compare to that of the platinum conjugate. Both species showed moderate cytotoxicity, with IC_{50} values in the range of 20–40 μM. Further data would be required to assess any differences between the cytotoxicity of the two; it may be expected that the transferrin conjugate would be more toxic, since it is more readily internalised into the cell *via* TfR1.

The inactivity of the platinated transferrin conjugate QD–Tf–L6–Pt (**19**) is surprising, since the majority of Pt^{II} chlorido complexes show some degree of toxicity at this concentration; furthermore both CdSe–ZnS/DHLA QDs and QD–Tf show moderate cytotoxicity at equimolar cadmium concentrations. This therefore suggests that **19** is unable to enter cells following platination. CdSe–ZnS/DHLA QDs are known to be able to penetrate the cell membrane *via* passive

delivery (although still *via* endocytosis)[65] and transferrin is readily internalised by endocytosis upon binding to TfR1;[53] indeed, the protein has previously been employed to increase cellular uptake of drug molecules with selective targeting of cancer cells. The ICP-MS data suggest a high degree of platination of the transferrin conjugate, and it is likely this would have a great effect on the surface properties of the quantum dots, such as charge and hydrophobicity; this may render the conjugate non-penetrable through the cell membrane and hence non-cytotoxic.

4.4 Platinum Complexes with Porphyrins

4.4.1 Introduction

Porphyrins are macrocyclic compounds consisting of four pyrrole units connected by methine bridges. They are highly conjugated, aromatic systems and as such display intense absorption in the visible region. The centre of the porphyrin forms a cavity in which metal ions can be accommodated, bound by the four nitrogens of the pyrrole rings. Such compounds are termed metalloporphyrins and are ubiquitous in Nature. The haem prosthetic group, consisting of an iron porphyrin, is essential to many metalloproteins such as haemoglobin, myoglobin and the cytochromes, and is involved in oxygen and electron transfer; in addition, many related structures carry out similar biological functions.

Porphyrins have found medicinal applications in photodynamic therapy (PDT), a technique involving the selective damage of tissue using a photosensitising drug, light and oxygen, which is used in the treatment of certain cancers and skin conditions. The majority of photosensitisers are porphyrins or related molecules, which can be excited by the wavelengths of light which show the deepest penetration through human skin (600–1000 nm).[66] Irradiation of the photosensitiser induces excitation to a singlet excited state, ^{1}PS*, which can undergo intersystem crossing (ISC) to the triplet excited state, ^{3}PS*; this process is relatively efficient in the case of tetrapyrrolic systems. From here, the photosensitiser can react in two ways, defined as Type I or Type II processes.[67] Type II processes involve the direct interaction of ^{3}PS* with molecular oxygen; since this has a triplet ground state the interaction results in triplet-triplet annihilation, regenerating the ground state of the photosensitiser and forming singlet oxygen, $^1O_2$, which shows high and indiscriminate reactivity with biomolecules and is largely responsible for the cytotoxic effects of PDT. Type I processes involve either reduction or oxidation of the photosensitiser by biological substrates, generating free radicals which react rapidly with molecular oxygen and

form numerous reactive oxygen species, including $O_2^{\bullet-}$, $OH^{\bullet}$, OH^- and H_2O_2; these are also expected to contribute to cell death.

An advantage of porphyrins for this purpose is their selective uptake into tumour cells over healthy cells;[68] it is believed porphyrins are transported by low density lipoproteins (LDL) which are internalised *via* receptor mediated endocytosis, and cancer cells are known to express elevated levels of LDL receptors.[69] Given the success of porphyrins in PDT and their tumour accumulating properties, there has been increasing interest in the incorporation of porphyrins into cytotoxic Pt^{II} complexes, to potentially yield complexes with a dual mode of action.[68] One study found significant tumour accumulation of such complexes,[70] and another reported a series of Pt-porphyrin conjugates that showed both phototoxicity upon irradiation and cytotoxicity due to the platinum fragment.[68]

It was therefore hypothesised that a Pt^{II} azido complex containing a porphyrin could show interesting photochemical behaviour, given the rich photochemistry of both moieties alone. The azide anion is known to be an efficient quencher of singlet oxygen;[71] however this may be negated upon photoactivation if the porphyrin were to become dissociated and distant from the platinum moiety, or perhaps alternative photoactivation pathways could be induced. Furthermore, porphyrins exhibit strong absorbance in the visible region and may therefore allow for activation of a Pt^{II} azido complex at these wavelengths. In this section, the synthesis and photochemistry of a Pt^{II} chlorido and a Pt^{II} azido complex containing a simple porphyrin ligand is described.

4.4.2 Experimental

4.4.2.1 Materials

Pyrrole (≥ 97%), 4-pyridinecarboxaldehyde (>96%), propionic acid (99%), and 5,10,15,20-Tetra(4-pyridyl)porphyrin (97%) were purchased from Sigma-Aldrich. Benzaldehyde (>99%), pyridine (anhydrous, reagent grade) and sodium azide

were obtained from Fisher. *cis*-[$Pt(DMSO)_2Cl_2$] and K[$PtNH_3Cl_3$] were synthesised as described in Chapter 3. All column chromatography was carried out using silica gel (60 Å), and under subdued laboratory lighting conditions in order to minimise exposure of the porphyrins to light.

4.4.2.2 Synthesis

5-(4-Pyridyl)-10,15,20-triphenylporphyrin (PyTPP)

4-Pyridinecarboxaldehyde (2.5 mL, 26 mmol) and benzaldehyde (7.5 mL, 74 mmol) were added to propionic acid (250 mL) in a round-bottomed flask. The solution was heated to reflux (423 K), after which pyrrole (7.0 mL, 100 mmol) was added dropwise over a 20 min period. The mixture was heated at reflux for 1 h with vigorous stirring, then cooled for 6 h at room temperature and stored at 277 K overnight. A purple solid (2.72 g) was collected by filtration, and washed with methanol until the filtrate ran colourless. The product was purified by column chromatography, with the desired porphyrin eluting as the second band with 99% $CHCl_3$/1% EtOH.

Yield: 0.57 g (3.7%)
R_f = 0.45 (98:2 $CHCl_3$:EtOH)
^{1}H NMR (400 MHz, $CDCl_3$): δ 9.03 (d, 2H), 8.90–8.79 (m, 8H), 8.22 (d, 6H), 8.18 (d, 2H), 7.78 (m, 9H), –2.80 (s, NH, 2H).
ESI-MS: 616.2499 $[M + H]^+$, $C_{43}H_{30}N_5$ requires 616.2496 *m/z*.

***Cis*-[Pt(PyTPP)(DMSO)Cl_2]**

5-(4-Pyridyl)-10,15,20-triphenylporphyrin (PyTPP) (64.5 mg, 0.105 mmol) was dissolved in dichloromethane (20 mL), and to this was added *cis*-[$Pt(DMSO)_2Cl_2$] (48 mg, 0.116 mmol) in dichloromethane (10 mL). The mixture was stirred overnight at room temperature in the dark, after which all solvent was removed.

The crude product was purified by column chromatography, with the required product eluting as the main band with 95% $CHCl_3$/5% EtOAc.

Yield: 75 mg (74%)

R_f = 0.64 (5:1 $CHCl_3$:EtOAc)

^{1}H NMR (400 MHz, $CDCl_3$): δ 9.18 (d, 2H), 8.95–8.76 (m, 8H), 8.28 (d, 2H), 8.22 (d, 6H), 7.78 (m, 9H), 3.62 (s, 6H), –2.77 (s, NH, 2H).

ESI-MS: 960.1668 $[M + H]^+$, $PtC_{45}H_{36}N_5Cl_2OS$ requires 960.1660 *m/z*.

***Cis*-[Pt(PyTPP)(Py)Cl_2] (20)**

Cis-[Pt(PyTPP)(DMSO)Cl_2] (61 mg, 0.064 mmol) was dissolved in chloroform (15 mL), pyridine (6.13 μL, 0.076 mmol) was added, and the mixture heated at reflux for 24 h in the dark. Solvent was removed and the crude product purified by column chromatography. The required product eluted as the second band using a solvent system of 5:1 $CHCl_3$:EtOAc.

Yield: 15 mg (25%)

R_f = 0.90 (5:1 $CHCl_3$:EtOAc)

^{1}H NMR (400 MHz, $CDCl_3$): δ 9.35 (d, 2H), 9.07 (d, 2H), 8.94–8.79 (m, 8H), 8.22 (d, 6H), 8.18 (d, 2H), 7.87 (t, 1H) 7.79 (m, 9H), 7.42 (t, 2H), –2.80 (s, NH, 2H).

ESI-MS: 961.1965 $[M + H]^+$, $PtC_{48}H_{35}N_6Cl_2$ requires 961.1943 *m/z*.

***Cis*-[Pt(PyTPP)(Py)(N_3)$_2$] (21)**

Cis-[Pt(PyTPP)(Py)Cl_2] (**20**) (15 mg, 0.016 mmol) was dissolved in dimethylformamide (4 mL), and to this was added a solution of NaN_3 (10 mg, 0.160 mmol) in methanol (1.5 mL). The mixture was stirred in the dark for 48 h, after which H_2O (50 mL) was added and the solution lyophilised. The product was

washed with water then purified by column chromatography; the required product eluted as the main band with 5:1 $CHCl_3$:EtOAc.

Yield: 4 mg (26%)

R_f = 0.85 (5:1 $CHCl_3$:EtOAc)

^{1}H NMR (400 MHz, $CDCl_3$): δ 9.22 (d, 2H), 9.00 (d, 2H), 8.94–8.78 (m, 8H), 8.30 (d, 2H), 8.21 (d, 6H), 7.96 (t, 1H) 7.79 (m, 9H), 7.56 (t, 2H), –2.80 (s, NH, 2H).

UV-Vis (DMF): λ_{max} 418, 514, 549, 590, 646 nm; ε 290 000, 18 100, 7300, 5400, 3600 M^{-1} cm^{-1}.

ESI-MS: 974.2755 $[M + H]^+$, $PtC_{48}H_{35}N_{12}$ requires 974.2753 *m/z*.

4.4.2.3 Methods

4.4.2.3.1 Photoreactions

Saturated solutions of *cis*-[Pt(PyTPP)(Py)Cl_2] (**20**) and *cis*-[Pt(PyTPP)(Py)$(N_3)_2$] (**21**) in DMF-d_7 were irradiated at 310 K in an LZC-ICH2 photoreactor equipped with LZC-VIS UV-Visible light lamps (λ = 400–700 nm, P = 0.27 mW cm^{-2}), with ^{1}H NMR spectra recorded after 0, 30, 60 and 120 min in the case of **20**, and 0, 5, 10, 20, 30, 60 and 120 min for **21**.

4.4.3 Results

A porphyrin was synthesised incorporating one pyridyl group to act as a ligand for platinum, and subsequently reacted to form novel Pt^{II} chlorido and azido complexes. The photochemical behaviour of both complexes was investigated upon irradiation with visible light.

4.4.3.1 Synthesis and Characterisation of PyTPP and Platinum Complexes

A simple porphyrin, 5-(4-Pyridyl)-10,15,20-triphenylporphyrin (PyTPP), was chosen, containing three phenyl rings and one pyridyl ring bound to the methine bridges of the porphyrin core. This was synthesised as previously described,[72,73] by an Adler-type condensation of pyrrole, benzaldehyde and 4-pyridinecarboxaldehyde[74] as shown in Scheme 4.6.

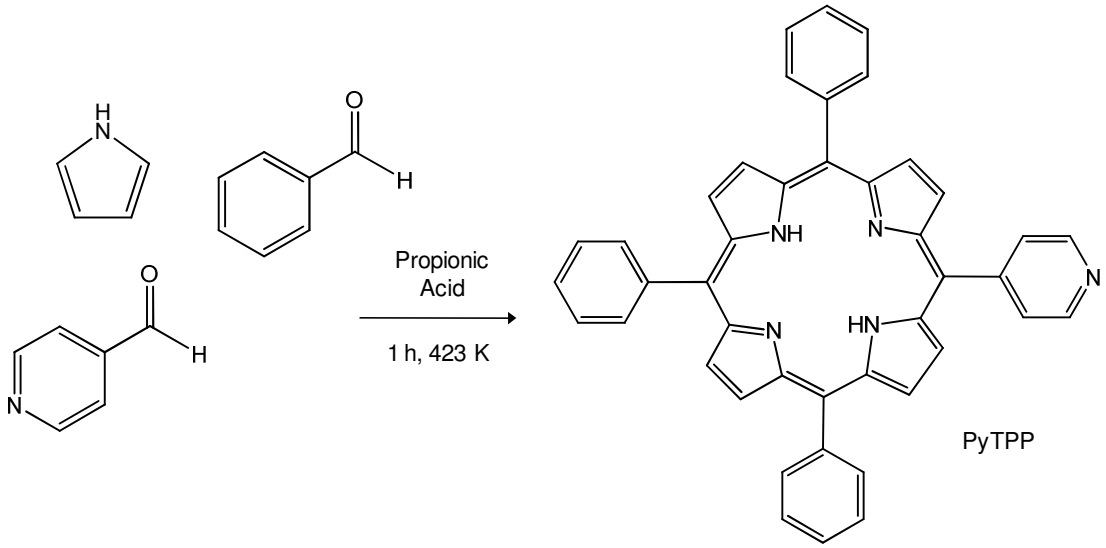

Scheme 4.6 The synthesis of PyTPP.

The crude product consisted of a mixture of at least 5 different porphyrin species as shown by TLC. The major product was tetraphenylporphyrin, with small quantities of bis-pyridyl species also present as well as the required mono-pyridyl product. This was isolated by column chromatography and characterised by ^{1}H NMR spectroscopy and mass spectrometry. The synthetic routes to the Pt^{II} complexes of this porphyrin are shown in Scheme 4.7.

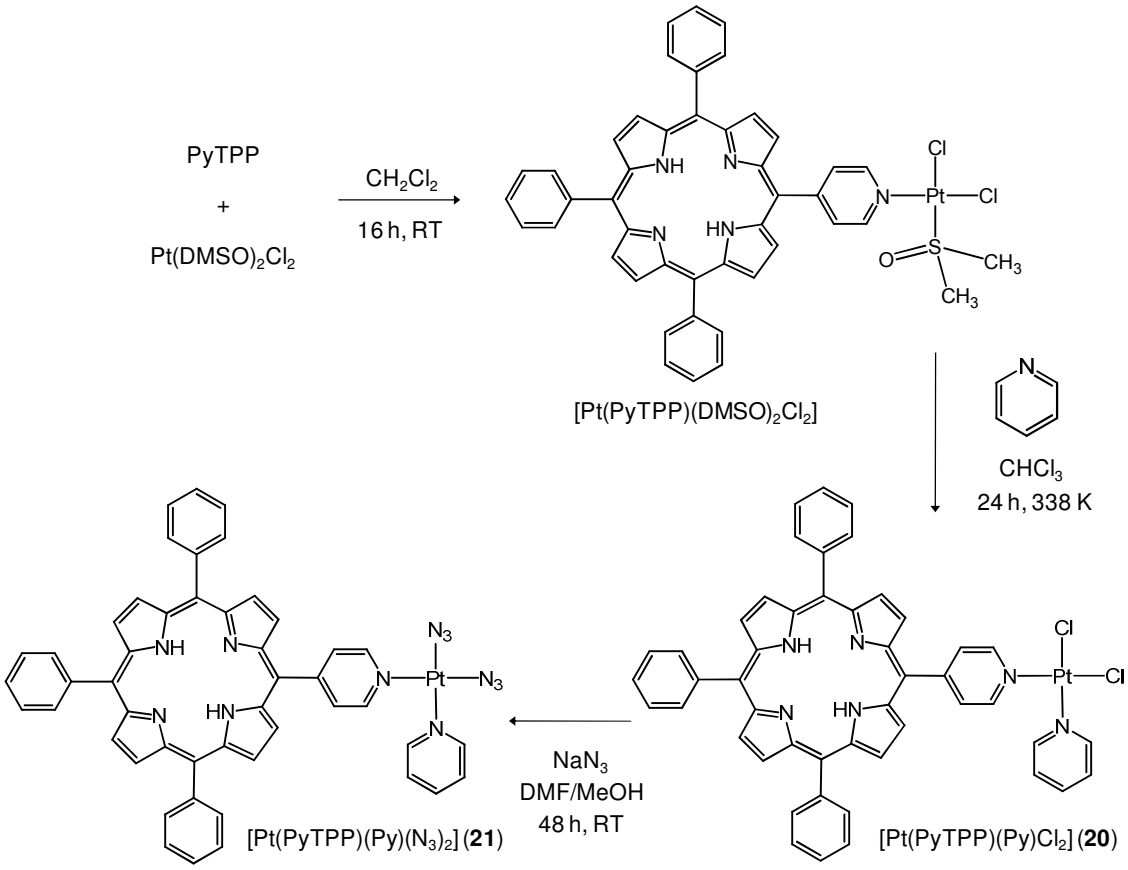

Scheme 4.7 Synthetic routes to Pt^{II} complexes of PyTPP.

Coordination of platinum was achieved by the reaction of PyTPP with the Pt^{II} complex *cis*-$[Pt(DMSO)_2Cl_2]$, as previously described.[75] The ^1H NMR spectrum showed clear evidence of the retention of one DMSO ligand in the complex. A singlet arising from six protons was seen at 3.62 ppm and, in contrast with the platinum starting material, platinum satellites were not evident. Satellites can be broadened by chemical shift anisotropy relaxation, and large molecules tumble slowly, hence relaxation becomes more significant and can result in the broadening of satellites beyond detection;[76] the peaks of the pyridyl protons closest to the bound nitrogen also showed no visible satellites. The signal corresponding to the internal pyrrole protons, appearing at high field (–2.80 ppm) as a result of shielding by the ring current, was also still present in the complex

confirming the platinum was not coordinated inside the porphyrin cavity. Replacement of the remaining DMSO ligand of *cis*-[Pt(PyTPP)(DMSO)Cl_2] was achieved by reaction with pyridine to form the novel complex *cis*-[Pt(PyTPP)(Py)Cl_2] (**20**), although this reaction was low-yielding and significant quantities of the free porphyrin were observed. The chlorido groups were then directly exchanged with azide *via* a well-documented method using NaN_3 in DMF/MeOH,[77] to form the azido complex *cis*-[Pt(PyTPP)(Py)$(N_3)_2$] (**21**).

Attempts were also made to synthesise a multinuclear complex *via* the attachment of platinum to all four pyridyl groups of tetrapyridylporphyrin (TPyP). Reaction of this porphyrin with *cis*-[Pt$(DMSO)_2Cl_2$] was attempted in a similar manner to that of Scheme 4.7; an alternative method involved reaction with K[Pt$(NH_3)Cl_3$], in which the porphyrin should replace the chlorido group *cis* to the ammonia ligand. However, all attempts to form a multinuclear complex were unsuccessful. Although a purple product was precipitated in all cases, this was invariably insoluble in most common solvents, with DMF-d_7 the only solvent in which NMR spectra could be obtained. Whilst the spectra did indicate reaction had taken place, the products were not clean and could not be identified, and the poor solubility in any solvents suitable for column chromatography prevented purification attempts.

4.4.3.2 UV-Vis Spectroscopy of *cis*-[Pt(PyTPP)(Py)$(N_3)_2$] (21)

The UV-visible absorption spectrum of *cis*-[Pt(PyTPP)(Py)$(N_3)_2$] (**21**) in DMF is shown in Figure 4.4.1, and displays the typical spectral profile of a free-base (i.e. non-metallated) porphyrin.

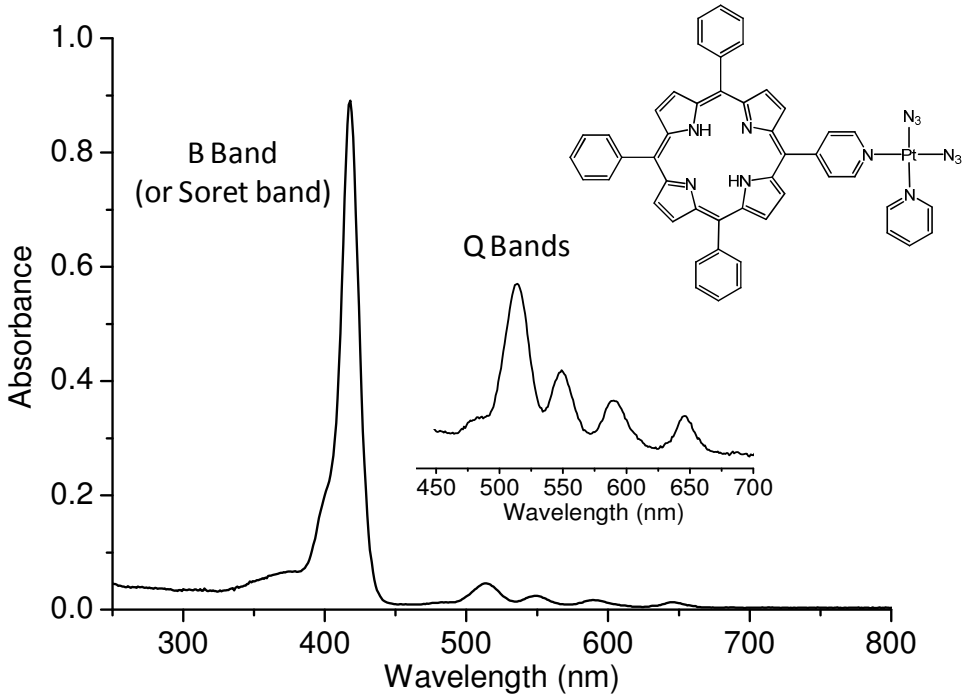

Figure 4.16 The UV-visible absorption spectrum of [Pt(PyTPP)(Py)(N_3)$_2$] (**21**), with (inset) an expansion of the Q band region.

The intense band at 418 nm is known as the B band, or Soret band, and arises from a π-π* transition from the ground state to the second excited singlet state.[78] The bands in the lower energy region are known as Q bands, the number and relative intensity of which depends upon the substituents on the pyrrole or meso carbons and whether or not the porphyrin is metallated; in free base porphyrins such as this, four bands are seen. Their intensity is much lower than that of the Soret band, since they arise from pseudoparity forbidden transitions to the first singlet excited state. The absorption bands of the platinum complexes are virtually unchanged from those of the uncoordinated porphyrin, hence platinum coordination to the pyridyl ring does not seem to significantly perturb the electronic properties of the porphyrin system.[75]

4.4.3.3 Photoreactions of [Pt(PyTPP)(Py)Cl_2] (20) and [Pt(PyTPP)(Py)$(N_3)_2$] (21) with Visible Light

a) [Pt(PyTPP)(Py)Cl_2] (**20**)

After 30 min a new singlet had emerged at 10.41 ppm, which increased in intensity upon further irradiation (Figure 4.17). This was believed to arise from hydrogen peroxide, with evidence provided by the growth of this peak upon spiking the irradiated sample with 4 μL of a 30% H_2O_2 solution. Hydrogen peroxide is known to be among the reactive oxygen species potentially formed upon irradiation of porphyrins, and unlike others is detectable by ^{1}H NMR spectroscopy.

There was little change in the aromatic region throughout the experiment, except for a slight decrease in intensity of the signals. However, several smaller peaks were formed at low field. After 30 min a singlet was apparent at 11.50 ppm, however this decreased in intensity upon further irradiation. Conversely, a peak at 12.09 ppm steadily increased in intensity throughout the experiment. It was thought the latter peak could arise from the pyridyl protons of a Pt^{IV} complex, formed upon oxidation of the Pt^{II} species by the hydrogen peroxide generated *in situ*. An NMR spectrum was thus run 36 h after spiking the irradiated sample with H_2O_2, however there was no increase in intensity of the peak at 12.09 ppm. To test if an oxidation reaction could be facilitated by irradiation, the spiked sample was irradiated for 30 min, however again no increase in this peak was found, suggested the assignment as a Pt^{IV} species may be incorrect.

Irradiation of the free porphyrin PyTPP produced only a very small quantity of H_2O_2 after 30 min (not illustrated). It is suggested that the increased yield in the case of the Pt^{II} chlorido complex could be due to the heavy-atom effect. Singlet oxygen production, upon which formation of H_2O_2 is likely dependent, arises from the interaction of oxygen with a triplet excited state of the photosensitiser; this triplet state is produced *via* intersystem crossing from a singlet excited state.

A heavy metal in the molecule can increase the rate of intersystem crossing (the heavy-atom effect),[22] which may in turn increase $^1O_2$ and H_2O_2 production.

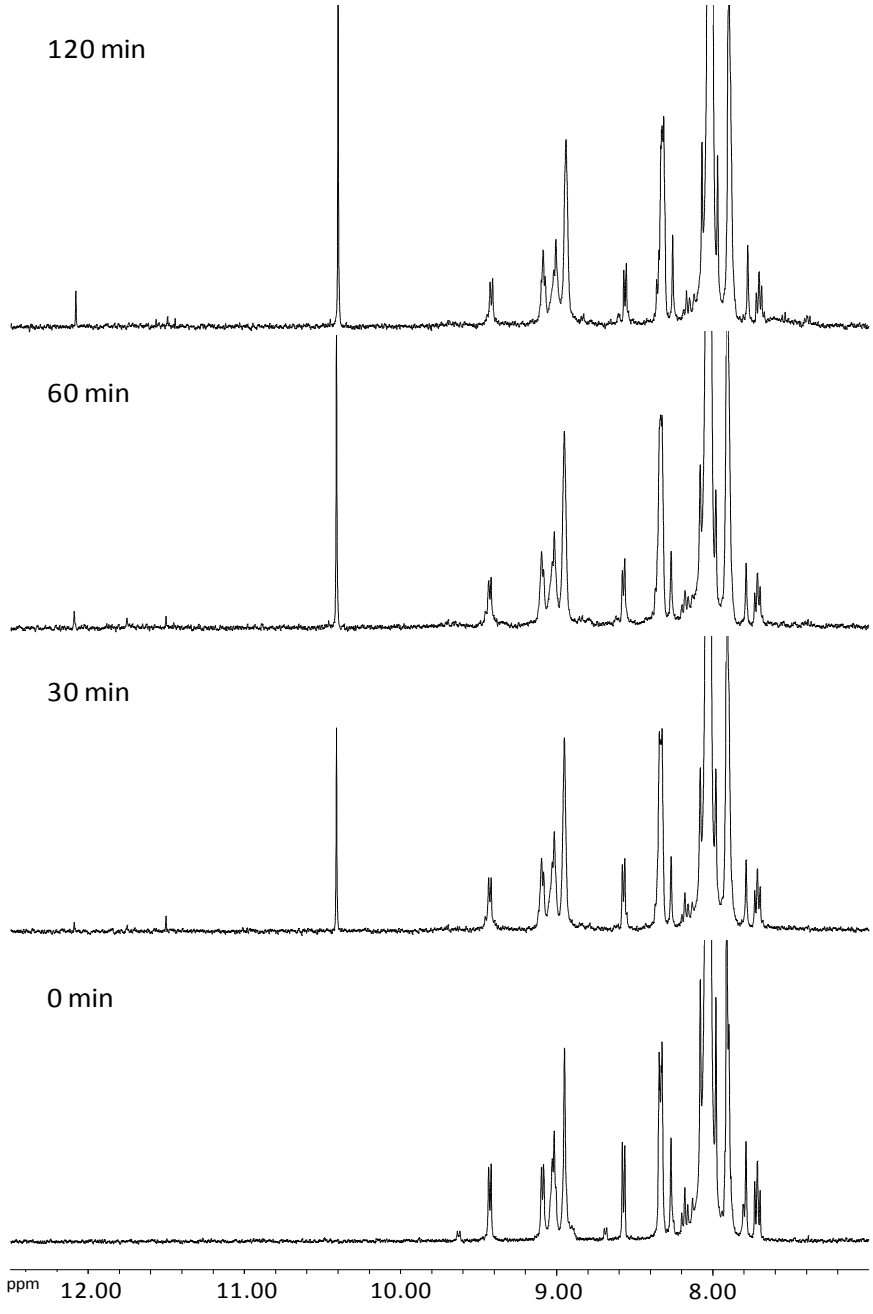

Figure 4.17 ^{1}H NMR spectra recorded in DMF-d_7 at various timepoints during the irradiation of [Pt(PyTPP)(Py)Cl_2] (**21**) with visible light.

b) [Pt(PyTPP)(Py)$(N_3)_2$] (**21**)

In the case of the Pt^{II} azido complex changes were seen in the aromatic region after 5 min irradiation; notably the emergence of two small peaks around the doublet at 8.68 ppm, and new peaks slightly downfield of the pyridyl protons at 9.37 ppm. It is likely these arise from species which have undergone loss of the azido ligands; this is a known photochemical reaction of Pt^{II} azido complexes, and has been demonstrated in Chapter 3. These new peaks increase in intensity upon further irradiation, with a concomitant decrease in intensity of the peaks from the initial complex.

Contrary to the case of [Pt(PyTPP)(Py)Cl_2] (**21**), only very small amounts of hydrogen peroxide were detected upon irradiation of the Pt^{II} azido complex. It is suggested this could be due to the known quenching effect of the released azide anions on singlet oxygen ($^1O_2$), which is a precursor to the generation of hydrogen peroxide upon irradiation of porphyrins.

There is no evidence of new peaks around 11–12 ppm. This observation suggests the peaks seen upon irradiation of the Pt^{II} chlorido complex (**20**) may indeed be related to the formation of hydrogen peroxide, although such evidence was not found in that particular experiment.

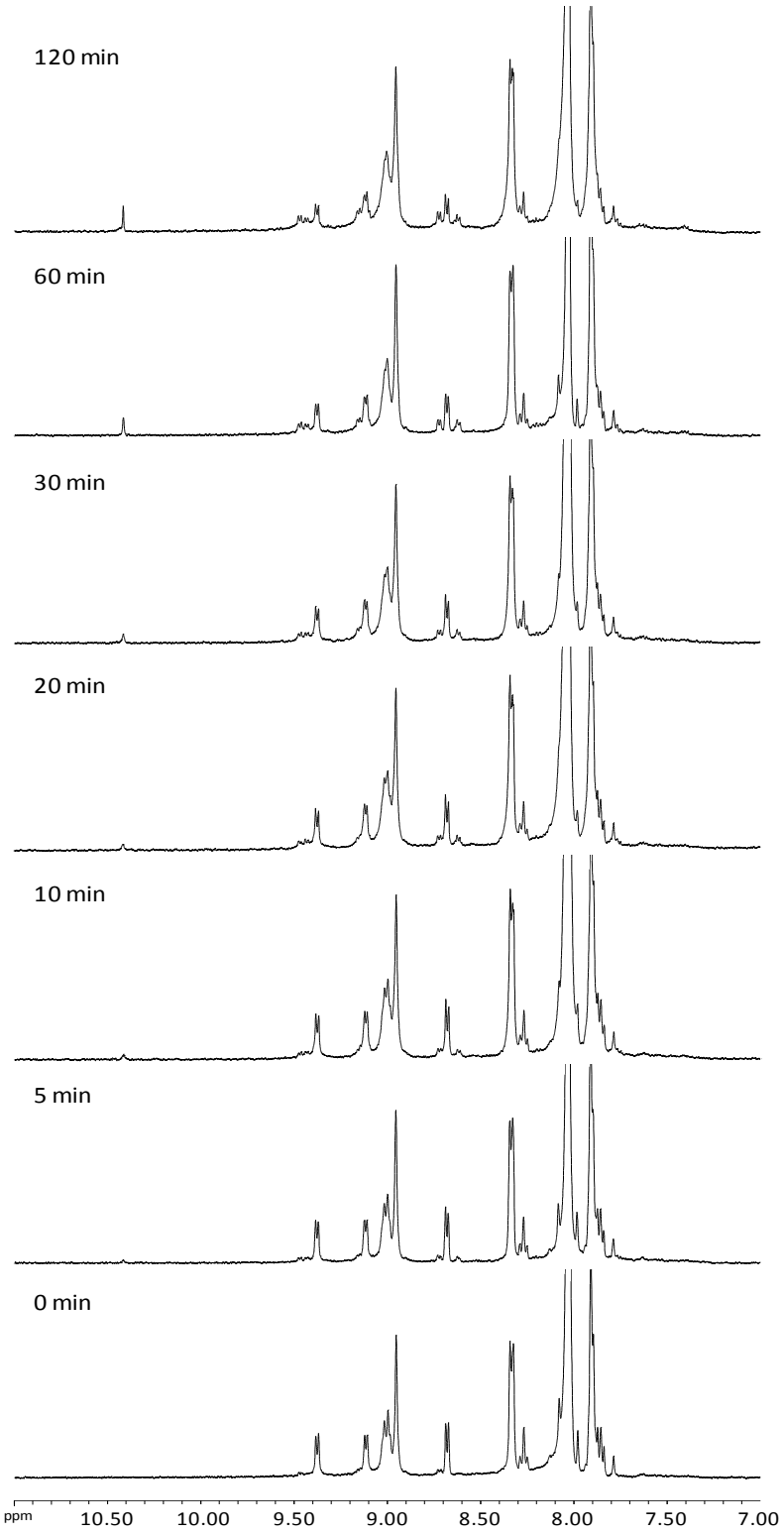

Figure 4.18 ^{1}H NMR spectra recorded in DMF-d_7 at various timepoints during the irradiation of [Pt(PyTPP)(Py)$(N_3)_2$] (**21**) with visible light.

4.4.4 Discussion

4.4.4.1 Synthesis of PyTPP and Platinum Complexes

For an initial study of the photochemistry of Pt^{II} chlorido and azido complexes containing porphyrins, a simple porphyrin was chosen with one pyridyl ligand for coordination to platinum (PyTPP). This porphyrin was synthesised according to published procedures,[72,73] although was obtained in a typically low yield, since reactions to produce mixed aryl porphyrins can potentially form six different porphyrin products. One report[72] suggests a higher yield can be obtained by using an excess of 4-pyridinecarboxaldehyde compared with benzaldehyde (1.18:1). However in this work, whilst this method was found to be successful in reducing the proportion of tetraphenylporphyrin in the product, relatively large quantities of the two *bis*-pyridyl porphyrin isomers were also formed. These were difficult to separate from the required monopyridyl product by column chromatography due to their very similar R_f values; additionally, increases in yield were only modest. Hence an alternative method using an excess of benzaldehyde was preferred.[73]

Although the platination of the porphyrin with *cis*-[$Pt(DMSO)_2Cl_2$] proceeded in good yield to form *cis*-[$Pt(PyTPP)(DMSO)Cl_2$], attempts to replace the remaining DMSO ligand with pyridine led to significant quantities of free PyTPP. At room temperature, detachment of the porphyrin from the platinum centre was found to predominate, with only very small quantities of the desired product detected by TLC. Heating the reaction to reflux led to a greater proportion of the required product *cis*-[$Pt(PyTPP)(Py)Cl_2$] (**20**), evidently replacement of the second DMSO ligand requires elevated temperatures as previously suggested,[75] although free PyTPP was still evident. It is likely that pyridine has an affinity for platinum similar to or greater than that of PyTPP, hence is able to readily displace the porphyrin. A similar displacement of PyTPP was found upon reaction of **20** with sodium azide, although to a lesser extent. This problem could be overcome by the use of a different aromatic amine ligand with a lower affinity for platinum, or by

the coordination of platinum to a chelating amine moiety on a porphyrin, which would impart greater stability to the complex.

It was believed that a complex containing multiple platinum centres bound to one porphyrin could show interesting DNA interactions and photochemical properties. Indeed, very recent studies of ruthenium and osmium complexes of tetrapyridyl porphyrin have found such complexes are both cytotoxic and phototoxic upon irradiation with red light, and their fate inside cells can be followed by the fluorescence of the porphyrin moiety.[79,80] Attempts were made to form an analogous platinum complex in this work, however these were not successful. Since it was desirable to retain two chlorido ligands in the product to allow for potential cross-linking to DNA, as well as two amine ligands, the target complexes were neutral and thus the reaction products showed very poor solubility; previous examples of Pt^{II} complexes of tetrapyridylporphyrin have a high positive charge overall.[81] However, it may also be of interest to prepare a charged monochlorido or monoazido complex, since the DNA interactions of such a complex are likely to be very different from those of cisplatin-type complexes.

4.4.4.2 Photoreactions of Porphyrin-containing Platinum Complexes

The apparent formation of hydrogen peroxide upon irradiation of the chlorido complex [Pt(PyTPP)(Py)Cl_2] (**20**), but not of the azido complex [Pt(PyTPP)(Py)$(N_3)_2$] (**21**), is interesting. Typically, the irradiation of porphyrins yields singlet oxygen by reaction of the excited photosensitiser with molecular oxygen, and this is believed to be the primary cause of cell death in PDT. The generation of many other reactive oxygen species, including hydrogen peroxide, is also possible, although these are typically formed as a result of the initial reaction of the excited photosensitiser with biological substrates to form radicals, which subsequently interact with oxygen.[67] Indeed, there are reports of the detection of H_2O_2 in *in vitro* experiments of cells treated with photosensitisers and light,[82,83]

with biomolecules such as ascorbate[84] and NADPH oxidase[83] implicated in its formation.

The irradiation study of **20** was carried out on the porphyrin alone, however there are some studies to suggest the formation of hydrogen peroxide from the irradiation of porphyrins in the absence of biological substrates.[85,86] These suggest formation is dependent upon the substituents on the porphyrin and whether or not it aggregates in aqueous solutions, however the mechanism of hydrogen peroxide generation was not discussed. Knör and Vogler report the formation of hydrogen peroxide from the irradiation of an aerated ethanolic solution of a Sb^{III} porphyrin, with concurrent oxidation of the metal to the Sb^{V} state;[87] however, since the Pt^{II} complex **20** is likely to show markedly different chemistry from a Sb^{III} metalloporphyrin, comparisons cannot readily be drawn. It is suggested in this work that the hydrogen source could be H_2O, which is present in significant quantities in the DMF-d_7 in which the spectra were obtained.

It is known that hydrogen peroxide can be produced in relatively small amounts as a secondary oxidant after initial singlet oxygen formation.[83] The generation of hydrogen peroxide in this way could account for its lack of formation upon irradiation of the azido complex **21**. It is known that Pt^{II} azido complexes can release free azide upon photoactivation,[88] and the azide anion is a very efficient quencher of singlet oxygen.[89] Should quenching occur, this would minimise the amount of singlet oxygen that could subsequently form hydrogen peroxide.

It is clear that many more studies would need to be performed in order to elucidate the photoproducts of the irradiation of **20** and **21**. Of all the reactive oxygen species that could be produced upon irradiation, ^{1}H NMR can only detect hydrogen peroxide, although its presence should ideally be confirmed by another method such as the luminol chemiluminescence test.[86] Monitoring changes in the UV-visible absorption spectrum may also give valuable information on any changes to the porphyrin system. Factors to be determined could include the dependence upon oxygen and involvement of singlet oxygen, the role of the solvent (although solubility issues would prevent the irradiation of these particular

porphyrins in aqueous solutions), and the influence of the light source; higher energy UV light could give rise to different photoproducts.

The initial investigation into the photochemistry of these systems is intriguing, suggesting that a Pt^{II} azido porphyrin complex gives rise to different photoproducts from that of a chlorido complex. The question of whether free azide quenches the singlet oxygen produced upon irradiation remains to be answered. However even if this were the case, it may not necessarily be detrimental. Singlet oxygen could react with a variety of biomolecules *in vivo*, where the quenching effect may not be so pronounced; additionally, the rich photochemistry of both porphyrins and azido complexes could lead to the activation of novel photochemical pathways.

4.5 Conclusions

This Chapter was concerned with the functionalisation of platinum complexes with bioactive species.

The conjugation of the fluorescent probe MIA to $[Pt(L1)(N_3)_2]$ (**5**) confirms the possibility of functionalisation of the pendant hydroxyl group. The relatively large degree of fluorescence quenching in comparison to that of the free probe suggests a longer spacer length between the probe and platinum may be desirable in the design of complexes for intracellular fluorescence monitoring applications; however, the large increase in fluorescence should the probe become detached from the platinum may also be of use in monitoring intracellular reactions.

The reaction of $[Pt(en)(N_3)_2(OH)_2]$ (**3**) with MIA yielded a complex in which only one axial hydroxyl group of a Pt^{IV} azido complex was modified. The rapid increase in fluorescence upon irradiation of this complex, as a result of loss of the axial groups and reduction to Pt^{II}, could be a useful monitor of the reduction event and not solely applicable to photoactivated complexes.

Although the functionalisation of the protected amine groups of Pt^{II} and Pt^{IV} azido complexes was unsuccessful in the isolation of a clean product, the formation of a

fluorescent sulfonamide indicates some degree of success, and suggests the deprotection of such groups is feasible and a valid way of introducing an amine-reactive moiety into the complex.

The synthesis of water soluble quantum dots was achieved, however the subsequent amide coupling and platinum coordination rendered the resulting conjugate insoluble in aqueous solutions. The conjugation of transferrin to quantum dots was evidenced by iron uptake studies, and subsequent reactions prepared the platinum conjugate which showed good water solubility and essentially no fluorescence quenching. However, this conjugate was found to be non-cytotoxic towards the A2780 human ovarian cancer cell line, likely as a result of extensive surface modification due to the high degree of platination, rendering the complex impenetrable through the cell membrane.

Pt^{II} chlorido and azido complexes containing a porphyrin were found to undergo differing behaviour upon irradiation with visible light in DMF solution. Evidence of H_2O_2 was seen in the case of the Pt^{II} chlorido complex but was much reduced in the case of the azido analogue; it is suggested that H_2O_2 production may be dependent upon singlet oxygen, which could be rapidly quenched by any azide ion release from the Pt^{II} azido complex upon irradiation.

This chapter therefore demonstrates the ability to functionalise platinum azido complexes, and suggests that conjugation of bioactive species may be of interest in the monitoring of reactions or reduction upon photoactivation, or by generating complexes with a novel mode of action upon irradiation.

4.6 References

[1] S. Dhar, Z. Liu, T. Zhuang, J. Thomale, H. Dai and S. J. Lippard, *J. Am. Chem. Soc.*, 2008, **130**, 11467.

[2] S. Mundwiler, B. Spingler, P. Kurz, S. Kunze and R. Alberto, *Chem. Eur. J.,* 2005, **11**, 4089.

[3] K. R. Barnes, A. Kutikov and S. J. Lippard, *Chem. Biol.*, 2004, **11**, 557.

[4] P. de Hoog, C. Boldron, P. Gamex, K. Sliedregt-Bol, I. Roland, M. Pitie, R. Kiss, B. Meunier and J. Reedijk, *J. Med. Chem.*, 2007, **50**, 3148.

[5] T. W. Hambley, *Aust. J. Chem.*, 2008, **61**, 647.

[6] E. J. New, R. Duan, J. Z. Zhang and T. W. Hambley, *Dalton Trans*., 2009, 3092.

[7] A. K. Larsen, A. E. Escargueil and A. Skladanowski, *Pharmacol. Ther*., 2000, **85**, 217.

[8] C. Molenaar, J.-M. Teuben, R. J. Heetebrij, H.J. Tanke and J. Reedijk, *J. Biol. Inorg. Chem.*, 2000, **5**, 655.

[9] R. J. Heetebrij, E. G. Talman, M. A. van Velezen, R. P. M. van Gijlswijk, S. S. Snoeijers, M. Schalk, J. Wiegant, F. van der Rijke, R. M. Kerkhoven, A. K. Raap, H. J. Tanke and J. Reedijk, *ChemBioChem*, 2003, **4**, 573.

[10] E. J. New, C. Roche, R. Madawala, J. Z. Zhang and T. W. Hambley, *J. Inorg. Biochem.*, 2009, **103**, 1120.

[11] L. Ronconi and P. J. Sadler, *Chem. Commun*., 2008, 235.

[12] P. J. Bednarski, R. Grunert, M. Zielzki, A. Wellner, F. S. Mackay and P. J. Sadler, *Chem. Biol.*, 2006, **13**, 61.

[13] T. Hiratsuka, *J. Biol. Chem.*, 1982, **257**, 13354.

[14] F. Muñoz-Martinez, C. P. Reyes, A. L. Perez-Lomas, I. A. Jimenez, F. Gamberro and S. Castanys, *Biochim. Biophys. Acta.*, 2006, **1758**, 98.

[15] A. Y. Jan, E. F. Johnson, A. J. Diamonti, K. L. Carraway III and K. S. Anderson, *Biochemistry*, 1998, **37**, 792.

[16] F. Zobi, B. Balali Mood, P. A. Wood, F. P. A. Fabbiani, S. Parsons and P. J. Sadler, *Eur. J. Inorg. Chem.*, 2007, 2783.

[17] M. D. Hall, C. T. Dillon, M. Zhang, P. Beale, Z. Cai, B. Lai, A. P. J. Stampfl and T. W. Hambley, *J. Biol. Inorg. Chem.*, 2003, **8**, 726.

[18] J. M. Walker, *Methods Mol. Biol.*, 1994, **32**, 321.

[19] P. Roux, A. Le Saux, C. Fiore, C. Schwimmer, A.-C. Dianoux, V. Trezeguet, P. V. Vignaism G. J.-M. Lauquin and G. Brandolin, *Anal. Biochem.*, 1996, **234**, 31.

[20] G. T. Hermanson, *Bioconjugate Techniques*, Elsevier, San Diego, USA, 2nd edn. 2008.

[21] M. Reithofer, M. Galanski, A. Roller and B. K. Keppler, *Eur. J. Inorg. Chem.*, 2006, 2612.

[22] S. K. Lower and M. A. El-Sayed, *Chem. Rev.*, 1966, **66**, 199.

[23] J. F. Hartwig, P. M. Pil and S. J. Lippard, *J. Am. Chem. Soc.*, 1992, **114**, 8292.

[24] R. Guddneppanavar, G. Saluta, G. L. Kucera and U. Bierbach, *J. Med. Chem.,* 2006, **49**, 3204.

[25] B. Das Sarma and J. C. Ballar Jr, *J. Am. Chem. Soc.*, 1969, **91**, 5958.

[26] S. Ren, L. Cai and B. M. Segal, *Dalton Trans.*, 1999, 1413.

[27] J. N. Jolley, A. I. Yanovsky, L. R. Kelland and K. B. Nolan, *J. Inorg. Biochem.*, 2001, **83**, 91.

[28] F. Di Costanzo, A. Sdrobolini and S. Gasperoni, *Crit. Rev. Oncol. Hematol.*, 2000, **35**, 101.

[29] D. Wang and S. J. Lippard, *Nat. Rev. Drug. Discov.*, 2005, **4**, 307.

[30] F. S. Mackay, N. J. Farrer, L. Salassa, H.-C. Tai, R. J. Deeth, S. A. Moggach, P. A. Wood, S. Parsons and P. J. Sadler, *Dalton Trans.*, 2009, 2315.

[31] Y.-A. Lee, S. S. Lee, K. M. Kim, C. O. Lee and Y. S. Sohn, *J. Med. Chem.*, 2000, **43**, 1409.

[32] W. H. Ang, S. Pilet, R. Scopelliti, F. Bussy, L. Juillerat-Jeanneret and P. J. Dyson, *J. Med. Chem.*, **48**, 8060.

[33] W. H. Ang, I. Khalaila, C. S. Allerdyce, L. Juillerat-Jeanneret and P. J. Dyson, *J. Am. Chem. Soc*, **127**, 1382.

[34] R. P. Feazell, N. Nakayama-Ratchford, H. Dai and S. J. Lippard, *J. Am. Chem. Soc.*, 2007, **129**, 8438.

[35] R. Song, K. M. Kim, S. S. Lee and Y. S. Sohn, *Inorg. Chem.*, 2000, **39**, 3567.

[36] R. Song, K. M. Kim and Y. S. Sohn, *Inorg. Chim. Acta*, 2002, **338**, 89.

[37] A. Fleischer, A. Roller, V. B. Arion, B. K. Keppler and F. Mohr, *Can. J. Chem.*, 2009, **87**, 146.

[38] C. B. Murray, D. J. Norris and M. G. Bawendi, *J. Am. Chem. Soc.*, 1993, **115**, 8706.

[39] X. Michalet, F. F. Pinaud, L. A. Bentolila, J. M. Tsay, S. Doose, J. J. Li, G. Sundaresan, A. M. Wu, S. S. Gambhir and S. Weiss, *Science*, 2005, **307**, 538.

[40] A. M. Smith, H. Duan, A. M. Mohs and S. Nie, *Adv. Drug Deliv. Rev.*, 2008, **60**, 1226.

[41] J. B. Delehanty, I. L. Medintz, T. Pons, F. M. Brunel, P. E. Dawson, H. Mattoussi, *Bioconjug. Chem.*, 2006, **17**, 920.

[42] C. Tekle, B. van Deurs, K. Sandvig and T.-G. Iversen, *Nano Lett.*, 2008, **8**, 1858.

[43] R. P. Bagwe, X. J. Zhao and W. H. Tan, *J. Dispers. Sci. Technol.*, 2003, **24**, 453.

[44] J. M. Tsay, M. Trzoss, L. Shi, X. Kong, M. Selke, M. E. Jung and S. Weiss, *J. Am. Chem. Soc*., 2007, **129**, 6865.

[45] J.-M. Hsieh, M.-L. Ho, P.-W. Wu, P.-T. Chou, T.-T. Tsaib and Y. Chi, *Chem. Commun*., 2006, 615.

[46] N. G. Blanco, C. R. Maldonado and J. C. Mareque-Rivas, *Chem. Commun.*, 2009, **35**, 5257.

[47] J. Sambrook, T. Maniatis and E. F. Fritsch, *Molecular Cloning: A Laboratory Manual*, Laboratory Press, New York, 2nd. Edn., 1989, volume 3, appendix B.12.

[48] T. Jin, F. Fiji, H. Sakata, M. Tamura and M. Kinjo, *Chem. Commun.*, 2005, 4300.

[49] A. R. Clapp, E. R. Goldman and H. Mattoussi, *Nat. Protoc*., 2006, **1**, 1258.

[50] X. Peng, M.C. Schlamp, A.V. Fadavanish and A.P. Alivisatos, *J. Am. Chem. Soc.*, 1997, **119**, 7019.

[51] W. W. Yu, L. Qu, W. Guo and X. Peng, *Chem. Mater*., 2003, **15**, 2854.

[52] S. A. Johannesen, B. O. Petersen, J. Ø. Duus and T. Skrydstrup, *Inorg. Chem*., 2007, **46**, 4326.

[53] Z. M. Qian, H. Li, H. Sun and K. Ho, *Pharmacol. Rev*., 2002, **54**, 561.

[54] Evitag Protocols Recipe Book, Evident Technologies, 2006.

[55] A. R. Montoro Bustos, J. Ruiz Encinar, M. T. Fernandez-Arguelles, J. M. Costa-Fernandez and A. Sanz-Medel, *Chem. Commun*., 2009, 3107.

[56] M. Grabolle, J. Ziegler, A. Merkulov, T. Nann and U. Resch-Genger, *Ann. N. Y. Acad. Sci*., 2008, **1130**, 235.

[57] B. O. Dabbousi, J. Rodriguez-Viejo, F. V. Mikulec, J. R. Heine, H.

Mattoussi, R. Ober, K. F. Jensen, and M. G. Bawendi, *J. Phys. Chem. B*., 1997, **101**, 9463.

[58] S. Pathak, S.-K. Choi, N. Arnheim and M. E. Thompson, *J. Am. Chem. Soc.*, 2001, **123**, 4103.

[59] C. -A. J. Lin, R. A. Sperling, J. K. Li, T.-Y Yang, P.-Y. Li, M. Zanella, W. H. Chang and W. J. Parak, *Small*, 2008, **4**, 334.

[60] X. Gao, L. Yang, J. A. Petros, F. F. Marshall, J. W. Simons and S. Nie, Curr. Opin. Biotech., 2005, **16**, 63.

[61] M. G. Sandros, M. Behrendt, D. Maysinger and M. Tabrizian, *Adv. Funct. Mater*., 2007, **17**, 3724.

[62] J. Qian, K.-T. Yong, I. Roy, T. Y. Ohulchanskyy, E. J. Bergey, H. H. Lee, K. M. Tramposch, S. He, A. Maitra and P. N. Prasad, *J. Phys. Chem. B*, 2007, **111**, 6969.

[63] A. R. Timerbaev, C. G. Hartinger, S. S. Aleksenko, and B. K. Keppler, *Chem. Rev*., 2006, **106**, 2224.

[64] J. M. Tsaya and X. Michalet, *Chem. Biol*., 2005, **12**, 1159.

[65] J. B. Delehanty, H. Mattoussi and I. L. Medintz, *Anal. Bioanal. Chem*., 2009, **393**, 1091.

[66] S. Wan, J. A. Parrish, R. R. Anderson and M. Madden, *Photochem. Photobiol.*, 1981, **34**, 679.

[67] L. B. Josefsen and R. W. Boyle, *Metal-Based Drugs*, 2008, 1.

[68] H. Brunner, M. R. Arndt and B. Trettinger, *Inorg. Chim. Acta.*, 2004, **357**, 1649.

[69] B. A. Allison, E. Waterfield, A. M. Richter and J. G. Levy, *Photochem. Photobiol.*, 1991, **54**, 709.

[70] R. Song, Y.-S. Kim and Y. S. Sohn, *J. Inorg. Biochem.*, 2002, **89**, 83.

[71] J. R. Harbour and S. L. Issler, *J. Am. Chem. Soc.* 1982, **104**, 903.

[72] M. T. Barton, N. M. Rowley, P. R. Ashton, C. J. Jones, N. Spencer, M. S. Tolley and L. J. Yellowlees, *New. J. Chem.*, 2000, **24**, 555.

[73] E. B. Fleischer and A. M. Shachter, *Inorg. Chem*., 1991, **30**, 3763.

[74] A. D. Adler, F. R. Longo, J. D. Finarelli, J. Goldmacher, J. Assour and L. Korsakoff, *J. Org. Chem.*, 1967, **32**, 476.

[75] H. Yuan, L. Thomas and L. K. Woo*, Inorg. Chem.*, 1996, **35**, 2808.

[76] P. J. Hore, *Nuclear Magnetic Resonance*, Oxford University Press, New York, 2004.

[77] S. S. Kamath, V. Uma and T. S. Srivastava, *Inorg, Chim. Acta.,* 1989, **161**, 49.

[78] K. Kalyanasundaram, *Photochemistry of Polypyridine and Porphyrin Complexes*, Academic Press, London, 1992.

[79] F. Schmitt, P. Govindaswamy, G. Süss-Fink, W. H. Ang, P. J. Dyson, L. Juillerat-Jeanneret and B. Therrien, *J. Med. Chem*., 2008, **51**, 1811.

[80] F. Schmitt, P. Govindaswamy, O. Zava, G. Süss-Fink, L. Juillerat-Jeanneret and B. Therrien, *J. Biol. Inorg. Chem*., 2009, **14**, 101.

[81] L. Scolaro, M. Plutino, A. Romeo, R. Romeo, G. Ricciardi, S. Belviso and A. Albinati, *Dalton Trans.*, 2006, 2551.

[82] F. Bohm, R. Edge, S. Foley, L. Langea and T. G. Truscott, *J. Photochem. Photobiol. B*, 2001, **65**, 177.

[83] N. Rubio, S. P. Fleury and R. W. Redmond, *Photochem. Photobiol. Sci.*, 2009, **8**, 457.

[84] G. G. Kramarenko, S. G. Hummel, S. M. Martin and G. R. Buettner *Photochem. Photobiol.*, 2006, **82**, 1634.

[85] I. A. Menon, M. A. Becker, S. D. Persad and H. F. Haberman, *Clin. Chim.*

Acta. 1990, **186,** 375.

[86] K. Komagoe and T. Katsu, *Anal. Sci*., 2006, **22**, 255.

[87] G. Knor and A. Vogler, *Znorg. Chem.,* 1994, **33**, 314.

[88] J. Sima, *Coord. Chem. Rev.*, 2006, **250**, 2325.

[89] J. R. Harbour and S. L. Issler, *J. Am. Chem. Soc*. 1982, **104**, 903.

Chapter 5

Platinum Complexes with Azopyridine Ligands

5.1 Introduction

In the search for photoactive platinum complexes as potential anticancer agents, efforts have focused mainly upon Pt^{IV} complexes of the general formula $[Pt(amine)_2(N_3)_2(OH)_2]$.[1,2,3] These complexes possess a LMCT band ($N_3 \rightarrow Pt^{IV}$), typically centred around 260–290 nm depending upon the geometry of the azide ligands (*cis* or *trans* respectively). Irradiation with UVA light effects a photoreduction from Pt^{IV} to Pt^{II}, during which the two azide ligands are lost to generate reactive, cytotoxic species.

For phototherapy applications, the use of visible (ideally red) light is preferable to UVA, as it penetrates skin to a greater extent and results in minimised damage to surrounding healthy cells.[4] However, these Pt^{IV} complexes show little absorbance in the visible region, and as such irradiation at these wavelengths is less effective compared with UVA. For example, although *trans,trans,trans*-$[Pt(NH_3)(py)(N_3)_2(OH)_2]$ was found to be as cytotoxic as cisplatin towards HaCaT keratinocytes upon irradiation at 420 nm, this complex is over an order of magnitude more potent when irradiated with UVA light.[3] In addition, TD-DFT calculations indicate 476 nm is the longest predicted singlet transition for this complex; the longest wavelength at which the absorption of light is formally allowed (L. Salassa, unpublished results).

Shifting the wavelength of activation to longer wavelengths is therefore a key aim in the development of new photoactivatable platinum complexes. Photoreduction has thus far been achieved by irradiation into the $N_3 \rightarrow Pt^{IV}$ LMCT band; however, shifting this band to significantly longer wavelengths may not be feasible and, in order to achieve photoactivity in the visible region, it may be necessary to modify the design of the complex. It was believed that the incorporation of highly coloured ligands could result in a change in the nature of the absorption bands, the desired absorbance at visible wavelengths, and the potential for photoactivity in this region. For these reasons, it was decided to investigate platinum complexes containing azo compounds as ligands.

Azo compounds are characterised by the presence of the R–N=N–R' functional group (R/R' = alkyl or aryl). Due to extensive delocalisation of π electrons throughout the system, aryl azo compounds are highly coloured and are widely used as dyes; it is estimated that around 60–70% of all dyes used in the food and textile industries contain an azo linkage.[5] In addition to their intense colours, azo compounds show interesting photochemical behaviour, undergoing reversible *cis-trans* isomerisation about the N=N bond upon irradiation.[6] The differing geometries and spectral properties of the two isomers means these systems find application as molecular photoswitches[7] and in optical data storage.[8]

Compounds such as 2-(phenylazo)pyridine (azpy) are able to act as chelating ligands for metals, coordinating *via* the pyridyl and aza nitrogens. These ligands are of interest due to their excellent π-accepting ability; by receiving electron density into the azo π* orbital, they are able to stabilise metals in low oxidation states.[9] This is demonstrated by remarkably air-stable azo complexes of Mo^0, Cr^0 and W^0,[10] and the greater stability of Ru^{II} azo complexes compared with those of bipyridine.[11] Several ruthenium complexes containing such ligands have been reported previously, and our group has recently investigated the anticancer activity of Ru^{II} arene azopyridine complexes with chlorido and iodido ligands. The chlorido complexes show hydrolysis of Ru–Cl and Ru–arene bonds to varying extents, and their cytotoxicity may result from interactions with DNA.[12] The iodido complexes, however, are inert to hydrolysis and their cytotoxicity is thought to arise from an increase in reactive oxygen species (ROS); intriguingly, these complexes are also able to catalytically oxidise glutathione.[13] In addition, a Au^{III} complex of azpy has recently been reported,[14] which exhibits cytotoxic activity as well as an interesting metal-mediated reaction giving rise to an organic cation.

In contrast to other transition metals, platinum complexes of azo dyes are relatively scarce. Cyclometallated azobenzene complexes of Pt^{II} and Pt^{IV} containing catecholato ligands have been reported as liquid crystalline materials,[15] and the photochemistry of an azobenzene-conjugated Pt^{II}–terpyridine

complex has been investigated.[16] However, despite reports of Pd^{II} analogues as early as 1983,[17] Pt^{II} complexes of chelating azopyridine ligands remained unexplored until 2001, and only two such studies have been reported to date. These have focused upon the spectra and electrochemistry of catecholato complexes,[18] and aromatic ring amination reactions on the ligand as well as oxidative halogen addition to yield Pt^{IV} complexes.[19] However, despite the rich photochemistry of both azopyridine ligands and complexes such as $[Pt(bipy)_2]Cl_2$, photochemical studies of Pt^{II} azopyridine complexes are apparently absent in literature.

In this Chapter, the synthesis, characterisation and photochemistry of a series of Pt^{II} chlorido and azido complexes containing phenylazopyridine ligands are described. The structures of the complexes prepared are shown below.

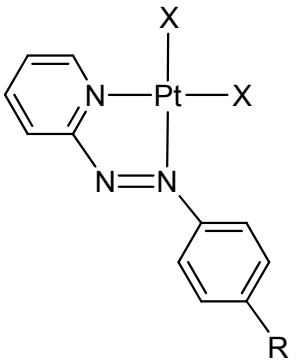

R = H (azpy)
NMe$_2$ (azpyNMe$_2$)
OH (azpyOH).
X = Cl, N_3

Complex	Azo Ligand	X
22	azpy	Cl
23	azpy	N_3
24	azpyNMe$_2$	Cl
25	azpyNMe$_2$	N_3
26	azpyOH	Cl
27	azpyO$^-$	N_3

Figure 5.1 Pt^{II} chlorido and azido complexes studied in this Chapter.

5.2 Experimental

5.2.1 Materials

2-(Phenylazo)pyridine (azpy) and 4-(2-pyridylazo)phenol (azpyOH) were kindly donated by Dr Sarah Dougan, and were synthesised as previously described.[12] The former was purified by column chromatography prior to use (silica gel, eluting with 100% dichloromethane), whilst the latter was used as received. 4-(2-pyridylazo)-*N,N*-dimethylaniline (azpyNMe$_2$) was purchased from Sigma-Aldrich, and *cis*-[Pt(DMSO)$_2$Cl$_2$] was synthesised as described in Chapter 3. UV grade dioxane (Sigma-Aldrich) and HPLC grade methanol and water (Fisher) were used as solvents for UV-visible spectroscopy. All other reagents were obtained from commercial sources, and used as received.

5.2.2 Synthesis

[Pt(azpy)Cl$_2$] (22)

2-(Phenylazo)pyridine (75 mg, 0.41 mmol) was dissolved in dichloromethane (5 mL) and added to a solution of *cis*-[Pt(DMSO)$_2$Cl$_2$] (174 mg, 0.41 mmol) in dichloromethane (30 mL). After five minutes the orange solution began to darken; it was then stirred at room temperature for 4 h. The solvent volume was reduced and the mixture stored overnight at 277 K. A brick-red solid was filtered off, washed with dichloromethane, and dried under vacuum.

Yield: 165 mg (90%).
Elemental analysis: Found: C, 29.36; H, 1.86; N, 9.12. $PtC_{11}H_9N_3Cl_2$ requires: C, 29.41; H, 2.02; N, 9.35%.
^{1}H NMR (500 MHz, $CDCl_3$): δ = 9.89 (d, $^3J(^{195}Pt\text{-}^1H)$ 30 Hz, 1H), 8.56 (d, 1H), 8.39 (td, 1H), 7.99 (m, 3H), 7.61 (t, 1H), 7.55 ppm (t, 2H).
ESI-MS: 471.97 $[M + Na]^+$, $NaPtC_{11}H_9N_3Cl_2$ requires 471.97 *m/z*.

[Pt(azpy)(N_3)$_2$] (23)

[Pt(azpy)Cl_2] (75 mg, 0.17 mmol) was dissolved in dimethylformamide (10 mL), and sonicated to ensure dissolution. To this, a solution of NaN_3 (109 mg, 1.7 mmol) in methanol (6.5 mL) was added, upon which there was an immediate colour change from orange to deep pink. The solution was stirred in the dark at room temperature for 48 h, after which all solvent was removed by rotary evaporation. Water (5 mL) was added to dissolve any excess NaN_3, and the insoluble black product was filtered off, washed with small quantities of water, ethanol and diethyl ether, and dried under vacuum.

Yield: 66 mg (85%).
Elemental analysis: Found: C, 28.01; H, 1.82; N, 26.50. $PtC_{11}H_9N_9$ requires: C, 28.58; H, 1.96; N, 27.27%.
^{1}H NMR (500 MHz, $CDCl_3$): δ = 9.21 (d, $^3J(^{195}Pt\text{-}^1H)$ 27 Hz, 1H), 8.48 (d, 1H), 8.34 (td, 1H), 8.05 (d, 2H), 7.94 (t, 1H), 7.65 (t, 1H), 7.58 ppm (t, 2H).
ESI-MS: 485.05 $[M + Na]^+$, $NaPtC_{11}H_9N_9$ requires 485.05 *m/z*.

[Pt(azpyNMe$_2$)Cl_2] (24)

4-(2-Pyridylazo)-*N,N*-dimethylaniline (100 mg, 0.44 mmol) was dissolved in dichloromethane (20 mL), and added to a solution of *cis*-[Pt(DMSO)$_2Cl_2$] (185 mg, 0.44 mmol) in dichloromethane (55 mL). Upon mixing, a colour change from orange to blue was observed; the solution was then stirred at room temperature for 4 h. The solvent volume was reduced and the mixture stored overnight at 277 K. A shiny, green-gold solid was filtered off, washed with dichloromethane, and dried under vacuum.

Yield: 195 mg (90%).
Elemental analysis: Found: C, 31.62; H, 2.79; N, 11.28. $PtC_{13}H_{14}N_4Cl_2$ requires: C, 31.72; H, 2.87; N, 11.38%.
^{1}H NMR (500 MHz, $CDCl_3$): δ = 9.62 (d, $^3J(^{195}Pt\text{-}^1H)$ 30 Hz, 1H), 8.39 (d, 2H),

8.15 (td, 1H), 8.08 (d, 1H), 7.57 (t, 1H), 6.74 (t, 2H), 3.22 ppm (s, 6H).
ESI-MS: 498.09 $[M - Cl + MeCN]^+$, $PtC_{15}H_{17}N_5Cl$ requires 497.90 *m\z*.

$[Pt(azpyNMe_2)(N_3)_2]$ (25)

$[Pt(azpyNMe_2)Cl_2]$ (25 mg, 0.05 mmol) was dissolved in dimethylformamide (5 mL) to give a blue solution. NaN_3 (33 mg, 0.51 mmol) in methanol (2 mL) was added; no colour change was observed. The solution was stirred in the dark at room temperature for 48 h, then water (100 mL) was added and the solution lyophilised. To the residue, water (5 mL) was added to dissolve any excess NaN_3, and the insoluble green solid was filtered off, washed with small quantities of water, ethanol and diethyl ether, and dried under vacuum.

Yield: 19 mg (75%).
Elemental analysis: Found: C, 30.79; H, 2.74; N, 27.42. $PtC_{13}H_{14}N_{10}$ requires: C, 30.89; H, 2.79; N, 27.71%.
^1H NMR (500 MHz, $CDCl_3$): δ = 9.01 (d, $^3J(^{195}Pt\text{-}^1H)$ 32 Hz, 1H), 8.47 (d, 2H), 8.12 (t, 1H), 8.02 (d, 1H), 7.54 (t, 1H), 6.78 (t, 2H), 3.24 ppm (s, 6H).
ESI-MS: 528.09 $[M + Na]^+$, $NaPtC_{13}H_{14}N_{10}$ requires 528.09 *m/z*.

$[Pt(azpyOH)Cl_2]$ (26)

4-(2-Pyridylazo)phenol (56 mg, 0.28 mmol) was dissolved in methanol (50 mL) and added to a solution of *cis*-$[Pt(DMSO)_2Cl_2]$ (100 mg, 0.24 mmol) in methanol (100 mL). The mixture was sonicated for five minutes to aid dissolution of the starting materials, during which time it began to darken from orange to a deep red-brown colour. It was then stirred overnight at room temperature. The volume was reduced and the mixture stored at 277 K for 4 h. A shiny brown solid was filtered off, washed with methanol and collected in a glass vial. To ensure total removal of *cis*-$[Pt(DMSO)_2Cl_2]$, dichloromethane (8 mL) was added and the mixture stirred, sonicated for 10 sec, then filtered off and collected again.

Yield: 79 mg (68%).

Elemental analysis: Found: C, 27.81; H, 2.15; N, 8.82. $PtC_{11}H_9N_3Cl_2O$ requires: C, 28.40; H, 1.95; N, 9.03%.

^{1}H NMR (400 MHz, MeOD): δ = 9.60 (d, $^3J(^{195}Pt\text{-}^1H)$ 32 Hz, 1H), 8.59 (d, 1H), 8.48 (td, 1H), 8.03 (d, 2H), 8.00 (t, 1H), 6.91 ppm (t, 2H).

ESI-MS: 487.96 [M + Na], $NaPtC_{11}H_9N_3Cl_2O$ requires 486.97 *m/z*.

Na[Pt(azpyO)(N_3)$_2$] (27)

[Pt(azpyOH)Cl_2] (25 mg, 0.05 mmol) was dissolved in dimethylformamide (5 mL) to give a dark orange solution. NaN_3 (35 mg, 0.54 mmol) in methanol (2 mL) was added; there was an immediate colour change to deep blue. The solution was stirred in the dark at room temperature for 48 h, then water (100 mL) was added and the solution lyophilised. To the residue, water (5 mL) was added to dissolve any excess NaN_3; the product was also partially soluble, however a quantity of black product was isolated and washed with small quantities of water, ethanol and diethyl ether, and dried under vacuum.

Yield: 18 mg (65%).

Elemental analysis: Found: C, 26.61; H, 1.79; N, 23.95. $PtC_{11}H_8N_9ONa$ requires: C, 26.41; H, 1.61; N, 25.20%.

^{1}H NMR (500 MHz, $CDCl_3$): δ = 8.63 (d, $^3J(^{195}Pt\text{-}^1H)$ 32 Hz, 1H), 8.46 (d, 2H), 8.05 (t, 1H), 7.76 (d, 1H), 7.30 (t, 1H), 6.49 ppm (d, 2H).

ESI-MS: 501.04 [M + H], $NaPtC_{11}H_9N_9O$ requires 501.04 *m/z*.

5.2.3 Methods

5.2.3.1 X-ray Crystallography

The crystal structure of **22** was solved by Dr Guy Clarkson at the University of Warwick. Data were collected and refined as described in Chapter 2.

5.2.3.2 Computational Methods

TD-DFT calculations on the azopyridine ligands and platinum complexes were carried out with the help of Dr Luca Salassa at the University of Warwick. Gaussian 03[20] was employed for all the calculations. Geometry optimisation calculations of the ground state were performed in the gas phase with the gradient-corrected correlation functional PBE1PBE.[21] The LanL2DZ basis set[22] and effective core potential were used for the Pt atom and the 6–31G** basis set[23] was used for all other atoms, respectively. Ligands were optimised at the PBE1PBE/6–31G** level. The nature of all stationary points was confirmed by performing a normal-mode analysis.

Sixteen singlet excited states for the ligands and thirty-two for the complexes were calculated with time-dependent density functional theory (TD-DFT)[24,25] employing ground-state geometries optimised in the gas phase.

The conductor-like polarisable continuum model method (CPCM)[26] with methanol as solvent was used to calculate all the electronic structure and excited states in solution. The electronic distribution and the localisation of the singlet excited states were visualised using the electron density difference maps (EDDMs).[27] GaussSum 1.05[28] was used for EDDMs calculations and for the electronic spectrum simulation.

5.2.3.3 Kinetic Studies of Azopyridine Ligands and Pt^{II} Complexes by UV-Visible Spectroscopy

The UV-visible absorption spectra of the ligands azpy, azpyNMe_2 and azpyOH, as well as the complexes **22**–**27**, were monitored over a 12 h period in dioxane at 298 K. Sample preparation, carried out under subdued laboratory light, involved dissolution of the compound in dioxane, filtration, appropriate dilution and, where necessary, addition of acid. To allow for this, a delay of five minutes was set between dissolution and recording the first spectrum. Spectra were subsequently recorded every 2 min for 1 h, every 5 min for a further 1 h, every 10 min for 3 h, then every 30 min for the remaining 7 h. In the case of azpyOH and [Pt(azpyOH)Cl_2] (**26**), 10 µL (~3 eq) of 0.01 M HNO_3 was added to ensure the phenolic group remained protonated. For Na[Pt(azpyO)$(N_3)_2$] (**27**), the study was carried out in methanol due to the insolubility of the complex in dioxane.

5.2.3.4 Stability of Complex 27 in Aqueous Solution and Cell Culture Medium

The stability of Na[Pt(azpyO)$(N_3)_2$] (**27**) in aqueous solution was monitored at 310 K over a 12 h period by UV-visible spectroscopy. Following dissolution of **27**, spectra were recorded every 2 min for 1 h, every 5 min for a further 1 h, every 10 min for 3 h, then every 15 min for the remaining 7 h.

The stability of this complex was also assessed under solution conditions similar to those employed in cytotoxicity testing. Following dissolution of the complex in DMSO, appropriate dilutions were performed so that the final solution comprised 1% DMSO, 12.5% saline (0.9% solution) and 86.5% RPMI-1640 medium. Since the medium is pink in colour, a solution of the same composition but without complex was used as a baseline for the UV-visible absorption spectra, so that any absorbance observed was solely from the complex.

5.2.3.5 Stability of Pt^{II} Complexes in Acetone

The stability of complexes **22**–**27** was monitored over time by ^{1}H NMR spectroscopy. Saturated solutions of the complexes were prepared in acetone-d_6 and a spectrum recorded immediately following dissolution (~5 min); spectra were then re-recorded after 1, 3, 6, 18 and 113 d. Samples were stored at ambient temperature in the dark between measurements.

5.2.3.6 Cytotoxicity Testing

Experiments to determine the cytotoxicity of **27** towards human ovarian A2780 cancer cell lines were performed by Dr Ana Pizarro at the University of Warwick, according to the procedure outlined in Chapter 2.

5.2.3.7 Photoreactions

Photoreactions of complexes **22**–**26** in dioxane, and complex **27** in methanol, were monitored by UV-visible spectroscopy. For all complexes, irradiations were performed using a LZC-ICH2 photoreactor equipped with LZC-UVA lamps (λ_{max} = 365 nm, P = 1.7–2.2 mW cm^{-2}) and LZC-VIS UV-Visible light lamps (λ = 400–700 nm, P = 0.27–0.29 mW cm^{-2}). For complexes **22** and **23**, irradiations in the visible region were also carried out using four green LEDs (λ_{max} = 525 nm, P = 0.19 mW cm^{-2}). For complex **24**, non-irradiated controls were included, as the spectral profile of this complex changed over time in the dark. These controls were placed in the photoreactor but covered in tinfoil to avoid exposure to light. Further details and the spectral outputs of all light sources can be found in Chapter 2.

All irradiations were carried out at 298 K unless otherwise stated, with spectra recorded after the following total irradiation times: 30 s, 1, 2, 3, 5, 10, 15, 20, 30, 45, 60, 90 and 120 min.

5.2.3.8 Phototoxicity Testing

The phototoxicity of complex **27** towards the HaCaT keratinocyte human skin cell line was determined by Dr Julie Woods and Kim Robinson at the Photobiology Unit in Ninewells Hospital, Dundee, as described in Chapter 2.

5.2.3.9 Fluorescence Spectroscopy

Fluorescence spectra of the ligands azpy, azpyNMe$_2$ and azpyOH, and of complexes **22**–**27**, were obtained at 298 K in dioxane. The excitation wavelength (λ_{ex}) was set to the λ_{max} for each absorption band of the compound.

5.3 Results

Pt^{II} chlorido and azido complexes of three azopyridine ligands azpy, azpyNMe$_2$ and azpyOH were prepared and characterised. The UV-visible absorption spectra of the ligands and complexes were calculated using TD-DFT methods, allowing the nature of the transitions to be determined. The photochemical behaviour of the complexes upon irradiation with UVA and broadband visible light was examined, and attempts were made to rationalise the observed changes in the absorption spectra with regard to the transitions involved. In addition, the cytotoxicity of the water-soluble complex (**27**) towards A2780 human ovarian cancer cells, and its phototoxicity towards HaCaT keratinocytes has been investigated.

5.3.1 Synthesis of Platinum Complexes of Azopyridine Ligands

5.3.1.1 Synthesis of Pt^{II} Chlorido Complexes

The Pt^{II} chlorido complexes were obtained by addition of the appropriate azopyridine ligand to a solution of *cis*-$[Pt(DMSO)_2Cl_2]$, according to the scheme shown.

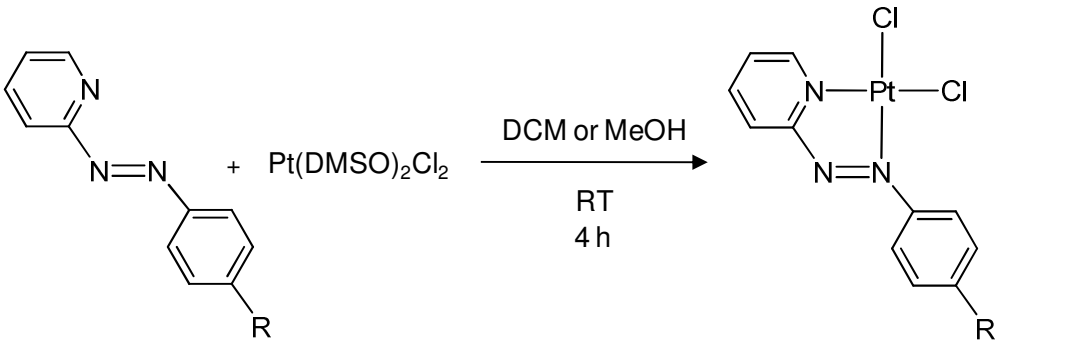

Scheme 5.1 The synthesis of Pt^{II} chlorido complexes with azopyridine ligands

$[Pt(azpy)Cl_2]$ (**22**) and $[Pt(azpyNMe_2)Cl_2]$ (**24**) were produced by this method, analytically pure in yields of 90%. In the case of $[Pt(azpyOH)Cl_2]$ (**26**), methanol was chosen as the solvent due to the low solubility of azpyOH in dichloromethane. However, *cis*-$[Pt(DMSO)_2Cl_2]$ is poorly soluble in methanol and was commonly observed in the ^1H NMR spectrum of the product. Purification by column chromatography was unsuccessful; excess starting material was therefore eliminated by briefly sonicating the obtained product in a small volume of dichloromethane and isolating once more.

Attempts were made to prepare the Pt^{II} chlorido complex of another azopyridine ligand, 4-(2-pyridylazo)resorcinol; this ligand is similar to azpyOH, but contains an additional OH group on one ortho position of the phenyl ring. The synthesis

was carried out as for **26**; however, despite ^{1}H NMR evidence of a pure Pt^{II} product, elemental and mass spectral analyses were inconclusive and this product was not identified.

5.3.1.2 Synthesis of Pt^{II} Azido Complexes

The Pt^{II} azido complexes were prepared by direct substitution of the chlorido ligands with an excess of sodium azide in DMF, according to Scheme 5.2.

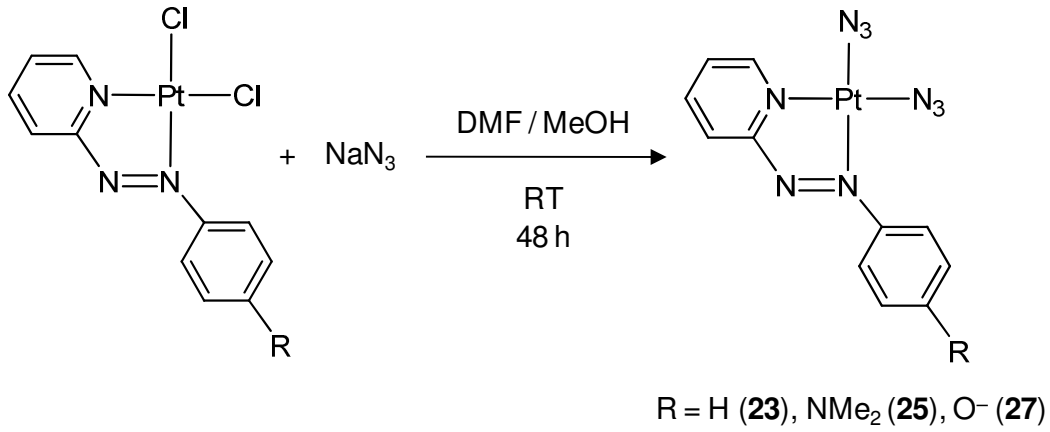

Scheme 5.2 The synthesis of Pt^{II} azido complexes of azopyridine ligands

$[Pt(azpy)(N_3)_2]$ (**23**) and $[Pt(azpyNMe_2)(N_3)_2]$ (**25**) were synthesised by the above method in yields of around 80%. Complex **27** was isolated as a salt with the ligand in its deprotonated form, $Na[Pt(azpyO)(N_3)_2]$. In an attempt to isolate the protonated product, the complex was dissolved in water and acidified, causing a colour change from deep blue to brown. However, although a small amount of product was recovered, it was found to be impure and all further studies were carried out on the deprotonated complex $Na[Pt(azpyO)(N_3)_2]$ (**27**).

5.3.1.3 Investigating the Oxidation of Pt^{II} Complexes

Efforts to oxidise [Pt(azpy)$(N_3)_2$] (**23**) under a variety of conditions were unsuccessful. The use of aqueous solutions of hydrogen peroxide returned unreacted starting material. Two methods previously employed for the oxidation of Pt^{II} complexes of cyclometallated azobenzenes were also attempted. However, reaction with I_2 in acetone[15] yielded a mixture of products as seen by NMR spectroscopy, and the organic oxidising agent *meta*-chloroperoxybenzoic acid (mCPBA)[29] was found to decolourise the deep pink solution to pale brown, suggesting decomposition of the azo chromophore.

5.3.2 X-ray Crystallography

The structure of [Pt(azpy)Cl_2] (**22**) was determined by single crystal X-ray diffraction, and corresponds well with that previously reported in the literature.[18] The complex crystallised as orange plates, in the monoclinic system and of space group C2/c. The asymmetric unit contains three crystallographically independent Pt^{II} complexes, differing in the angle of the pendent phenyl group and the distance of the chlorido groups from the plane of the platinum and the chelating azo ligand. Close contacts between the chlorines and the pyridine hydrogens of a neighbouring complex lead to the formation of infinite ribbons (seen for each independent complex). Two such ribbons are associated *via* close Pt-Pt contacts of 3.6 Å. No significant π-π stacking is seen.

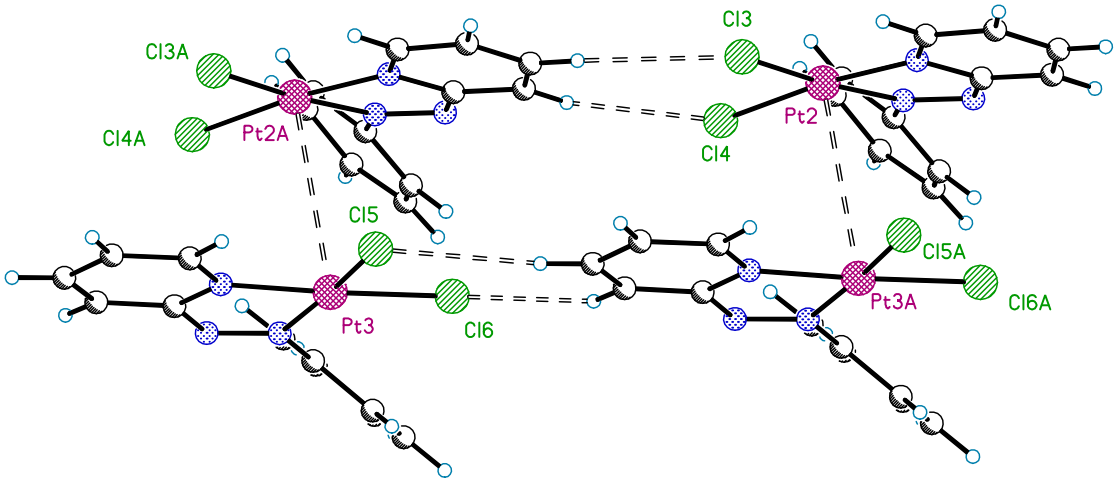

Figure 5.2 A section of the ribbons formed by each crystallographically independent complex of [Pt(azpy)Cl_2] (**22**), and the interaction of these ribbons via close Pt-Pt contacts (picture courtesy of Dr Guy Clarkson).

5.3.3 Computed Geometries

According to DFT calculations, similar structural features are observed for all three azopyridine ligands. All display planar geometry and have comparable N=N distances of around 1.25 Å.

Upon coordination to platinum, the phenyl ring of the ligand is twisted out of the Pt–py–azo plane, by between 29˚ and 39˚ in complexes **22**–**26**. In complex **27**, however, this twist is reduced to 3˚ and the ligand remains essentially planar.

Selected calculated bond lengths for complexes **22**–**27** are tabulated below; in the case of **22**, the values are compared with those obtained from the crystal structure, and show good agreement. In all Pt^{II} chlorido complexes (**22**, **24** and **26**), the N=N bond lengthens to a similar extent (1.28–1.29 Å) upon coordination. Pt–Cl bonds are of a similar length (~2.32 Å) in all complexes, with the two bonds within each

complex also comparable despite differing ligands in the *trans* position (one pyridyl and one aza nitrogen).

In the azido complexes, Pt–N_3 distances are shorter in all cases than the corresponding Pt–Cl, with a concomitant increase in the Pt–N(py) and Pt–N(aza) bond lengths. The N=N distances are similar to those in the chlorido complexes, with the exception of complex **27** in which this bond is significantly lengthened.

Table 5.1 Selected bond distances (Å) of complexes **22**–**27** in calculated ground state geometries, and comparison with the X-ray crystal structure of **22**.

Pt^{II} Chlorido Complex	N=N	Pt–N(py)	Pt–N(aza)	Pt–Cl (trans-py)	Pt–Cl (trans-aza)
[Pt(azpy)Cl_2] (**22**) Calculated	1.275	2.016	2.003	2.316	2.318
[Pt(azpy)Cl_2] (**22**) X-ray	1.291(9)	2.018(8)	1.965(8)	2.281(2)	2.288(3)
[Pt(azpyNMe_2)Cl_2] (**24**)	1.286	2.012	2.019	2.326	2.324
[Pt(azpyOH)Cl_2] (**26**)	1.282	2.013	2.002	2.325	2.325
Pt^{II} Azido Complex	N=N	Pt–N(py)	Pt–N(aza)	Pt–N_3 (trans-py)	Pt–N_3 (trans-aza)
[Pt(azpy)(N_3)$_2$] (**23**)	1.280	2.021	2.019	2.002	1.989
[Pt(azpyNMe_2)(N_3)$_2$] (**25**)	1.289	2.017	2.049	2.012	1.995
Na[Pt(azpyO^-)(N_3)$_2$] (**27**)	1.327	2.013	2.080	2.039	2.018

5.3.4 Orbital Analysis

5.3.4.1 Azopyridine Ligands

The HOMO of azpy has n character, localised on the nitrogen lone pair, whereas HOMO–1 is a π* orbital delocalised over the whole molecule. This order is reversed for azpyNMe$_2$ and azpyOH – they both possess π* HOMOs, residing in part upon the NMe$_2$ and OH groups, while for both HOMO–1 displays n symmetry.

The LUMO of all three ligands is π* in character and delocalised over the whole molecule, with little involvement from the NMe$_2$ and OH groups. LUMO+1 is located mainly on the pyridyl ring in each case. The HOMO–LUMO energy gaps are 4.33, 3.43 and 4.00 eV for azpy, azpyNMe$_2$ and azpyOH, respectively.

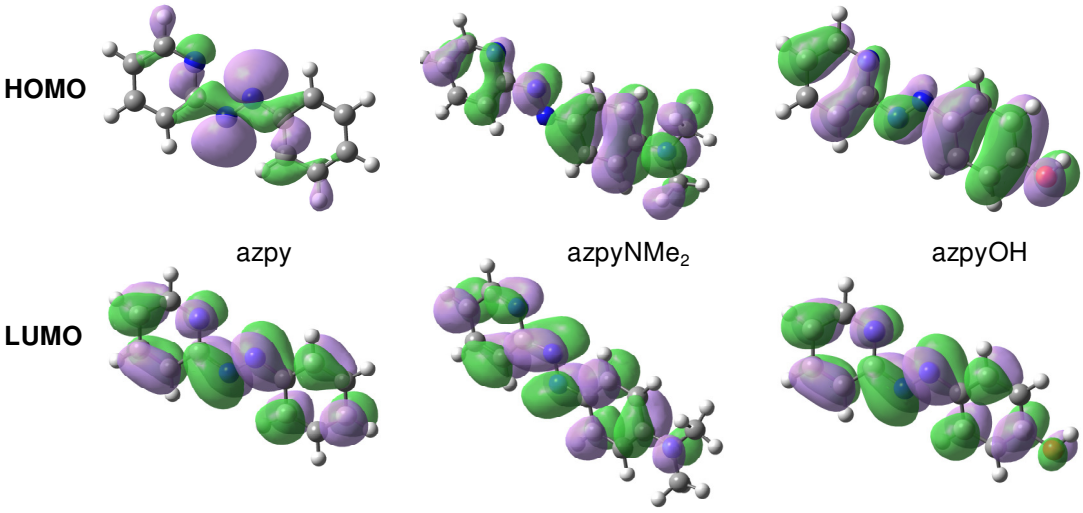

Figure 5.3 HOMO and LUMO representations of azpy, azpyNMe$_2$ and azpyOH. Green indicates a positive phase, and lilac a negative phase.

5.3.4.2 Pt^{II} Complexes

The HOMO of **22** is a π* orbital delocalised over the whole molecule, with a significant part residing on the platinum and chlorido ligands; similarly HOMO–1 is also of π* symmetry but with a lesser involvement of the Pt–Cl region. In contrast, the π* HOMO of **23** is located almost entirely on the platinum and azido ligands. HOMO–1 is more delocalised, but still with very little based on the phenyl ring of azpy. The HOMOs of **24**–**27** are alike; π* in character and predominately based on the azo ligands, including the NMe_2 and OH groups. Each HOMO–1 of **24**–**27** is also similar, and located mainly on the platinum and chlorido/azido ligands.

The LUMOs of complexes **22**–**27** are similar; π* orbitals delocalised mainly over the azopyridine ligand and the metal, with little density based on the chlorido or azido ligands. With the exception of **23**, the LUMO+1 of all complexes show a similar σ* antibonding character towards the Pt–ligand bonds, with small but variable degrees of density on the azopyridine ligand, whilst LUMO+2 resides mainly upon the pyridyl ring. In complex **23**, however, the nature of these orbitals is reversed. The HOMO–LUMO energy gaps are 3.54, 2.80, 2.67, 2.69, 2.97 and 2.75 eV, for complexes **22**–**27**, respectively.

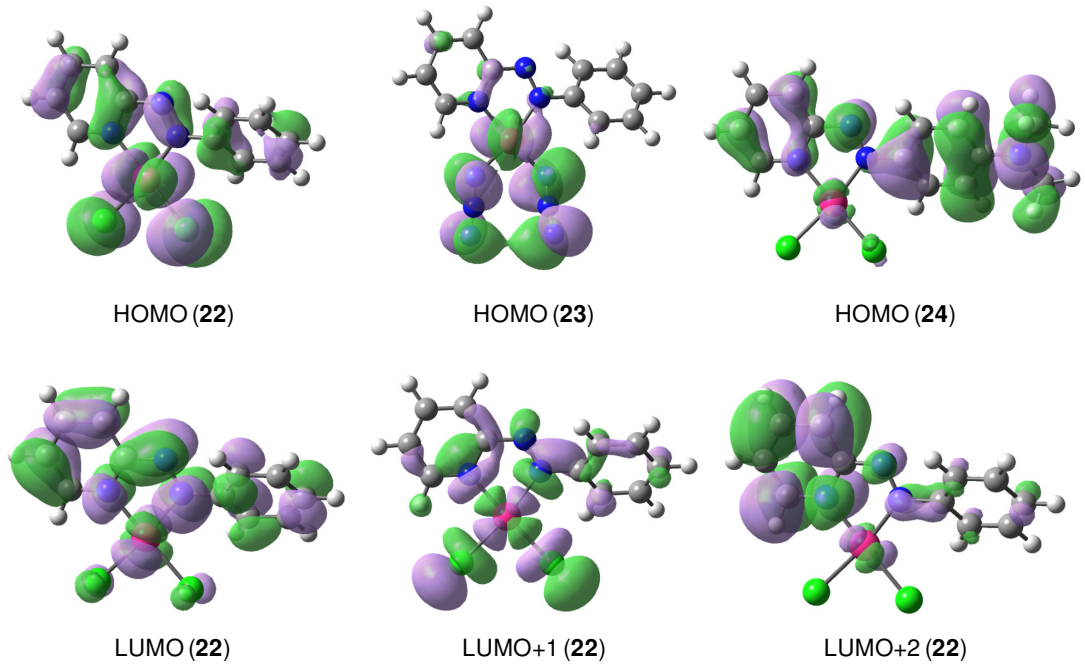

Figure 5.4 Selected orbitals of platinum complexes. Top: The HOMOs of **22**, **23** and **24**. Bottom: The lower unoccupied orbitals, similar for all complexes, are shown for **22**.

5.3.5 UV-Visible Absorption Spectra of Azopyridine Ligands

5.3.5.1 Absorption and Singlet Excited States of Azpy, $AzpyNMe_2$ and AzpyOH

UV-visible absorption spectra of the three azopyridine ligands were recorded in both methanol and dioxane, with the results listed in Table 5.2.

Table 5.2 Wavelength of maximum absorbances and extinction coefficients for azopyridine ligands in methanol and dioxane.

Compound	Methanol		Dioxane	
	λ_{max} (nm)	ε (M^{-1} cm^{-1})	λ_{max} (nm)	ε (M^{-1} cm^{-1})
Azpy	222	9000	222	11200
	317	14100	315	16400
	441	500	452	300
$AzpyNMe_2$	273	8700	258	9100
	432	29000	418	44300
AzpyOH[a]	247	8700	248	9300
	357	21600	355	22100

[a] Acidified with 3 eq HNO_3

Electronic absorption spectra of the three ligands in methanol were calculated using TD-DFT methods. Figure 5.5 shows these overlain with the experimental spectra, and includes the electron density difference maps (EDDMs) of the lowest energy singlet transition in each case. Table 5.3 lists the calculated singlet excited states for these ligands.

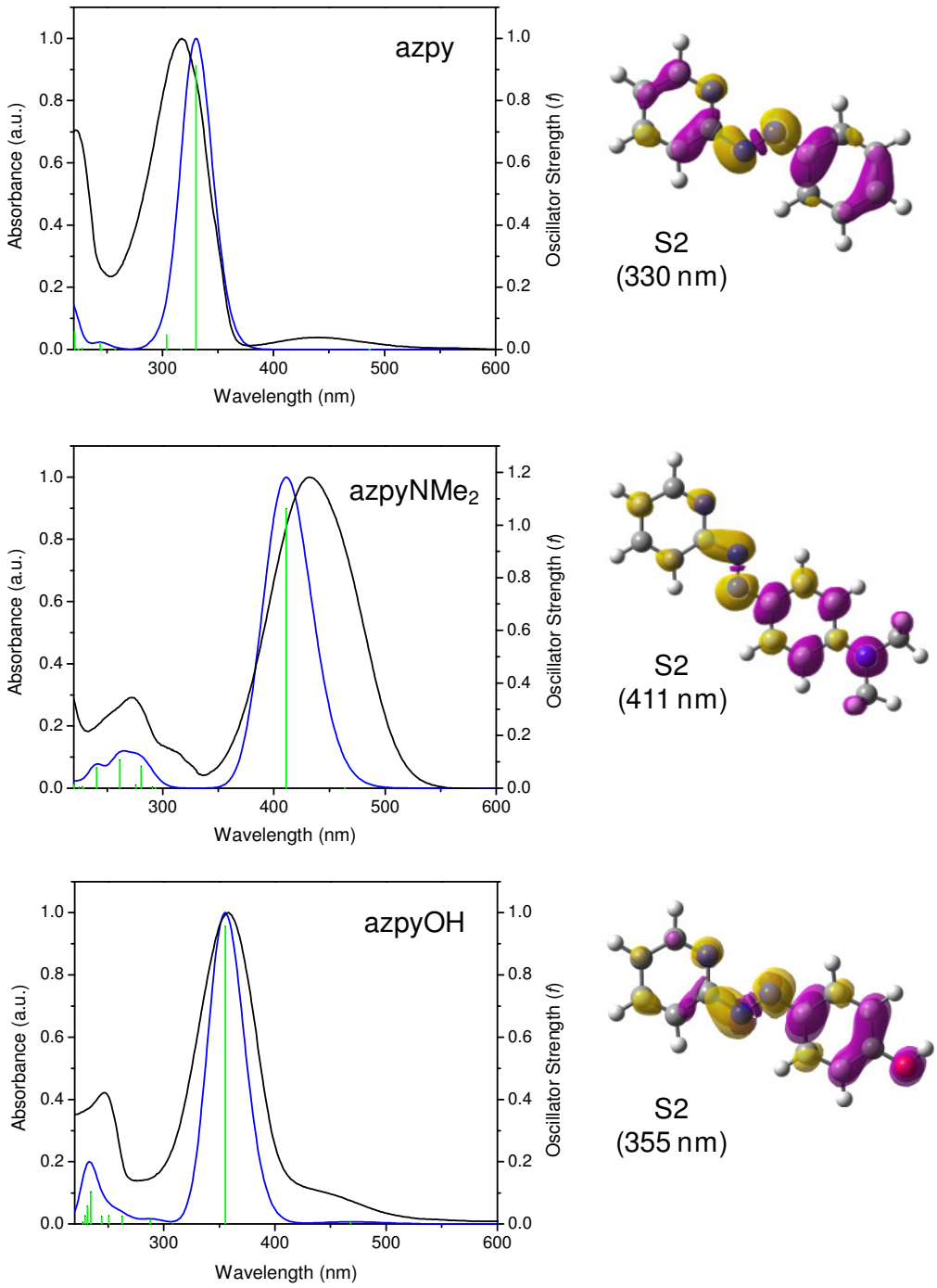

Figure 5.5 Normalised absorption spectra for azpy, azpyNMe$_2$ and azpyOH in methanol (black) and calculated spectra (blue). The excited states are shown as vertical bars. Inset: Electron density difference maps (EDDMs) of the lowest energy singlet electronic transition for each ligand. Electron density migrates from magenta to yellow areas.

Table 5.3 Calculated singlet excited states for azopyridine ligands in methanol. Tr = transition number, as obtained in the TD-DFT calculation output; *f* = oscillator strength.

	Tr	E^{calc}, eV (nm)	*f*	Major Contribution	Character
azpy	2	3.75 (330)	0.91	HOMO–1→LUMO (83%)	π–π*
	4	4.08 (304)	0.05	HOMO–2→LUMO (91%)	π–π*
	10	5.61 (220)	0.06	HOMO–1→LUMO+1 (66%)	π–π*
azpy	2	3.02 (411)	1.06	HOMO→LUMO (81%)	π–π*/CT
NMe_2	5	4.42 (281)	0.08	HOMO–2→LUMO (69%)	π–π*
	7	4.75 (261)	0.11	HOMO→LUMO+2 (72%)	π–π*
	9	5.16 (240)	0.08	HOMO–5→LUMO (76%)	π–π*
azpy	2	3.49 (355)	0.96	HOMO→LUMO (79%)	π–π*/CT
OH	8	5.29 (234)	0.10	HOMO→LUMO+2 (70%)	π–π*
	9	5.36 (231)	0.06	HOMO–5→LUMO (50%)	π–π*

The results of TD-DFT calculations were used to assign the absorption bands of the spectra; these confirm the previous assignment of these transitions based on experimental data. The main absorption band of azpy in methanol is centred at 317 nm, corresponding to a π–π* transition in which electron density migrates onto the aza nitrogens. A weak band is also seen at 441 nm in the experimental spectrum, resulting from a formally forbidden n-π* transition. AzpyNMe_2 displays a strong absorption band at 432 nm, arising from a mixed π–π*/CT state in which charge transfer from the NMe_2 group makes a strong contribution. This

results in the significant red shift of this band compared with the purely π–π* transition of azpy. A significant charge transfer contribution is also seen in the main transition of azpyOH, although to a lesser extent than in azpyNMe$_2$. Higher energy absorptions in both azpyNMe$_2$ and azpyOH can be ascribed to π–π* states.

Comparing the spectra of these ligands in dioxane and methanol, the transitions display solvatochromism as expected from their assigned character. Although dioxane is known to show anomalous solvatochromic effects,[30] in this case the expected trends are observed. π–π* bands are red-shifted upon changing to the more polar methanol, since attractive polarisation forces between the solvent and the absorbing molecule lower the energy of the excited state to a greater extent than the ground state, decreasing the energy between the two. In contrast the n–π* transition of azpy is blue-shifted in methanol; this is due to the increased solvation of the lone pair in a more polar solvent, decreasing the energy of the n orbital.[31]

5.3.5.2 Kinetic Studies of Azopyridine Ligands in Dioxane

The electronic absorption spectral profiles of the ligands azpy, azpyNMe$_2$ and azpyOH in dioxane were measured over a 12 hour period, as described in section 5.2.3.3.

The spectrum of azpy remained unchanged during the course of the experiment. However, the main absorption band of azpyNMe$_2$ (λ_{max} = 418 nm) showed an increase in intensity of approximately 7% over 12 hours, with no change in energy. Repetition of the experiment found that, although the trend was reproducible, the absolute values varied between 5 and 8%. This is displayed in Figure 5.6.

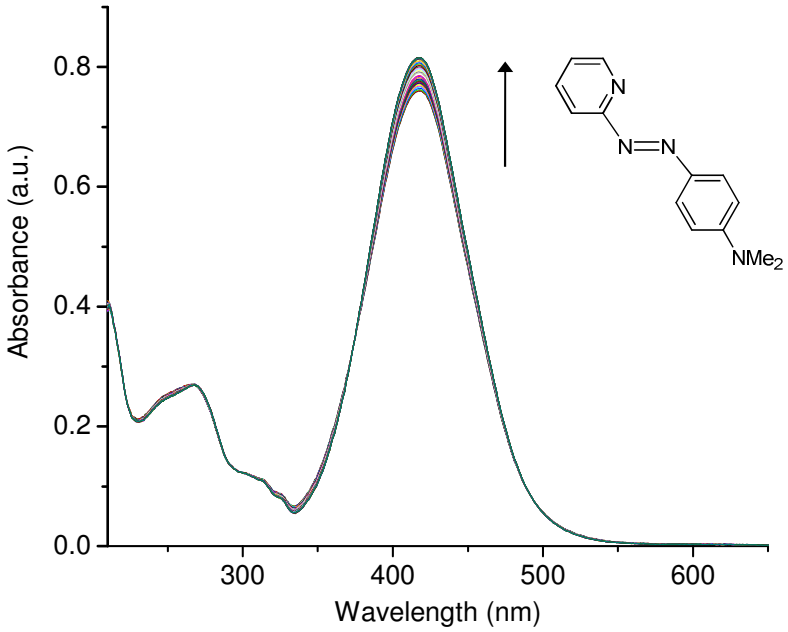

Figure 5.6 The spectrum of azpyNMe$_2$ in dioxane, showing an increase in intensity of the main absorption band over time.

Initial experiments showed that the spectrum of azpyOH also changed over time, with an absorbance band growing at 471 nm. However, further investigation suggested this change is related to the protonation state of the phenolic OH group. A subsequent experiment, in which ~3 mol eq HNO_3 were added to ensure the OH group remained protonated, showed no change in the spectral profile over 12 hours.

5.3.6 UV-Visible Absorption Spectra of Pt^{II} Complexes

5.3.6.1 Absorption and Singlet Excited States of Complexes 22-27

UV-visible absorption data for complexes **22**–**27**, in methanol and dioxane, are shown in Table 5.4.

Table 5.4 Wavelength of maximum absorbances and extinction coefficients for complexes **22–27** in methanol and dioxane.

Complex	Methanol		Dioxane	
	λ_{max} (nm)	ε (M^{-1} cm^{-1})	λ_{max} (nm)	ε (M^{-1} cm^{-1})
22	267	7500	222	11200
	381	13500	395	16400
	495	3200	452	3000
23	380	8700	391	9100
	529	3700	566	4300
24[a]	298	4400	301	7200
	602	16000	613	19600
			647	22000
25[a]	293	7700	298	9800
	614	24000	618	28600
26[b]	272	11000	273	12200
	475	17000	461	18900
			481	19800
27	270	7900	n/a	n/a
	340	4000		
	584	22900		
	619	25900		

[a] 95:5 methanol/dioxane:DMF. [b] Acidified with 3 eq HNO_3

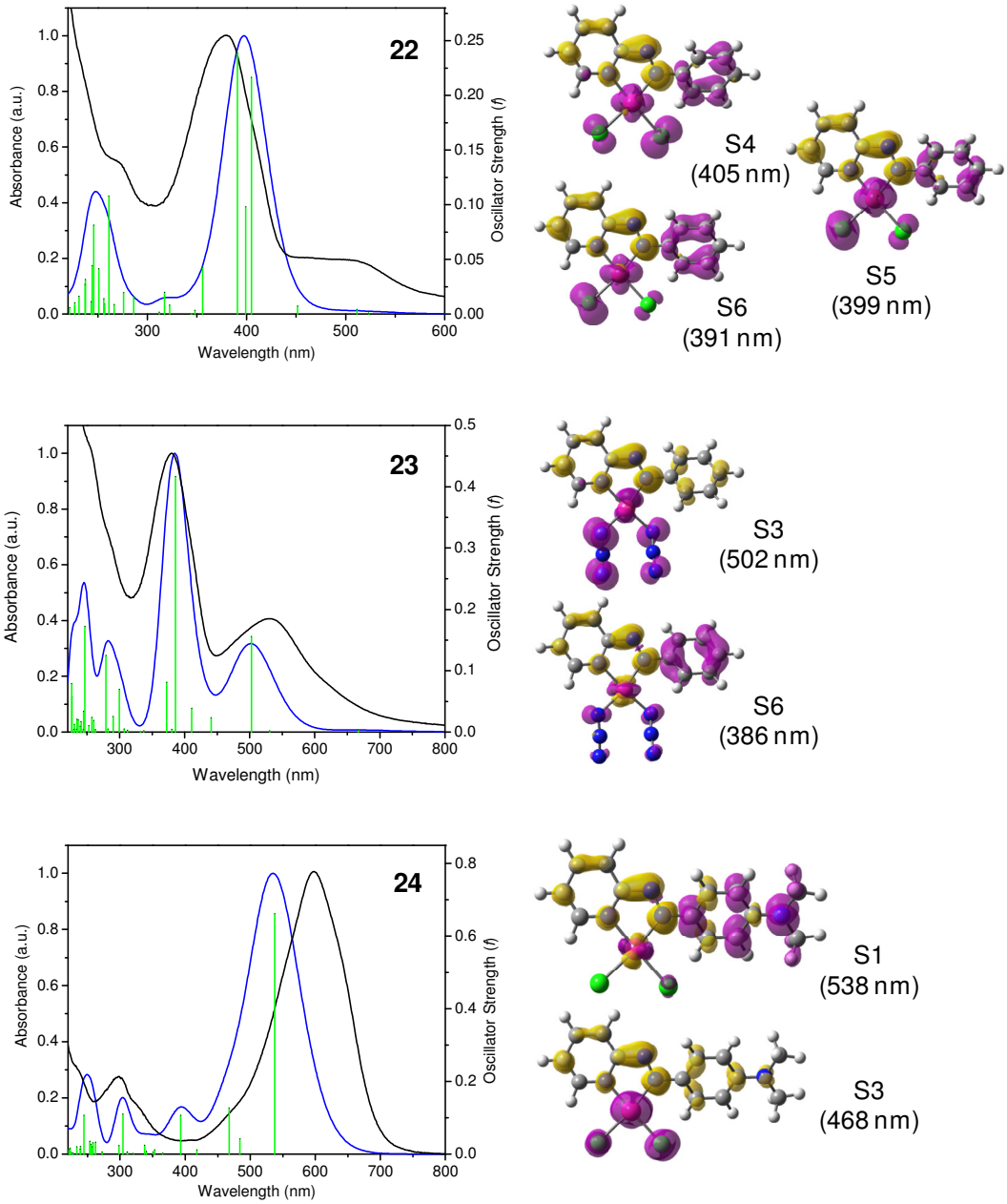

Figure 5.7 Normalised absorption spectra for complexes **22**–**24** in methanol (black) and calculated spectra (blue). Inset: Electron density difference maps (EDDMs) of the lowest energy singlet electronic transition for each complex.

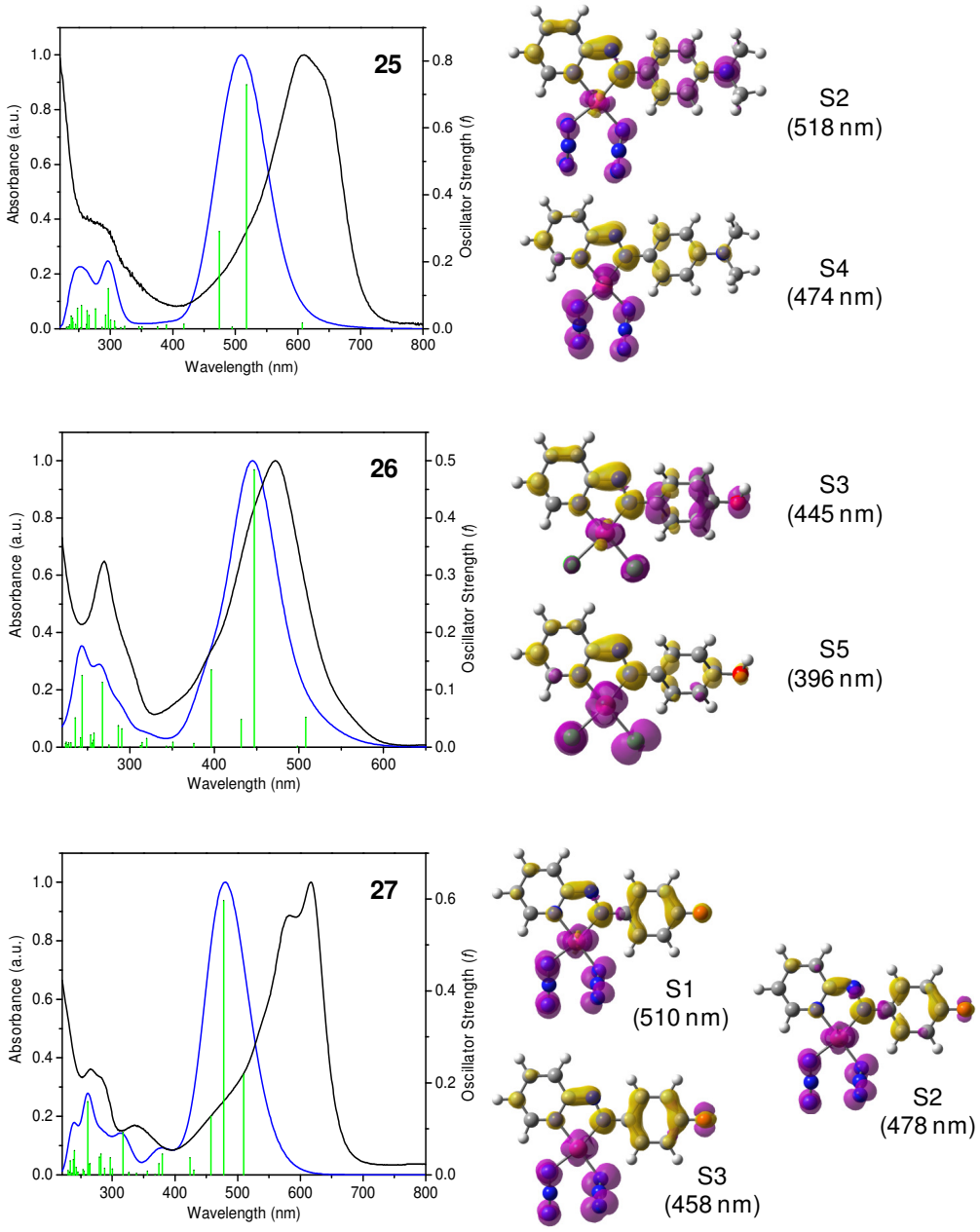

Figure 5.8 Normalised absorption spectra for complexes **25**–**27** in methanol (black) and calculated spectra (blue). Inset: Electron density difference maps (EDDMs) of the lowest energy singlet electronic transition for each complex.

Table 5.5 Calculated singlet excited states for complexes **22**-**27** in methanol.

	Tr	E^{calc}, eV (nm)	*f*	Major Contribution	Character
22	4	3.06 (405)	0.22	HOMO–1→LUMO (40%)	MLCT
	5	3.11 (399)	0.10	HOMO–4→LUMO (46%)	MLCT
	6	3.17 (391)	0.24	HOMO–5→LUMO (48%)	MLCT
	16	4.75 (261)	0.10	HOMO→LUMO+2 (64%)	MLCT
	20	5.05 (246)	0.08	HOMO–1→LUMO+2 (38%)	MLCT
23	3	2.47 (502)	0.16	HOMO–1→LUMO (84%)	MLCT
	6	3.21 (386)	0.42	HOMO–3→LUMO (51%)	LC
	8	3.33 (372)	0.08	HOMO→LUMO+2 (59%)	LC/MC
	13	4.14 (300)	0.07	HOMO→LUMO+1 (58%)	MLCT
	16	4.45 (279)	0.13	HOMO–1→LUMO+1 (38%)	MLCT
	21	5.03 (247)	0.17	HOMO–4→LUMO+2 (29%)	MC/MLCT
24	1	2.31 (538)	0.66	HOMO→LUMO (69%)	LC
	3	2.65 (468)	0.13	HOMO–1→LUMO (37%)	MLCT
	5	3.15 (393)	0.11	HOMO–3→LUMO (38%)	MLCT
	14	4.08 (304)	0.11	HOMO→LUMO+2 (82%)	LC
	23	5.07 (244)	0.11	HOMO–3→LUMO+2 (40%)	MLCT
25	2	2.39 (518)	0.73	HOMO→LUMO (54%)	MLCT/LC
	4	2.61 (474)	0.29	HOMO–2→LUMO (75%)	MLCT
	15	4.17 (297)	0.12	HOMO→LUMO+2 (53%)	MLCT/LC
	18	4.49 (276)	0.06	HOMO–2→LUMO+2 (80%)	MLCT
	20	4.71 (263)	0.05	HOMO→LUMO+3 (77%)	LC
	22	4.68 (254)	0.07	HOMO–1→LUMO+6 (21%)	MC
26	1	2.44 (508)	0.05	HOMO–1→LUMO (53%)	MLCT
	3	2.77 (445)	0.46	HOMO→LUMO (48%)	MLCT/LC
	4	2.87 (433)	0.06	HOMO–4→LUMO (68%)	MLCT
	5	3.13 (396)	0.13	HOMO–3→LUMO (71%)	MLCT
	16	4.64 (267)	0.11	HOMO→LUMO+2 (66%)	LC
	21	5.09 (244)	0.12	HOMO–3→LUMO+2 (61%)	MLCT
27	1	2.43 (510)	0.22	HOMO–1→LUMO (58%)	MLCT
	2	2.60 (478)	0.60	HOMO→LUMO (37%)	MLCT
	3	2.71 (458)	0.13	HOMO–2→LUMO (50%)	MLCT
	6	3.26 (380)	0.45	HOMO–5→LUMO (59%)	MLCT
	13	3.91 (317)	0.09	HOMO→LUMO+2 (79%)	LC
	17	4.40 (282)	0.05	HOMO–8→LUMO (36%)	MLCT
	21	4.76 (261)	0.16	HOMO→LUMO+3 (65%)	MC/LC

The results of TD-DFT calculations were used to assign the transitions observed in the spectra of complexes **22**–**27**. The spectrum of **22** consists of a main band centred at 381 nm, with a weaker band at lower energy. The three transitions comprising the main band all have mixed character, with electron density migrating to the azo group and pyridyl ring. The formally forbidden n–π* band at lower energy is more intense here than for azpy. Complex **23** shows a different spectral profile. The band centred at 380 nm results from a primarily ligand-centred (LC) transition with some contribution from the metal, whilst a lower energy band at 529 nm arises from a metal-to-ligand charge transfer (MLCT) transition with a very strong contribution from the azido ligands.

The main absorption band of **24** arises from an LC transition in which electron density migrates from the NMe_2 region to the aza nitrogens, with only a small involvement of the metal and chlorido ligands. A lesser contribution to this absorption band is made from a transition at slightly higher energy, MLCT in character with a strong involvement of the chlorido ligands. The spectrum of **25** is similar, with an asymmetric band centred at 614 nm, again comprised of two transitions. Although charge transfer (from the NMe_2 group to the azo nitrogens and pyridyl ring) dominates the main transition, the metal and azido groups also contribute. The second transition is MLCT in character, with a strong contribution from the azido groups.

The relatively broad absorption band in the spectrum of **26** results from two main transitions, with two others making a lesser contribution. The dominant transition is mixed in character, in which electron density migrates to the azo group and pyridyl ring; similar to that seen for complex **22** but here with contribution from the OH group also. The second transition is MLCT in character, with strong involvement of the chlorido groups. Complex **27** shows the poorest agreement between theoretical and experimental spectra, however the nature of the transitions involved can still be established. Three main transitions are found to comprise the absorption band. All are MLCT in character with strong

contributions from the azido ligands, with charge transfer from the oxygen involved to various extents.

5.3.6.2 Effects of pH on the Absorption Spectra of Complexes 26 and 24

Solutions of [Pt(azpyOH)Cl_2] (**26**) were found to readily change colour, from brown to deep blue, upon addition of certain reagents or solvents, during chromatography attempts and, at times, upon filtration. Further investigation revealed this to result from deprotonation of the OH substituent of the azopyridine ligand. As the protonated forms of the azpyOH complexes are poorly soluble in water, an accurate pH titration by NMR spectroscopy could not be performed; instead UV-visible absorption spectra were obtained at several pH values. Complex **26** was dissolved in a basic NaOH solution and the pH gradually decreased by addition of 0.01 M HNO_3. The coexistance of both protonated and deprotonated species at pH 5.21 and 6.24 indicates the pK_a lies between the two.

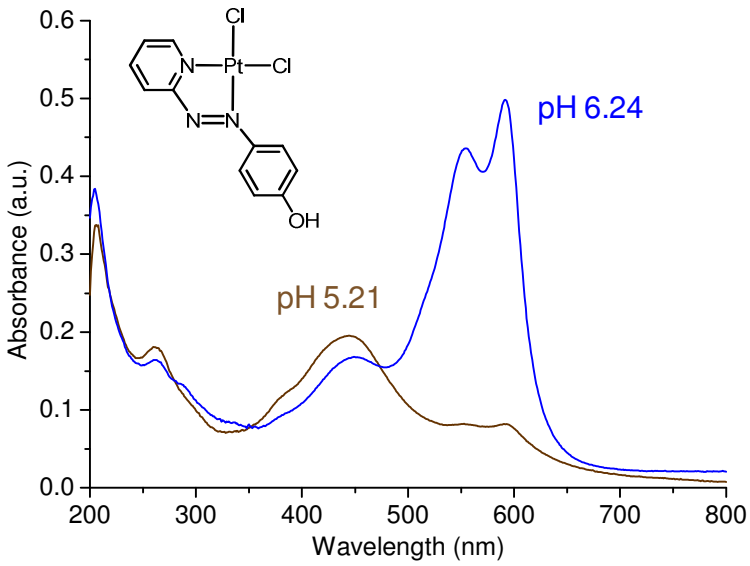

Figure 5.9 The absorption spectrum of [Pt(azpyOH)Cl_2] (**26**) at pH 5.21 and 6.24.

Protonation of the NMe_2 group of complex **24** was also investigated. Extremely acidic conditions (pH ~ 0) were required to effect protonation, which resulted in a colour change from deep blue to orange. The resulting spectral profile is similar to that of [Pt(azpy)Cl_2] (**22**), confirming the influence of charge transfer from the NMe_2 group on the absorption properties of **24**. The effect of coordination to platinum is also demonstrated, since the pK_a of azpyNMe_2 alone has been determined as 2.11.[32]

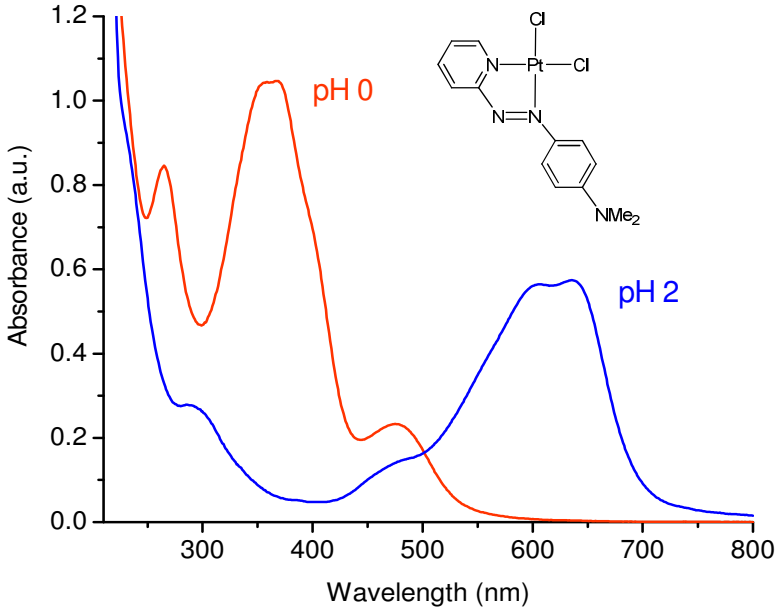

Figure 5.10 The dependence of the absorption spectrum of complex **24** on pH.

5.3.6.3 UV Kinetic Studies of Pt^{II} Complexes in Dioxane

The electronic absorption spectra of complexes **22**–**26** in dioxane, and **27** in methanol, were measured over a 12 hour period as described in section 5.2.3.3.

The spectra of [Pt(azpy)Cl_2] (**22**) and [Pt(azpy)$(N_3)_2$] (**23**) remained unchanged throughout the experiment. The two complexes of azpyNMe_2, however, showed

contrasting behaviour. The main absorption bands of [Pt(azpyNMe$_2$)Cl$_2$] (**24**), at 613 nm and 647 nm, showed a 6% decrease in intensity over time, whilst that of [Pt(azpyNMe$_2$)(N$_3$)$_2$] (**25**) (618 nm) increased in intensity by 7%, consistent with the behaviour of the ligand alone (section 5.3.5.2). This is illustrated in Figure 5.11.

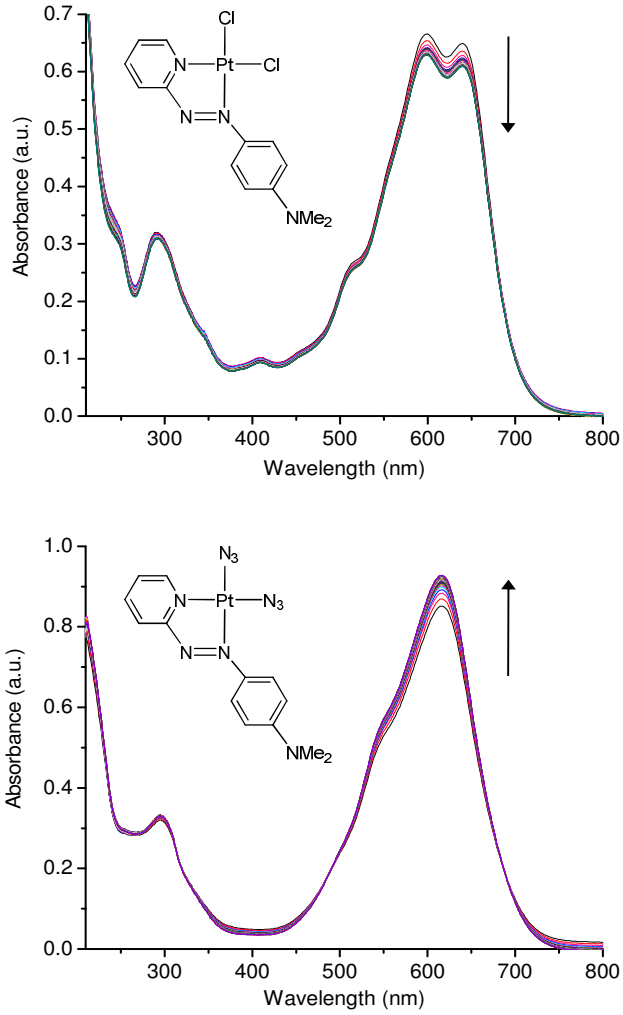

Figure 5.11 The change in UV-Visible absorption spectra of complexes **24** and **25** over a 12 h period.

Initial experiments showed that the spectrum of [Pt(azpyOH)Cl_2] (**26**) also changed over time; however, as in the case of azpyOH alone, further investigation suggested this was due to the protonation state of the phenolic OH group, the pK_a of which is decreased upon coordination to platinum (section 5.3.6.2). Repetition of the experiment, with the addition of 3 mol eq HNO_3 to ensure the phenolic OH group remained protonated, showed no change to the spectral profile over 12 hours. Na[Pt(azpyO)$(N_3)_2$] (**27**), in methanol, showed a 5% decrease in intensity of the absorption band at 619 nm, whilst that at 584 nm remained essentially unchanged.

5.3.7 Fluorescence Studies

The fluorescent properties of the three azopyridine ligands and complexes **22–27** were investigated. All were found to be non-fluorescent under the conditions employed (298 K, dioxane).

5.3.8 Kinetic Studies of Complex 27 in Aqueous Solutions and Cell Culture Media

The spectrum of Na[Pt(azpyO)$(N_3)_2$] (**27**) was followed over a 12 hour period in aqueous solution. The main absorption bands around 600 nm rapidly decreased over time, with A_{594} decreasing by 16% in the six minutes following the first acquisition, followed by the emergence of a new peak at 425 nm. The change was also noted visually, as the intense blue colour had been lost at the end of the experiment and the solution appeared pale grey-brown.

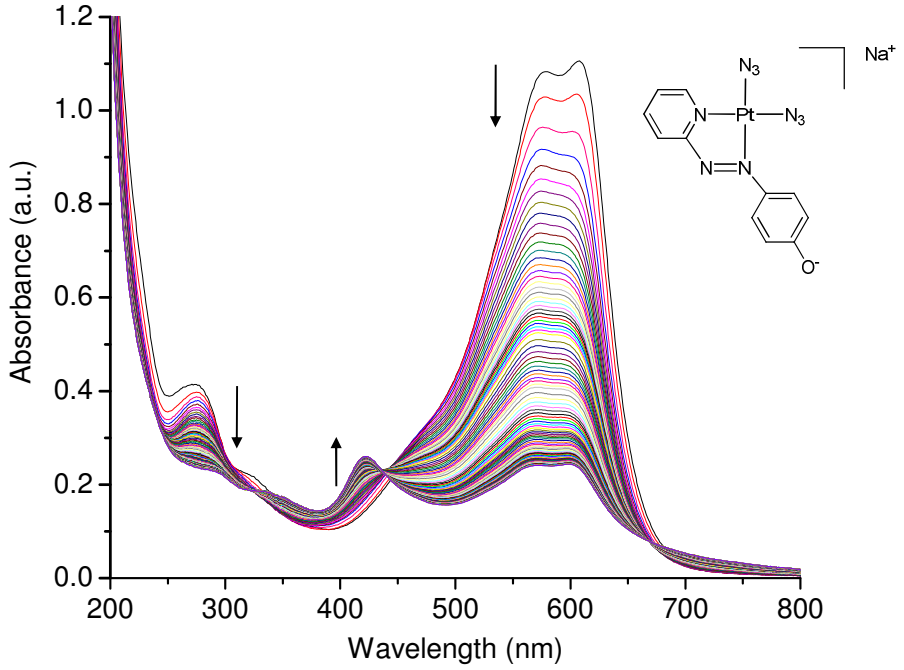

Figure 5.12 The change in absorption profile of **27** over a 12 h period in aqueous solution.

Comparing the final spectrum with those obtained during the pH titration experiment, it appears that the phenolate group became protonated over time in water. This was confirmed by addition of 2 mol eq HNO_3, after which the peak at 425 nm continued to grow and the two peaks around 600 nm decreased in intensity further. Conversely, addition of dilute NaOH restored the spectrum to its original profile.

Since **27** is a potential candidate for cytotoxicity and phototoxicity testing, a stability study was carried out in buffered (pH 7.3) RPMI cell culture medium, to mimic conditions in such experiments, as described in section 5.2.3.4. A similar but much reduced change was seen in this case, indicating the complex remained predominantly in its deprotonated form. This is supported by observations during the cell tests, in which the blue colour of the solution remained following the 24 hour exposure of the cells to the drug.

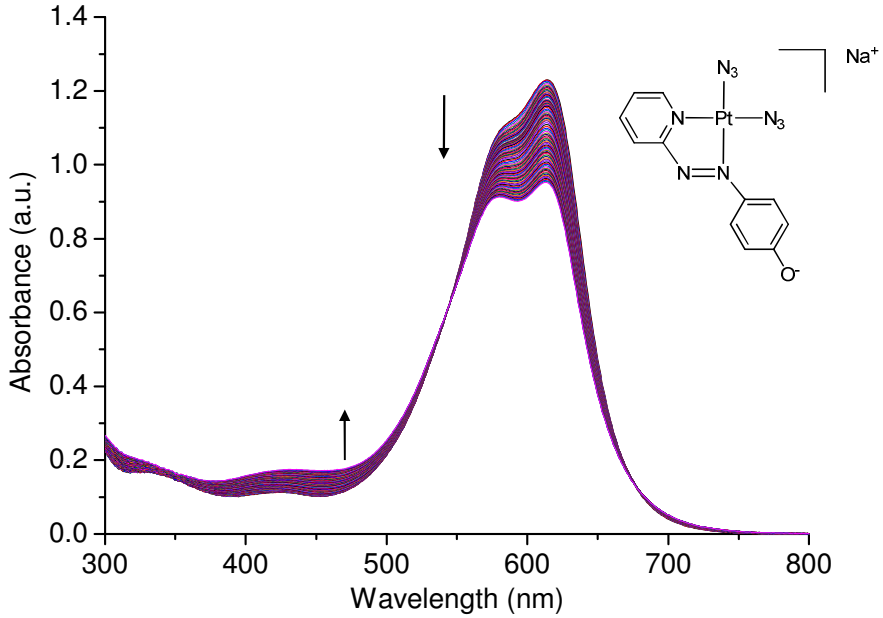

Figure 5.13 The change in absorption profile of **27** over a 12 h period in cell culture medium.

5.3.9 Stability of Pt^{II} Complexes by NMR in Acetone

The NMR spectra of complexes **22**–**27**, recorded in acetone, showed no change over a period of 113 days following storage at ambient temperature in the dark. It can therefore be concluded that these complexes are very stable in solution under these conditions, as there is no evidence of decomposition or formation of new species.

5.3.10 Cytotoxicity of $Na[Pt(azpyO)(N_3)_2]$ (27)

Complex **27** was tested for cytotoxicity against the A2780 human ovarian cancer cell line. Although the complex showed moderate cytotoxicity, results were

variable with the two tests performed giving IC_{50} values of 62 and 83 μM (cisplatin 1.3 μM).

5.3.11 Photoreactions of Pt^{II} Complexes in Dioxane

The photoreactions of the Pt^{II} complexes **22–27** upon irradiation with UVA and visible light were followed by UV-visible absorption spectroscopy. Experiments were carried out in dioxane due to the increased solubility in this solvent over methanol, with the exception of complex **27**, for which methanol was used. Unless otherwise stated, the power levels and total irradiation times were as described in section 5.2.3.7.

5.3.11.1 [Pt(azpy)Cl_2] (22)

A) UVA Light

The spectral profile of **22** remained essentially unchanged following 120 min irradiation, with the main absorption band at 395 nm showing only a small decrease of 2%. This decrease continued upon prolonged irradiation, to a total of 4% after 210 min. However, given such small changes, the complex can be regarded as essentially stable under these conditions.

B) Visible Light

Following 120 min irradiation, no change was seen in the main absorption bands of **22**.

C) Green Light

Similarly, no change was seen following 120 min irradiation with green light.

5.3.11.2 [Pt(azpy)(N_3)$_2$] (23)

A) UVA Light

Irradiation with UVA light resulted in a decrease in intensity of both main bands in the absorption spectrum of **23** (Figure 5.14, A).

The lower energy band (566 nm) showed the most rapid change in absorbance, decreasing to less than half of its initial value by 45 min. Upon further irradiation a slight increase was seen, similar to the remainder of the lower energy region of the spectrum in which the absorbance increased gradually throughout the experiment. The band at 391 nm also decreased upon irradiation; this continued throughout the experiment. After 45 min, a new peak became apparent at 325 nm, which increased in intensity upon further irradiation. By the end of the experiment the sample had decolourised significantly, from deep pink to pale brown.

B) Visible Light

Irradiation with visible light also led to a decrease in intensity of both main bands in the spectrum of **23**. Similar changes in the spectral profiles suggest the same reaction is occurring upon irradiation with both UVA and visible light; however in this case the rate of change is slower compared with UVA. Following 120 min of irradiation, the band at 566 nm was still decreasing in intensity and the new peak at 325 nm had not clearly resolved.

C) Green Light

Following 120 min irradiation, no change was seen in the spectral profile of **23**.

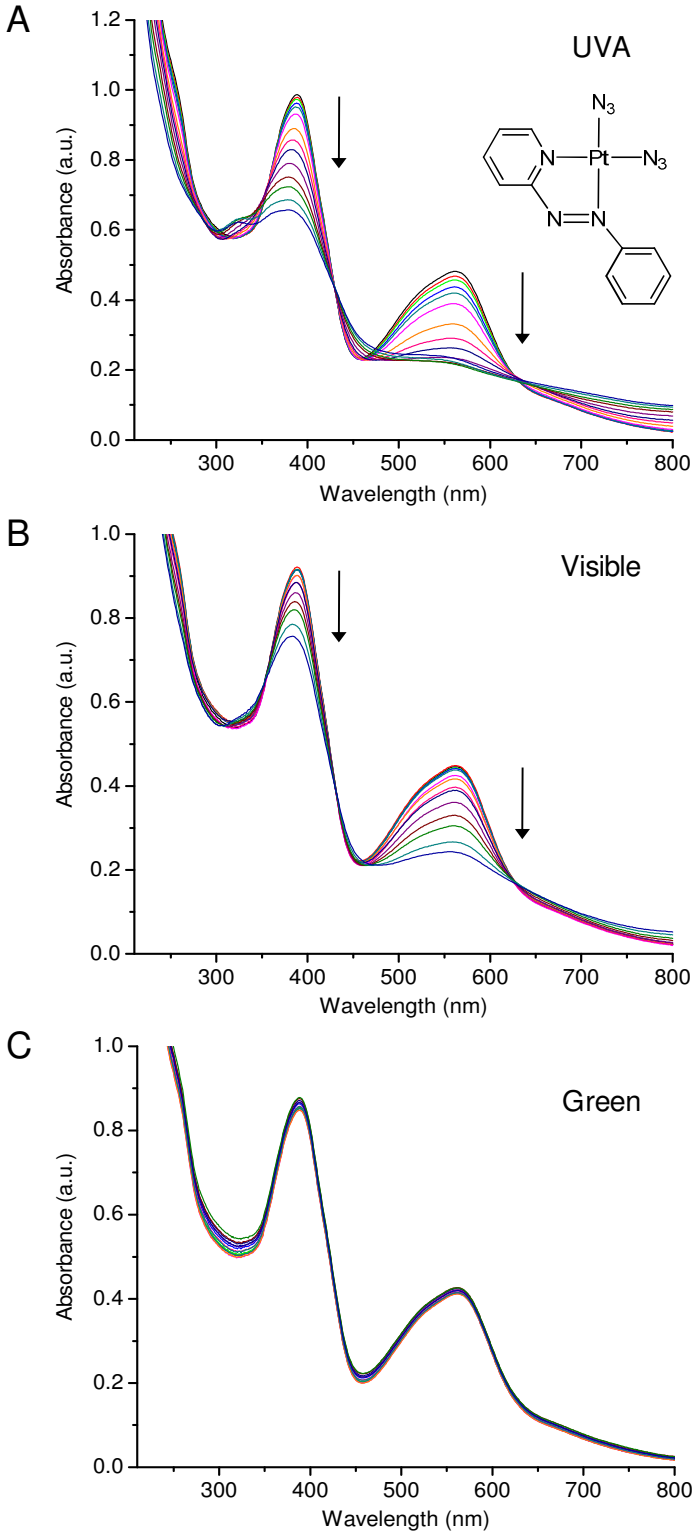

Figure 5.14. UV-visible absorption spectra of [Pt(azpy)(N_3)$_2$] (**23**) following irradiation with A: UVA, B: visible and C: green light, over 120 min in dioxane.

Attempts to elucidate the photoproducts of these reactions were unsuccessful. No platinum containing species could be detected by mass spectrometry, and following the reactions by NMR was limited by the poor solubility of the complex in many solvents suitable for irradiation experiments. An attempt in dioxane showed only weak signals in the spectrum of the initial complex, the intensity of which were rapidly lost upon irradiation and no photoproducts could be identified.

5.3.11.3 [Pt(azpyNMe$_2$)Cl$_2$] (24)

A) UVA Light

The main absorption bands at 613 and 647 nm showed a decrease in intensity of 8% following 120 min irradiation, with a smaller decrease (5%) also seen for the dark control. A reduction in intensity throughout the higher energy region was seen for both samples and was deemed not to be an effect of irradiation.

B) Visible Light

The decrease of the main absorption bands was, at 3%, smaller than that seen following UVA irradiation, however this trend was also seen for the dark control. Again, changes in the higher energy region of the spectrum were seen but appeared to be independent of irradiation.

Given the variable changes seen in the spectrum of this complex even under dark conditions, it is difficult to draw conclusions as to its stability upon irradiation. However, it can be concluded that the effect of irradiation is not large, and the complex is relatively stable under the conditions employed.

5.3.11.4 [Pt(azpyNMe$_2$)(N$_3$)$_2$] (25)

A) UVA Light

The irradiation of complex **25** resulted in changes to the main absorption band at 618 nm. Initially this band decreased in intensity with a broadening of the maxima, and after 30 min began to resolve into two separate peaks. Upon further irradiation, the peak at lower energy (621 nm) decreased in intensity faster than that at higher energy (574 nm). Irradiation was continued beyond 120 min, with additional spectra recorded at 180 and 240 min (grey and violet lines, respectively). The trend was continued, although the intensity difference between the two peaks began to decrease. A decrease in the higher energy absorption band at 298 nm was also observed.

B) Visible Light

Initial changes were similar to those seen upon irradiation with UVA light, although again occurred at a slower rate. Irradiation was continued beyond 120 min, with additional spectra recorded at 150, 180, 210, 240, 300 and 360 min. Following 180 min irradiation, the broadened band again began to resolve into two separate peaks, both of which decreased in intensity upon continued irradiation, although in this case the higher energy peak appeared to decrease at a slightly faster rate. Again a decrease in the higher energy absorption band at 298 nm was observed.

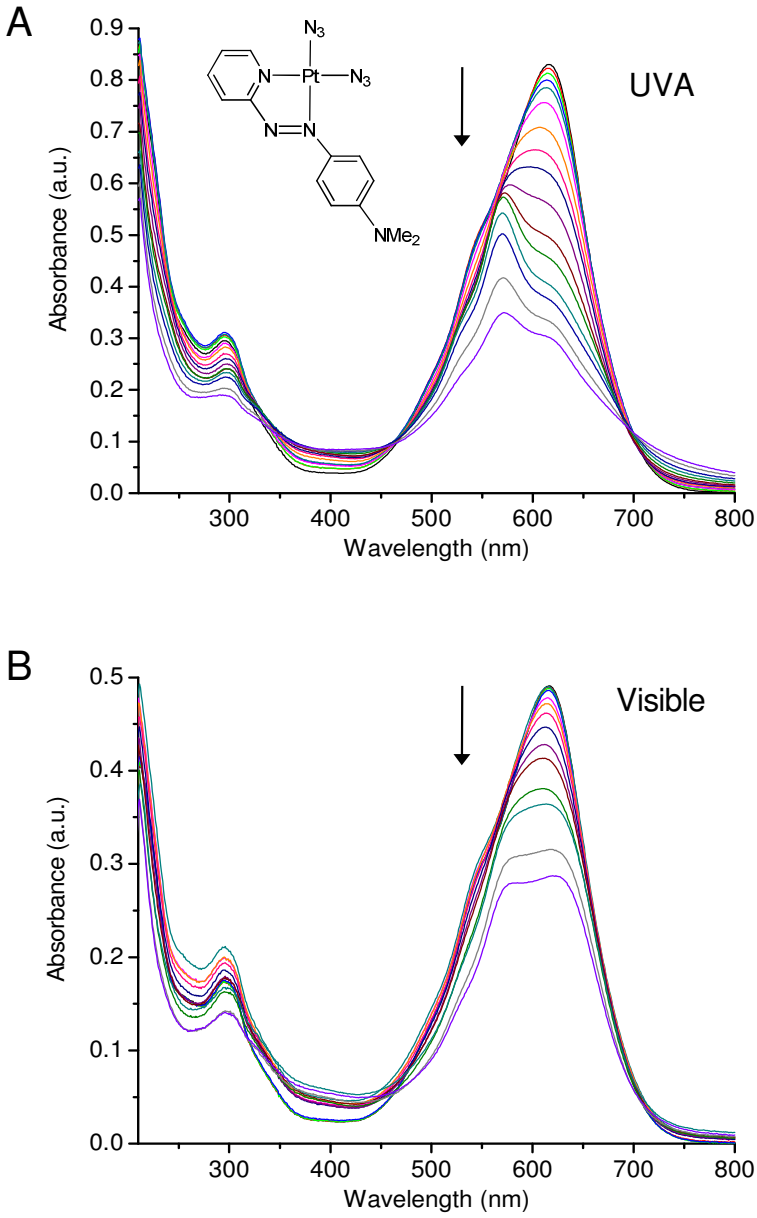

Figure 5.15 UV-visible absorption spectra of [Pt(azpyNMe$_2$)(N$_3$)$_2$] (**25**) following irradiation with UVA and visible light, over 120 min in dioxane.

5.3.11.5 [Pt(azpyOH)Cl_2] (26)

A) UVA Light

A 2% decrease in intensity was seen in the main absorption bands of **5** following 120 min irradiation; again the complex can be regarded as essentially stable under these conditions.

B) Visible Light

Following 120 min irradiation, no change was seen in the main absorption bands of **26**.

5.3.11.6 Na[Pt(azpyO)$(N_3)_2$] (27)

A) UVA Light

In comparison to complexes **23** and **25**, relatively little change was seen in the absorption spectra of **27** upon irradiation. Both peaks at 619 nm and 584 nm decreased in intensity by a total of 10% after 120 min irradiation, with an accompanying blue shift of 11 nm in each case. Whilst no further blue shift was seen after 45 min, the intensity decrease continued throughout the experiment.

B) Visible Light

Little change was seen in the spectra of the complex upon irradiation with visible light. As with UVA, a blue shift of both peaks was again observed, although at 5 nm was smaller in magnitude in this case. A small (3%) increase in intensity of these peaks was seen over the course of the experiment.

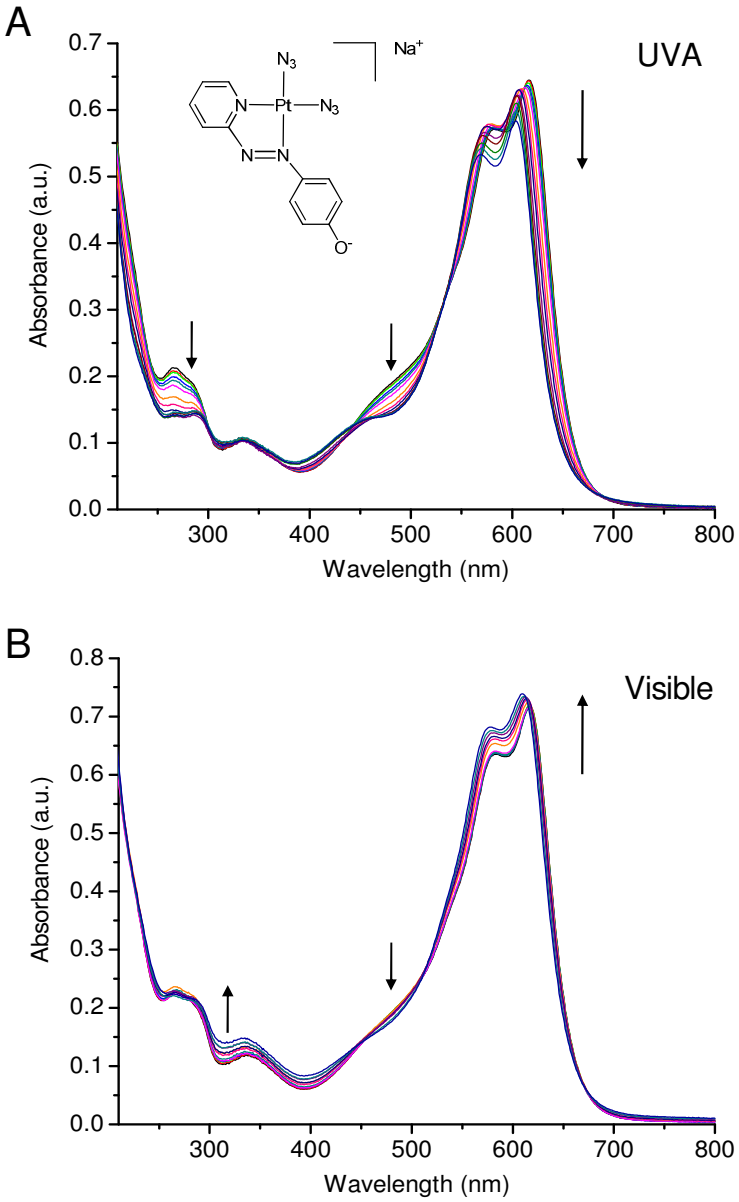

Figure 5.16 UV-visible absorption spectra of Na[Pt(azpyO)(N_3)$_2$] (**27**) following irradiation with UVA and visible light, over 120 min in methanol.

5.3.12 Phototoxicity of $Na[Pt(azpyO)(N_3)_2]$ (27)

Complex **27** was tested for phototoxicity towards HaCaT keratinocytes, irradiating with UVA light as described in Chapter 2. The complex was found to be toxic both upon irradiation with UVA light and in the dark (sham-irradiated control), with IC_{50} values of 72.1 and 112.9 μM respectively, which indicate an increase in toxicity upon irradiation.

During testing, it was observed that the intense blue colour caused staining of the cells, and thus provided a means of visualising the complex within the cells. This staining was evident in the majority of cells in the sample; estimated at around 80% by visual inspection. Following the 1 h incubation period prior to irradiation, the blue colour appeared to be localised in the nuclear region, with only punctate staining of the cytoplasm, as shown in Figure 5.17. This suggests that a platinum complex reaches the nucleus, since the ligand alone does not give rise to a blue solution, and that uptake into the nucleus is rapid.

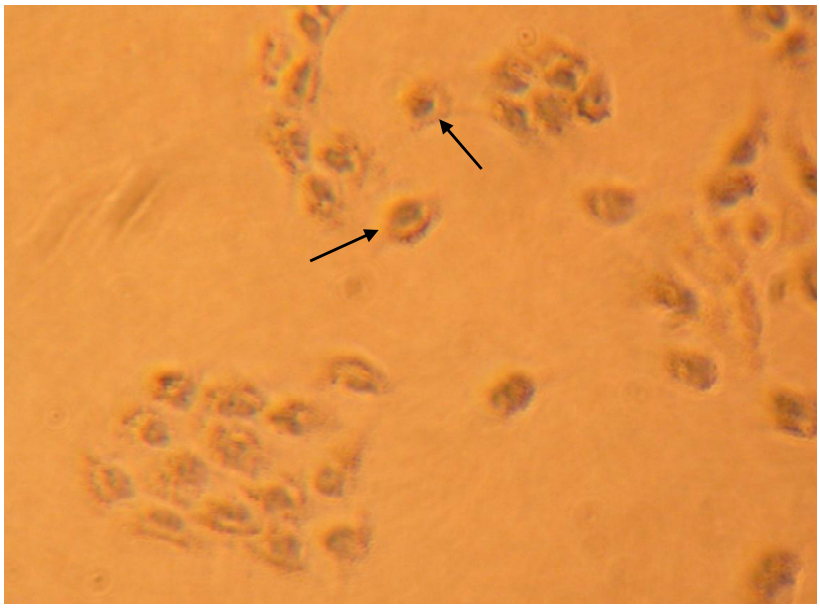

Figure 5.17 A microscope image of HaCaT cells prior to irradiation, 1 h after addition of complex **27**. The staining of the cells by the complex is evident, with the blue colouring appearing to be localised in the nuclei.

During the 24 h development period following irradiation, the blue colour began to fade. This seemed to occur to a lesser extent in the irradiated sample than in the sham-irradiated control, however this was not quantified and would need further investigation.

5.4 Discussion

5.4.1 Synthesis and Characterisation of Platinum Complexes of Azopyridine Ligands

Pt^{II} chlorido complexes of several azopyridine derivatives have been reported in literature.[18,19] Typically, synthesis has involved reaction of the appropriate azopyridine ligand with K_2PtCl_4 in boiling aqueous acetonitrile, with purification in some cases by column chromatography. Attempts were made here to simplify this procedure and reduce the need for refluxing and chromatography. *Cis*-$[Pt(DMSO)_2Cl_2]$ was chosen as the starting material due to the ease of replacement of the two DMSO groups by incoming ligands.[33] The synthetic methods described here produced, in the case of **22** and **24**, analytically pure complexes in higher yields and on a shorter timescale than previously reported methods. The yield was reduced, however, in the synthesis of **26** due to the need for an additional purification step. Solubility constraints led to the use of methanol as the reaction solvent in this case, leading to the contamination of the product with the poorly soluble starting material *cis*-$[Pt(DMSO)_2Cl_2]$. During column chromatography, a colour change from brown to blue was observed. It is likely that the phenolic OH of the ligand was deprotonated, and the resulting, more polar complex was retained on the silica.

Attempts to synthesise the Pt^{II} chlorido complex of 4-(2-pyridylazo)resorcinol were unsuccessful; although evidence of a pure, platinum-containing product was obtained by NMR spectroscopy, it could not be identified. The ligand is well

known for its excellent metal binding ability, and has been used in the spectrometric determination of over 40 different metals.[34] Tridentate (*N,N,O*) coordination of this ligand is most common, and may be favoured over bidentate (*N,N*) coordination in a proton-accepting solvent such as methanol.[35] However, mass spectral and elemental analyses suggested the product formed was neither the tridentate nor the intended bidentate complex, and its identity could not be elucidated.

Formation of a Pt^{II} azido complex is commonly carried out by chloride extraction with silver nitrate in aqueous solution, followed by addition of sodium azide as described previously.[36] However, the poor aqueous solubility of the Pt^{II} chlorido complexes, combined with the reported unsuitability of this method for Pt^{II} bipyridine complexes,[37] led to the use of an alternative method in this case, whereby sodium azide was added directly to the complex in DMF. This method, previously employed in the synthesis of Pt^{II} azido complexes containing bipyridines,[38] was found to be equally suitable in this case and the required complexes were isolated in good yields. Complex **27** was isolated as a sodium salt with the ligand in its deprotonated form, $Na[Pt(azpyO)(N_3)_2]$. Subsequent experiments indicated that the phenolic OH group of the ligand has a pK_a ~5–6 when coordinated to platinum (section 5.3.6.2), and the methanolic solution of NaN_3 used in the reaction was sufficiently basic to effect deprotonation. In order to isolate the protonated product, it was not possible to acidify the reaction solution during synthesis due to the presence of excess sodium azide, since the azide anion forms an extremely toxic gas, HN_3, upon exposure to acid. Acidifying an aqueous solution of the isolated, deprotonated sample was also unsuccessful and could be a result of instability to highly acidic conditions, since several metal complexes of azpyOH have previously been found to be unstable and sensitive to changes in pH.[39]

Given the interesting photochemistry of Pt^{IV} azido complexes previously synthesised in our group, attempts were made to oxidise $[Pt(azpy)(N_3)_2]$ (**23**) in order to investigate the properties of the Pt^{IV} derivative. However, attempts using

a variety of conditions were not successful. The oxidation of $[Pt(bipy)(N_3)_2]$ and similar complexes is difficult to achieve, due to the π-accepting nature of bipy and its ability to stabilise metals in their low oxidation states.[40] Azpy is a better π-acceptor than is bipy, demonstrated by the greater stability of $[Ru(azpy)_2Cl_2]$ compared with $[Ru(bipy)_2Cl_2]$ with respect to oxidation to Ru^{III}.[11] Therefore it is perhaps not surprising that the oxidation of **23** was problematic, and it may be that a stronger oxidising agent and/or reaction conditions would be required than can be tolerated by the azo functionality and the azido groups.

5.4.2 UV-Visible Absorption Spectra of Azopyridine Ligands and Complexes 22–27

The experimental absorption spectra of the three ligands azpy, $azpyNMe_2$ and azpyOH were compared with those generated by TD-DFT calculations; the results of which also enabled the transitions comprising each band to be assigned.

Each ligand displays a large band arising from a π–π* transition. The charge transfer character of this transition increases with the σ-donating ability of the para substituent on the phenyl ring (H < OH < NMe_2), resulting in a progressive red shift of this band in the absorption spectrum. Azpy displays a weak n–π* transition at lower energy; the major contribution is presumably from a HOMO–LUMO transition, since the HOMO of this ligand is of n symmetry. Although formally forbidden on symmetry grounds, the selection rules are seemingly violated to a small extent and a very weak band resulting from this transition is observed.

The absorption bands of complexes **22**–**27** are comprised of two or more main transitions, generally with LC or MLCT character. The LC transitions typically show involvement of the NMe_2 or OH group (**24**–**27**), whilst the MLCT transitions often contain a strong contribution from the chlorido or azido groups. In all transitions listed, electron density migrates to the azo group and pyridyl

nitrogens. The influence of the NMe_2 and OH groups of **24**–**27** can be seen by the red shift and increased molar extinction coefficient of the absorption bands compared with complexes **22** and **23**. σ-Donation from these groups decreases the π-accepting capability of the azo group, increasing the energy of the metal-based orbitals thus decreasing the energy of the MLCT transitions. A similar energy decrease is seen for ligand-centred transitions, due to the increased delocalisation of electron density. [Pt(azpy)Cl_2] (**22**) again shows a weak band at lower energy (495 nm). Not predicted by singlet excited state calculations, this is likely due to a formally forbidden triplet transition. The presence of a heavy metal centre increases spin-orbit coupling, allowing for a violation of the spin selection rule and a weak band to be observed.

The agreement between calculated and experimental spectra is generally good, although less so for complexes of azpyNMe_2 (**24** and **25)** and for **27**, containing the deprotonated ligand azpyO^-. It has been previously observed that such predictions are less valid in the presence of strongly electron-donating or withdrawing groups;[41] presumably the calculated energy of the orbitals is less accurate in these cases.

5.4.2.1 Kinetic Studies of Ligands and Platinum Complexes by UV-Visible Absorption Spectroscopy

The main absorption band of azpyNMe_2 shows an increase in intensity over time; the magnitude of which appears to be variable. The same is seen for the Pt^{II} azido complex of this ligand, **25**, whilst the chlorido complex **24** shows the opposite trend, with the two main bands decreasing in intensity. The reason for this behaviour is unclear. Stacking interactions are common in aromatic π-systems and could give rise to such variations in the spectra. Although no significant π-π stacking was seen in the crystal structure of [Pt(azpy)Cl_2] (**22**), σ-donation from the NMe_2 group renders the aromatic system of azpyNMe_2 complexes more electron- rich in comparison, which could increase the likelihood of such

interactions. However, the deviation of the ligand from planar geometry in complexes **24** and **25** would be expected to hinder stacking, and these spectral changes are minimal in complex **27**, which is essentially planar according to DFT calculated geometries. Additionally, although the aggregation of azo dyes is fairly well documented, it is typically favoured in aqueous solutions of high ionic strength and not in organic solvents.[42] The phenomenon seen here could be further explored by concentration- and temperature-dependent NMR and UV-visible spectroscopic experiments.

5.4.3 Effects of pH on Complexes 24 and 26

The effect of charge transfer from the NMe_2 and OH groups on the absorption properties of these complexes is demonstrated by the UV spectra of **24** and **26** at varying pH values. At very low pH (around 0), the NMe_2 group of **24** is protonated and essentially all donating ability is lost; the solution turns from deep blue to orange and the spectral profile resembles that of [Pt(azpy)Cl_2] (**22**). Although a pK_a value was not determined, it is certainly below that of the free ligand, 2.11[32]. The lower tendency towards protonation reflects the greater conjugation of the nitrogen lone pair into the π system when the ligand is coordinated to platinum. Similarly, the σ-donating ability of the OH group is greatly enhanced upon deprotonation, as can be seen by the large red shift in the main absorption band of **27** compared with that of **26**. An accurate pK_a of the OH group of complex **26** could not be determined; however at around 5–6 this is significantly lower than that of the free ligand at 8.08. A similar effect was seen in the ruthenium complex [(η^6-p-cym)Ru(azpyOH)Cl]PF_6, where the pK_a was decreased to 6.48 upon coordination to the metal.[32] This suggests that electron density from the phenolate group is more readily delocalised in the metal complex. Additionally, at physiological pH (around 7.4) the complex will exist predominately in its deprotonated form, with an overall negative charge.

5.4.4 Stability Studies of Pt^{II} Complexes

5.4.4.1 Stability of 22–27 by NMR

The synthesis and biological properties of the Au^{III} complex $[Au(azpy)Cl_2]Cl$ have been recently reported.[14] Intriguingly, the complex was found to undergo a metal-mediated reaction to form a cationic, tricyclic organic derivative of azpy over 12 days in an acetone solution. This cation showed higher cytotoxicity than the parent complex in a number of cancer cell lines.

Complexes **22**–**27** were therefore investigated for their tendency to undergo this or a similar reaction, with ^1H NMR spectra in acetone showing no observable changes over 113 days. It was therefore concluded that complexes **22**–**27** are stable over a long time period in solution, and show no tendency to undergo such reactions.

The mechanism of formation of this cation has not been elucidated, though Au^{III} mediated organic transformations are well-known.[43] Although Pt^{II} is isoelectronic with Au^{III}, the two display markedly different chemistries. The Pt^{II} complex of azpy is neutral whilst that of Au^{III} is cationic, and the electronic properties of these complexes will differ significantly.

5.4.4.2 Stability of $Na[Pt(azpyO)(N_3)_2]$ (27) in Aqueous Solution and Cell Culture Media

The rapid change in the UV-visible spectrum of **27** upon dissolution in water appears to result from protonation of the phenolate group. The pK_a of this group has been determined as 5–6 so at pH values close to this a mixture of the two species will be present in solution. The spectral profile will thus change as an equilibrium is reached following dissolution of a purely deprotonated sample in water. However, the observed rate of change is slower than expected, since protonation is typically instantaneous. This reduced rate could indicate the

involvement of the phenolate group in intermolecular interactions, reducing its tendency to protonate. Indeed, an osmium complex of this ligand was recently crystallised, in which the phenolate oxygen was found to show a strong hydrogen bond to a water molecule (Y. Fu, unpublished results). The stability of this complex in methanol also supports the theory, since such a process could not readily occur in this solvent. Furthermore, the suppression of this change in RPMI cell culture medium, buffered at pH 7.3, provides additional evidence. This indicates that, during cytotoxicity testing, the complex should remain predominately in its deprotonated form with an overall negative charge.

5.4.5 Cytotoxicity of Na[Pt(azpyO)(N_3)$_2$] (27)

The cytotoxicity of several Ru complexes of azopyridines has been reported, as well as that of an Au^{III} azpy complex.[14] However, despite several reports of Pt^{II} azopyridine complexes, cytotoxicity studies appear to be absent in the literature. The aqueous insolubility of the complexes synthesised here hampered the testing of all but complex **27**, which is reasonably water soluble due to its isolation as a sodium salt. This was found to be moderately cytotoxic towards the human ovarian A2780 cancer cell line, although different IC_{50} values were obtained in the two plates tested (62 and 83 μM). The rapid change in the absorption spectrum of **27** in aqueous solution, believed to be influenced by its protonation state, appears to be reduced upon dissolution in buffered, alkaline cell media. However should this occur to any extent (during sample preparation, for example), it would result in the testing of two complexes with differing properties and solubilities, and in unknown proportions.

It is also noteworthy that whilst the complex remains predominately deprotonated in cell culture media, upon uptake into cancer cells, which typically show pH values 0.3 to 0.5 units lower than those of healthy cells,[44] protonation of the complex may be more probable.

5.4.6 Photoreactions of Pt^{II} Complexes

The photoreactions of Pt^{IV} azido complexes, and their potential for use as photoactivated anticancer agents, are the subject of much current interest. Chapter 3 was also concerned with investigations of the photochemistry and phototoxicity of Pt^{II} azido complexes. However, both the Pt^{II} and Pt^{IV} analogues studied thus far show very low absorbance at visible wavelengths of light, which are preferred for phototherapy due to their deeper penetration into tissues compared with UVA. Therefore photoactivation of these complexes with visible light, whilst sometimes achievable, is much less efficient than with UVA.[3] Azo compounds show very strong absorbance at visible wavelengths, hence it was believed that their incorporation into platinum azido complexes may allow for activation with light in the visible region.

The three Pt^{II} chlorido complexes showed little change upon irradiation with UVA or visible light, whilst the azido analogues appeared more photoactive but to varying degrees. Attempts were made to rationalise the observed behaviour considering information from TD-DFT calculations, which predict the nature of the transitions and the orbitals involved in singlet excited states.

The fate of a complex upon irradiation will depend partly upon what transitions can be induced by the energy of light, and the nature of the orbitals populated during these transitions. For example, the population of strongly antibonding orbitals is likely to result in dissociation of the parts of the molecule for which this character is seen. Complexes **22**–**27** all contain an orbital with σ-antibonding character towards most of the molecule (Figure 5.4): LUMO+1 for all except complex **23** (LUMO+2). The strong antibonding character suggests all transitions having contributions from this orbital will be dissociative.

Complex **23** is perhaps the most photoactive of all three azido complexes, and undergoes a rapid decrease in its absorption bands upon irradiation. The strongest predicted transition in this complex (386 nm, f = 0.42), has a small (9%) contribution from a HOMO→LUMO+2 transition, corresponding to population of

this strongly antibonding orbital. An additional transition at 372 nm has a much smaller oscillator strength ($f = 0.08$), but a large contribution from the HOMO→LUMO+2 transition (59%), and is likely also to be significant. Furthermore, there are a number of higher energy states, with low probability but some contribution involving LUMO+2. The changes in spectral profile are similar upon irradiation of **23** with visible light, although occur at a slower rate. The transitions around 386 nm and 372 nm could potentially be accessed by this light source, especially since the output spectrum shows spikes of intensity in this region. Irradiation with green light ($\lambda_{max} = 525$ nm) resulted in no change to the absorption spectrum of **23**, apparently being of insufficient energy to induce dissociative transitions. However, as the power level of the LEDs is very low in comparison to the other light sources used, confirmation of this is required by repeating this experiment using a more powerful light source, such as a laser, with a similar spectral output.

Since LUMO+2 is σ-antibonding towards most of the molecule, it is likely that dissociation of the complex is extensive. The loss of intense colour and rapid decrease in signal intensity both in the absorption and NMR spectra is in accordance with significant decomposition. However, elucidation of photoproducts may be difficult even if dissociation is less extensive. For example, were free azopyridine to be released it would undergo *cis-trans* isomerisation upon irradiation, resulting in changes to the spectral profile which would hinder its identification.

Complex **25** also shows a decrease in intensity of its absorption bands upon irradiation, although in this case the spectral profiles differ following irradiation with UVA and visible light. The transitions involving population of the strongly antibonding LUMO+1 have a lesser probability (lower oscillator strength) than those of complex **23**, with the most accessible at 376 nm ($f = 0.006$, HOMO–1→LUMO+1 77%), 345 nm ($f = 0.006$, HOMO–2→LUMO+1 67%, HOMO→LUMO+1 20%) and 317 nm ($f = 0.03$, HOMO–3→LUMO+1 48%), with some additional transitions at higher energy. Although of a low probability,

the contributions made to these transitions involving LUMO+1 are high. No transitions involving this orbital can be found at lower energies accessible by irradiation with visible light. However, the complex is photoactive upon irradiation in this region, and it is possible that small spikes in the spectral output of the visible lamps (at around 370 nm and 320 nm) could induce such changes. The resulting spectral profile is different from that produced by UVA light; since irradiation with different wavelengths is likely to induce different transitions, which can give rise to different photoproducts.

Complex **27** is much less photoactive than **23** or **25**, the absorption spectrum showing only a small decrease upon UVA irradiation and a slight increase with visible light. Considering the accessible transitions involving the population of LUMO+1, a greater photoactivity may be expected. Two transitions (380 nm, $f = 0.045$, HOMO–1→LUMO+1 20%, and 374 nm, $f = 0.0245$, HOMO–1→LUMO+1 66%) show fairly reasonably high probabilities and contributions from the σ-antibonding orbital, in comparison with **23** and **25**. However, it was mentioned earlier that the calculation of orbital energies is often less accurate in the presence of strongly electron-donating groups such as the phenolate anion, which could partially account for the difference between theoretical and experimental observations.

Additionally, whilst TD-DFT calculations can predict the nature of transitions and the relevant orbitals involved, they cannot predict their effects on the complex and its subsequent fate. For example, the population of a strongly σ-antibonding orbital could lead merely to a lengthening of the appropriate bonds and destabilisation of the complex, rather than dissociation. This could explain why none of the chlorido complexes appear to be photoactive, despite having accessible transitions (albeit with low probabilities) involving the population of an antibonding orbital. In the case of the azido complexes, dissociation may be more probable. The azido group is known to display a rich photochemistry, involving the generation of nitrenes and radicals amongst other species,[45] both of which could induce further reaction or decomposition of the photoproducts.

Furthermore, these calculations involve solely the singlet excited state. A more thorough analysis would involve triplet states, the contribution of which may be significant in these complexes due to the heavy-atom effect. The calculation of potential energy surfaces along Pt–ligand bonds would also give insight into which ligands are the most likely to dissociate, and which are the most dissociative states.

5.4.7 Phototoxicity of [Pt(azpyO)(N_3)$_2$] (27)

The activity shown by Na[Pt(azpyO)(N_3)$_2$] (**27**) is promising in the search for new phototoxic complexes. Although toxic in the dark, there is a significant increase in activity upon irradiation with UVA light. Furthermore, the strong absorbance at visible wavelengths provides the possibility of photoactivation in this region, which has been hindered for previous Pt^{IV} azido complexes due to their low absorbances. Work is now ongoing to investigate the phototoxicity of **27** upon irradiation with a broadband red light source.

Additionally, the intense blue colour of solutions of **27** allows for its presence in cells to be clearly visualised, providing information on its localisation. Since the colour is characteristic of the complex and not the free ligand, it could also aid in identification of the intact complex and any transformations it may undergo. The fact that the complex can be visualised alone in this way offers an advantage over those to which fluorescent probes are attached. In such cases, incorporation of a probe into the complex can significantly alter properties such as cellular uptake and distribution, especially since such probes must be located remote from the metal centre in order to minimise quenching of the fluorescence.

Several observations during the testing of this complex warrant further investigation. The punctate staining in the cytoplasm could result from accumulation in mitochondria as well as in the nucleus, which could be determined by co-localisation experiments. It is also interesting that the cells appear to retain the blue colour to a greater extent upon UVA irradiation than

sham irradiation, since a blue colour is indicative of the intact complex. However, this observation was only visual and the experiment would need to be repeated quantitatively.

5.5 Conclusions

The Pt^{II} chlorido and azido complexes of three azopyridine ligands have been studied in this Chapter. All complexes were synthesised in good yields and fully characterised. Attempts to oxidise [Pt(azpy)$(N_3)_2$] (**23**) to a Pt^{IV} derivative were unsuccessful, presumably due to the stabilising effect of the π-accepting azo group on the Pt^{II} oxidation state.

TD-DFT calculations allowed for an analysis of the frontier orbitals of the ligands and complexes. All complexes were found to have a low-lying unoccupied orbital with a strong σ-antibonding character towards the majority of the molecule. The results of TD-DFT calculations were also used to assign the transitions observed in the UV-visible absorption spectra of these complexes; mainly ligand centred or MLCT with strong contributions from the chlorido and azido groups. σ-Donation from the NMe_2 and OH/O^- groups result in a red shift of the main absorption bands of **24**–**27** compared with those of the unsubstituted complexes.

UV-visible absorption spectra of Pt^{II} chlorido complexes showed very little change upon irradiation with UVA and visible light. The Pt^{II} azido complexes **23** and **25** were found to be photoactive in both cases, with dissociation likely induced by population of a σ-antibonding orbital. Although **23** showed similar changes upon irradiation with UVA and visible light, **25** showed differing behaviour between the two; it is likely different transitions were induced in each case, giving rise to different photoproducts. Complex **27** showed some photoactivity upon irradiation with UVA light, but very little was observed with visible light. This complex showed moderate, although variable cytotoxicity against the human ovarian A2780 cancer cell line (IC_{50} 62–83 μM). It was also found to be cytotoxic towards HaCaT keratinocytes, with activity increasing upon

irradiation with UVA light, with IC_{50} values of 112.9 and 72.1 μM in the dark and upon irradiation, respectively. This complex was also found to stain treated cells blue, allowing for its location within the cells to be visualised.

One of the aims of this work was to synthesise Pt^{II} azido complexes with ligands exhibiting strong absorbance in the visible region, to investigate whether this would lead to photoactivity upon irradiation at these wavelengths. TD-DFT calculations suggest dissociative transitions for all complexes occur in the UVA region (around 370–380 nm); even so complexes **23** and **25** show photoactivity upon irradiation with both UVA and broadband visible light, and work is ongoing to investigate if the phototoxicity of **27** shown upon irradiation with UVA light is maintained with red light. As well as strong absorbance in the visible region, these complexes have a large scope for design by, for example, changing the substituents on the phenyl ring, which has been shown here to have a vast influence on their properties. These results therefore suggest that further exploration of the use of ligands which absorb strongly in the visible region may lead to successful attempts to increase the wavelength of photoactivation of platinum azido complexes.

5.6 References

[1] P. J. Bednarski, F. S. Mackay and P. J. Sadler, *Anti-Cancer Agents Med. Chem.*, 2007, **7**, 75.

[2] F. S. Mackay, J. A. Woods, H. Moseley, J. Ferguson, A. Dawson, S. Parsons and P. J. Sadler, *Chem. Eur. J.*, 2006, **12**, 3155.

[3] F. S. Mackay, J. A. Woods, P. Heringová, J. Kašpárková, A. M. Pizarro, S. A. Moggach, S. Parsons, V. Brabec and P. J. Sadler, *Proc. Natl. Acad. Sci. U. S. A.*, 2007, **104**, 20743.

[4] S. Wan, J. A. Parrish, R. R. Anderson and M. Madden, *Photochem. Photobiol.*, 1981, **34**, 679.

[5] F. Soponara, A. Cătălin Moţa and C. Sârbu, J. *Chromatogra. A.*, 2008, **1188**, 295.

[6] N. Tamai and H. Miyasaka, *Chem. Rev.*, 2000, **100**, 1875.

[7] S. Kawata and Y. Kawata, *Chem. Rev.*, 2000, **100**, 1777.

[8] Z. F. Liu, K. Hashimoto and A. Fujishima, *Nature*, 1990, **347**, 658.

[9] A. H. Velders, K. van der Schilden, A. C. G. Hotze, J. Reedijk, H. Kooijman and A. L. Spek, *Dalton Trans.*, 2004, 448.

[10] W. Kaim and S. Kohlmann, *Inorg. Chem.*, 1987, **26**, 68.

[11] R. A. Krause and K. Krause, *Inorg. Chem.*, 1980, **19**, 2600.

[12] S. J. Dougan, M. Melchart, A. Habtemariam, S. Parsons and P. J. Sadler, *Inorg. Chem*., 2006, **45**, 10882.

[13] S. J. Dougan, A. Habtemariam, S. E. McHale, S. Parsons and P. J. Sadler, *Proc. Natl. Acad. Sci. U. S. A.*, 2008, **105**, 11628.

[14] A. Garza-Ortiz, H. den Dulk, J. Brouwer, K. Jaap, S. Huub, A. L. Spek and J. Reedijk, *J. Inorg. Biochem.*, 2007, **101**, 1922.

[15] M. Ghedini, D. Pucci, A. Crispini and G. Barberio, *Organometallics*, 1999,

18, 2116.

[16] T. Yutaka, I. Mori, M. Kurihara, J. Mitzutani, N. Tamai, T. Kawai, M. Irie and H. Nishihara, *Inorg. Chem.*, 2002, **41**, 7143.

[17] P. Bandyopadhyay, D. Bandyopadhyay, A. Chakravorty, F. A. Cotton, L. R. Falvello and S. Han, *J. Am. Chem. Soc.*, 1983, **105**, 6327.

[18] G. K. Rauth, S. Pal, D. Das, S. Chittaranjan, A. M. Z. Slawin and J. D. Woollins, *Polyhedron*, 2001, **20**, 363.

[19] M. Panda, S. Das, G. Mostafa, A. Castiñeiras and S. Goswami, *Dalton Trans.*, 2005, 1249.

[20] M. J. Frisch, G. W. Trucks, H. B. Schlegel, G. E. Scuseria, M. A. Robb, J. R. Cheeseman, J. A. J. Montgomery, T. Vreven, K. N. Kudin, J. Tomasi, V. Barone, B. Mennucci, M. Cossi, G. Scalmani, N. Rega, G. A. Pettersson, H. Nakatsuji, M. Hada, M. Ehara, K. Toyota, R. Fukuda, J. Hasegawa, M. Ishida, T. Nakajima, Y. Honda, O. Kitao, H. Nakai, M. Klene, X. Li, J. E. Knox, H. P. Hratchian, J. B. Cross, V. Bakken, C. Adamo, J. Jaramillo, R. Gomperts, R. E. Stratmann, O. Yazyev, A. J. Austin, R. Cammi, C. Pomelli, J. W. Ochterski, P. Y. Ayala, K. Morokuma, G. A. Voth, P. Salvador, J. J. Dannenberg, V. G. Zakrzewski, S. Dapprich, A. D. Daniels, M. C. Strain, O. Farkas, D. K. Malick, A. D. Rabuck, K. Raghavachari, J. B. Foresman, J. V. Ortiz, Q. Cui, A. G. Baboul, S. Clifford, J. Cioslowski, B. B. Stefanov, G. Liu, A. Liashenko, P. Piskorz, I. Komaromi, R. L. Martin, D. L. Fox, T. Keith, M. A. Al-Laham, C. Y. Peng, A. Nanayakkara, M. Challocombe, P. M. W. Gill, B. Johnson, W. Chen, M. W. Wong, C. Gonzalez and J. A. Pople, *Gaussian 03*, (Revision D 0.1); Gaussian Inc.: Wallingford CT, 2004.

[21] J. P. Perdew, K. Burke and M. Ernzerhof, *Phys. Rev. Lett.*, 1996, **77**, 3865.

[22] P. J. Hay and W. R. Wadt, *J. Chem. Phys.*, 1985, **82**, 270.

[23] A. D. McLean and G. S. Chandler, *J. Chem. Phys.*, 1980, **72**, 5639.

[24] M. E. Casida, C. Jamorski, K. C. Casida and D. R. Salahub, *J. Chem. Phys.*

1998, **108**, 4439.

[25] R. E. Stratmann, G. E. Scuseria and M. J. Frisch, *J. Chem. Phys.*, 1998, **109**, 8218.

[26] M. Cossi, N. Rega, G. Scalmani and V. Barone, *J. Comput.*, *Chem.* 2003, **24**, 669.

[27] W. R. Browne, N. M. O'Boyle, J. J. McGarvey and J. G. Vos, *Chem. Soc. Rev.*, 2005, **34**, 641.

[28] N. M. O'Boyle and J. G. Vos, *GaussSum*, Dublin City University. Available at http://gausssum.sourceforge.net. 2005.

[29] S. Chattopadhyay, C. Sinha, P. Basu and A. Chakravorty, *Organometallics*, 1991, **10**, 1135.

[30] P. Suppan and N. M. Ghoneim, *Solvatochromism*, Royal Society of Chemistry, Cambridge, 1997.

[31] J. B. Lambert, H. F. Shurvell, D. A. Lightner and R. G. Cooks, *Organic Structural Spectroscopy*, Prentice-Hall, New Jersey, 1998.

[32] S. J. Dougan, Ph.D. Thesis, University of Edinburgh, 2007.

[33] F. F. Rochon, C. Bensimon and C. Tessier, *Inorg. Chim. Acta,* 2008, **361**, 16.

[34] S. Srijaranai, S. Chanpaka, C. Kukusamude, G. Chutima and K. Grudpan, *Talanta*, 2006, **68**, 1720.

[35] Y. Kudo, N. Yoshida and M. Fujimoto, *Bull. Chem. Soc. Jpn.*, 1986, **59**, 795.

[36] P. Muller, B. Schroder, J. Parkinson, N. Kratochwil, R. A. Coxall, A. Parkin, S. Parsons and P. J. Sadler, *Angew. Chem. Int. Ed.*, 2003, **42**, 335.

[37] S. Wimmer and P. Castan, *Inorg. Chim. Acta*, 1988, **142**, 13.

[38] S. S. Kamath, V. Uma and T. S. Srirastava, *Inorg. Chim. Acta*, 1989, **161**,

49.

[39] R. G. Anderson and G. Nickless, *Anal. Chim. Acta*, 1967, **39**, 469.

[40] F. S. Mackay, N. J. Farrer, L. Salassa, H.-C. Tai, R. J. Deeth, S. A. Moggach, P. A. Wood, S. Parsons and P. J. Sadler, *Dalton Trans.*, 2009, 2315.

[41] L. Salassa, C. Garino, A. Albertino, G. Volpi, C. Nervi, R. Gobetto and K. I. Hardcastle, *Organometallics*, 2008, **27**, 1427.

[42] L. C. Abbott, S. N. Batchelor, J. Oakes, J. R. Lindsay Smith and J. N. Moore, *J. Phys. Chem. B.*, 2004, **108**, 13726.

[43] S. P. Nolan, *Nature*, 2007, **445**, 496.

[44] J. L. Wike-Hooley, J. Haveman and H. S. Reinhold, *Radiother. Oncol.*, 1984, **2**, 343.

[45] J. Šima, *Coord. Chem. Rev.*, 2006, **250**, 2325.

Courses Attended

Transferable Skills course: Searching Research Literature, University of Edinburgh, October 2004.

Laser Safety course, University of Edinburgh, November 2004.

Postgraduate course in Nuclear Magnetic Resonance, University of Edinburgh, April 2005.

Crystallography lecture course (4th year undergraduate level) given by Professor Simon Parsons, University of Edinburgh, February 2006.

Basic Radiation Protection course, University of Edinburgh, April 2006.

EaStCHEM and CRUK Training Day: Cancer Medicinal Chemistry, University of St Andrews, January 2007.

Chemical Biology postgraduate research seminars, weekly during term time, University of Edinburgh (September 2004 – May 2007), and University of Warwick (June 2007 – June 2009).

Conferences Attended

1st European Chemistry Congress, Budapest, Hungary, August 2006. Poster displayed.

Inaugural Scottish Cancer Medicinal Chemistry Symposium, University of St Andrews, Scotland, March 2007.

Dalton Discussion 10: Applications of Metals in Medicine and Healthcare, University of Durham, England, September 2007.

European COST program D39 conference, Verona, Italy, November 2007. Oral presentation.

10th International Symposium on Platinum Coordination Compounds in Cancer Chemotherapy (ISPCC), Verona, Italy, November – December 2007. Poster displayed.

Publications

Controlling Emission Energy, Self-Quenching, and Excimer Formation in Highly Luminescent N^C^N-Coordinated Platinum(II) Complexes

Sarah J. Farley, David L. Rochester, Amber L. Thompson, Judith A. K. Howard and J. A. Gareth Williams

Inorganic Chemistry, 2005, **44**, 9690.